Deflection-Based Field Testing for Quality Management of Earthwork

Technical Report 0-6903-1

Cooperative Research Program

CENTER FOR TRANSPORTATION INFRASTRUCTURE SYSTEMS
THE UNIVERSITY OF TEXAS AT EL PASO
EL PASO, TX 79968
HTTP://CTIS.UTEP.EDU

in cooperation with the
Federal Highway Administration and the
Texas Department of Transportation

TECHNICAL REPORT STANDARD TITLE PAGE

1. Report No.	2. Government Accession No.	3. Recipient's Catalog No.
FHWA/TX-19/0-6903-1		

4. Title and Subtitle	5. Report Date
Deflection-Based Field Testing for Quality Management of Earthwork	July 2018; Published March 2019
	6. Performing Organization Code

7. Author(s)	8. Performing Organization Report No.
C. Tirado, S. Rocha, A. Fathi, M. Mazari, and S. Nazarian	TX 0-6903-01

9. Performing Organization Name and Address	10. Work Unit No.
Center for Transportation Infrastructure Systems The University of Texas at El Paso El Paso, Texas 79968-0516	11. Contract or Grant No. 0-6903

12. Sponsoring Agency Name and Address	13. Type of Report and Period Covered
Texas Department of Transportation Research and Technology Implementation Office P.O. Box 5080 Austin, Texas 78763-5080	Technical Report Jan. 1, 2016 – July 31, 2018
	14. Sponsoring Agency Code

15. Supplementary Notes

Project performed in cooperation with Texas Department of Transportation and the Federal Highway Administration.
Project Title: Assess Deflection-Based Field Testing for Project Acceptance

16. Abstract

TxDOT current practice for field compaction quality control and acceptance for base, subbase and soil layers is to determine the compacted density and sometimes moisture content by nuclear density gauge (NDG). TxDOT has also considered several stiffness-based devices to replace the NDG because stiffness parameters are more relevant to pavement design. Since spot tests cannot represent the uniformity of the compaction in a continuous manner, less stiff areas can be easily missed. For design-build projects an additional challenging step is the design verification. The current process based on laboratory resilient modulus tests is tedious and marginally representative of the in situ properties. Even though modulus-based nondestructive testing (e.g., with FWD, LWD or DCP) can be conceptually considered as a straightforward solution to this problem, a recent NCHRP study has shown the level of detail that is needed to consider for obtaining meaningful values from the modulus-based devices. This research study has been carried to develop procedures and specifications to improve the process of design verification of compacted materials to ensure quality, performance and durability using a combination of proof rolling with the intelligent compaction rollers and deflection-based devices and to identify less stiff spots, to achieve uniformity, of compacted geomaterials.

17. Key Words	18. Distribution Statement
Modulus, Light-Weight Deflectometer, Intelligent Compaction, Geomaterial, Stiffness	No restrictions. This document is available to the public through the National Technical service, 5285 Port Royal Road, Springfield, Virginia 22161, www.ntis.gov

19. Security Classif. (of this report)	20. Security Classif. (of this page)	21. No. of Pages	22. Price
Unclassified	Unclassified	202	

Form DOT F 1700.7 (8-72) Reproduction of complete page authorized (art. 5/94)

Deflection-Based Field Testing for Quality Management of Earthwork

Cesar Tirado, PhD
Aria Fathi, MSCE
Sergio Rocha, BSEE
Mehran Mazari, PhD
Soheil Nazarian, PhD, PE

Research Project 0-6903

Conducted for

Texas Department of Transportation

Final Report

July 2018

Center for Transportation Infrastructure Systems
The University of Texas at El Paso
El Paso, TX 79968-0516

DISCLAIMERS

The contents of this report reflect the view of the authors who are responsible for the facts and the accuracy of the data presented herein. The contents do not necessarily reflect the official views or policies of the Texas Department of Transportation or the Federal Highway Administration. This report does not constitute a standard, a specification or a regulation.

The material contained in this report is experimental in nature and is published for informational purposes only. Any discrepancies with official views or policies of the Texas Department of Transportation or the Federal Highway Administration should be discussed with the appropriate Austin Division prior to implementation of the procedures or results.

NOT INTENDED FOR CONSTRUCTION, BIDDING, OR PERMIT PURPOSES

Cesar Tirado, PhD
Sergio Rocha, BSEE
Aria Fathi, MSCE
Mehran Mazari, PhD
Soheil Nazarian, PhD, PE (66495)

Acknowledgements

The authors would like to express their sincere appreciation to the Project Management Committee consisting of Jimmy Si, Richard Izzo, Andy Naranjo, Brett Haggerty, Joe Fiello, Miguel Arellano, Richard Williammee Jr and Ruben Carrasco for their support.

We are grateful to a number of employees of TxDOT, especially Jaime Aparicio, Lawrence (Larry) D. Cannon and Richard Williammee of Fort Worth District, Ramon Rodriguez of Laredo District, Seve Sisneros of Lubbock District, Ray Brady of Atlanta District, and Delmy Reyes of Bryan District, and Ruben Carrasco of CST, for their assistance in field testing.

The help from a number of construction companies to accommodate us is also acknowledged.

We are also grateful to a number of undergraduate and graduate students from UTEP for their assistance in the project.

Abstract

TxDOT current practice for field compaction quality control and acceptance for base, subbase and soil layers is to determine the compacted density and sometimes moisture content by nuclear density gauge (NDG). TxDOT has also considered several stiffness-based devices to replace the NDG because stiffness parameters are more relevant to pavement design. Since spot tests cannot represent the uniformity of the compaction in a continuous manner, less stiff areas can be easily missed. For design-build projects an additional challenging step is the design verification. The current process based on laboratory resilient modulus tests is tedious and marginally representative of the in situ properties.

Even though modulus-based nondestructive testing (e.g., FWD, LWD or DCP) can be conceptually considered as a straightforward solution to this problem, a recent NCHRP study has shown the level of detail that is needed to consider for obtaining meaningful values from the modulus-based devices. This research study has been carried to develop procedures and specifications to improve the process of design verification of compacted materials to ensure quality, performance and durability using a combination of proof rolling with the intelligent compaction rollers and deflection-based devices and to identify less stiff spots, to achieve uniformity, of compacted geomaterials.

Table of Contents

List of Figures

List of Tables

1 INTRODUCTION

1.1 Problem Statement

The Texas Department of Transportation's (TxDOT) current practice for field compaction quality control and acceptance for soil and base layers is to determine the compacted density and occasionally moisture content by nuclear density gauge (NDG). TxDOT has considered several stiffness-based devices to replace density measurement because stiffness parameters are more relevant to and used in pavement design. Since both density and stiffness measurements are spot tests, they cannot represent the quality and uniformity of compaction in a continuous manner.

For design-build projects an additional challenging step is the design verification. The current process based on laboratory resilient modulus tests is tedious and marginally representative of the in situ properties. Even though modulus-based nondestructive testing (e.g., with FWD, LWD or DCP) can be conceptually considered as a straightforward solution to this problem. One cannot simply extrapolate the use of the FWD on existing roads to the design verification using FWD or other devices.

Conventional proof-rolling is oftentimes specified by TxDOT as a way of evaluating the uniformity of the compacted materials. Proof-rolling or mapping subgrade and base using the intelligent compaction rollers after completing compaction can effectively identify the less stiff spots and significantly improve the compaction uniformity of the compacted layers.

1.2 Objective

The primary objective of this research is to develop procedures and specifications to estimate the mechanical properties of compacted geomaterials for design verification. This objective could be interpreted as the approach to improve the quality acceptance process of compacted materials instead of conducting laboratory MR tests. In that context, by using existing devices this research aims at developing practical test protocols and specifications to improve the general quality of compaction for subgrade, embankment, and base construction, and facilitate the design verification. The secondary objective is to identify the less stiff spots (or more broadly to achieve uniformity) of compacted geomaterials by means of deflection-based field testing and intelligent compaction.

A generic flowchart of the steps to implement deflection-based design verification process is illustrated in Figure 1.1. This flow chart will act as a living document that will be modified in consultation with TxDOT partners throughout the project as warranted by the experimental and numerical results of the study. The main components for a successful and implementable specification are shown in Figure 1.2.

To achieve these objectives, a number of tasks were proposed and completed. These tasks include:

Task 1. Optimization of Processes and Specifications
Task 2. Develop Prototype Specification
Task 3. Address Theoretical and Technological Limitations
Task 4. Address Practical Limitations
Task 5. Pilot Evaluation of Specification
Task 6. Modification of Preliminary Specifications
Task 7. Validation of Specification
Task 8. Development of Final Deliverables

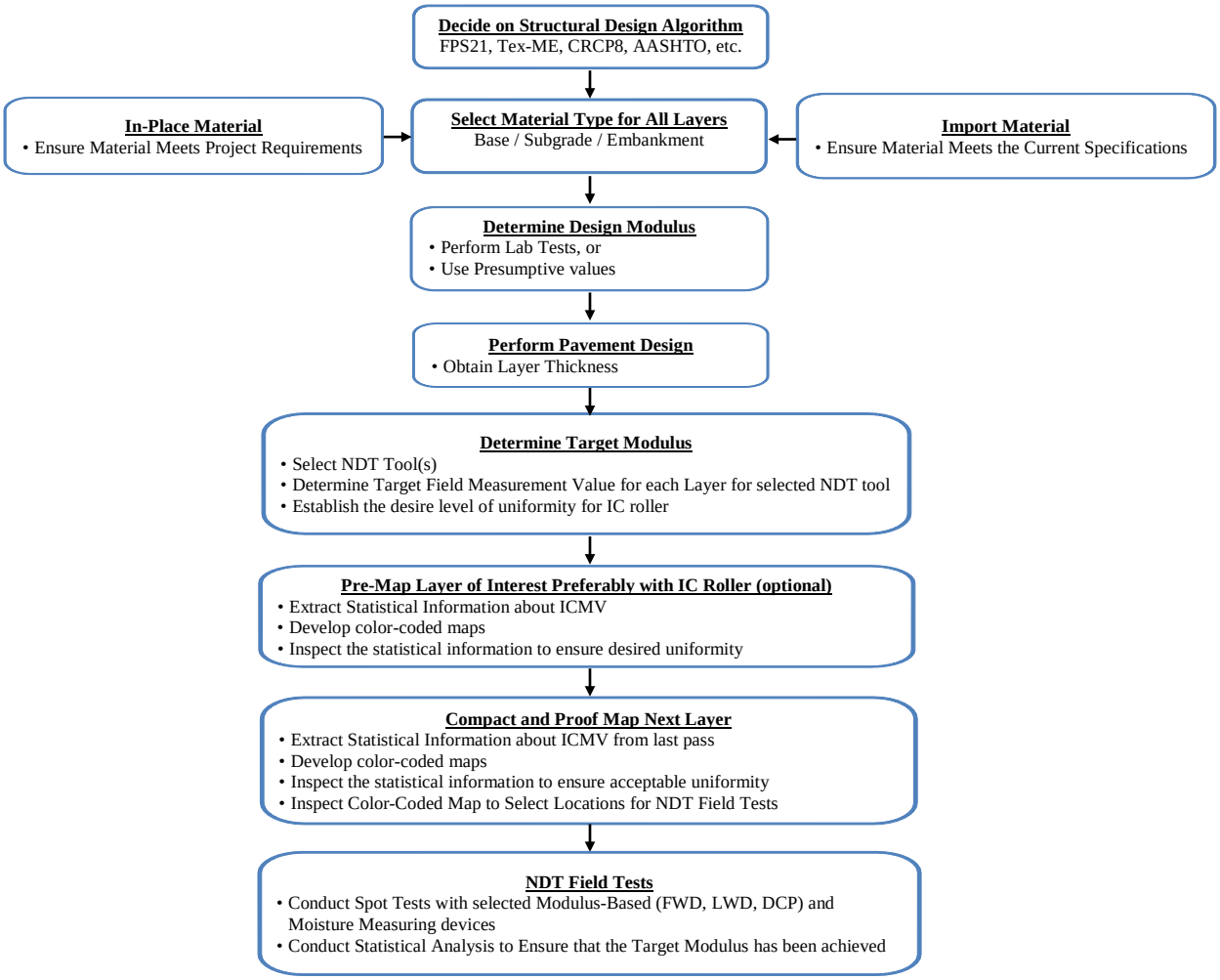

Figure 1.1 - A generic flowchart of implementing design verification.

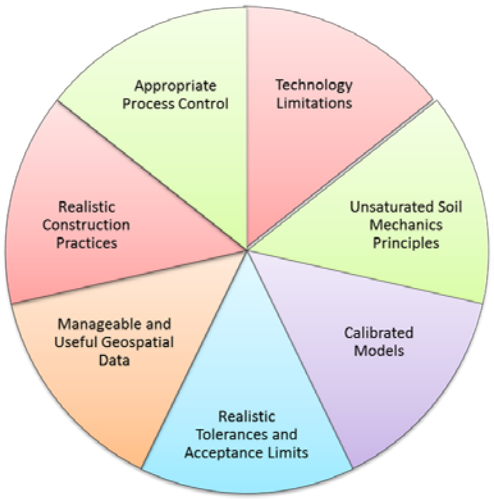

Figure 1.2 - Major items to be addressed in the proposed specification.

1.3 Organization of Report

In addition to this introductory chapter, the report consists of the following six chapters:

- Chapter 2 provides a summary of the review of the state of the practice for the estimation of stiffness of geomaterials.
- Chapter 3 provides a summary of the use of Intelligent Compaction (IC) technology as a tool of qualify control.
- Chapter 4 reviews the theoretical and technological limitations of the selected technologies for estimating stiffness of geomaterials and IC technology.
- Chapter 5 present the process of data collection during the implementation of IC and deflection-based testing in the participating districts. This includes a list of test sections, spot tests, IC data collection, and the practical limitations and major issues encountered during the data collection and data reduction processes. Geospatial analysis and correlation studies between the different technologies implemented are also presented. The chapter concludes with a proposed protocol for project acceptance developed after the interpretation of the presented analyses.
- Chapter 6 briefly summarizes key findings and recommendations for the implementation of the selected technologies used for quality management of earthwork.

In addition to these chapters, the following seven appendices complement this report:

- Appendix A includes the revised Special Specification for Deflection-based Design Verification.
- Appendix B includes the Field Test Procedure for Determining Deflection or Modulus of Geomaterials using Light Weight Deflectometer.
- Appendix C includes the Field Test Procedure for Determining Intelligent Compaction Measurement Value (ICMV) Using Intelligent Compaction (IC) Technology.
- Appendix D contains a summary of constitutive models and models to predict modulus for field test devices.
- Appendix E includes a summary of the current state DOT practices.
- Appendix F summarizes the field evaluation and analysis of subgrade and base in I-35W test section in Fort Worth, TX.
- Appendix G summarizes the field evaluation and analysis of subgrade and base in SH 183 test section in Irving, TX.
- Appendix H summarizes the field evaluation and analysis of subgrade and base in FM 1460 test section in Georgetown, TX.
- Appendix I summarizes the field evaluation and analysis of cement treated base in US 77 test section near Victoria, TX.
- Appendix J summarizes the field evaluation and analysis of cement treated subgrade at SH 149 in Carthage, TX.
- Appendix K summarizes the field evaluation and analysis of subgrade and base in SH 349, near Lamesa, TX.
- Appendix L summarizes the field evaluation and analysis of subgrade and base at FM 133, near Cotulla, TX.
- Appendix M summarizes the field evaluation and analysis of subgrade and base in I-45, near Huntsville, TX.

2 MODULUS BASED QUALITY MANAGEMENT

2.1 Introduction

The traditional quality assurance (QA) approach for transportation infrastructure and more specifically highway construction includes quality control (QC), acceptance, and sometimes, independent assurance (Burati et al. 2003). The stiffness/modulus of a layer is the one of the main design parameters used in modern mechanistic-empirical pavement design guides. The current state of the practice in quality management is widely based on the density (and to less extent the moisture content) measured by a nuclear density gauge (NDG). As such the link between the parameters used in the design and quality management is rather weak. The transformation to stiffness-based quality management through nondestructive testing (NDT) has been under continuous development during the past decades. Technological improvement of construction technologies has resulted in the popularity of Intelligent Compaction (IC) techniques. Even though the basic concept of using IC was developed in the early 1970s, this technology has been under continuous development and implementation during the past decade. The application of the IC in the construction of transportation infrastructure as a more rigorous stiffness-based quality management procedure has attracted the attention of a number of highway agencies (HAs) and departments of transportation (DOTs). This chapter summarizes the current body of research relevant to the stiffness/modulus-based quality management methods including the IC applications.

2.2 Estimating Stiffness of Compacted Geomaterials

The stiffness/modulus of compacted geomaterial layers can be estimated either from laboratory or in-situ test methods. Along with the evolution of laboratory test methods, the modulus/stiffness-based in-situ methods have been under continuous improvement as well. The limitations associated with empirical correlations for design of flexible pavement structures have raised the need to employ mechanistic-based concepts. However, the key to successful implementation of mechanistic approaches is to understand the complex behavior of the pavement structures under the wheel loads. The unbound aggregate pavement layers are one of the most important components of the pavement structures sine most of the deficiencies in the performance of pavements could be traced to unbound aggregate geomaterial layers. Understanding the response of unbound materials has been the focus of many research efforts during the past decades.

Lekarp et al. (2000) included a comprehensive review of the concepts and definitions regarding the resilient response of unbound aggregates. The stresses beneath a rolling wheel load could be defined in terms of time-dependent vertical, horizontal and shear components. Although a resilient response has been assumed satisfactory to represent the behavior of unbound geomaterials under repeated loads, the true nature of such behavior could be the result of consolidation, distortion and attrition (Loung, 1982). Puppala (2008) and Tutumluer (2013) synthesized the body of literature regarding the estimation of resilient modulus of unbound geomaterials. Puppala (2008) synthesized different laboratory and in-situ methods for determining the stiffness/modulus of unbound compacted geomaterials. He also discussed the direct and indirect correlations between the laboratory and in situ moduli.

Tables 2.1 and Table 2.2 summarize the laboratory and field approaches to estimate the stiffness/modulus of the compacted geomaterials. Besides these test methods and devices, several direct and indirect correlations have also been developed to determine the resilient modulus parameters from basic soil properties and some compaction-related parameters.

Laboratory tests are essential to study the parameters that affect the properties of materials. The behavior of a material in terms of variation in modulus with stress level, strain amplitude, and the strain rate is best established by conducting laboratory tests such as the resilient modulus test. However, moduli from laboratory tests are moderately or significantly different than the in situ results. A review of the literature on the recent efforts in studying the fundamental differences between the laboratory and field moduli is summarized in Table 2.3.

Table 2.1 – Summary of Laboratory Methods to Estimate Stiffness of Geomaterials

Methods and Devices	Standard	Strengths	Limitations
California Bearing Ratio (CBR)	- AASHTO T-193 - ASTM D1883	- Relatively easy and inexpensive to perform - Well known among pavement professionals - Established correlations with some in-situ test devices (e.g. DCP and LWD)	- Not used directly in Mechanistic-Empirical (M-E) design - Not dependent of state of stress and therefore not representing the actual response of geomaterial layers under repeated wheel loads
Static Triaxial	- ASTM D4767 - ASTM D2850	Common among DOTs	Does not measure the moduli at the strain levels associated with NDT
Resonant Column	- ASTM D4015	- Directly correlated to field seismic moduli without the need for transfer functions - Relatively easy and inexpensive to perform	- Estimates the low-strain linear elastic modulus of geomaterials and is not representative of nonlinear behavior
Resilient Modulus (MR)	- AAHTO T307 - NCHRP 1-28A	- Relatively complicated and expensive - The test device required comprehensive training to perform the test	- Directly used in M-E design process - The test is performed under various ranges of confining pressure and deviatoric stress - Different models are available to correlate MR to the state of stress - Correlation to the material properties have been under continuous investigation

Table 2.2 – Summary of Field Methods to Estimate the Stiffness of Geomaterials

Methods and Devices	Standard	Strengths	Limitations
Falling Weight Deflectometer (FWD)	ASTM D4694	- Provides a reasonable estimation of layer moduli - Well-known among pavement professionals	- Requires backcalculation of test results to determine layer moduli - The backcalculated results are uncertain due to the variation in layer thickness
Light Weight Deflectometer (LWD)	- ASTM 2583 - ASTM 2835	- Equipment is readily available - community is familiar with concept of deflection-based testing	- Moduli can be influenced by the underlying layers, resulting in more variable moduli
Portable Seismic Property Analyzer (PSPA)	- NA	- Measures layer-specific modulus independent of thickness of layer - No back calculation necessary - Results can be calibrated to specific material being tested prior to construction when M-D relationship is measured in lab	- Need to calibrate the test results to the material and site conditions under evaluation - Requires more sophisticated training of technicians. - Low repeatability, with a high standard deviation due to capability to detect anisotropic conditions
Soil Stiffness Gauge (SSG) - Geogauge	ASTM D6758	- Training and technical requirements are similar to nuclear density gauge - Provides a reasonable estimate of laboratory measured moduli with proper calibration	- Proper intimate contact between Geogauge and soil is difficult to achieve in practice without preparation - Underlying materials can influence results especially for relatively thin unbound layers
Dynamic Cone Penetrometer (DCP)	ASTM D6951	- Several correlations have been established to correlate DCP test results to CBR and modulus/stiffness - Widely used among state highway agencies - Relatively inexpensive and easy to use	- It requires intruding a metal rod into compacted layer - The correlations between DCP index and stiffness are empirical

Table 2.3 – Summary of Studies about Differences between Lab and Field Moduli

Reference	Objectives and Approach	Concluding Remarks	Devices and Test Methods
Nazarian et al (2014)	to investigate laboratory-field transfer functions as a part of developing modulus-based construction quality control of unbound geomaterials	The seismic methods were employed to develop the laboratory-field transfer functions since the field moduli estimated by PSPA could be directly correlated to laboratory moduli values determined from Free-Free Resonant Column (FFRC) test	Lab MR and FFRC tests; Field LWD and PSPA
Oh et al (2011)	to determine correlation factors (CFs) between laboratory resilient moduli and moduli from in-situ tests for unbound geomaterials	A reasonable correlation was found between the backcalculated FWD moduli and the corresponding CFs to correlate to laboratory MR values. However, the backcalculated FWD moduli were not realistic due to uncertainties associated with layer thickness	DCP; FWD; lab MR
Mohammad et al (2007)	To correlate resilient modulus of subgrade geomaterials from NDT, in-situ and laboratory methods	- A reasonable correlation found between the predicted MR results using DCP index and the actual laboratory results - The DCP soil-property model found to be the most reliable approach to correlate the laboratory and field test results as compared to other field test deices	DCP; FWD; Miniature Cone Penetrometer; Lab MR
Gudishala (2004)	To investigate the correlations between in-situ and laboratory resilient moduli	- Correlations developed for specific soil types between in-situ and laboratory resilient moduli - Developed models were associated with some level of uncertainty	DCP; LWD; Lab MR
Ping et al (2002)	To investigate correlations between laboratory and field moduli of granular subgrade materials	- Field backcalculated moduli were about 60% greater than those from laboratory tests - A reasonable correlation between lab MR and in-situ plate load test was not found	FWD; In-Situ Plate Load Test (PLT); Lab MR
Tanyu et al (2003)	To compare the elastic moduli from lab MR tests to those obtained from backcalculation of FWD deflections	- The minimum bulk stress in the laboratory resilient modulus test can be higher than the bulk stress under field conditions. - The low-strain elastic modulus from laboratory tests were lower than the elastic moduli backcalculated from field data	Lab MR test, Large Scale Model Experiment (LSME), FWD

Field tests are more practical and more desirable because they are rapid to perform, and because they test a large volume of material in its natural state. Field tests typically fall into two categories: *material characterization* and *design simulation*. In *material characterization* one attempts to determine the engineering properties of a material (such as modulus) in a way that is the most theoretically correct. The material properties measured in that way are fundamental material properties that are not related to a specific modeling scenario. To use these material properties in a certain design methodology, they should be combined with an appropriate analytical or numerical model (and often additional laboratory tests) to obtain the design output. In the *design simulation*, one tries to her/his best ability to simulate the design condition experimentally and then back-figure some material parameter that is relevant to that condition. These methods usually measure the response (typically the stiffness) of the pavement system.

Both approaches have advantages and disadvantages. In the design simulation, the state of stress applied to the geomaterials ideally should be similar to those from the actual scenario they are attempting to simulate. However, since the state of stress in the pavement depends on the modulus of the layers, it would be difficult

to use a measured modulus from one pavement structure to another with different layer thicknesses or underlying layers. The moduli that resemble material characterization can be used universally, but they have to be tied to a pavement design model.

The correlations developed by various studies in the literature predict the moduli only within the range geomaterials types used for model development. However, most models exhibit poor predictive power when they are tested on different soils not used to develop the relationships (Von Quintus and Killingsworth, 1998; Yau and Von Quintus, 2002; Wolfe and Butalia, 2004; Malla and Joshi, 2007). Such problems should be expected because correlations are developed from data that may have shown large variations for similar types, similar compaction, and stress conditions. Practically speaking, it may never be possible to develop a universal correlation that can be used nationally. However, it may be feasible for each highway agency to develop soil-specific relationships for their most common geomaterials.

The stresses imposed by the compaction equipment during construction process are sometimes the largest stress states that the compacted unbound geomaterials could experience during their service life. The particle interlock which is formed during the compaction process along with the lateral confining pressure forms a residual stress within the geomaterial layer that could affect the response of pavement layers during repeated traffic loading. Tutumluer (2013) contains a summary of research body regarding the consideration of initial stress states induced by compaction. D'Appolonia et al. (1969) and Duncan et al. (1991) have investigated the residual stresses as a result of compaction process. Due to such stresses locked in the geomaterial layers, the separation/loosening of materials could happen towards the final stages of compaction (Mooney and Reinhart, 2009).

Due to the complexity and nonlinearity of the behavior of unbound pavement geomaterials under repeated wheel loads, it is crucial to investigate the parameters affecting the resilient response of such materials (Lekarp et al, 2000). Nonlinear resilient modulus constitutive models have evolved during the past decades. A summary of different nonlinear resilient modulus constitutive models using various definitions of stress state to explain the nonlinear behavior of compacted geomaterials is available in Appendix D.

2.3 Impact of Moisture Variation, Density, Gradation and Plasticity

Significant efforts have been dedicated to study the impact of moisture variation in terms of moisture content or matric suction in the literature. Most of these studies were based on the concepts of unsaturated soil mechanics. Overviews of such evaluations are included in Richter (2006), Gupta et al. (2007), and Cary and Zapata (2010). On the other hand, the behaviors of geomaterials under saturated conditions were also investigated in a number of studies such as Wolfe and Butalia (2004), Hopkins et al (2004) and Ooi et al. (2006). In general, the studies regarding the impact of moisture variation on modulus of compacted geomaterials could be divided into the following categories:

- Unsaturated conditions
    - Models based on matric suction concepts
    - Models based on gravimetric/volumetric moisture content
    - Models based on degree of saturation
- Saturated conditions

Table 2.4 summarizes a number of research efforts in documenting the impact of moisture variations, in specific, and environmental changes, in general, on the modulus/stiffness of compacted earthworks and unbound geomaterials. Comprehensive syntheses of such studies are reported in Puppala (2008) and Tutumluer (2013).

Table 2.4 – Summary of Studies in Evaluation of Moisture Variation on Modulus

Reference	Objectives and Approach	Concluding Remarks	Approaches and Concepts
von Quintus and Killingsworth (1998)	Investigating the performance of cohesive and granular subgrade soils	Moisture content of cohesive subgrades increases after compaction of the layer which affects the resilient modulus of compacted layer	The data were extracted from long term pavement performance (LTPP) database
Maher et al. (2000)	Investigating the parameters affecting resilient modulus including moisture variation. Proposing statistical approached to predict resilient modulus from soil properties	Initiation and dissipation of pore pressure significantly impacts the strength of subgrade geomaterials. Statistical models were developed and calibrated to predict the resilient modulus of subgrade geomaterials at different moisture contents and stress states.	A number of subgrade materials were selected to perform the resilient modulus tests under different water contents to investigate their sensitivity to moisture variation and cyclic stress ratio
Yuan and Nazarian (2003)	Seismic non-destructive testing approaches were utilized to evaluate the variation of resilient modulus and moisture content	The variations in seismic modulus with moisture seems to be different for subgrade soils compared to base materials Moisture susceptibility of geomaterials are dependent of their fine content and soil type The effect of moisture content variation on design modulus should be considered	Drying and wetting cycles were applied to both fine- and coarse-grained materials Laboratory seismic tests were performed to evaluate the sensitivity to moisture variations
Kung et al. (2006)	Evaluating the variation of resilient modulus and plastic strain with post compaction moisture content	An increase in matric suction would result in decrease in resilient deformation and hence increase in resilient modulus. higher moisture content of subgrade materials as well as the lower matric suction results in decline of resilient modulus	Resilient modulus and plastic strain were investigated on two types of cohesive subgrade soils under different moisture content and suction conditions A prediction model using matric suction and deviatoric stress was proposed to estimate resilient modulus
Zaman and Khoury (2007)	Investigating the effect of post-compaction moisture content on resilient modulus	Resilient modulus exhibited a hysteric loop with changes of moisture content The initial moisture content affects the drying/wetting loop from both suction-based and moisture content-based models The increase in resilient modulus with increase in soil suction was dependent of the soil type	Resilient modulus tests performed during wetting and drying cycles for a number of subgrade soils both matric-suction and moisture content were evaluated during the experiments
Pacheco and Nazarian (2011)	Investigating the impact of compaction and testing moisture content and density on modulus of compacted geomaterials	Modulus of samples compacted at dry side of optimum showed higher values For higher compaction moisture contents and constant density, the modulus is lower compared to optimum conditions The modulus of compacted geomaterials is dependent of the difference between time of compaction and testing	A number of subgrade geomaterial samples were prepared under different moisture and density conditions in the laboratory The seismic modulus of compacted samples were evaluated during wetting and drying cycles Impact of relative density on modulus were also evaluated

Table 2.4, cont. – Summary of Studies in Evaluation of Moisture Variation on Modulus

Reference	Objectives and Approach	Concluding Remarks	Approaches and Concepts
Khoury et al. (2013)	Evaluate the variation in resilient modulus, unconfined compressive strength and modulus of elasticity with changes in moisture content after compaction	The resilient and elastic modulus as well as the unconfined compression strength of the compacted subgrade samples decreased when subjected to wetting and increased after drying The variation of materials strength and modulus is affected by soil type and stabilizing agent Modulus-moisture models were developed to be implemented in the design process Parameters for MEPDG environmental adjustment factor have been estimated for modulus and strength tests	Both untreated and stabilized soils were evaluated during resilient modulus, unconfined compression strength and modulus of elasticity
Nazarian et al. (2014)	Developing specifications for modulus-based construction quality control of soils and unbound aggregate geomaterials	The moisture content of geomaterials at the time of compaction affects the modulus-moisture correlations. The rate of modulus change with respect to moisture variation is not the same for different geomaterials The modulus-moisture correlations developed under laboratory conditions are different than those developed under field conditions Transfer functions are needed to correlate field and laboratory modulus-moisture correlations The variability of moisture measurement devices affects the modulus-moisture correlations-	A number of subgrade soils and unbound granular materials were evaluated under laboratory, small-scale and field conditions The materials were compacted at different moisture contents and then modulus-based tests were performed during drying and wetting cycles A number of modulus-moisture correlations were developed under laboratory, small-scale and field conditions
Li and Sun (2015)	Investigating the impact of moisture fluctuation on resilient modulus of compacted clay using simulation and laboratory experiments	The amplitude of moisture fluctuation has inverse correlation with resilient modulus of compacted clay. The reduction factor for moisture fluctuation was proposed to reflect its impact on long-term resilient modulus changes.	Wetting and drying cycles with respect to optimum and equilibrium moisture content
Abu-Farsakh et al. (2015)	Developing/modifying a resilient modulus constitutive model to incorporate the impact of moisture content for unsaturated subgrade geomaterials	Nonlinearity of the relationship between resilient modulus and matric suction. Due to the complexities associated with the existing models in the literature, a modified constitutive model was proposed to consider the nonlinearity of the modulus-suctions correlation by incorporating normalized moisture content and including the effect of soil type.	Four subgrade soil types were selected to perform the laboratory tests The soil-water characteristic curves (SWCC) were evaluated using axis-translation and chilled hygrometer

The lack of correlation between modulus of compacted geomaterials and field moisture content was discussed in Richter (2006). Such concern have addressed in some research efforts later in Von Quintus et al. (2010) and Pacheco and Nazarian (2011). The importance of the difference between the moisture content at the time of compaction and at the time of acceptance testing was addressed in Khoury and Zaman (2004) and most recently as a part of developing modulus-based construction quality approaches for unbound geomaterials and earthworks in Nazarian et al (2014).

The new and improved Mechanistic-Empirical Design Guide (MEPDG) recommends to consider the effects of the environmental factors on the resilient modulus using the following function:

$$MR = F_{env} \times MR_{opt} \tag{2.1}$$

where F_{env} is the environmental adjustment factor and MR_{opt} is the resilient modulus at optimum moisture content. The model was further calibrated using a series laboratory experiments under different moisture conditions in terms of degree of saturation as follows:

$$\log\left(\frac{MR}{MR_{opt}}\right) = a + \frac{b-a}{1+e^{\beta+K_m\left(S-S_{opt}\right)}} \tag{2.2}$$

where MR = modulus at any degree of saturation, S = current degree of saturation (decimal), MR_{opt} = modulus at OMC and MDD, S_{opt} = degree of saturation at OMC (decimal), a = minimum of $log(MR/MR_{opt})$, b = maximum of $\log(MR/MR_{opt})$, β = regression parameter = $\ln(-b/a)$, and K_m = regression parameter.

Many other studies have also focused on developing correlations to predict the resilient modulus of compacted geomaterials using the moisture/suction variables. A synthesis of these studies is included in Appendix D.

Variation of modulus of compacted geomaterials has been correlated to the density in a limited number of studies in the literature. Some of these efforts were aimed at investigating the impact of density combined with moisture content in terms of degree of saturation as well explained in Cary and Zapata (2011). However, in other studies (e.g., Mooney et al., 2010; Von Quintus et al., 2010; Pacheco and Nazarian, 2011), a direct correlation between modulus and density could not be established.

Nazarian et al. (2014) evaluated the impact of relative density on a set of well-controlled laboratory specimens. Again, not a strong correlation were established between density and modulus under laboratory conditions. Evaluation of such correlation were extended to field conditions where density values were estimated using an NDG device. Besides the uncertainties associated with estimation of density by NDG, a reasonable correlation was not found between any of the in-situ modulus and density values.

There are limited number of studies with regards to the impact of moisture content variation on the stiffness and ICMVs of compacted geomaterials during intelligent compaction process. A synthesis of these studies is included in Table 2.5.

Indirect modulus models predicts the resilient modulus of geomaterials using index properties such as gradation parameters and plasticity indices. Such prediction models have been evolved enormously during the past two decades. Puppala (2008), Richter (2006) and Tutumluer (2013) include reviews of the impact of gradation parameters and plasticity indices on modulus. Other attempts to develop these predictions models could be found in Santha (1994), Titus-Glover and Fernando (1995), Mohammad (1999), Amber (2002), Malla and Joshi (2007), Malla and Joshi (2008), Nazzal and Tatari (2013), Kim et al. (2014) and Gu et al. (2014).

Nazarian et al. (2014) and Navarro et al. (2012) summarized a synthesis of the prediction models for regression parameters of the resilient modulus constitutive models that utilize index properties of geomaterials. However, not such an effort to predict model parameters for stiffness of compacted geomaterials during application of intelligent compaction was found in the literature.

Table 2.5 – Summary of Studies Including Correlation between ICMVs and Density

Reference	Objectives and Approach	Concluding Remarks
White et al. (2007)	Evaluating the use of intelligent compaction for quality control and quality assurance of earthworks and soils Developing correlations between ICMVs and in-situ soil properties such as dry density during field evaluations and laboratory compaction of soil samples	The vibratory compaction method was deemed insufficient to establish moisture-density correlations under laboratory conditions ICMVs may not reflect the actual soil compaction in terms of density for unbound granular soils Moisture-density correlations were affected by impact energy for cohesive soils Not a clear correlation was found between different ICMVs and the in-situ dry unit weight of the compacted geomaterials
White et al. (2008)	ICMVs and spot tests were performed on test sections to establish possible correlation	At project scale, the ICMVs and spot test could be correlated using average values. However, such correlations revealed lower correlation coefficient for density tests compared to modulus tests
White and Thompson (2008)	Two types of ICMVs were collected on test sections to establish their correlations with in-situ spot tests	Correlations between ICMVs and in-situ dry density were established as a function of soil type Overall, not a significant correlation was observed between ICMVs and dry unit weights
Mooney et al. (2010)	Review and evaluation of different intelligent soil compaction systems Evaluating the correlations between in-situ spot tests and ICMVs Recommending specifications for roller-integrated continuous compaction control	A common quality control/quality assurance approach utilize ICMVs to identify weak areas to further perform spot tests such as density Areas with low ICMV were not necessarily representing the areas with low density The measured ICMVs are more sensitive to the compaction process compared to density values
Cao et al. (2010)	The theoretical analysis consisted of developing a dynamic model of roller vibration and its impact on degree of compaction of the soil A number of clayey soils were selected to perform the experimental study A test section was selected to perform the vibratory tests on subgrade geomaterials	A linear correlation found between degree of compaction of subgrade layer and acceleration of vibratory drum from theoretical analyses Results of experimental evaluations showed that there is a correlation between vibration acceleration harmonic ratio and degree of compaction Kinetic parameters of the vibratory roller were reasonably correlated to the variation of density of compacted layer
Xu et al. (2012)	A systematic approach was developed to analyze and manage data from IC operations for HMAs as well the unbound geomaterial layers	The linear correlation between ICMVs and moduli of in-situ spot tests were more consistent compared to density
Siddagangaiah et al. (2014)	To develop roller-integrated quality management approaches for earthworks and unbound granular materials in Texas A number of field evaluations along with a series of laboratory test were performed under different moisture and density conditions ICMVs were compared to the results of modulus-based spot tests as well as the in-situ density and moisture test results	Some correlations were observed between ICMVs and in-situ modulus results from LWD and DCP but not a clear correlation was found between ICMVs and density values from NDG

2.4 Estimating Modulus for Quality Assurance

2.4.1 Modulus and Deflection-Based Devices

The most common portable modulus-based devices available in the market are Dynamic Cone Penetrometer (DCP), Electro-Mechanical Stiffness Device (Geogauge), Lightweight Deflectometer (LWD), Falling Weight Deflectometer (FWD), Plate Bearing Test, and Portable Seismic Property Analyzer (PSPA). Table 2.6 compares the costs, speed and easiness of use of the more portable devices. A detailed compilation of the literature review for each device is included in Nazarian et al. (2014). A summary of each device's advantages and limitations are included in Table 2.7. Many DOTs have moved away from the Plate Bearing Test because of the time necessary to perform the test and the popularity of FWD. On the other hand, the logistics of the statewide implementation of the FWD may be problematic. For this reason, the use of faster and more portable devices is on the rise. LWDs work on the same principles at a small fraction of the FWD cost.

Table 2.6 - Comparison of Tools for Measuring Modulus

Device	DCP	Geogauge	LWD	PLT	PSPA
Parameter Reported	Penetration Rate (in./blow)	Modulus	Deflection/ Modulus	Modulus of Subgrade Reaction	Modulus
ASTM Standard	D-6951	D-6758	E-2583	D-1196	None
Expertise Needed	Minimal	Moderate	Moderate	Advanced	Moderate
User-friendliness	Easy	Easy	Easy	Difficult	Easy
Speed	10 minutes	2 minutes	2 minutes	2 hours	30 seconds
Initial Costs	$3,000 (basic) $40,000 (automated)	$6,000	$15,000	$15,000	$20,000

Dynamic Cone Penetrometer (DCP). The Dynamic Cone Penetrometer (DCP) test, shown in Figure 2.1, involves driving a cone shaped probe into the soil using a dynamic load and measuring the advancement of the device for each applied blow or interval of blows. The depth of penetration is a directly impacted by the drop height of the weight, cone size, and cone shape. Also, the resistance to penetration is dependent on the strength of the material. The strength, in turn, is dependent on density, moisture, and material type of the layer evaluated. Detailed documentation of the history and applications of the DCP is provided by Amini (2003). They also summarized relationships of DCP penetration rate with CBR, resilient modulus and strength. Chen et al. (2001) indicated that the DCP was useful for determining the layer thickness, and could be a useful tool when the FWD backcalculated moduli were not accurate. Correlations of measurements with the DCP to other devices, such as the PFWD and FWD were studied by Siekmeier et al. (2000), Abu-Farsakh et al. (2005) and Von Quintus et al. (2009).

Geogauge. Geogauge, shown in Figure 2.2, is a hand-portable gauge that provides a means of estimating lift stiffness and soil modulus for compaction process control. The Geogauge measures the impedance at the surface of an unbound layer by imposing a known stress to the surface of a layer and measuring the resulting surface velocity as a function of time at 25 steady state frequencies between 100 and 196 Hz. Alshibli et al. (2005) assessed the potential use of the Geogauge as a QC/QA device for testing subgrades, base courses, and compacted soil layers and indicated it can be used to calculate the modulus/stiffness characteristics of compacted layers; however, problems with its field use have been reported in several studies, including Simmons (2000), Miller and Mallick (2003), Ellis and Bloomquist (2003) and Nazarian et al. (2014), particularly with the seating of the Geogauge at the soil-foot interface and the disturbance in the results due to vibration caused by nearby vehicles.

Table 2.7 - Advantages and Disadvantages of Modulus-Based Devices (Nazarian et al., 2014)

Device	Description	Advantages	Disadvantages
Dynamic Cone Penetrometer (DCP)	DCP test involves driving a cone shaped probe into a geomaterial and measuring advancement of the device for several intervals of hammer drops. The rate of penetration of the probe is used to obtain layer thicknesses and moduli.	Adapted by selected agencies in QA operations. Does not require extensive support software for evaluating test results. Can test multi-layers	Takes time to perform a test. Not strictly a stiffness/ modulus measuring device as the penetration rate has to go through two levels of empirical correlations to estimate modulus
Electro-Mechanical Stiffness Device (Geogauge)	Geogauge provides stiffness property of a geomaterial by measuring applied force and resulting displacement induced by a small harmonic oscillator operating over a frequency of 100 to 200 Hz.	Acceptable success rate in identifying areas with different physical conditions or anomalies. Simple training. Provides a reasonable estimate of laboratory measured moduli with proper calibration.	Intimate contact between Geogauge and soil is difficult to achieve without through site preparation. Moduli do not represent stress levels that occur under truck loading. Underlying materials can influence results especially for relatively thin unbound layers.
Portable Falling Weight Deflectometer (PFWD) **aka Light Weight Deflectometer (LWD)**	PFWD operates in a similar fashion to the FWD with one to three sensors. The FWD analysis method is applicable to PFWD as long as three sensors are used. PFWD with one sensor is often used with a so-called "forward-calculation" to estimate stiffness of the layer.	State of stress is closer to vehicular stresses than any other device. Pavement community is familiar with concept of deflection-based testing.	Unable to consistently identify areas with anomalies. Underlying materials can influence results especially for relatively thin unbound layers. Any error in thickness of the layer being tested can result in large errors and variability in modulus.
Portable Seismic Property Analyzer (PSPA)	PSPA consists of two accelerometers and a source packaged into a hand-portable system. PSPA measures the linear elastic average modulus of a layer based on generating and detecting stress waves.	Measures layer-specific modulus independent of thickness of layer. No backcalculation necessary. High success rate in identifying areas with different physical conditions or anomalies. Results can be calibrated to specific material being tested prior to construction when M-D relationship is measured in lab	Need to calibrate the test results to the material and site conditions under evaluation. Lowest repeatability, with a high standard deviation due to capability to detect anisotropic conditions.

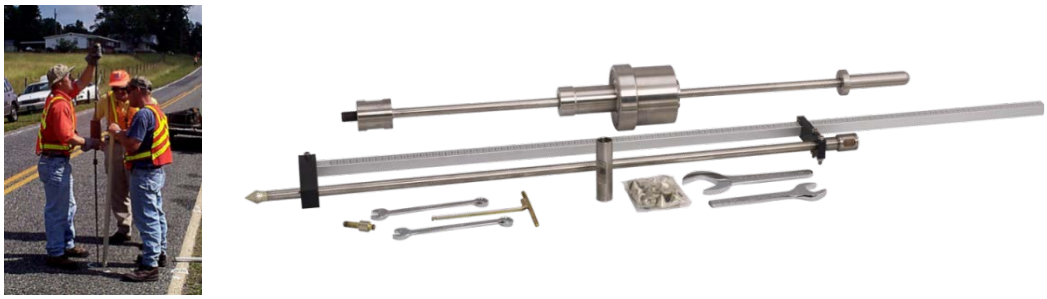

Figure 2.1 – Dynamic Cone Penetrometer (DCP).

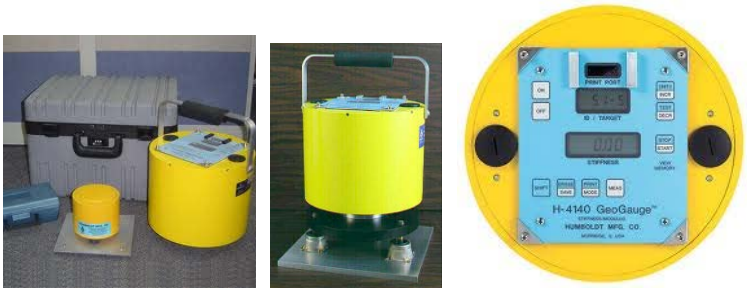

Figure 2.2 – Geogauge.

Light Weight Deflectometer (LWD). The Light Weight Deflectometer (LWD), shown in Figure 2.3, is a portable Falling Weight Deflectometer (PFWD) that has been developed as an alternative in-situ testing device to the plate load test. Generally, the LWD consists of a loading device that produces a defined load pulse, a loading plate, one center displacement sensor (and up to two optional additional sensors) to measure the center deflection or a deflection bowl. Similar to FWD, the LWD determines the stiffness of pavement system by measuring the material's response under the impact of a load with a known magnitude and dropped from a known height. Its potential use of the LWD as a QC/QA device for testing subgrades, base courses, and compacted soil layers has been assessed by Alshibli et al. (2005) and Fleming et al. (2007). Both studies concluded that the device was a useful and versatile field quality control and pavement investigation tool if an understanding of the device issues was considered by the data users. Yet, Petersen et al. (2007) found that the equivalent predicted moduli from laboratory resilient modulus tests did not correlate with the in-situ stiffness moduli. Vennapusa and White (2009) evaluated key features of 8 commonly used LWD devices and found that LWD moduli are affected by the size of loading plate, plate contact stresses, type and location of deflection sensor; plate rigidity, loading rate, and buffer stiffness. They provided a comparative shown in Table 2.8. Tirado et al. (2015) using finite element modeling showed the variation of results are related to the design of the devices. Vennapusa and White (2009) also compiled extensive relationships between the different LWD devices and other spot test devices.

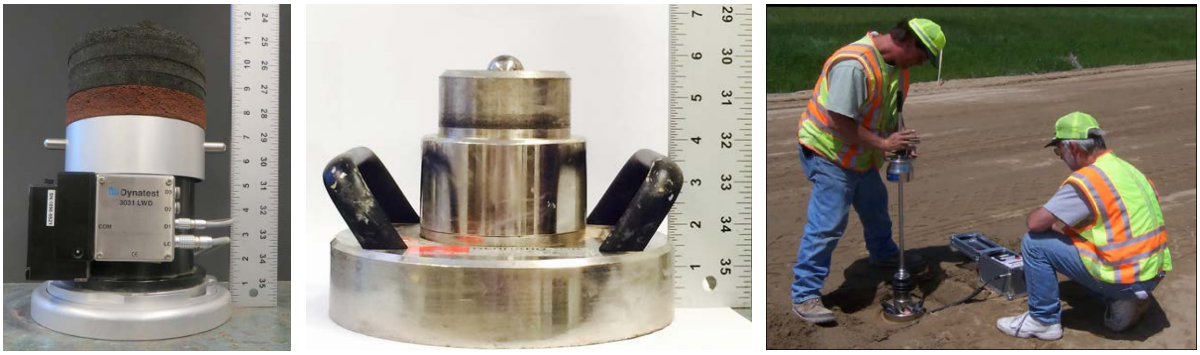

Figure 2.3 – Light-Weight Deflectometer (LWD).

Table 2.8 - Comparison of Different LWD Devices (Vennapusa and White 2009)

Device	Plate Diameter (mm)	Plate Thickness (mm)	Falling Weight (kg)	Maximum Applied Force (kN)	Load Cell	Total Load Pulse (ms)	Type of Buffers	Deflection Transducer		
								Type	Location	Measuring Range (mm)
Zorn	100, 150, 200, 300	124, 45, 28, 20	10, 15	7	No	18±2	Steel Spring	Acceler-ometer	Plate	0.2-30 (±0.02)
Keros	150, 200, 300	20	10, 15, 20	15	Yes	15-30	Rubber (Conical shape)	Velocity	Ground	0-2.2 (±0.002)
Dynatest 3031	100, 150, 200, 300	20	10, 15, 20	15	Yes	15-30	Rubber (Flat)	Velocity	Ground	0-2.2 (±0.002)
Prima	100, 200, 300	20	10, 20	15	Yes	15-20	Rubber (Conical shape)	Velocity	Ground	0-2.2 (±0.002)
Loadman	110, 132, 200, 300	-	10	18	Yes	25-30	Rubber	Acceler-ometer	Plate	-
ELE	300	-	10		Yes			Velocity	Plate	-
TFT	200, 300	-	10	8.5	Yes	15-25	Rubber	Velocity	Ground	-
CSM	200, 300	-	10	8.8	Yes	15-20	Urethane	Velocity	Plate	-

Portable Seismic Property Analyzer. The Portable Seismic Property Analyzer (PSPA) uses the Spectral-Analysis-of-Surface-Waves (SASW) method which is based upon measuring surface waves propagating in layered elastic media. The SASW test is a non-intrusive seismic test method that relies on the measurement of Rayleigh type surface waves. The key point in the SASW method is the measurement of the dispersive nature of the surface waves, which are used to determine the shear wave velocity of the pavement, the base, and the subgrade. The generation and detection of surface waves are controlled by an impact source and two receivers (or accelerometers) placed on the pavement surface, as shown in Figure 2.4. The two vibration transducers are located at known distances from the source. Typically, one of the distances is kept equal to two times the shorter distance. Nazarian et al. (2002 and 2004) developed several field protocols and test equipment that combine the results from laboratory and field tests with those used for quality control during construction based on seismic technology. The study focused on repeatability, reproducibility of the methods, means of relating the measured parameters to the design moduli, and relating the parameters to performance of the pavement. Relationship between the resilient modulus and seismic modulus was further documented in Williams et al. (2002) and Nazarian et al. (2003). Von Quintus et al. (2009) found the device that had the highest success rate in identifying areas with different physical conditions or anomalies. The potential and effectiveness as a combined laboratory and field quality management technique has been evaluated Toohey et al. (2010), Schuettpelz et al. (2010) and Celaya et al. (2010).

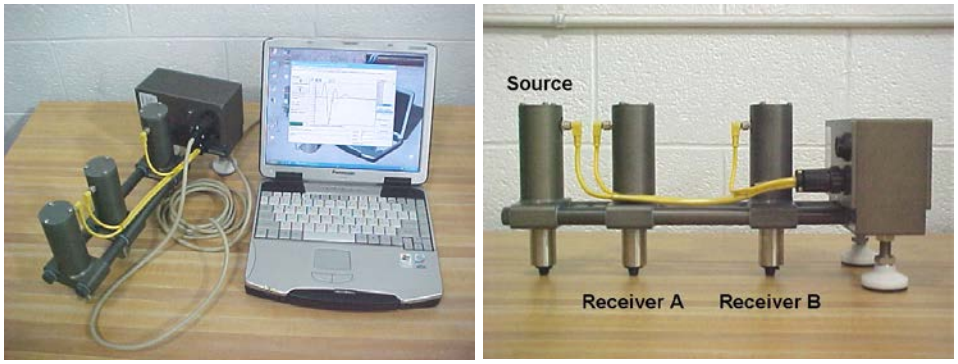

Figure 2.4 – Portable Seismic Property Analyzer (PSPA).

Falling Weight Deflectometer (FWD). The falling weight deflectometer (FWD) has been employed by state highway agencies (SHAs) for over three decades now. It applies an impulse load, through a circular plate, to the pavement surface from a specific height. A load cell measures the actual impulse load for further estimation of pavement layers' moduli. A number of deflection sensors measure the surface deflections at different offsets from the loading plate. The applied load and the measured deflections will be stored in a data acquisition system for further analyses. The observed deflection basin (see Figure 2.5) is used to back-calculate the elastic modulus of each pavement layer considering the layer thicknesses. FWD is categorized as a NDT method and furthermore it is cost effective and repeatable. However, similar to the other test methods described in this section, FWD is a spot test and the results are not representing the structural conditions of the complete section. FWD has been evaluated in many investigations including evaluation of structural performance of in-service pavements, quality control of geomaterial pavement layer during construction, design of overlays and estimating the level of pavement distress and deterioration. Schmalzer (2006), as a part of long-term pavement performance (LTPP) program, provided the background information and field operation guidelines for the use of FWD on LTPP test sections. This guideline provided the test procedure as well as the equipment calibration and test locations. Alavi et al. (2008) synthesized the usage of FWD among state highway agencies and department of transportation. Based on the results of the survey from forty-five SHAs, most of them were using their own specifications rather than the LTPP guidelines. The synthesis also reviewed different FWD devices available in the market. One of the many applications of FWD data collection reviewed in this NCHRP synthesis was project acceptance and evaluation which particularly includes the assessment of geomaterial pavement layers during construction phases. Majidzadeh et al. (2014) evaluated the risk and cost of different devices, including FWD, during subgrade QC/QA program. They concluded that the cost of quality management process using NDT devices, such as FWD and LWD, is about half the cost of conventional methods. Petersen and Peterson (2008) investigated the use of FWD during a design-build project in the state of Washington. They concluded that using FWD to analyze the existing pavement conditions would lead to a more concise pavement design rather than a conservative design using only cores and bore holes data. Kim and Park (2002) evaluated the use of multi-load level FWD deflections for assessment of layer conditions and performance predictions. They developed a dynamic finite element program and a forward model to estimate the remaining life of pavement including rutting performance and fatigue cracking.

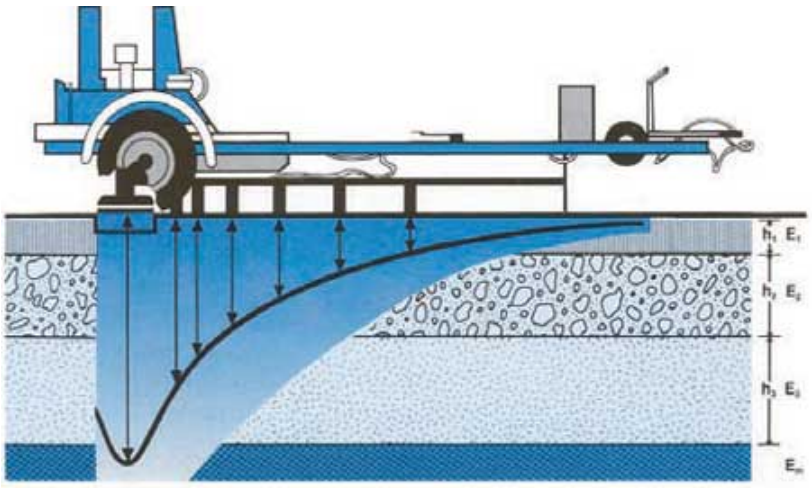

Figure 2.5 – Falling Weight Deflectometer (FWD) and deflection basin (image courtesy of CLRP).

Estimation of Mechanical Properties Using Modulus-Based NDT Devices. A table with models developed for determining mechanical properties as determined by each of the reviewed modulus-based NDT devices is provided in Appendix D.

Evaluation of Modulus-Based NDT Devices

Von Quintus et al. (2009) conducted a utility analysis under NCHRP Project 10-65 to objectively evaluate NDT technologies, among them modulus-based NDT devices. Based on this utility analysis, Nazarian et al. (2014) under NCHRP Project 10-84 evaluated different modulus-based devices considering different characteristics, among them their

- ***applicability*** to develop a specification that relates field quality management to the structural pavement design. This includes
  - the ability to harmonize pavement design parameters and field measurements. Ideally the selected device should provide a stiffness or modulus measurement that is compatible or that can be readily related to the lab modulus.
  - and to make layer specific measurements.
- ***suitability*** for field measurements, that include
  - the ability to detect construction defects and sensitiveness to poor quality due to segregation and under-compaction.
  - repeatability, precision and sensitivity of device. The repeatability, defined as the variation in the measured parameter when the measurements are made at a given point without removing the device, is an indication of the stability of the hardware and robustness of the software used in each device. Precision is defined as the variability in the measured parameter when the device is moved over a small area. It is not only controlled by the repeatability but also by the variability in the material tested, the uniformity of coupling the device to the compacted geomaterials and the test boundary conditions. The sensitivity of the device to the way the modulus of the layer is obtained.
- ***practicality***, which include the applicability of the device to different types of compacted geomaterials, the availability of commercial equipment, availability of ASTM or AASHTO standards, reliability and ruggedness, user friendliness, expertise needed for data collection and interpretation, and the initial and operational costs.

The PSPA was found to be most appropriate in terms of applicability to the goals of that study since it makes layer-specific and direct measurement of the modulus while the DCP and LWD ranked the highest in terms of practicality. Nazarian et al. (2014) at the end recommended the LWD as the most pragmatic device for quality management of the earthwork given their availability, impact on the resources of the DOTs and the data analysis. They showed that achieving quality compaction (defined as achieving adequate layer modulus) is weakly associated with achieving density. With regards to the application of LWD in a modulus-based quality management approach, Nazarian et al. (2014) found that different LWDs estimate different moduli at the same test spot. As such, the specification should be clear which LWD should be used. It is also important to consider the properties of the underlying layers in setting the LWD target values, especially when the layer of interest is overlying a layer with a significantly different modulus. On the other hand, they concluded that the DCP is simple to use and inexpensive. However, since DCP strictly measures the strength not the modulus of the layer, setting its target should be done with care. The DCP results were not very sensitive to moisture content and material changes.

2.5 Moisture and Density-Based Devices

Figure 2.6 depicts images of these devices. The nuclear density gauge (NDG) is still the most widely-used device for measuring moisture and density. The field of measuring moisture and density with non-nuclear devices is evolving quite rapidly. Improvements to software and hardware are also being implemented on a number of existing devices. These devices include Soil Density Gauge (SDG, also known as SQI), Electrical Density Gauge (EDG), M+DI device and Speedy Moisture Tester (SMT), along with a number of less known devices.

Electrical Density Gauge (EDG)

Soil Density Gauge (SDG)

Moisture+Density Indicator (M+DI)

Speedy Moisture Tester

Roadbed Water Content Meter (DOT600)

Figure 2.6 – Non-nuclear moisture and density measurement devices.

A number of less used and known devices are also available (Sebesta et al., 2012). Of course the nuclear density gauge is still widely used and is a viable option. Due to the fact that extensive information is available to the community, its performance and limitations are not discussed here. These devices (except NDG) have not been used as extensively as the modulus-based device. The field of measuring moisture and density with non-nuclear devices is evolving quite rapidly. Improvements of software and hardware are also being carried out on number devices. Advantages and disadvantages of the devices that estimate the moisture content and/or density of the compacted geomaterials are included in Table 2.9.

Electrical Density Gauge (EDG). The Electrical Density Gauge (EDG) is a non-nuclear alternative for determining the moisture and density of compacted soils used in road beds and foundations. The EDG is a portable, battery-powered instrument capable of being used anywhere without the concerns and regulations associated with nuclear safety. Von Quintus et al. (2009) reported that the EDG consistently provided coefficients of variation of measurements of less than 1%, though they recommended that this device and technology be evaluated in more detail and that studies be initiated to improve its accuracy.

Moisture+Density Indicator (M+DI). The Moisture+Density Indicator (M+DI) uses Time Domain Reflectometry (TDR) to measure the travel time of an electromagnetic step pulse produced by the TDR pulse generator through four soil spikes in the ground. M+DI readings have been found not comparable to the NDG readings, mainly attributed to the TDR's soil constant calibration procedure. The dry densities recorded by the M+DI were typically less than those from the nuclear gauges (Khalid et al., 2005; Bennert and Maher, 2008).

Table 2.9 - Advantages and Disadvantages of Moisture/Density Devices

Device	Description	Advantages	Disadvantages
Electrical Density Gauge (EDG)	EDG is a portable, battery-powered instrument that uses a radio signal between four spikes to measure capacitance, resistance, and impedance of the soil. These parameters are used to determine the density and water content of an unbound layer.	Does not require a licensed technician. Repeatable with standard deviation in density measurements less than 1 pcf.	The necessity to run a series of lab and in situ tests for correlation purposes. Poor success rate in identifying areas with anomalies.
Moisture + Density Indicator (M+DI)	**M+DI** utilizes time domain reflectometry (TDR) to measure voltage time histories of an electromagnetic step pulse at four soil spikes in the ground. The voltage signal is analyzed to determine the water content and density of an unbound layer.	Requires no certified operators or safety training or instrument calibration.	Prior calibration of the device for each specific soil using laboratory compaction molds is required. May not be appropriate for aggregates or earth-rock mixtures that either interfere with penetration of the probes or have numerous and large void spaces. Time required to conduct a test may be of concern.
Soil Density Gauge (SDG)	SDG produces a radio-frequency electromagnetic field using a transmitter and receiver to estimate the in-place density, and moisture content of unbound pavement materials using electrical impedance spectroscopy (EIS).	Requires no certified operators or safety training or instrument calibration. Unit provides GPS logging for database management and offers fast, reliable and repeatable readings in real time.	The technology is new and limited research has been performed using this device.
Speedy Moisture Tester (SMT)	SMT measures the moisture content of geomaterial by measuring the rise in gas pressure within an air-tight vessel containing a mix of soil sample and a calcium carbide reagent.	Portable and requires no external power source. Can measure many materials over a wide moisture content range.	Not suitable for all geomaterials, especially highly plastic clay soils The reagent used is considered as a hazardous product Compacted geomaterials have to be excavated before they can be tested.
Road-Bed Water Content Meter (DOT 600)	DOT600 estimates the volumetric water content of soil samples by measuring the dielectric permittivity of the material.	Sample bulk density and compaction force are monitored. The system is completely portable.	The technology is new and limited research has been performed using this device Prior calibration of the device for each specific soil is needed Compacted geomaterials have to be excavated before they can be tested

Soil Density Gauge (SDG). The SDG builds on the technology of the Pavement Quality Indicator (PQI). The SDG uses electrical impedance spectroscopy (EIS) for determining the in-place density, and moisture content of unbound pavement materials. The SDG generates and monitors radio frequency range electromagnetic field using a transmitter and receiver. Wacharanon et al. (2008) evaluated and compared this device to other density devices on three types of pavement materials (sand embankment, soil-aggregate subbase, and crushed rock base), and recommended the device for use in the pavement and subgrade property evaluation during construction phase. Pluta and Hewitt (2009) found wet densities differed by 19% when compared to the NDG's wet densities.

Speedy Moisture Tester. Speedy moisture tester (a.k.a. speedy calcium carbide moisture tester) is a portable system for measuring moisture content of soils typically used for roads and foundations. Dai and Kremer (2006) and Oman (2004) compared the results from the Speedy Moisture Meter and traditional oven burner methods. They reported a strong relationship between the moisture contents from the two methods.

Evaluation of Moisture and Density-Based Devices. A comprehensive evaluation of these devices is difficult since they have not been used as extensively as the modulus-based devices. Berney et al. (2011) conducted a comprehensive evaluation of many of these devices. Nazarian et al. (2014) evaluated these devices, and the results of the utility analysis of moisture devices are summarized in Table 2.10. Nazarian et al. (2014) recommended the use of a microwave oven, or a well-calibrated nuclear density gauge for moisture content determination.

Table 2.10 - Comparison of Tools for Measuring Moisture Density

Device	EDG	M+DI*	SDG/SQI	Speedy Moisture Tester
Parameter Reported	Density & Moisture Content	Density & Moisture Content	Density & Moisture Content	Moisture Content
ASTM Standard	None	D 6780	None	D 4944
Expertise Needed	Moderate	Moderate	Moderate	Minimal
User-friendliness	Difficult	Difficult	Easy	Easy
Speed	20 minutes	20 minutes	1 minute	5 minutes
Initial and Operational Costs	$8,000	$6,000	$10,000	$2,000

* sale of M+DI has been discontinued.

2.6 Field Quality Control and Acceptance

Field quality control consists of conducting modulus-based tests with an appropriate tool at a number of points for a specified lot. A moisture measuring device should be used concurrent with the modulus measuring device to obtain the in-place moisture content. The measured moisture content can be used to adjust the measured modulus to a common moisture content (say optimum moisture content). The field and laboratory moduli at the same moisture content and density may be different due to differences in compaction processes. A fair and equitable acceptance process requires appropriate tolerances based on the uncertainties in establishing the target modulus and the measuring devices.

The purpose of a Quality Assurance (QA) plan is to measure important quality characteristics which impact production at a time when a corrective action can be taken to prevent nonconforming material from being accepted. State and federal departments of transportation understand the importance of quality assurance since achieving a high quality pavement is their primary objective. Over the past several years, agencies have been working with the construction industry to implement quality control/quality assurance specifications to improve the quality of pavement construction. This effort is a result of the understanding that failure to conform to either material or construction specifications can result in the premature failure of highway components. Therefore, construction QA programs are intended to ensure that the quality of the materials and construction incorporated in the highway products is satisfactory.

In the past, state and federal departments of transportation used the average of absolute deviations from a target value as the quality measure to control the process, but using only the average has a disadvantage because it does not provide a measure of variability, and it is now recognized that variability is often an important predictor of pavement performance. To overcome the problems associated with using the only mean for QA, additional quality measures have been developed and implemented by state highway agencies, including the percent defective (PD), the Percent within Limits (PWL), the Conformal Index (CI), the average absolute deviation (AAD) and the moving average (Parker et al., 1993; Akkinepally and Attoh-Okine, 2006)

In a synthesis published in 2005 by the National Highway Research Program (NCHRP), it is shown that in the U.S the most common quality measure used for acceptance of soils and embankments is an individual value followed by the range, average, and PWL (Hughes, 2005). The most common quality measure for acceptance of the aggregate base and subbase is an individual value, followed by PWL, average, and the range (Hughes, 2005). The most effective statistical quality measure can translate into economic savings for the transportation agencies, because it can reduce the inspection and lessen the probability of a poor or defective product being accepted.

Table 2.11 shows a summary and the main advantages and disadvantages of the different specification compliance measures commonly used in the pavement industry. There are other quality assurance methods which have been developed but they have never been used for QA of flexible pavements.

Table 2.11 - Advantages and Disadvantages for Different Specification Compliance Measures

Quality Measure	Equation	Advantages	Disadvantages
Percent Within Limit (PWL)	$Q_L = \frac{\bar{x} - LSL}{s}$ $Q_U = \frac{USL - \bar{x}}{s}$ where: Q_L = quality index for the lower specification limit. Q_U = quality index for the upper specification limit. LSL = lower specification limit. USL = upper specification limit. $\bar{x}$ = the sample mean for the lot. s = sample standard deviation for the lot.	• Using the PWL combines two important statistical measures, mean and standard deviation, in one parameter. • PWL as a quality measure is susceptible to variability. • The method offers control over production for the contractor. • PWL is applied; a varying sample size is accounted for in the estimate of quality.	• The method does not distinguish between uniformity around a desirable target and uniformity around the threshold of unacceptable properties. • PWL does not correlate strongly with performance • One of the problems of PWL is that the number of samples can be infinite. In this case, it is not clear what is the defect and what are the consequences from this defect.
Percent Defective (PD)	$PWL = 100\text{-}PD$ where: PWL = Percent within limit PD = Percent defective.	• Using the PD as a quality measure in two sided specifications, it can determine the total PD because the PD below the lower specification limit can simply be added to the PD above the upper specification limit.	• Using the PD quality measure without combined with PWL; it does not have same efficiency combining both methods.
Average Absolute Deviation (AAD)	$AAD = \frac{\sum x_i - T}{n}$ where: x_i = individual test results. T = target value. n = number of tests per lot.	• This quality measure is currently structured to allow greater deviations from the target for smaller sample sizes. • This statistically method maintains consistent levels of control for both central tendency and variability of absolute deviations from the job mix formula (JMF).	• The primary drawback is that they can only be used when there is a target value. They cannot be used when there is only one specification limit. • Variability of the material in the lot may not be adequately measured. Specifically, very different sets of test results can give identical AAD values.
Conformal Index (CI)	$CI = \frac{\sqrt{\sum (x_i - T)^2}}{n}$ where: x_i = individual test results. T = target value. n = number of tests per lot.	• The attractiveness of this statistic method is that it focuses on the target value and it is this target value that is defining the quality level. • This quality measure may be used for one sided or two sided specification acceptance. • This approach also provides for the use of percent defective and percent within limits as quality indicators.	• The CI discourages mid-lot process adjustments by not allowing positive and negative deviations from the target to cancel out one another. • It is not recommended for a one sided specification and of potentially having the same CI value for greatly different sample results.
Moving Average (MA)	$\chi = \mu + \varepsilon\iota + \sum_{i=1}^{q} \theta i \varepsilon\iota - i$ where: μ = mean of the series. q = order of the MA model $\mathcal{E}t$ = white noise error terms. θi = parameters of the model.	• The moving average has been mostly applied for process control purposes, and is mostly useful when continuous processes are involved. • The use of the moving average provides a smoothing effect compared to plotting individual test results.	• The use of the moving average is not consistent with the use of lot by lot acceptance. Since each individual test result appears in multiple moving averages, it is difficult to determine when or where a lot begins or ends.

3 INTELLIGENT COMPACTION SYSTEMS

3.1 Data Collection in Intelligent Compaction

The advantages of intelligent compaction have been investigated by several groups (e.g., Anderegg and Kaufman, 2004; White et al., 2006; Hossian et al., 2006; Peterson et al., 2006; Mooney et al., 2010; Gallivan et al., 2011 and Chang et al., 2012). The advantages are summarized as listed below:

a) Improved quality of compaction/uniformity
b) Reduced over/under compaction costs
c) Reduced time of compaction
d) Identification of soft or weak spots
e) Increased lifetime of the roller
f) Integration of design, construction and performance

The challenges in implementing the intelligent compaction for quality control and assurance are primarily evaluating the influence of machine operating conditions and underlying heterogeneity on the roller measurement values.

The compaction of a material using an IC roller is controlled with the continuous feedback of the IC measurement values (ICMVs). The intelligent compactors include sensors to measure vibration characteristics or rolling resistance of the drum, onboard electronics to record and process sensor output and record the compaction level, and optional feedback system controls to adjust the compaction effort according to the measured compaction level. The onboard GPS system records the geospatial information. The data measurements and location details are stored in a data storage system (Peterson et al., 2006, Mooney and Adam, 2007). The data storage system and measurement value vary with the type and make of the IC roller. The descriptions of roller measurement values are discussed in detail in Mooney et al. (2010). The different data measurement units used for compaction control are listed in Table 3.1.

Studies have been carried out to evaluate the ICMVs for the compaction quality management of different pavement layers and embankment soils. Research has also been carried out to correlate the roller measurement values with the in situ point test measurements. Table 3.2 summarizes various studies and their significant findings.

3.2 IC Technology as Quality Control (QC) and Quality Acceptance (QA) Tools

Different manufacturers recommend different IC measurement values. Irrespective of the ICMV used, the vertical, longitudinal and transverse heterogeneity of the underlying soil strata is the most important factor influencing the ICMVs and the modulus-based spot test results. The correlations developed with the ICMVs and the spot tests change whenever there is a change in the underlying condition. The heterogeneity stems from the change in material type, compaction effort and moisture contents at the time of compaction and testing (Nazarian et al., 2011). The depth of influence for a regular (11 to 15 ton) roller is reported to vary between 2.5 ft to 4 ft (Mooney et al., 2010). Hence, the ICMVs measured will reflect the composite stiffness of the geomaterials up to a depth of 2.5 ft to 4 ft. However, the spot tests typically reflect the material property up to a depth of 0.5 ft to 1 ft (Mooney et al., 2010). Fathi et al. (2018) evaluated the depth of influence of a regular-sized IC-roller (17 ton) through an extensive parametric study using a (3D) finite element (FE) model. They found that the depth of influence of the vibratory roller is about 2.5 and 2.2 times greater than the depth of influence of LWD for single and two-layer geosystems, respectively.

Table 3.3 summarizes the findings from selected studies in use of the IC in quality control and acceptance testing. Whenever there is a high variability in the underlying ground strata, the use of IC for quality control and acceptance might be challenging. Research studies have recommended construction of individual test strips whenever the variability in the underlying ground conditions is high.

Table 3.1 - Commercially Available Roller Measurement Values (Mooney et al., 2010)

Measurement Value	Manufacturers	Parameters Used	Relations Used
Compaction Meter Value (CMV)	Dynapac, Caterpillar, Hamm, Volvo,	Ratio of vertical drum acceleration amplitudes at fundamental vibration frequency and its first harmonic	$CMV = c\frac{A_{2\Omega}}{A_{\Omega}}$ where, c is constant around 300 $A_{2\Omega}$ is the amplitude of the second harmonic A_{Ω} is the amplitude of the fundamental frequency
Compaction Control Value (CCV)	Sakai	Algebraic relationship of multiple vertical drum vibration amplitudes, including fundamental frequency, and multiple harmonics and sub harmonics	$CCV=[\frac{A_1+A_3+A_4+A_5+A_6}{A_1+A_2}]$ where, A_i are the amplitudes at the excitation frequencies
Stiffness, k_s	Ammann	Vertical drum displacement, drum-soil contact force	$k_s = \Omega^2\left[m_d + \frac{m_o e_o \cos(\emptyset)}{z_d}\right]$ where, m_d is the drum mass m_0e_0 is the eccentric mass moment ϕ is the phase angle z_d is the drum displacement Ω is the frequency
Vibration Modulus, E_{vib}	Bomag	Vertical drum displacement, drum-soil contact force	$z_d = \frac{2\times(1-v^2)}{\pi\times E_{vib}}\times\frac{F_s}{L}\times\left(1.8864 + ln\frac{L}{b}\right)$ where, F_s is the drum soil interaction force L is the drum length b is the contact width ν is the Poisson ratio z_d is the drum displacement
Machine Drive Power (MDP)	Caterpillar	Difference of gross power and the power associated with sloping grade and machine loss	$MDP = P_g - WV\left[sin\theta + \frac{a}{g}\right] - (mV + b)$ where, P_g is the gross power W is the roller weight a is the acceleration g is the acceleration due to gravity θ is the slope angle V is the roller velocity m and b are internal loss coefficients

Table 3.2 - Summary of Quality Control and In Situ Correlations

Reference	Objective and scope	Key findings/comments
White et al., 2005	Evaluated the utilization of intelligent rollers in real time compaction monitoring. A pilot field study was carried out in Illinois on a cohesive glacial till soil. Spot measurements of density, moisture content, DCP and Clegg impact hammer values were correlated to roller measurement values.	The variation in the machine drive power was observed to be the result of inherent soil and moisture variations in the compacted layer. The compaction effort was found to be significant only up to a depth of 40 cm. Consideration of moisture content in the regression analysis resulted in a better understanding of measurements and correlation between them.
White et al., 2006	Evaluated the relationship between machine drive power and measures of soil compaction at a test section in Peoria, Illinois. Two moisture contents were adopted. Vibratory pad foot roller was used. Well-graded silty sand was evaluated with nuclear gauge, moisture meter and DCP.	Demonstrated the use of machine drive power as a tool for compaction control. Variability of DCP index reduced with increase in roller passes.
Anderegg et al., 2006	Demonstrated the compaction monitoring using single drum vibratory intelligent compactor.	Linear relation with high correlation was established between moduli from the plate bearing tests and roller measurement values.
Mooney et al., 2006	Investigated the influence of heterogeneity on vibratory roller compactor response in Colorado. Lift thickness and moisture content were also considered along with varying depth to bedrock. A double smooth drum roller was used. The soil type was poorly graded sand (A-1-b) and DCP was used for the point measurements.	Roller parameters found to be sensitive to underlying stiffness when operated near resonance. At higher frequencies the roller parameters were insensitive to changes in the underlying soil conditions.
Hossian et al., 2006	Demonstrated intelligent compaction control concepts in identifying soft spots in Kansas. The relation of roller measured stiffness with density and moisture content was established. A single drum vibratory roller was used. Soil type was clayey sand and nuclear gauge, moisture meter and DCP were used for point measurements.	Poor correlation was observed between the roller measurement values and the CBR from DCP due to empirical nature. The target stiffness values needs to be function of the dry density since both high and low densities results in lower IC roller stiffness. Authors also showed the limitations of QC based on dry density alone.
Petersen and Peterson, 2006	Compared CMV with the point test measurements such as LWD, DCP and Geogauge	The roller measurements vary greatly with point measurements. The variation in the roller measurements is due to the difference in the area of measurements between drum and sensors of spot tests, and the response is greatly influenced by moisture, material and support.
White and Thompson, 2008	Evaluated compaction meter value and machine drive power with five different types of subbase materials including RAP in Illinois. Single drum intelligent roller with Clegg Impact tester, SSG, LWD, DCP and PLT were used as compaction control tools.	Machine drive power was observed to be more variable as compared to compaction meter value. Multivariate analyses may be used to relate the roller measured values and in situ point test values.
Mooney and Rinehart, 2007	Explored relationship between vibration characteristics and soil properties in a test section in Denver. Double drum smooth intelligent compactor was used.	Heterogeneity causes significant challenge to vibration based assessment of soil properties. Roller measurements for QC/QA were found to be greatly influenced by the stress dependent nature of soil.
Rahman et al., 2007	Studied the use of subgrade stiffness obtained from the IC technology using Bomag single smooth steel drum variocontrol intelligent roller. Three sections were considered in Kansas.	Demonstrated the potential benefits of IC technology in identifying weak areas of compaction. Revealed the sensitivity of the roller measurements to moisture content variation.

Table 3.2, cont. - Summary of Quality Control and In Situ Correlations

Reference	Objective and scope	Key findings/comments
White et al., 2011	Review of the field assessment studies and examining the factors influencing roller measurement values, correlations between the spot test measurements and spatial uniformity.	Roller measurement values are highly influenced by the variability of soil properties across the width of roller drum and moisture content. Establishing the target values, acceptance limits, correlations between field measurements being technology specific and based on local experience are the potential limitations of existing IC specifications.
Gallivan et al., 2011	Evaluated the use of intelligent compaction for QC/QA	Established the advantage of roller measurement values in detecting the deeper weak spots that cannot be identified with the density measurements.
Rahman et al., 2012	Developed correlations between the in situ measurements and roller measurement values in Kansas. Single drum intelligent roller was used along with nuclear gauge, SSG, LWD, DCP and PLT.	Study showed that the change in layer modulus with depth is a potential source of problem to compare stiffness and modulus results from different test and roller measurement values.
Rinehart et al., 2012	Evaluated the European CCC specifications on a pilot project in Colorado. Pilot study was implemented on a 30 cm thick subbase, of 12 m width and 300 m long. Dynapac roller was used in the study.	Study recommends lowering the acceptance criteria using spot test results on the weak areas identified through roller based measurement values. For process and acceptance control, study recommends for additional analysis beyond correlation to establish roller compaction target values.
White et al., 2013	Evaluated 16 sections of stabilized pavement foundations covering 4.8 mi, with ground conditions ranging from soft to very stiff using FWD, LWD, and roller-integrated compaction monitoring systems.	The CMV values correlated better with LWD and FWD values than with MDP values. CMV values correlated better with FWD values than with LWD values.
Nazarian et al., 2014	Developed a modulus-based construction specifications for compaction of earthwork and unbound aggregate.	Study showed there is not a strong correlation between NDG and CMV from IC roller .
Barman et al., 2016	Evaluated the Intelligent Compaction Analyzer (ICA) developed at the University of Oklahoma in quality control and quality improvement during compaction of stabilized subgrade.	ICA modulus correlated reasonably with subgrade modulus backcalculated from FWD data (R^2 = 0.63), fairly with the DCP test results (R^2 = 0.50) and excellently with the in-situ subgrade resilient modulus (R^2 = 0.72 to 0.97).
	CBR- California Bearing Ratio RAP- Reclaimed Asphalt Pavement CCC- Continuous Compaction Control SSG- Soil Stiffness Gauge	LWD- Light Weight Deflectometer DCP- Dynamic Cone Penetrometer PLT- Plate Load Test

Table 3.3 - IC in Quality Control and Quality Acceptance Testing

Reference	Findings
White et al. (2005)	Statistical analysis of the data help to reduce the IC measurement variations, position error and explains the underlying support conditions
Hossain et al. (2006)	By continuous nature of stiffness measurements by IC rollers, it is possible to identify soft spots during production control and acceptance testing
Mooney and Rinehart (2007)	The IC roller identified the weak areas that were not identified by a static proof roll test during acceptance testing
White et al. (2008)	The variations in the RMVs are important for interpreting layered soil conditions
Gallivan et al. (2011)	Minimal or inconsistent rolled areas are easily identified when IC roller is used for production control
Rahman et al. (2012)	Variability in soil properties is reduced when IC roller is used for production process. Proof rolling using IC roller identified poorly compacted locations. High variability in the stiffness measurements within a short distance contradicts the concept of uniform compaction using IC rollers.
Heersink et al. (2013)	Improved IC and QA of compaction process using a sequential, spatial back-fitting of RMVs coupled with multiresolution scale space analysis to generate estimates of compaction level.
Cai et al. (2015)	Correlations between IC CMV and MDP to DCP, LWD and FWD, confirm the promise of IC for reducing sampling requirements for acceptance criteria but not entirely replacing current QA sampling.
Xu and Chang (2016)	Developed a material–machine–information–human decision integrated system approach for adaptive QC/QA for compaction of asphalt pavements. In a case study, they found NDG density measured after each roller pass at one spot location had a fairly good linear correlation with ICMV growth (Sakai CCV) by roller pass.

Table 3.4 presents the findings from the selected studies on influence of geomaterials on ICMVs. The IC specification is applicable to both cohesive and cohesionless soil and base materials. However, several studies (e.g., Mooney et al. 2010; and Hossian et al., 2006) have demonstrated that the ICMVs are less reliable on cohesive soils if careful attention is not paid to soil moisture content variations. It is also important to account for the soil moisture variation for the stabilized materials. The European specifications limit the fine content (<0.06 mm) for materials compacted using IC technology. Also, Sweden specifications limit the fines content to 7%. Hence, the IC technology is by default used predominantly for cohesionless soils (Mooney et al., 2010).

Table 3.4 - Influence of Geomaterials Types on Quality Acceptance

Reference	Findings
Hossian et al. (2006)	The influence of moisture content on the ICMVs was found to be more pronounced for clay-type soils.
White et al. (2008)	ICMVs are dependent on the soil type
Rahman et al. (2012)	The LWD measured stiffness on fine graded soil control strip exhibit a high variability

3.3 Acceptance Testing

Table 3.5 summarizes different specifications for acceptance testing. The acceptance is typically based on spot tests performed at the weak areas identified using the target ICMV.

Table 3.5 - Specifications for Acceptance Testing

Specifications	Acceptance Criteria
MnDOT	All segments shall be compacted so that at least 90% of the MVs are at least 90% of the moisture-corrected RTV prior to placing the next lift. All of the RMVs must be at least 80% of the moisture-corrected RTV. If a significant portion of the grade is more than 20% in excess of the selected moisture-corrected RTV, the Engineer shall reevaluate the selection of the RTV.
FHWA	A minimum coverage of 90% of the individual construction area shall meet the optimal number of roller passes and 70% of the target RMV determined from test strips.
INDOT	A minimum of 90% of the construction area shall be mapped. A minimum of 70% of the mapped construction area shall exceed the target RMV.
ISSMGE/ Austria	The mean RMV must be $\geq$ ME[1] (based on 1.05*E_{LWD}[2]) 100% of RMVs must be $\geq$ 0.8 MIN[3] (based on 0.95*E_{LWD}) 90% of RMVs must be $\geq$ MIN (0.95*E_{LWD})
Germany	90% of all RMVs in an evaluation area must exceed the RTV.
Sweden	Swedish specifications use roller-integrated CCC to identify weak spots for PLT

[1]Mean RMV, [2]Modulus from LWD, [3]Min. RMV

3.4 Target Value Selection

For an efficient utilization of the IC technology, it is desirable that the contractor reach the targeted compaction specification without over-compacting the material. The selection of the target value can either be tied to the pavement design parameters or obtained from field test strips. In general, the former option is more desirable than the latter. One of the impediments to the wide implementation of the IC technology has been the tedium and excessive efforts necessary to construct the test strips. The downside of tying the target values to the pavement design parameters are the need for upfront advanced laboratory testing (such as resilient modulus testing) and a lack of an algorithm to estimate the target value.

Nazarian et al. (2014) under NCHRP Project 10-84 explain a process to select target values for devices that measure the response of the geomaterials (e.g., LWD, PLT and Geogauge) based on the pavement design parameters. The approach they proposed, especially for multi-layer earthwork, is to utilize a nonlinear structural algorithm. The nonlinear algorithm is used to develop straightforward relationships for estimating field target moduli from resilient modulus parameters (k'_1-k'_3) from Equation 3.1. This relationship makes use of a modified version of the MEPDG nonlinear material model (Ooi et al, 2004) that was found to yield more representative responses of the modulus-based devices than the model recommended by the MEPDG shown in Equation 3.2.

$$MR = k_1' P_a \left(\frac{\theta}{P_a} + 1 \right)^{k_2'} \left(\frac{\tau_{oct}}{P_a} + 1 \right)^{k_3'} \tag{3.1}$$

$$MR = k_1 P_a \left(\frac{\theta}{P_a} \right)^{k_2} \left(\frac{\tau_{oct}}{P_a} + 1 \right)^{k_3} \tag{3.2}$$

where θ = bulk stress, τ_{oct} = octahedral shear stress, P_a = Atmospheric pressure, and $k'_{1,2,3}$ and $k_{1,2,3}$ = regression constants. The authors provided relationships to convert parameters k_1 through k_3 recommended by the MEPDG to k'_1 through k'_3 utilized in that study considering the practical problems that this change may cause for highway agencies that utilize the MEPDG material model. The relationships provided in that report are based on the AASHTO T-307-03 Specification.

LWD: The target modulus/deflection is set in a way that is compatible with the algorithm used during the structural design of the pavement. The following steps shall be used to set the target values:

Step 1: Determine the resilient modulus parameters of the layer under test and the underlying layer(s).

Step 2: Convert the regression parameters k_1 through k_3 from Equation 4.2 to k'_1 through k'_3 using the following relationships:

$$k_1' = k_1 e^{-1.32 k_2} \tag{3.3}$$

$$k_2' = 1.88 k_2 \tag{3.4}$$

$$k_3' = k_3 \tag{3.5}$$

Step 3: Calculate the effective modulus of the geomaterial, E_{eff}, from:

$$E_{eff} = \frac{\left(1-\nu^2\right)F}{\pi a d_{eff}} \times f \tag{3.6}$$

where a = radius of load plate, d_{eff} = peak deflection on top the compacted layer, ν = Poisson's ratio of the geomaterials, f = plate rigidity factor.

Step 4: Establishing adjustment factor, K_{adj}. Obtain, K_{adj}, from Equation 3.7 following the two step procedure described below:

$$K_{adj} = K_{lab\text{-}field}\, K_{moist} \tag{3.7}$$

where $K_{lab\text{-}field}$ is an adjustment factor that accounts for differences in lab and field moduli at the same moisture content and density and K_{moist} is an adjustment factor for differences in the compaction and testing moisture contents. Estimate $K_{lab\text{-}field}$ from the following relationship:

$$K_{lab\text{-}field} = (F_{env})^{\lambda} \tag{3.8}$$

where λ = - 0.36 and F_{env} is calculated from

$$\log F_{env} = \left[-0.40535 + \frac{1.20693}{1 + e^{\left[0.68184 + 1.33194 \cdot \left(\frac{S - S_{opt}}{100}\right)\right]}} \right], \tag{3.9}$$

where S_{opt} = degree of saturation at optimum moisture content and S = degree of saturation at compaction moisture content. Estimate K_{moist} in the following manner

$$K_{moist} = e^{\eta(\omega C - \omega T)} \tag{3.10}$$

where η = 0.18 for fine-grained soils and 1.19 for unbound aggregates; ω_T = moisture content at time of testing (in percent); ω_C = moisture content at time of compaction (in percent);

Step 5: Estimate the adjusted modulus, E_{adj}, from:

$$E_{adj} = E_{eff} \times K_{adj} \tag{3.11}$$

PSPA: The target modulus, $E_{T\text{-}PSPA}$, is directly determined from laboratory Free-Free Resonant Column (FFRC) test (conforming to ASTM C 215) results using the following equation:

$$E_{T-PSPA} = \frac{E_{FFRDC-Lab}}{\left[\frac{(1+\nu)(1-2\nu)}{1-\nu}\right]}, \tag{3.12}$$

where $E_{FFRC\text{-}Lab}$ = measured modulus with the FFRC device on the laboratory specimen and ν = Poisson's ratio of the material. Further details are available in Appendix A of the NCHRP 10-84 Final Report (Nazarian et al. 2014).

3.4.1 Limitations of Existing Guidelines

White et al. (2011) conducted a thorough review of existing specifications for implementing intelligent compaction. That study noted that one of the major limitations of the existing intelligent compaction specifications is that the acceptance requirements (i.e., percent target value limits, acceptable variability, etc.) are technology specific and somewhat based on local experience. This limitation hinders widespread acceptance of these specifications into practice, as there are currently at least ten different Roller Integrated Compaction Monitoring (RICM) technologies.

White and Vennapusa (2004) have documented the following as the key attributes in order to generalize the acceptance of the intelligent compaction specification:

1. Identification of the rollers and descriptions of their configurations,
2. General guidelines for operations (speed, vibration frequency and amplitude, and track overlap)
3. Records to be reported (time stamp, operations/mode, soil type, moisture content, layer thickness, etc.)
4. Repeatability and reproducibility measurements for intelligent compaction values
5. Ground conditions (smoothness, levelness, isolated soft/wet spots),
6. Calibration procedures for rollers and selection of calibration areas,
7. Regression analysis between intelligent compaction values and point measurements,
8. Number and location of quality control (QC) and quality assurance (QA) tests,
9. Operator training/certification, and
10. Acceptance procedures/corrective actions based on achievement of minimum RICM target values and associated variability.

3.5 Geostatistics in IC

Geostatistics are statistical techniques developed to analyze and predict values of a characteristic that is spatially distributed. It begins with a type of autocorrelation analysis called variography or semivariance analysis, in which the degree of spatial self-similarity is displayed as a variogram. A curve is fit to the variogram, and the equation that describes the curve, called the variogram model, is used to predict unsampled locations by kriging or conditional simulation. Kriging is a geostatistical method used for spatial interpolation and it is different from other methods because it can assess the quality of the prediction with estimated errors. Kriging uses the semivariogram to measure spatially correlated component or spatial dependence. This produces provide optimal unbiased estimates of the property across the entire spatial domain. The same analysis can also be performed with temporal data such as hourly or daily measures of some property to interpolate through time. Geostatistical analyses also provide tools for spatial data exploration, identification of data anomalies, evaluations of errors in prediction of surface models, statistical estimation and optimal surface creation.

Summary of studies on using geostatistics in evaluating the compaction quality are listed in Table 3.6. The use of geostatistics in IC as QA/AC tool in the acceptance of compacted soil will be more meaningful than just spot test because it can demonstrate the spatial variability of compaction and depict soft/hard spot areas that can be targeted for repeated compaction. The FHWA is recommending using Veta software (formerly Veda) which is developed to analyze data collected from GPS and roller monitoring and displays simple statistical graphs like a histogram, semivariogram and spatial distribution of ICMVs.

3.6 Best Practices for Quality Control/Quality Assurance

Traditionally the compaction process is aimed at achieving the target density at specified level of moisture content. The type of roller and lift thickness are selected based on the type of material and layer of pavement structure. The optimum number of passes to attain the desired level of density is determined based on the control section characteristics. The compaction effort is more or less maintained constant throughout the process (6 to 10 roller passes). These practices do not allow to monitor the compaction process and to vary the compaction effort during construction.

Table 3.6 – Geostatistics in Intelligent Compaction

Reference	Objective and scope	Key findings/comments
White et al., 2007	Evaluated the utilization of intelligent compaction monitoring for unbound materials in the field. Test sections with different site conditions, rollers with different data measurements and storage system were evaluated.	Study demonstrated the use of variogram models to effectively characterize the uniformity of compaction by quantifying spatial variability. The study showed that the range from a variogram plot can be potentially used as a maximum separation distance between spot tests measurements. Also study showed that to reduce any significant error, roller measurement values from the middle of drum shall be considered.
Peterson et al., 2007	Evaluated the application of geostatistical tools to judge the adequacy of compaction and uniformity, assisting in the QC/QA process.	Traditional descriptive statistics were found to be inadequate to address the concern of uniform compaction. The use of IC data and geostatistics help to identify and fix the problematic areas of poor compaction, which in turn improve the overall life cycle of pavements.
White et al., 2008	To characterize the uniformity of the compacted soil layer using intelligent compaction technology with variable feedback control.	Findings from the study showed the limitations of univariate analysis in determining the uniformity of the compacted soil layer. Study identified the use of variogram model parameters to characterize the uniformity of compacted soil layer.
Vennapusa et al., 2010	To quantify the non-uniformity using spatial referenced roller measurements	Non-uniformity of compaction which cannot be explained with univariate analysis of roller measurements can be dealt with variogram analysis. Geostatistics can used to identify the areas of poor compaction and non-uniform conditions
White et al., 2011	Review of the field assessment studies and examined factors influencing the roller measurement values, correlations between the spot test measurements and spatial uniformity.	Geostatistical analysis of roller measurement values facilitate construction process control and characterize variations and non-uniformity.

A number of studies investigated the correlation between the roller measurement values (technology specific) and the spot test measurements to evaluate the compaction uniformity. A summary is provided in Table 3.7. The best practice is to determine the target roller measurement value (at constant roller parameters) based on correlations. The compaction process is monitored to meet the target value requirements. Individual agencies have identified their own limits of acceptance for target values to achieve compaction uniformity. With the advancement in the global positioning system (GPS), mapping compaction variability during the process in real time has been made easier (White et al., 2011). Geostatistical analysis of roller measurement values facilitate process control and characterize non-uniformity of compaction.

Table 3.7 – Summary of IC Measurements for Quality Control and In Situ Correlations

Reference	Objective and Scope	Key Findings/Comments
White et al., 2005	Evaluated the utilization of intelligent rollers in real time compaction monitoring. A pilot field study was carried out in Illinois on a cohesive glacial till soil. Spot measurements of density, moisture content, and DCP and Clegg impact hammer values were correlated to roller measurement values.	The variation in the machine drive power was observed to be the result of inherent soil and moisture variations in the compacted layer. The compaction effort was found to be significant only up to a depth of 40 cm. Consideration of moisture content in the regression analysis resulted in a better understanding of measurements and correlation between them.
White et al., 2006	Evaluated the relationship between machine drive power and measures of soil compaction at a test section in Peoria, Illinois. Two moisture contents were adopted. Vibratory pad foot roller was used. Well-graded silty sand was evaluated with nuclear gauge, moisture meter and DCP.	Demonstrated the use of machine drive power as a tool for compaction control. Variability of the DCP index reduced with increase in the roller passes.
Anderegg et al., 2006	Demonstrated the compaction monitoring using single drum vibratory intelligent compactor.	Linear relation with high correlation was established between moduli from the plate bearing tests and roller measurement values.
Mooney et al., 2006	Investigated the influence of heterogeneity on vibratory roller compactor response in Colorado. Lift thickness and moisture content were also considered along with varying depth to bedrock. A double smooth drum roller was used. The soil type was a poorly graded sand (A-1-b) and DCP was used for the point measurements.	Roller parameters found to be sensitive to the underlying stiffness when operated near resonance. At higher frequencies the roller parameters were insensitive to the changes in the underlying soil conditions.
Hossain et al., 2006	Demonstrated intelligent compaction control concepts in identifying soft spots in Kansas. The relation of the roller measured stiffness with density and moisture content was established. A single drum vibratory roller was used. Soil type was clayey sand and nuclear gauge, moisture meter and DCP were used for point measurements.	Poor correlation was observed between the roller measurement values and the CBR from DCP due to empirical nature. The target stiffness values needs to be function of the dry density since both high and low densities results in lower IC roller stiffness. Authors also showed the limitations of QC based on dry density alone.
Petersen and Peterson, 2006	Compared CMV with the point test measurements such as LWD, DCP and Geogauge	The roller measurements vary greatly with point measurements. The variation in the roller measurements is due to the difference in the area of the measurements between drum and sensors of spot tests, and the response is influenced by moisture, material and support.
Rahman et al., 2007	Studied the use of subgrade stiffness obtained from the IC technology using Bomag single smooth steel drum variocontrol intelligent roller. Three sections were considered in Kansas.	Demonstrated the potential benefits of the IC technology in identifying less stiff areas. Revealed the sensitivity of the roller measurements to moisture content variation.
Mooney and Rinehart, 2007	Explored relationship between vibration characteristics and soil properties in a test section in Denver. Double drum smooth intelligent compactor was used.	Heterogeneity causes significant challenge to vibration based assessment of soil properties. Roller measurements for QC/QA were found to be influenced by the stress dependent nature of soil.
White and Thompson, 2008	Evaluated compaction meter value and machine drive power with five different types of subbase materials including RAP in Illinois. Single drum intelligent roller with Clegg Impact tester, SSG, LWD, DCP and PLT were used as compaction control tools.	Machine drive power was observed to be more variable as compared to compaction meter value. Multivariate analyses may be used to relate the roller measured values and in situ point test values.

Table 3.7, cont. – Summary of IC Measurements for Quality Control and In Situ Correlations

Reference	Objective and Scope	Key Findings/Comments
White et al., 2011	Review of the field assessment studies and examining the factors influencing roller measurement values, correlations between the spot test measurements and spatial uniformity.	Roller measurement values are highly influenced by the variability of soil properties across the width of roller drum and moisture content. Establishing the target values, acceptance limits, correlations between field measurements being technology specific and based on local experience are the potential limitations of existing IC specifications.
Rahman et al., 2012	Developed correlations between the in situ measurements and roller measurement values in Kansas. Single drum intelligent roller was used along with nuclear gauge, SSG, LWD, DCP and PLT.	The change in layer modulus with depth is a potential source of problem to compare stiffness and modulus results from different test and roller measurement values.
Rinehart et al., 2012	Evaluated the European CCC specifications on a pilot project in Colorado. Pilot study was implemented on a 30 cm thick subbase, of 12 m width and 300 m long. Dynapac roller was used in the study.	Lowering the acceptance criteria using spot test results on the weak areas identified through roller based measurement values. For process and acceptance control, additional analysis beyond correlation is needed to establish roller compaction target values.
White et al., 2013	Evaluated 16 sections of stabilized pavement foundations covering 4.8 mi, with ground conditions ranging from soft to very stiff using FWD, LWD, and roller-integrated compaction monitoring systems.	The CMV values correlated better with LWD and FWD values than with MDP values. CMV values correlated better with FWD values than with LWD values.
	CBR - California Bearing Ratio RAP - Reclaimed Asphalt Pavement CCC - Continuous Compaction Control SSG - Soil Stiffness Gauge	LWD - Light Weight Deflectometer DCP - Dynamic Cone Penetrometer PLT - Plate Load Test

4 THEORETICAL AND TECHNOLOGICAL LIMITATIONS

4.1 Spot Testing with Light Weight Deflectometer

Adoption of mechanistic pavement design methodologies have led state highway agencies around the United States to gradually move from density-based tests to modulus-based tests for earthwork quality control/quality acceptance (QC/QA) (Vennapusa, 2008). Different nondestructive modulus-based in situ tests have been used for this purpose, including the plate load test (PLT), falling weight deflectometer (FWD), light weight deflectometer (LWD) and dynamic cone penetrometer (DCP). FWD has been in use for over 30 years and it is a trusted tool for assessment of built roads, but it may be not be suitable for the assessment of roads during construction, where the scale and frequency of testing can make it uneconomical. FWD is costly and its availability is limited. In addition, it is less suited to testing the pavement foundation layers, i.e. unbound granular base and subgrade, as these are typically subject to in-service stresses at the lower end of FWD stress range (Fleming et al., 2007). LWD offers several advantages to FWD, including lower initial cost, lower operational time and cost, and simplified testing procedure. A reduced load pulse duration and reduced maximum applied force allow the device to maintain portability. LWD helps to estimate the surface modulus of a material by dropping a weight from a known height to transmit a pulse load to a circular metal plate resting on the soil surface, and by measuring the deflection of either the plate or the soil.

Several aspects of the LWD tests may require further considerations for effective and defensible implementation, and for developing generic manufacturer-independent specifications. For instance, one factor that influences the reported surface modulus is the diameter of the loading plate (Lin et al., 2006). Other factors such as the loading rate, buffer stiffness, plate contact stress, and plate rigidity also contribute to the measured responses of LWDs (Vennapusa, 2008). In multi-layer soil systems, the layer thicknesses also affect the surface modulus estimation (Senseney et al., 2013). Also different makes of LWDs yield different surface moduli (Tirado et al., 2015).

The simplest way to model the behavior of pavements is by means of the layer elastic theory. This approach does not consider the load-induced nonlinear behavior of the materials and the plate-soil interaction. Finite element (FE) models have been developed to study the effects of the LWD design characteristics on the measured deflections. These models are often based on the elato-static, rather than dynamic, FE analyses. According to Guzina and Osburn (2002), the selection of a static-based model could lead to errors in the estimation of the surface moduli. Senseney et al. (2015) found that the dynamic vertical deflections were smaller than the static vertical deflections. Senseney et al. also demonstrated that the measurement depth of the LWD is 2 to 2.5 times the plate diameter. In contrast, Mooney and Miller (2009) found the influence depth of LWD to be 0.9 to 1.1 times the plate diameter. For the purpose of evaluating the depth of influence of LWD, a FE model was developed that considered the dynamic response, as well as the nonlinear behavior of soil, and the soil-plate interaction by means of a contact model. Different levels of sophistication of the FE model were considered to establish relationships among the more sophisticated (i.e., dynamic and nonlinear model) to the less sophisticated (i.e., linear-static) FE models. Though less representative of LWD field conditions, linear-static models provide fast execution times, as compared to the more sophisticated models. The responses between the different models were used for developing relationships that can be used to adjust the responses of the simpler models.

An axisymmetric dynamic nonlinear model was developed using LS-DYNA to simulate the LWD test on top of a geomaterial using a Zorn ZFG 2000 LWD (see Figure 4.1). About 75,000 elements were used to model an 80 in. wide and 100 in. deep soil section. The LWD impact was simulated using a half-sine pulse, with a 1500 lb peak force and a pulse duration of 17 msec applied as a pressure load on a 1 in. diameter area corresponding to the ball protruding from the top of the unit. A 2D surface-to-surface contact model that allowed the plate decoupling from the soil was implemented to better capture the responses comparable to those obtained during the field testing. In contrast, for the static model, which made use of the same soil mesh, a 30 psi pressure load was uniformly distributed at the soil surface as shown on Figure 4.1c. The time

histories of the responses were obtained underneath the center of the plate and along the soil surface with a 1 msec time interval for the dynamic FE analyses. With this information, the variations of the vertical deflection and stress with depth were calculated during the plate impact.

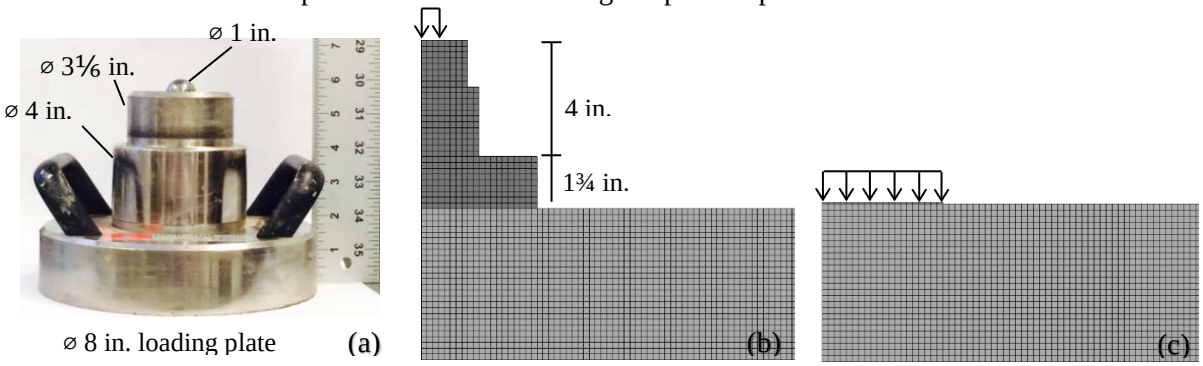

Figure 4.1 – Schematic and finite element models views from devices. (a) LWD device (b) FE LWD dynamic model (C) FE LWD static model.

Mazari et al. (2012) demonstrated that the nonlinear material model proposed by Ooi et al. (2006), shown in Equation 3.1, to be appropriate in representing the performance of the LWD. Mazari et al. (2012) also provided simple relationships for converting the nonlinear parameters obtained from Equation 3.1 to the more common k_1, k_2, and k_3 parameters proposed by NCHRP 1-28A (Oh and Fernando, 2011). The representative stresses recommended by NCHRP 1-28A, which are θ = 12.4 psi, τ_{oct} = 3 psi for subgrade and θ = 31 psi, τ_{oct} = 7.5 psi for unbound granular base materials, were used to estimate the representative linear elastic moduli.

A parametric study was performed on a single-layer geosystem (representing a uniform subgrade) and on a two-layer geosystem (representing a subgrade and a base layer). For each layer, a series of nonlinear k' parameters were randomly selected from a typical range of values shown in Table 4.1, as recommended by Velasquez et al. (2009). Following the traditional design practices, the pavement sections that yielded stiffer subgrades than base layers were excluded from the analysis.

Table 4.1 – Pavement Properties for One and Two Layer Geosystems

Pavement Properties	Range of Values
k'_1	100 – 3000
k'_2	0 – 3.0
k'_3	-4.0 – 0
Poisson's Ratio, v	0.35

4.2 Continuous Test with Intelligent Compaction Roller

Since the numerical modeling of soil response due to roller compaction is rather complex, a dynamic FE technique is necessary to evaluate the interaction of the roller with the geosystem. LS-DYNA, which is a multi-purpose FE program, was used in this study to address that need. Figure 4.2 shows a 3-D view of the geosystem and the roller. A 3-D mesh was assembled to represent a roller imparting energy to geomaterials at a given amplitude and vibrating frequency. The drum of the roller was modeled with rigid shell elements assuming common dimensions of IC rollers; i.e., 80 in. wide and 30 in. in radius. Due to the size of the drum, the geomaterial has been modeled as 160 in. wide, 160 in. long, and 100 in. deep with non-reflective boundaries. A mesh consisting of brick elements was used to represent the geosystem. About 64,000 elements wasen used to model the geomaterials. Smaller 2×2×2 in. elements were used underneath the roller up to 20 in. in depth, 24 in. longitudinally and 48 in. transversally from the center of the roller, after which the elements became larger. To establish better the contact of the drum nodes with the soil's mesh, about 75,000 shell elements have been used to simulate the drum.

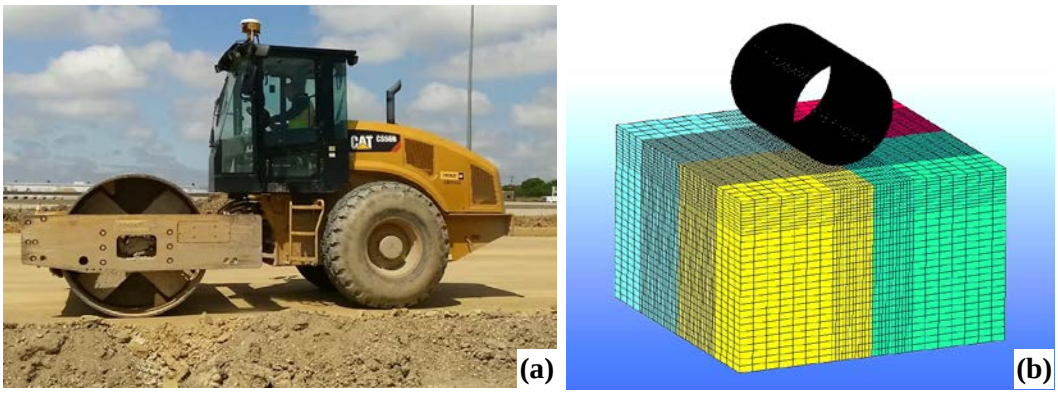

Figure 4.2 – Schematic and finite element models views from devices. (a) IC-Roller (b) 3-D FE dynamic model.

Figure 4.3 shows the drum to surface contact model. The interaction between the drum and the geosystem was simulated using LS-DYNA's "automatic single surface" contact type. The modified MEPDG resilient modulus constitutive model shown in Equation 3.1 was utilized to simulate the behavior of compacted geomaterials.

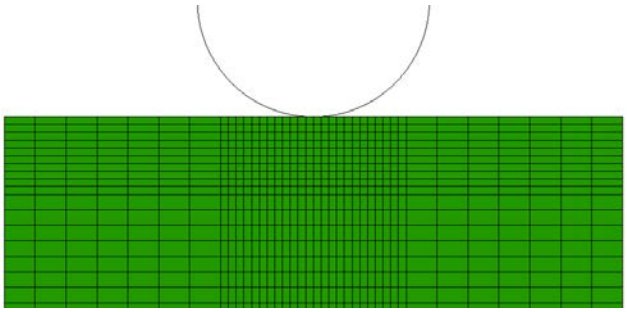

Figure 4.3 – Drum to Soil Contact.

The centrifugal force caused by the rotation of the eccentric masses inside the drum induces an excitation force, F_e, defined as:

$$F_e(t) = m_0 e_0 \Omega^2 \cos(\Omega t), \tag{4.1}$$

where Ω is the rotational frequency and e_0 is the eccentricity of the counter-rotating masses m_0. Typical values used for the simulated drum are shown in Table 4.2. The vibratory motion of the roller was maintained for t = 200 msec, equivalent to six load cycles. The stress, strain, and displacement time histories were calculated for every time interval of 1 msec underneath the center of the roller.

Table 4.2 – Specifications for Simulated Drum

Operating Parameter	Symbol	Value
Width of drum (compaction width)	*L*	2.0 m (80 in.)
Diameter of drum	*d*	1.5 m (60 in.)
Mass of drum	*md*	6000 kg (34.3 lb·s2/in)
Weight of drum	*mdg*	58,840 N (13,200 lb)
Mass-eccentricity	*m0e0*	5.36 kg·m (1.20 lb·s2)
Centrifugal force (Vertical excitation force)	*Fev*	170 kN (38 kips)
Frequency	*f*	28 Hz (1680 vpm)
Frequency	*Ω*	176 rad/s
Operating speed	*v*	0.9 m/s (3.24 km/h, 2.0 mph)

The Rayleigh damping as defined by Equation 4.3 was introduced to simulate material damping of the soil:

$$[C] = \alpha [M] + \beta [K] \tag{4.2}$$

where [*M*] is mass matrix, [*K*] is stiffness matrix, and Rayleigh constants were defined as $\alpha = 25$ and $\beta = 0.0002$ as recommended by Mooney and Facas (*2*) to minimize the dilatational and shear wave reflections.

4.3 Development of Database

A comprehensive database of linear and nonlinear cases with different input parameters was developed for single-layer and two-layer geosystems. The information stored in the database was used to evaluate the sensitivity of the geosystem response to different input parameters. The database contains the following general types of data:

1. Light Weight Deflectometer operating features, including plate dimensions, mass of plate, mass of hammer and vertical excitation impact.
2. Roller operating parameters, including drum dimensions, mass of drum, frequency, vertical excitation force and operating speed.
3. Geosystem structural and mechanical properties, including layer thickness, nonlinear *k'* parameters of layers, and the representative resilient modulus per layer.
4. Level of sophistication of the FE model, including the type of analysis (static, quasi-static or dynamic), and geomaterial constitutive model (linear elastic or nonlinear.
5. Pavement responses obtained after simulation of LWD and roller, including maximum surface vertical displacement, maximum stress observed under the load, and depth of influence.

Several levels of sophistication of the FE models for the LWD and IC-drum were considered, as represented in Tables 4.3 and 4.4. The models are identified with unique acronyms. For each geosystem type, 200 randomly generated cases were selected considering a uniform distribution within the feasible range of values shown in Table 4.1.

Table 4.3 – Specifications for Simulated LWD

FE Model Characteristics	Acronym	Load Type	Constitutive Model
Linear Static LWD	LS-LWD	Static	Linear Elastic
Nonlinear Static LWD	NS-LWD	Static	Modified MEPDG
Linear Dynamic LWD	LD-LWD	Dynamic	Linear Elastic
Nonlinear Dynamic LWD	ND-LWD	Dynamic	Modified MEPDG

Table 4.4 – Specifications for Simulated Drum

FE Model Characteristics	Acronym	Load Type	Constitutive Model	Roller Velocity
Static Stationary Linear	SSL	Static	Linear Elastic	-
Static Stationary Nonlinear	SSN	Static	Modified MEPDG	-
Vibratory Stationary Linear	VSL	Dynamic	Linear Elastic	-
Vibratory Stationary Nonlinear	VSN	Dynamic	Modified MEPDG	-
Vibratory Moving Linear	VML	Dynamic	Linear Elastic	0.9 m/s (3 mph)
Vibratory Moving Nonlinear	VMN	Dynamic	Modified MEPDG	0.9 m/s (3 mph)

4.4 Evaluation of Elastic Modulus under LWD

Stress distribution under a plate depends on the plate rigidity and soil type (Terzaghi and Peck, 1967). The surface moduli, E_{LWD}, is calculated using Equation 4.3, which is based on the Boussinesq theory:

$$E_{LWD} = \frac{\left(1-\nu^2\right) a\sigma_0}{d} \cdot f \tag{4.3}$$

where v is the Poisson's ratio, a is the radius of the plate, 4 in.,. σ_0 is the applied stress under the plate, 30 psi, and d is the deflection obtained from the FE model. The selection of appropriate value for parameter f, the shape factor that is a function of the soil type and stiffness and the rigidity of the plate, has been a subject of discussion within the engineering community. Parameter f is equal to $\pi/2$ for rigid plates. The first step is to compare the moduli and deflections measured by different models. The following observations were made:

- ***One Layer System:*** On average, the peak surface dynamic deflections were 1.3 times greater than the static deflections as shown on Figure 4.4a. Figure 4.4b demonstrates that the calculated dynamic E_{LWD} values from Equation 4.1 were about 71% of the static values. Nazarian et al. (2015) proposed a model to predict the target moduli of single layer pavement systems. In that approach, E_{LWD} is obtained from Equation 4.3 provided the bulk stress, θ, and octahedral shear stress, τ_{oct}, are calculated from:

$$\theta = \sigma_0\left[-0.193\ln\left(k_2'\right)+0.513\right], \text{ and} \tag{4.4}$$

$$\tau_{oct} = \sigma_0\left[\frac{1}{5.06+1.47k_2'^{1.5}}\right]. \tag{4.5}$$

The nonlinear static moduli obtained from that approach are compared to the nonlinear dynamic moduli from this study in Figure 4.5. The 17% difference in the results can be partially attributed to the dynamic vs. static natures of the two methods.

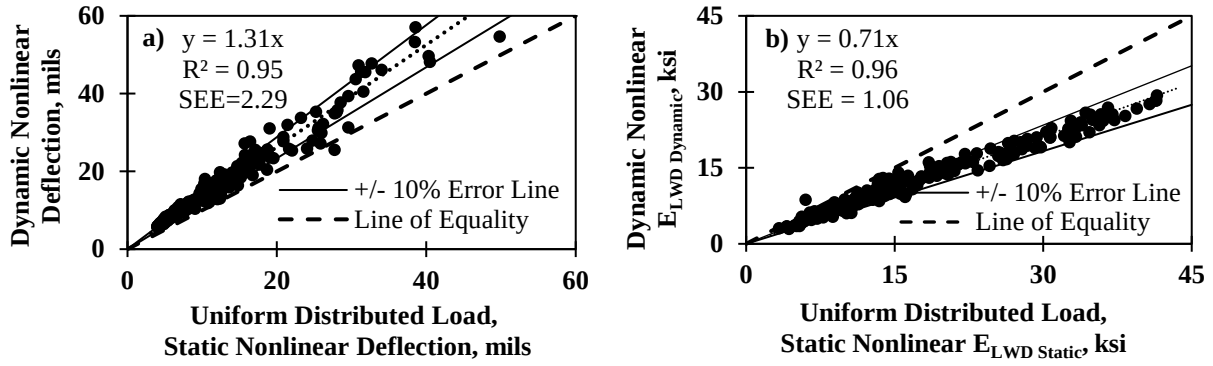

Figure 4.4 – Relationship of Dynamic and Static LWD Values for One-Layer Geosystem: (a) Deflection, and (b) Modulus.

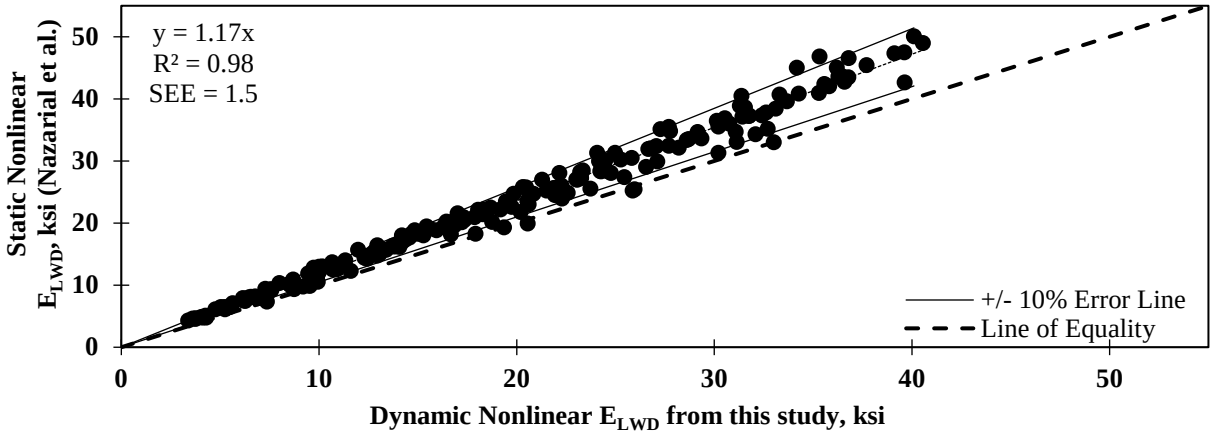

Figure 4.5 – Comparison of Static Moduli from Nazarian et al. (13) and Dynamic Moduli for Single Elastic Layer Geosystem of Static LWD Model.

- ***Two-Layer System:*** Seven different base layer thicknesses, varying from 6 in. to 18 in., in 2 in. increments, were considered. Equation 4.1 was used to calculate the moduli of the two layer systems after both the dynamic and static deflections were obtained for all cases. From Figure 4.6, the dynamic and static moduli are well correlated to one another. However, the dynamic moduli are on average about 63% of the static moduli.

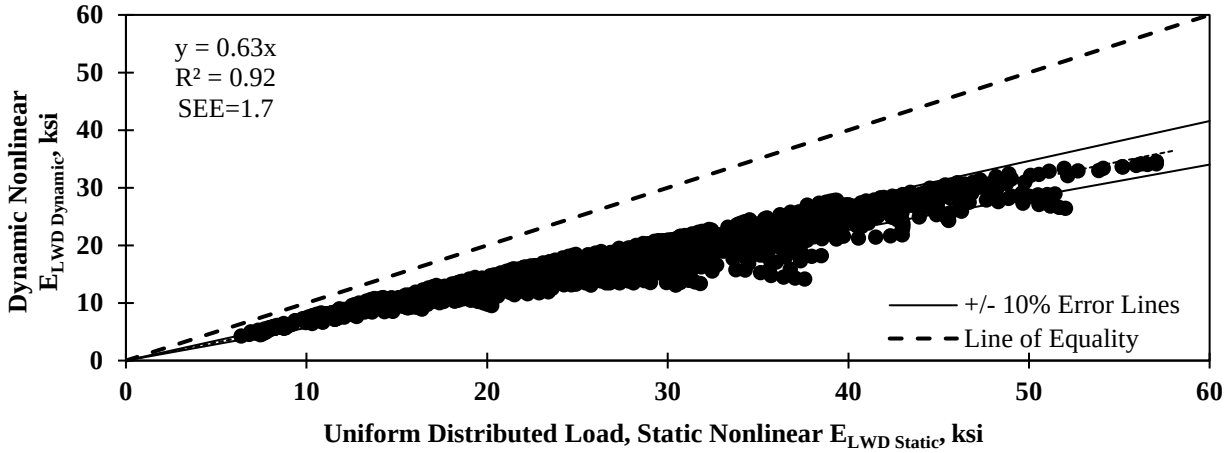

Figure 4.6 – Relationship of Dynamic and Static LWD Moduli for Two-Layer Geosystems.

4.5 Influence Depth of LWD

The deflection measured by LWD depends on the behavior of different layers down to a certain depth. Beneath that depth, the stresses and strains generated by LWD impact are significantly dissipated, and the geomaterial's properties below that depth do not have a significant effect on the measured deflections or surface moduli. Thus, the depth of influence plays a critical role in the quality control and quality assurance process of layered compacted geomaterials with dissimilar moduli. Given the importance of this matter on the development of a robust specification, the effects of the geomaterial properties, in terms of their nonlinear k' parameters, on the depth of influence of the LWD was investigated. For consistency, the depth of influence was defined as a depth where the response under the load (being stress, displacement or strain) was 10% of the corresponding surface response.

4.5.1 Influence Depth with Respect to Displacement

The depth of influence in this case is defined as the depth where displacement dissipates to 10% of the surface displacement. The ordinances are normalized with respect to the plate diameter, i.e. 8 in., for generality. The influence depth for the static model varies between 1.5 and 4 times the plate diameter. The descriptive statistics of the influence depth for single and two layer geosystems for nonlinear dynamic LWD FE model with respect to displacement are reported in Table 4.5a. The results indicate that the influence depth increases with an increase in the thickness of base.

4.5.2 Influence Depth with Respect to Stress

The depth of influence in this case is defined as the depth where stress decreases to 10% of the surface stress. The depth of influence is about 1.9 times the diameter, *D*, in static models. However, the results obtained from the dynamic analyses indicate that *z*/*D* varies between 2.1 and 2.8. The influence depth increases with an increase in k'_2 (as material becomes more granular), decreases only slightly with the increase in k'_3 (as material becomes more clayey) and decreases as k'_1 increases (the geomaterial becomes stiffer). The descriptive statics of the normalized depth of influence with respect to stress criterion for one and two-layer geosystems are reported in Table 4.5b. The average z/D decreases negligibly with an increase in the base thickness.

Table 4.5 – Descriptive Statistics of Influence Depth for Single and Two-Layer Systems for Nonlinear Dynamic LWD FE Model

Parameter	Normalized Depth of Influence (z/D)								
	One Layer System	Two-Layer System with Different Base Thicknesses							
		6 in.	7 in.	8 in.	10 in.	12 in.	14 in.	16 in.	18 in.
(a) Displacement Criterion									
Mean	3.59	4.30	4.38	4.44	4.52	4.57	4.60	4.61	4.62
Median	3.67	4.25	4.31	4.37	4.44	4.47	4.49	4.51	4.52
Standard Deviation	0.59	0.63	0.69	0.75	0.83	0.88	0.92	0.94	0.95
(b) Stress Criterion									
Mean	2.41	2.42	2.36	2.32	2.26	2.22	2.19	2.19	2.19
Median	2.39	2.42	2.37	2.33	2.28	2.25	2.21	2.18	2.15
Standard Deviation	0.15	0.12	0.15	0.19	0.25	0.29	0.30	0.29	0.26

4.6 Evaluation of IC Roller

The impact of geomaterials' properties, in terms of the nonlinear parameters, on the performance of the IC roller was studied using the database discussed above. In this section, the results obtained from different FE models with different levels of sophistication are discussed.

4.6.1 Influence Depth of Roller

A summary of the normalized depths of influence based on displacement criterion for stationary static models including both linear and nonlinear geosystems is provided in Table 4.6a. The influence depth from the single-layer SSL analyses is about 5.9 times the drum contact width. The drum contact width *B* was found to be about 12 in. for the simulated drum with operating features presented in Table 4.2. However, the influence depth varies between 4.5 and 6.8 times the drum contact width for the static stationary nonlinear (SSN) cases. The average z/B from the static stationary linear (SSL) models for the two-layer systems with 6 in. and 12 in. base thicknesses are between 5.8 and 6.8, and for SSN cases 18.

The average *z*/*B* slightly increases for linear and nonlinear geomaterials subjected to the vibratory drums at stationary and moving conditions as compared to the results gathered from static stationary (SSL and SSN) cases. The average *z*/*B* increases with an increase in thickness of the base (top) layer. The stiffer the geomaterial is, the deeper the depth of influence will become. The above-mentioned ratio obtained from vibratory moving nonlinear model (VMN, the most sophisticated model) for single layer and two-layer systems are 5.9, 6.21, respectively.

The descriptive statics of the normalized depth of influence with respect to stress criterion for different levels of sophistication of FE model are presented in Table 4.6b. The average z/B decreases with an increase in the base thickness, i.e. the stiffer the soil is, the shallower the penetration depth will be. The average z/B is 3.8 for the single layer geosystems for the VMN scenario. The normalized depth of influence for two-layer geosystems with 6 in. and 12 in. base thicknesses subjected to the vibratory moving drum are about 3.7 ft.

4.7 Impact of Nonlinear Material Parameters

The influence of the nonlinear nature of the geomaterials on the pavement responses was studied using Spearman's correlation (McDonald, 2014). The results of such activities are discussed for stress recovery ratio (SRR) and the depth of influence for one and two-layer geosystems subjected to both LWD and IC roller. Different levels of sophistication of the FE model were also taken into consideration.

Table 4.6 – Summary of Descriptive Statistics of Normalized Depth of Influence with Respect to Displacement for Different Levels of Sophistication of FE Model

Normalized Depth of Influence (z/B)	Different Levels of Sophistication of FE Model					
	One Layer System	Two-Layer System		One-Layer System	Two Layer System	
		6 in. Base	12 in. Base		6 in. Base	12 in. Base
(a) Displacement Criterion						
Static Stationary	***Linear Geomaterial (SSL)***			***Nonlinear Geomaterial (SSN)***		
Mean	5.89	6.12	6.29	5.82	6.01	6.18
Meadian	5.90	6.13	6.30	5.91	6.03	6.03
Standard Deviation	0.03	*0.17*	0.26	0.58	0.37	0.37
Vibratory Stationary	***Linear Geomaterial (VSL)***			***Nonlinear Geomaterial (VSN)***		
Mean	6.09	6.31	6.46	5.94	6.11	6.24
Median	6.11	6.30	6.46	5.99	6.13	6.30
Standard Deviation	0.06	0.19	0.28	0.40	0.30	0.28
Vibratory Moving	***Linear Geomaterial (VML)***			***Nonlinear Geomaterial (VMN)***		
Mean	6.12	6.33	6.49	5.91	6.08	6.24
Median	6.13	6.34	6.51	5.99	6.09	6.25
Standard Deviation	0.05	0.17	0.27	0.43	0.32	0.28
(b) Stress Criterion						
Static Stationary	***Linear Geomaterial (SSL)***			***Nonlinear Geomaterial (SSN)***		
Mean	4.11	4.17	4.06	4.08	4.08	4.05
Meadian	4.10	4.16	4.06	4.05	4.07	4.03
Standard Deviation	0.07	0.07	0.13	0.23	0.30	0.26
Vibratory Stationary	***Linear Geomaterial (VSL)***			***Nonlinear Geomaterial (VSN)***		
Mean	4.22	4.19	4.02	4.40	4.20	4.01
Median	4.21	4.19	4.01	4.27	4.15	4.06
Standard Deviation	0.07	0.10	0.06	0.43	0.24	0.39
Vibratory Moving	***Linear Geomaterial (VML)***			***Nonlinear Geomaterial (VMN)***		
Mean	3.76	3.61	3.53	3.77	3.70	3.64
Median	3.79	3.64	3.58	3.80	3.67	3.64
Standard Deviation	0.22	0.21	0.28	0.26	0.28	0.29

4.7.1 LWD Stress Recovery Ratio

Stress recovery ratio (SRR) can be used to correct the stress under the plate assuming uniform stress distribution (σ_0 ~ 30 psi), and consequently would substitute variable *f* in Equation 4.3, to estimate surface modulus E_{LWD}. Instead of using constant numbers for the shape function *f*, an actual magnitude (i.e. SRR) which may vary based on the mechanical properties of geomaterials can be taken into account.

The models based on the elastic half-space theory, without considering the plate-soil interaction, have been the preferred method for interpreting the results obtained with LWD. The soil responses obtained from the dynamic nonlinear FE model that considers the soil-plate interaction were compared to those obtained from the static analysis to study the distribution of the stresses under the plate. The stress recovery ratio, SRR, was used to quantify the stress transferred from the LWD plate to the soil surface as:

$$SRR = \frac{\sigma_{ave}}{\sigma_0} \cdot 100\%, \tag{4.6}$$

where σ_{ave} is the average stress applied to the pavement by the LWD plate and σ_0 is the stress under the plate assuming uniform stress distribution (~30 psi). As an example, the stress distribution under the LWD plate is compared to the uniformly distributed stresses in Figure 4.7. The stress concentration at the edge of the plate is clear. The level of stress concentration depends on the nonlinear parameters of the soil. This

matter is of practical importance because the degree of stress concentration impacts the parameter *f* selected in Equation 5.1 for day-to-day analysis of the LWD data.

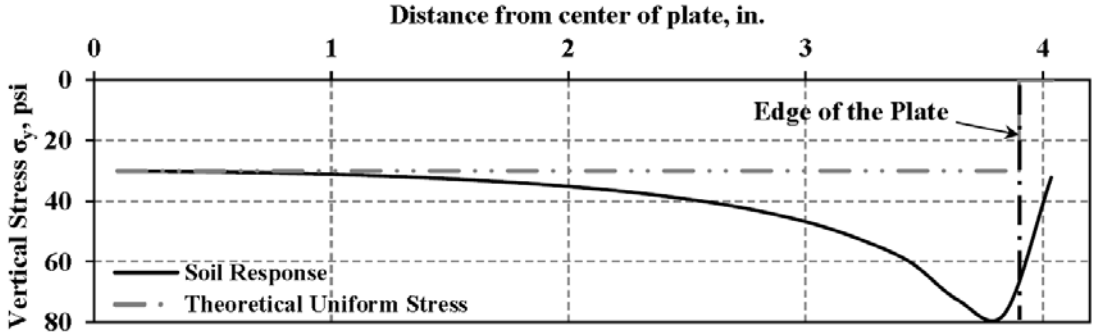

Figure 4.7 – Soil Responses under LWD and Theoretical Uniform Stress.

The impacts of the nonlinear k' parameters on SRR for this case are shown in Figure 4.8. SRR (stress concentration) increases with a decrease in k'_2 (material becomes less granular), and an increase in k'_3 (material becomes more cohesive).

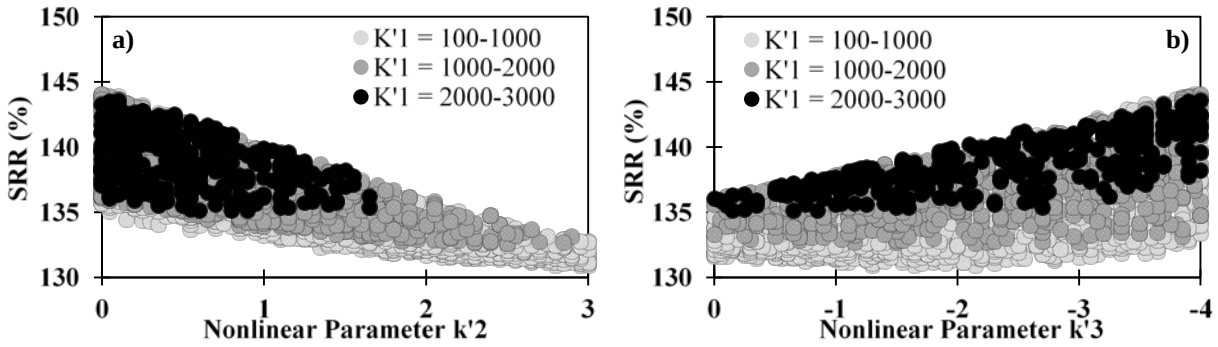

Figure 4.8 – Stress Recovery Ratio (SRR) for One-Layer Geosystem LWD Dynamic Analysis. (a) Impact of k'_2 of subgrade and (b) Impact of k'_3 of subgrade.

For the two layer geosystems, SRR can change with the variation of nonlinear parameters of base. The following equation was developed to estimate SRR so that the shape function *f* can be adjusted:

$$SRR(\%) = 142 + 5.02\ln\left(k'^{s}_{1} + 3.47 * 10^{-5}k'^{b}_{1}.h_b^2 - 0.0051k'^{b}_{1}.h_b\right) - 0.0195h_b - \\ - 4.98\ln\left(k'^{b}_{1}\right) - 6.89k'^{b}_{2} - 2.77k'^{b}_{3} \quad (4.7)$$

where k'^{b}_{i} are the nonlinear parameters for the base layer, and k'^{s}_{i} are nonlinear parameters for subgrade. Figure 4.9 presents the relationship between SRR estimated from the FE model and predicted from Equation 5.5. All estimated stress recovery ratios fall within a 10% uncertainty band.

Table 4.7 shows the influence of the nonlinear k' parameters on the stress recovery ratio calculated under dynamic LWD for the single and two-layer geosystems. For a single-layer system, parameter k'_2 impacts SRR the most. Parameter k'_1 is the second most significant factor for single layer systems. A two-layer system is more impacted by k'_2 of the base than the other nonlinear parameters. The nonlinear parameters of the subgrade tend to influence SRR less significantly, especially as the base thickness increases. With all this taken into account, the impact of nonlinear factors on the stress recovery ratio will become more constant when the base layer gets thicker, especially when the base is thicker than 10 in.

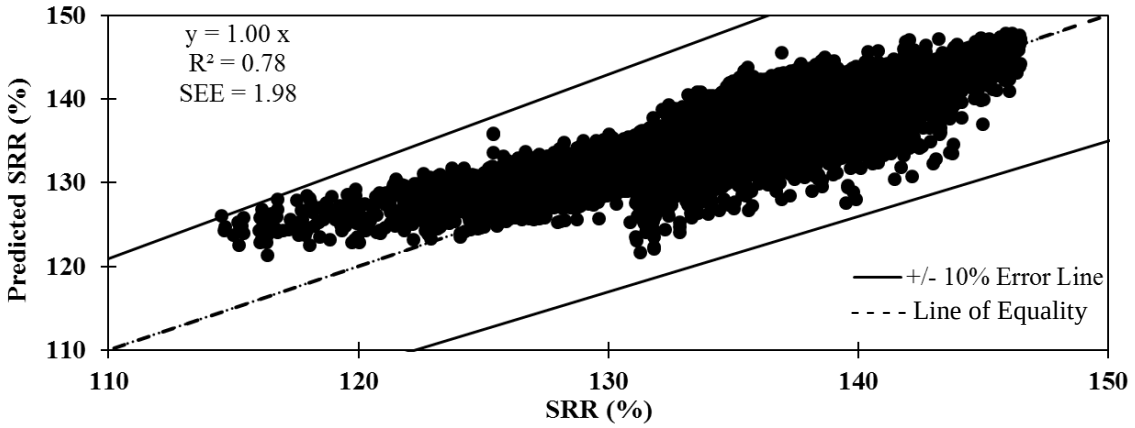

Figure 4.9 – Comparison of Estimated and Simulated Stress Recovery Ratios.

Table 4.7 – Impact of Nonlinear Material Parameters on Stress Recovery Ratio for Single and Two Layer Pavement Systems

Base Thickness, in.	Spearmann's Correlation Coefficients					
	Base Parameters			Subgrade Parameters		
	k'_1	k'_2	k'_3	k'_1	k'_2	k'_3
0 (Single Layer)	NA	NA	NA	0.64	-0.80	-0.53
6	0.12	-0.38	-0.13	0.44	-0.18	-0.03
7	0.22	-0.48	-0.15	0.39	-0.19	-0.05
8	0.32	-0.56	-0.17	0.33	-0.19	-0.06
10	0.49	-0.68	-0.21	0.19	-0.16	-0.06
12	0.59	-0.73	-0.24	0.09	-0.12	-0.05
14	0.64	-0.74	-0.27	0.02	-0.09	-0.04
16	0.67	-0.74	-0.29	-0.03	-0.07	-0.03
18	0.69	-0.74	-0.31	-0.06	-0.06	-0.03

4.7.2 LWD Depth of Influence

The results of the Spearman's correlation analysis carried out to determine the material nonlinear parameters that impact the depth of influence of one-layer geosystems are summarized in Table 4.8. The three nonlinear parameters show moderate to strong relationships to depth of influence. The greater k'_1 (stiffness of geomaterial) is, the shallower the depth of penetration will be. As parameter k'_2 increases (i.e., the material becomes more granular), and k'_3 decreases (i.e. material becomes less cohesive), the depth of influence increases.

Table 4.8 – Impact of Nonlinear Material Parameters on LWD's Depth of Influence for Single Layer Pavement Systems

Criterion for Determining Depth of Influence	Spearman's Correlation Coefficients					
	Static Analysis			Dynamic Analysis		
	k'_1	k'_2	k'_3	k'_1	k'_2	k'_3
Displacement	-0.46	0.65	-0.61	-0.54	0.71	-0.66
Stress	-0.49	0.54	-0.72	-0.54	0.82	-0.42

Table 4.9 shows the compiled results for the two layer geosystems. For the static model, k'_1 (stiffness) of the subgrade most significantly impact the depth of influence or both criteria being deflection or stress. The other parameters are of less of a significance. On the other hand, the depth of influence based on the dynamic models are influenced by different base and subgrade nonlinear parameters depending on the

response criterion selected. This study suggests that the nonlinearity of the soil and the dynamic nature of the impulse applied by LWD should be considered in selecting the target moduli.

Table 4.9 – Impact of Nonlinear Material Parameters on LWD's Influence Depth of for Two-Layer Pavement Systems

(a) Static Analysis

Criterion for Determining Depth of Influence	Spearman's Correlation Coefficients					
	Base Parameters			Subgrade Parameters		
	k'_1	k'_2	k'_3	k'_1	k'_2	k'_3
Deflection	0.13	0.19	-0.08	-0.56	0.07	-0.21
Stress	-0.33	0.04	-0.03	0.55	-0.05	0.10
Strain	0.01	0.26	0.17	-0.53	0.22	0.18

(b) Dynamic Analysis

Criterion for Determining Depth of Influence	Spearman's Correlation Coefficients					
	Base Parameters			Subgrade Parameters		
	k'_1	k'_2	k'_3	k'_1	k'_2	k'_3
Deflection	0.27	0.04	-0.07	-0.59	0.06	-0.26
Stress	-0.57	0.54	-0.10	0.12	0.12	0.03
Strain	0.29	0.66	-0.60	0.08	0.01	-0.05

4.7.3 IC Roller Depth of Influence

As shown in Table 4.10, k'_2 and k'_1 correlate the best with the depth of influence from stationary static nonlinear (SSN) models. The parameter k'_2 (granularity causing stress hardening) affects the most the influence depth from the vibratory stationary nonlinear (VSN). For the vibratory moving nonlinear (VMN) scenario, the parameters k'_3 (i.e. cohesiveness causing softening) and k'_1 (stiffness of geomaterial) impact the most the depth of influence based on displacement and stress criteria, respectively. For two layer geosystems, the nonlinear parameters of the subgrade affects the influence depth more, as shown in Table 4.10. However, the influence depth does not vary significantly.

Table 4.10 – Impact of Nonlinear Material Parameters on IC Roller Influence Depth for Single Layer System

Criterion for Determining Depth of Influence	Spearman's Correlation Coefficients					
	Based on Displacement Criterion			Based on Stress Criterion		
	Subgrade Parameters			Subgrade Parameters		
	k'_1	k'_2	k'_3	k'_1	k'_2	k'_3
SSN	-0.56	0.78	0.54	-0.54	0.26	0.32
VSN	0.02	0.08	-0.02	0.03	0.07	0.06
VMN	-0.58	0.63	0.70	-0.60	-0.28	0.03

4.8 Relating Pavement Responses under IC Roller and LWD

The displacements under different levels of sophistication of IC roller and LWD were compared in order to establish reliable relationships between the two devices. The results are summarized here.

4.8.1 Static LWD vs. Different Levels of Sophistication of IC-Roller

The displacements observed from the static LWD model and static stationary (SSN) IC-roller model agree well for single layer geosystems as shown in Figure 4.11. The average surface displacement under the static stationary IC roller with operating features mentioned in Table 4.2 is about 6 times the corresponding results gathered from the application of a uniformly distributed load (i.e., static LWD). However, the average pressure exerted by the drum was found to be about 51 psi which is 1.6 times the average pressure imposed by the LWD plate (i.e. 3030 psi).

Table 4.11 – Impact of Nonlinear Material Parameters on IC Roller Influence Depth for Two-Layer System

Level of Sophistication of FE Model		Spearman's Correlation Coefficients					
		Base Parameters			Subgrade Parameters		
		k'_1	k'_2	k'_3	k'_1	k'_2	k'_3
6 in. Base Thickness							
SSN	**Based on Displacement Criterion**	-0.09	0.30	0.18	-0.64	0.51	0.52
VSN		0.03	0.23	0.20	-0.62	0.29	0.58
VMN		0.01	0.14	0.24	-0.66	0.26	0.64
SSN	**Based on Stress Criterion**	0.04	-0.25	0.23	-0.66	0.55	0.44
VSN		0.04	-0.05	0.09	0.03	0.06	0.03
VMN		-0.08	-0.26	-0.08	-0.65	0.23	0.27
12 in. Base Thickness							
SSN	**Based on Displacement Criterion**	-0.06	0.35	0.15	-0.52	0.12	0.32
VSN		0.09	0.17	0.17	-0.51	0.03	0.34
VMN		0.09	0.11	0.23	-0.54	-0.03	0.36
SSN	**Based on Stress Criterion**	-0.17	-0.05	0.05	-0.51	0.53	0.39
VSN		-0.01	0.01	0.04	-0.17	0.08	0.02
VMN		-0.17	-0.31	0.02	-0.50	0.36	0.25

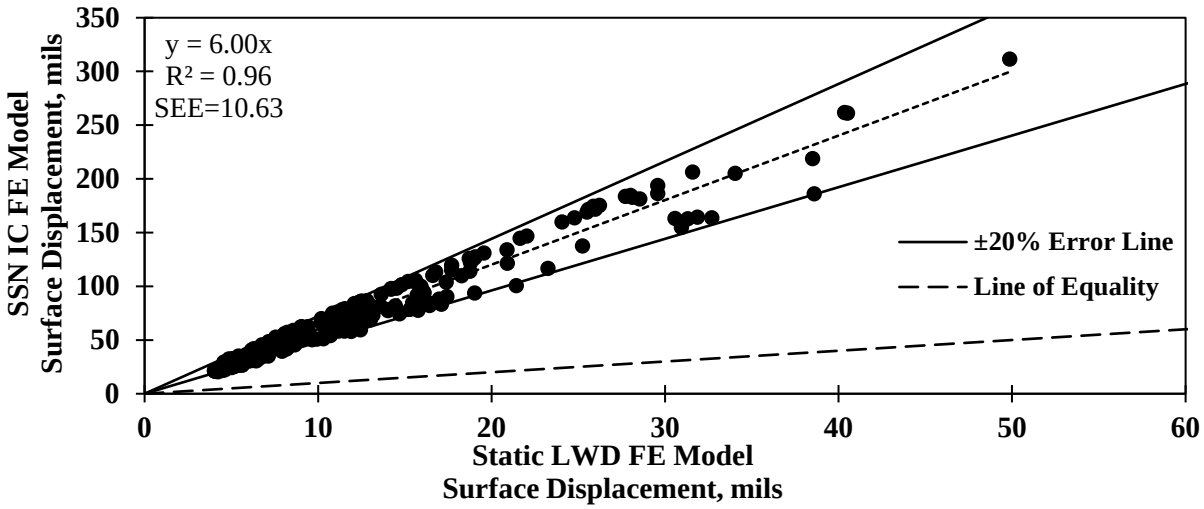

Figure 4.10 – Relationship of Surface Displacement between Static LWD and Static Stationary Nonlinear (SSN) IC Roller for Single Layer Systems.

The displacements for the two-layer geosystems obtained from the static stationary drum (SSN) and static LWD FE models for 6 in. and 12 in. base thickness are shown in Figure 4.11. The slopes of the fitted lines increased for the two-layered geosystems to about 7.6. In addition, the data points representing the displacements for the two layer systems are more dispersed in comparison to the corresponding ones obtained for single-layer systems. In other words, the surface displacements for the two layer systems seem to be correlated with some uncertainty as judged by the number of cases falling outside the ±20% error bounds. With a more sophisticated model that included more pavement parameters these relationships can be improved.

Table 4.12 demonstrates the descriptive statics for correlation of different levels of sophistication of the IC-roller with the corresponding results obtained from the static LWD model. Similar to the static cases, the dispersion in the results increases with an increase in the thickness of the base for vibratory FE models.

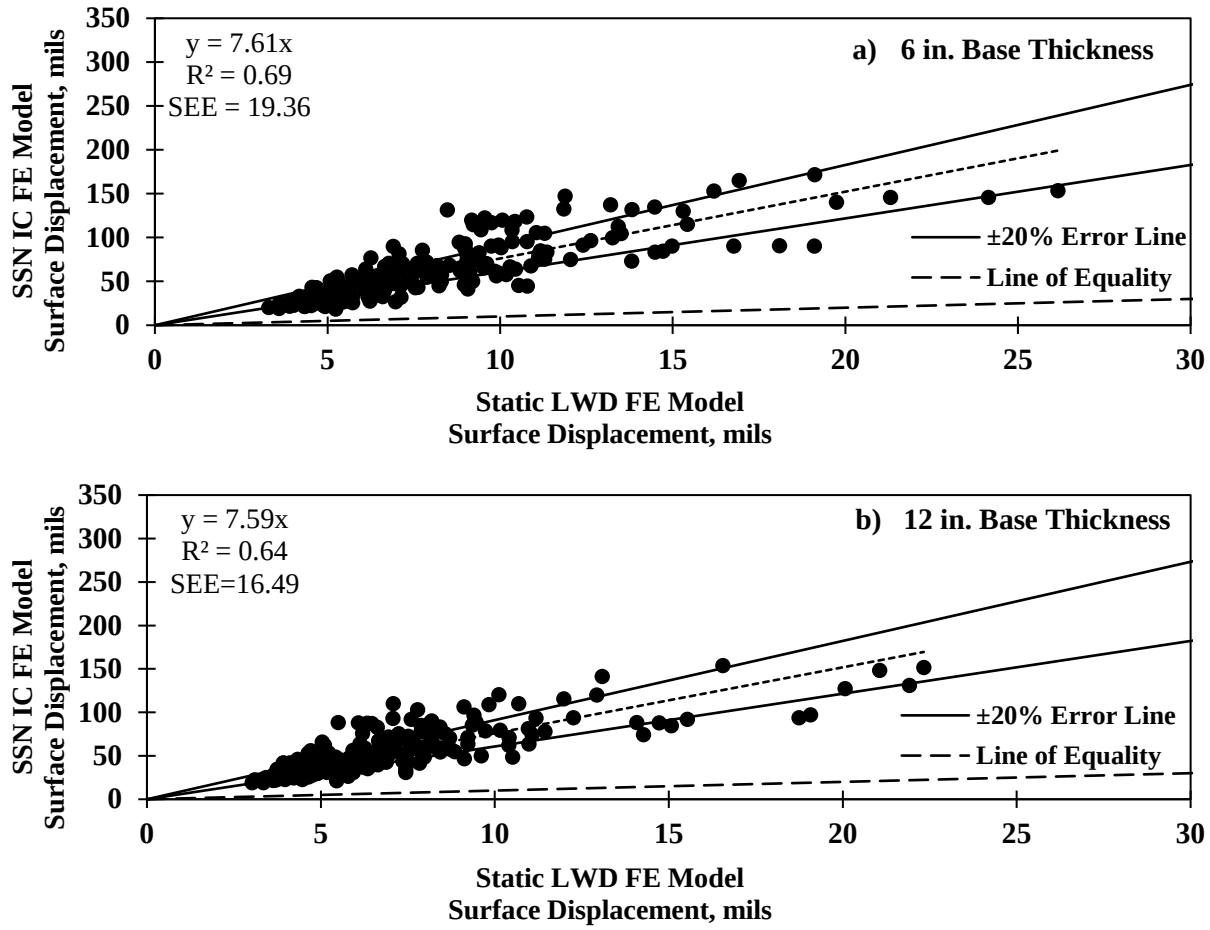

Figure 4.11 – Relationship of Surface Displacement between Static LWD and Static Stationary Nonlinear (SSN) IC Roller for Two Layer Systems.

Table 4.12 – Descriptive Statics for Correlation of Maximum Surface Displacement Obtained from Static LWD and Different Levels of Sophistication of IC Roller for Single and Two-Layer Systems

Model	Slope of Fitted Linear Relationship, S			Coefficient of Determination, R^2			Standard Error of Estimate, SEE		
	SSN	VSN	VMN	SSN	VSN	VMN	SSN	VSN	VMN
Single Layer System	6.00	5.58	6.08	0.96	0.93	0.87	10.63	7.89	10.82
6 in. Thick Base	7.61	7.45	8.40	0.69	0.75	0.58	19.36	16.14	22.22
12 in. Thick Base	7.59	7.82	8.28	0.64	0.56	0.48	16.49	16.56	17.25

4.8.2 Dynamic LWD vs. Different Levels of Sophistication of IC Roller

The maximum surface displacements recorded form the dynamic LWD (D-LWD) model and different levels of sophistication of the IC roller FE models are compared in Table 4.13. The average surface displacements recorded from different IC-roller scenarios are about 4.5 times the comparable results obtained from D-LWD cases for single layer geosystems. The same pattern was observed for the two layer systems.

Table 4.13 – Summary of Descriptive Statics for the Correlation of Maximum Surface Displacement Obtained From Dynamic LWD and Different Levels of Sophistication of IC Roller for Single and Two-Layer Systems

Model	Slope of Fitted Linear Relationship, S			Coefficient of Determination, R^2			Standard Error of Estimate, SEE		
	SSN	VSN	VMN	SSN	VSN	VMN	SSN	VSN	VMN
Single Layer System	4.45	4.17	4.54	0.86	0.92	0.84	19.95	13.22	16.54
6 in. Thick Base	5.03	4.95	5.59	0.65	0.75	0.60	20.59	16.17	21.92
12 in. Thick Base	4.91	5.09	5.40	0.59	0.58	0.53	17.93	16.73	17.11

4.9 Bridging Relationship

The linear relationships presented in the previous section may not reflect a robust relationship between the two devices. To improve those relationships, a comprehensive correlation analysis was carried out. This process was adopted to fit different nonlinear functions considering the transformation of all input parameters (e.g. $\sqrt{k_i'}, \ln k_i', \exp k_i'$). The development of such relationships from the numerical data are explored here.

4.9.1 Static Stationary Nonlinear (SSN) IC-Roller vs. Static Nonlinear LWD

Based on the Spearman's correlation analysis of the IC drum displacement and the nonlinear material parameters, the surface displacements for the single and two layer systems were found to be more sensitive to the nonlinear parameters of the subgrade. Hence, to develop a robust relationship between the LWD surface displacement, d_{LWD}, and the surface displacement under the IC-roller, the base thickness (h_b) and the nonlinear k' parameters of subgrade were taken into account in the general form of:

$$d_{IC-Roller} = f\left(k_i'^{S}, h_b, d_{LWD}\right) \tag{4.8}$$

The best prediction of the surface displacement (d_{SSN}) under the regular static stationary roller (SSN) with the operating features discussed in Table 4.2 is provided by Equation 88.2:

$$d_{SSN} = C_1 d_{S-LWD} + \frac{C_2 - C_3 h_b k_3'^{S}}{k_1'^{S}} - k_2'^{S} d_{S-LWD} \tag{4.9}$$

where $C_1 = 6.85$, $C_2 = 50.7$, $C_3 = 0.432$, $k_i'^{S}$ are the nonlinear parameters of subgrade, and $d_{S\text{-}LWD}$ the surface displacement obtained from the application of static LWD. As shown in Figure 4.12, the proposed equation provides a good estimate of the IC SSN responses, with an R^2 value of 0.91 and standard error of estimate of 12.2 mils. The proposed relationship adequately relates the two surface displacements.

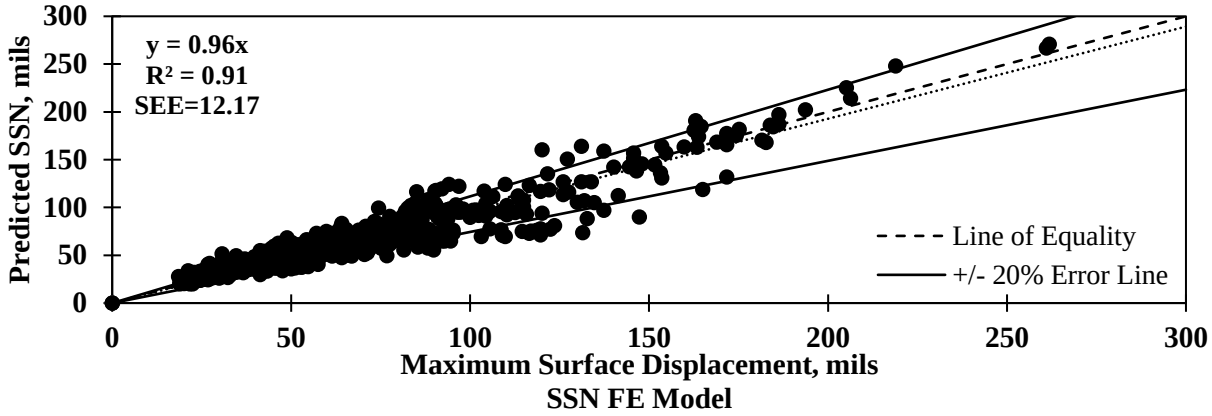

Figure 4.12 – Predicted SSN Surface Displacement vs. surface displacement from SSN FE Model.

4.9.2 Vibratory Stationary Nonlinear (VSN) IC-Roller vs. Dynamic Nonlinear LWD

Similar to the static FE nonlinear models for both IC and LWD, a function to predict the surface deflection of IC roller as obtained from the VSN FE model using the dynamic FE model of the LWD was developed. The Spearman's correlation study for the VSN IC model concluded the nonlinear parameters k'_1 and k'_2 of subgrade had a significant effect on the surface displacement for both single and two-layered systems. The following equation was found to be as a good predictor for the surface displacement for a vibratory stationary roller (VSN):

$$d_{VSN} = C_1 d_{D-LWD} + \frac{C_2 - C_3 h_b k_3'^s}{k_1'^s} - k_2'^s d_{D-LWD}, \quad (4.10)$$

where d_{VSN} is VSN IC roller surface displacement, C_1 = 4.83, C_2 = 134.29, C_3 = 0.372, and $d_{D\text{-}LWD}$ is the surface displacement obtained from the application of dynamic LWD.

The estimated displacements under the vibratory stationary drum agree well with the results gathered from the VSN forward model (shown in Figure 4.13). Equation 4.10 predicts VSN IC surface displacements with an R^2 value of 0.91 and the *SEE* magnitude of 10.8 mils.

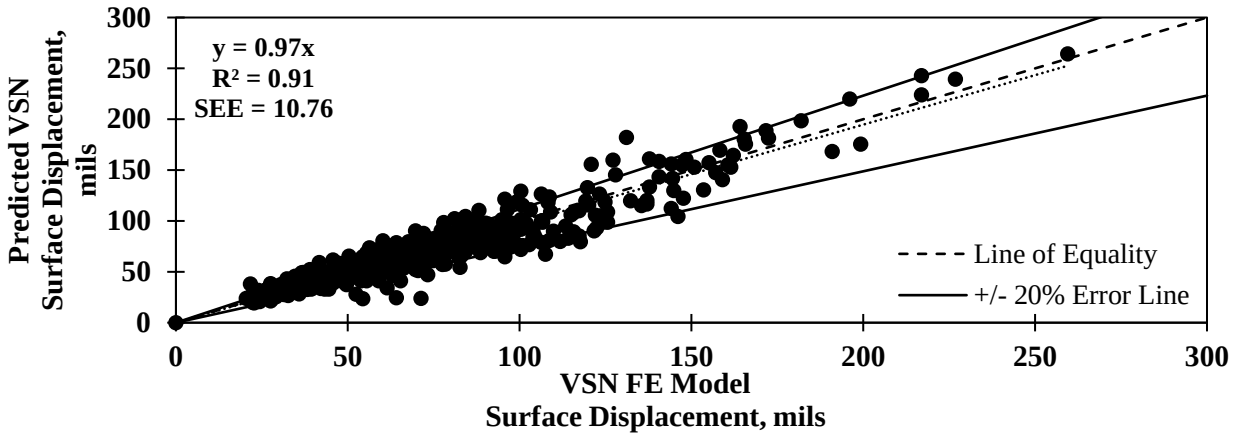

Figure 4.13 – Predicted VSN Surface Displacement vs. Surface Displacement from VSN FE Model.

4.9.3 Vibratory Moving Nonlinear (VMN) IC-Roller vs. Dynamic Nonlinear LWD

Similarly, the correlation analysis was carried out for the compiled results recorded from VSN IC-roller and D-LWD. The following equation is suggested to predict surface displacement (d_{VMN}) under a vibratory moving roller (VMN):

$$d_{VMN} = C_1 - \ln(k_1'^s) - C_2 k_2'^s + C_3 k_3'^s (C_4 h_b - 1) + C_5 {d_{D-LWD}}^2, \quad (4.11)$$

where C_1 = 8.59, C_2 = 0.725, C_3 = 0.389, C_4 = 0.0012, C_5 = 1.62, and $d_{D\text{-}LWD}$ is the surface displacement under dynamic LWD. Figure 4.14 shows that the predicted surface displacements for VMN cases are in a good agreement with the results obtained from VMN forward model.

4.10 Conclusion

This report consists of the determination of the different operational responses obtained from a LWD and a regular IC-roller. The report provides a means for accounting for the impact of these mechanisms on the measured responses and depths of influence. Both static and dynamic finite element models were studied considering the nonlinear material models for the geomaterials. Representative transfer functions were developed to adjust the surface deformations and moduli obtained from the elasto-static layered theory to account for the nonlinear and dynamic nature of the LWD tests. For the specific LWD studied here, the dynamic modulus was on average 0.58 times the LWD static modulus.

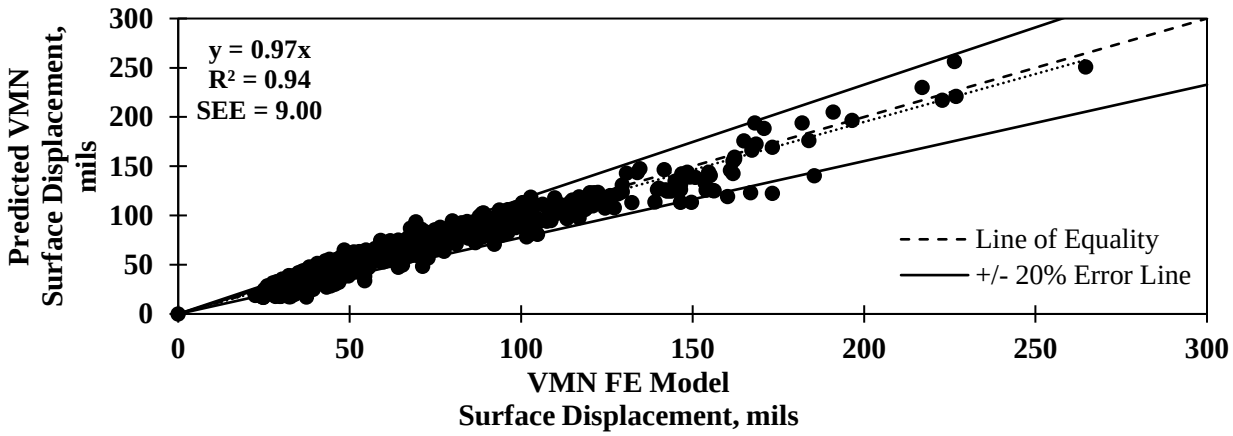

Figure 4.14 – Predicted VMN Surface Displacement vs. Surface Displacement from VMN FE Model.

The depth of influence of LWD plays an important role in setting the target moduli for layered geosystems. The depth of influence under the dynamic loads are deeper than from the static loads. Also, the nonlinear nature of the material and the response used to determine the depth of influence play a role in the final outcome. The rigidity factor used in the Boussinesq theory is also a source of uncertainty in the analysis. The stress distribution under the plate was represented with the stress recovery ratio, for dynamic and static models, for one and two layer systems. SRR for one layer geosystems varies from 130 to 145%. For the two layer geosystems, SRR varied from 110 to 150%. A relationship was proposed to predict SRR as a function of the thickness of the base and nonlinear parameters of the base and subgrade. The proposed relationships can be used to estimate more representative target LWD moduli using the nonlinear parameters obtainable from laboratory resilient modulus testing.

To quantify the effectiveness of the roller compaction, the effective depth of compaction must be considered. This depth depends on the underlying materials, in addition to the roller weight, dimension and operating conditions. A parametric study was carried out to evaluate the influence of the geomaterials' properties on the depth of influence by taking into account the different levels of sophistication of FE models. The normalized depth of influence with respect to the contact width is about $z/B = 6$ (about 80 in.) using a displacement criterion consisting of a depth where the displacement induced by the maximum load reduces to about 10% of the surface deflection. When a stress criterion is used, the normalized depth of influence reduces to about $z/B = 4$. Depth of influence increases 4 to 8% when a base layer is included. The stiffness of the subgrade, represented by nonlinear parameter k'_1, had the most significant impact on the depth of influence, followed by the stress hardening parameter k'_2 of the subgrade. The stiffer the geomaterial is, the shallower the depth of influence will be. Depth of influence also increased with granularity of the material, especially in single layer systems. Single layer systems also offered more variation in terms of depth of influence, ranging from $z/B = 4.3$ to 6.8.

The displacements under different levels of sophistication of IC roller and LWD were compared in order to establish reliable relationships between the two devices. Even though the average pressure exerted by the drum was found to be 1.6 times the average pressure imposed by the LWD plate, the average surface displacement under the static stationary IC-roller is about 6 times the corresponding results gathered from the application of a uniformly distributed load (i.e., static LWD). The average surface displacements recorded from different scenarios of IC-rollers are about 4.5 and 5 times the comparable results obtained from dynamic LWD cases for single and two layer geosystems, respectively. Different functions were used to bridge the responses of IC-roller and LWD. These functions includes thickness of the base and nonlinear parameters of the base and subgrade to predict surface displacement beneath a drum.

This study clearly demonstrate that a number of fundamental issues that impact the implementation of modulus-based specifications can be understood and reconciled in a scientific manner for an effective implementation.

5 DATA COLLECTION AND DESIGN VERIFICATION

5.1 Design Verification Process

The field tests performed in the construction sites, along with the additional tests in the laboratory, are part of the process proposed under the specification for estimating the uniformity and mechanical properties of compacted geomaterials for design verification. Figure 5.1 illustrates through a flowchart the design verification process.

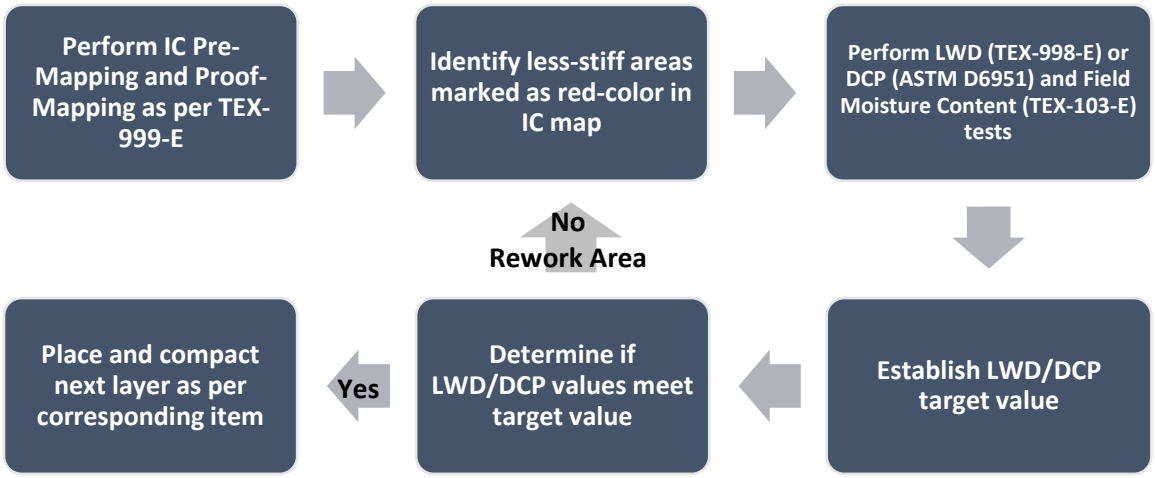

Figure 5.1 – Design Verification Process.

The field test protocol performed by the research team at each test bed for each layer is summarized in the following steps:

1. **Identify test strip.** The research team coordinated with the contractor and TxDOT personnel to identify a 250 ft (minimum) to 500 ft (maximum) long, full width test strip.
2. **Set up GPS.** The research team set up the GPS base station.
3. **Set up IC roller.** The research team coordinated with the contractor to setup the IC roller for proper data collection. This included verification of operating frequency, speed and amplitude. Compactor was instrumented with UTEP developed data acquisition system (DAQ).
4. **Carry out construction as normally done.** The research team observed the construction and compaction of test section but did not interfere with the operation. Shortly after compaction the following steps were performed at a time that was least disruptive to the contractor.
5. **Identify spot test locations.** Using the test section layout, the research team identified 44 locations for NDT spot test arranged as grid consisting of four rows along the full width, each consisting of 11 points. Each row was located at the below the coverage of each roller pass. All rows that were equally spaced, adjusted to meet the full width of the site. The selected number of spot test was used to establish the variability in the measurements.
6. **Proof-map test strip.** The research team and contractor personnel proof-mapped the compacted subgrade with IC roller or instrumented roller after compaction. Test section was proof-mapped using one forward pass of the IC roller shortly after compaction.
7. **Perform modulus-based NDT field tests.** NDT field tests were performed by the research team using modulus-based NDT devices, i.e., light weight deflectometer (LWD) and dynamic cone penetrometer (DCP), on prepared subgrade after proof-mapping.
8. **Perform in-situ moisture measurements.** Contractor or TxDOT representative performed nuclear density gauge (NDG) testing on the underlying layer.
9. **Retrieve samples for determination of moisture in the laboratory.** The research team collected samples for further laboratory testing to validate NDG moisture results.

10. **Prepare and compact the base layer.** The contractor carried out construction of base layer. The research team did not interfere with the operation.
11. **Proof-map the completed base with an IC roller after compaction.** After setup of GPS and IC roller (Steps 2 through 3) by the research team in coordination with the contractor and TxDOT personnel, the proof-mapping of the test section was performed where prior evaluation of the subgrade had carried out.
12. **Perform modulus-based NDT field tests.** NDT field tests were performed by the research team using modulus-based NDT devices, i.e., light weight deflectometer (LWD) and when available falling weight Deflectometer (FWD), on prepared base after proof-mapping.
13. **Perform in-situ moisture measurements.** Contractor or TxDOT personnel performed nuclear density gauge (NDG) testing on the underlying layer.
14. **Retrieve samples for determination of moisture in the laboratory.** The research team collected samples for further laboratory testing to validate NDG moisture results.

Laboratory resilient modulus and moisture-density tests were conducted on the samples extracted from the subgrade and unbound granular base at several moisture contents.

5.2 IC Data Collection Process and NDT Modulus-based Testing

At each construction site, the contractor's routine compaction process was followed by a proof mapping. The goal of the proof mapping, also known as final coverage, was to evaluate the compaction uniformity through the identification of less stiff spots and to ensure the complete coverage of the compacted section.

A map with IC data, in the generic form of Intelligent Compaction Measurement Values (ICMV), is rendered by vibratory compactors with IC technology. However, the research team had foreseen that IC rollers may not be readily available in construction sites. For that reason, a data acquisition system (DAQ) developed at UTEP was used to collect vibration data and ground response during IC operations. A schematic of the system is depicted in Figure 5.2. The system consists of two accelerometers that are mounted on the roller (drum), a data acquisition box, a real time kinematic (RTK) GPS antenna and receiver, a power supply and a laptop computer to monitor the data collection process, shown in Figure 5.3. Instrumentation of IC rollers is illustrated in Figure 5.4. This tool provides the operator with a detailed analysis of the input IC signal for each of the recording channels as well as an on-site mapping of the test area based on CMV values.

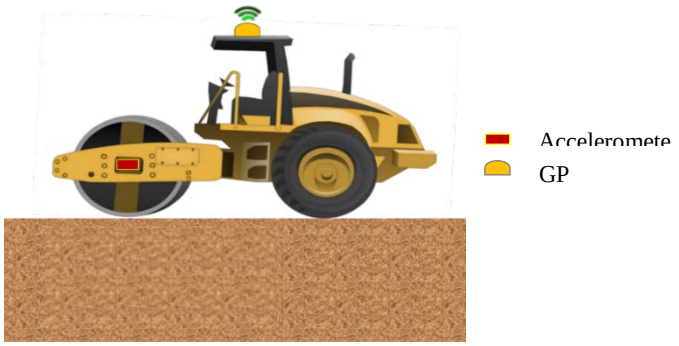

Figure 5.2 – Schematic of the IC Calibration System.

An example of an accelerometer time history is illustrated in Figure 5.5. A GPS unit mounted on the roller is used for geo-referencing. The measured time history is subjected to appropriate filtering and then transformed into the frequency domain using a Fast-Fourier Transform (FFT) algorithm. The FFT of a time signal represents the frequency composition of the signal. An example of the amplitude spectrum (amplitude vs. frequency) after those operations on the time-record data is shown in Figure 5.5. The fundamental frequency and its multiples as well their associated amplitudes were extracted from that amplitude spectrum.

Figure 5.3 – Components of the Data Acquisition System Developed at UTEP.

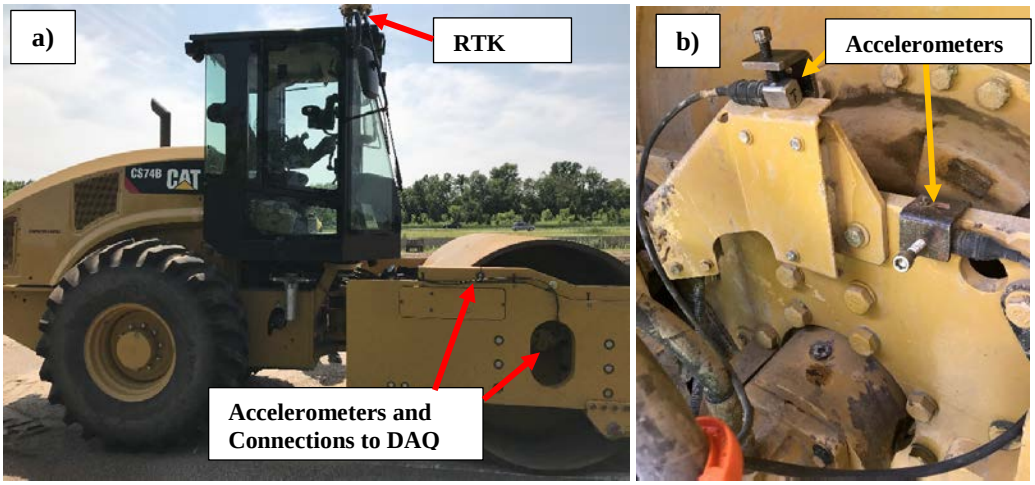

Figure 5.4 – Field Site Instrumentation of Roller Compactor: (a) RTK GPS and Wiring of Accelerometers to Data Acquisition System and (b) Installation of both Accelerometers to Measure Vertical and Horizontal Vibration on Roller Compactor Drum Frame.

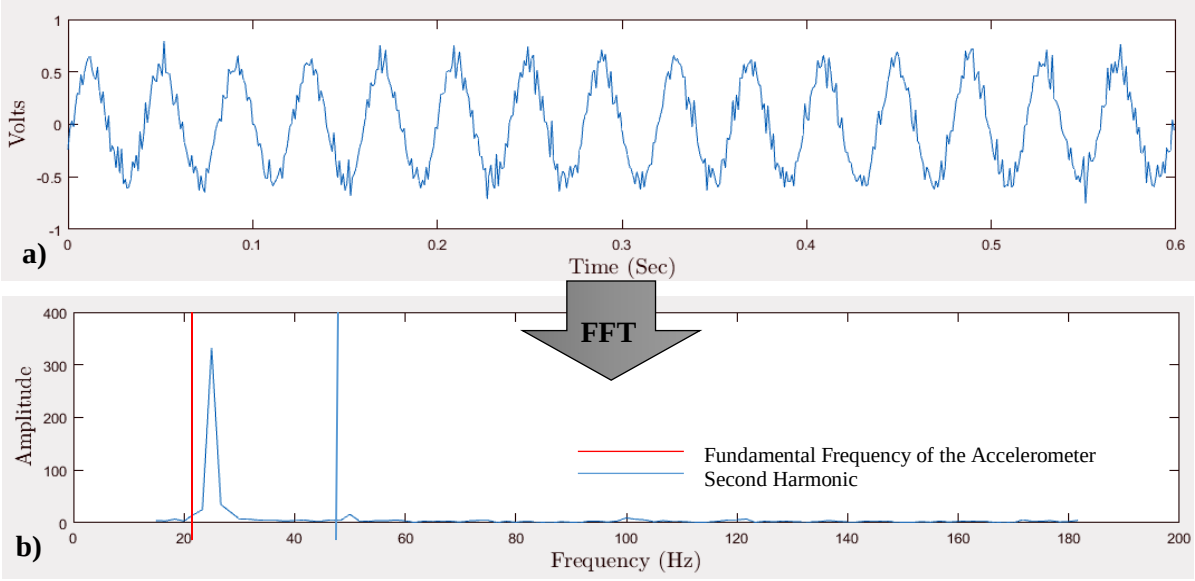

Figure 5.5 – Transforming Sensor Data from Time-Domain (a) to Frequency Domain (b) Employing an FFT Algorithm.

The precision of the analysis in the frequency-domain, Δf, is controlled by the number of data points selected from the time-domain record, N, and the rate of sampling the data in the time-domain, Δt, through:

$$\Delta f = \frac{1}{N\Delta t} \tag{5.1}$$

As such, the fewer the number of data points and the more densely the time records are sampled, the lower the resolution of the data analysis in the frequency domain. In the first glance, it may seem appropriate to utilize more data points to improve the frequency resolution even further. However, such action has an unintended consequence. As more data points are used, the length of the data collected increases. Since the roller is moving during the IC operation, the longer time length translates to longer distance between the data points reported, i.e., the ability of the roller to spot less stiff areas decreases.

Figure 5.6 demonstrates the steps performed to analyze accelerometer. Once the FFT algorithm is applied to a block of data, the appropriate calibration is applied to convert voltage output spectrum to acceleration spectrum. The accelerometer data are then integrated once to obtain velocity spectrum and once more to obtain deflection spectrum.

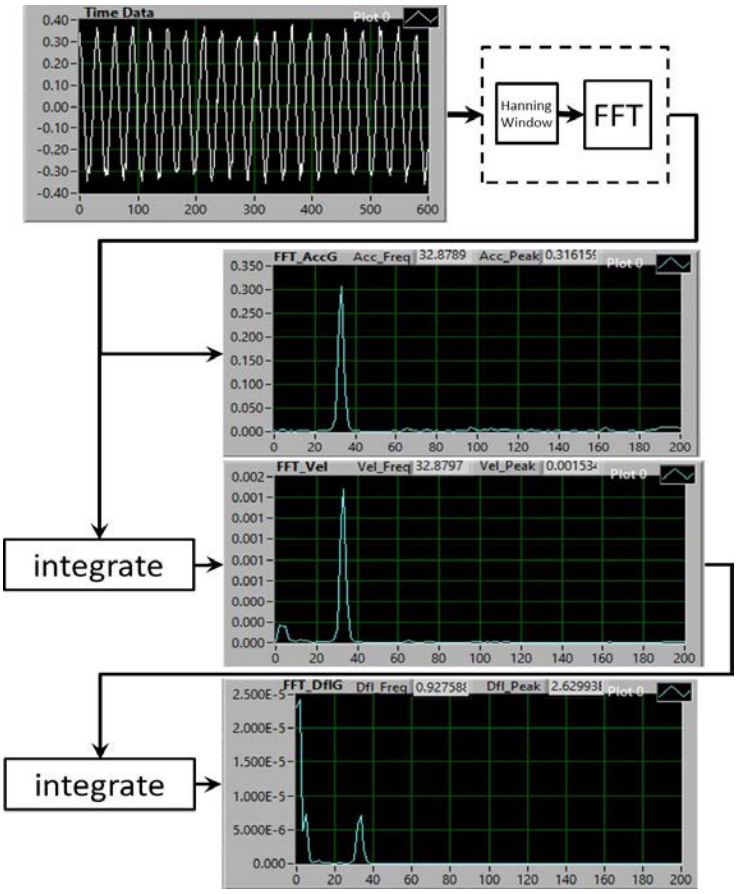

Figure 5.6 – Steps Performed to Analyze Accelerometer Data.

Figure 5.7 shows a map of the IC data points where ICMVs were obtained by the UTEP DAQ system during the mapping of in a section on SH 183 in Irving. Four passes, in both forward and reverse directions of the roller, are discernible. Each line, i.e. roller pass, is comprised by a series of points representing a GPS location where an ICMV reading is recorded. The UTEP DAQ system records five ICMV readings per second. For a roller speed of 3 mph, ICMVs are recorded at a rate of about 0.9 fps.

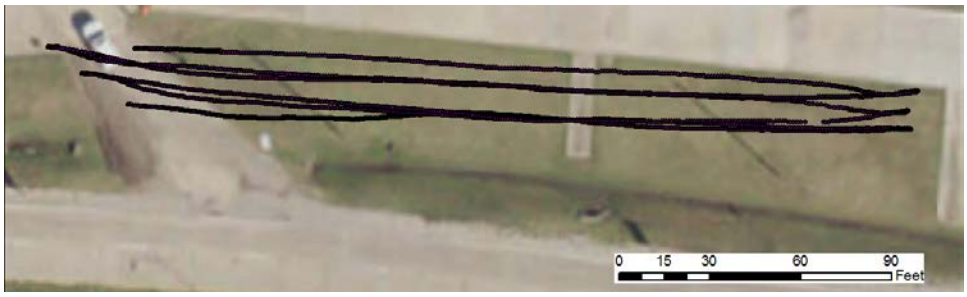

Figure 5.7 – IC Data Points Collected During Mapping of a Test Layer (SH 183 in Irving).

Geo-statistical and geospatial data analysis techniques were employed to visualize and interpret the IC data by means of color-coded maps. These maps display the geo-referenced or spatial data on a map in which each class is separated by different colors. In this study, three colors, green, yellow and red, were used for creating a color-coded map. The goal of using the ICMV color-coded maps is to identify the less stiff areas (usually marked as red spots) throughout the construction area. An example map is shown in Figure 5.8.

Figure 5.8 – CMV Variation Map Using ArcMap.

Compacted geomaterials may exhibit high spatial variability in their mechanical properties. Since it is impractical to estimate the exact position of the roller (due to its size), it is virtually impossible to estimate ICMV at a specific point so that it can be relate to other modulus-based measurements. For this reason, a grid was established equal to the width of the roller and the length equal to about 1/10th of the length of the test site. The grid is represented by rectangular (buffered) areas that are practical to rework, as shown in Figure 5.9 for the same test section mapped in Figure 5.7. For visualizing a simplified representation of IC data, all ICMV measurements falling inside each rectangular buffered area can be statistically analyzed by means of average or other summary statistics to represent the level of compaction and uniformity of that area.

Figure 5.9 – Data Collected by IC Roller on top of a Test Layer Divided in Rectangular Buffered Areas (SH 183 in Irving).

Modulus-based nondestructive measurements were carried in the vicinity of the center of each rectangular area for studying the relationship of the stiffness of the material as measured by these NDT devices with the ICMV measurements as obtained after proof-mapping with IC technology (see Figure 5.10).

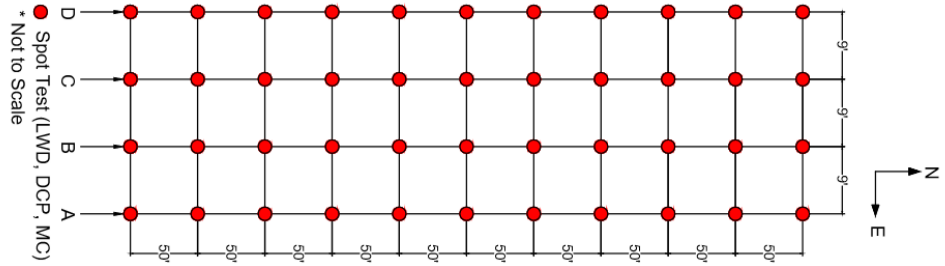

Figure 5.10 – Schematic of a Typical Test Section and Locations of Spot Tests.

5.3 Complications and Limitations in ICMV Data Acquisition

This section briefly describes some of the practical complications the research team encountered during the implementation of IC on the visited sites in this project, the observed practical limitations and corresponding suggestions to address the complications.

Most ICMV estimation algorithms implement a gridding algorithm that makes use of geostatistics to extrapolate the data for the purpose of generating a map. Rather than providing the raw data captured by the accelerometers as an output file, these software packages provide processed data. To address this issue, a data acquisition system has been developed to capture the accelerometer's readings, to calculates the CMV values, and to generate color-coded maps of the CMVs without any post-processing and extrapolation involved.

Figure 5.11a shows CMV distribution map obtained by UTEP system. The roller path is superimposed onto the rectangular blocks which are centered at the spot test (LWD and DCP) locations. The roller path is comprised of several geo-referenced points at which IC data is collected. Figure 5.11b illustrates the number of geo-referenced data points falling within each block. Some blocks are not covered by the roller, while some others contain few geo-referenced data points due to the roller passing very close to the edges of the rectangular blocks. No CMV values are assigned to blocks with no CMV values. In order to avoid this complication, it is imperative for the roller operator to drive on a straight line throughout each pass which would lead to complete coverage of the test area.

Another important factor that the roller operator needs to be aware of is the importance of maintaining a constant speed. Mooney et al. (2010) found that CMV and CCV decreased with increase in roller speed. At a constant rate of readings, any variation in the roller speed would lead to an uneven distribution of number of data points falling within each block which could dramatically impact the CMV average values for each of the blocks as well as the output map. Figure 5.12 shows how different number of data points results in different details in CMV values. CMV averages are computed for three different number of data points (200, 600 and 1000 data points). Even though the CMVs demonstrate roughly equal mean values, more detail is evident in CMV values computed for higher number of data points.

Figure 5.13 demonstrates the influence of variation in the roller vibration frequency by comparing the spectrograms from two data points in two different blocks. One of these blocks is at the beginning of a pass and the other one is located along the pass. As shown in Figure 5.13b, the second harmonic (first multiple of the operating frequency) has a relatively high amplitude as compared to the fundamental frequency, followed by high amplitude random noise. Conversely, the spectrogram in Figure 5.13c exhibits a lower ratio of second harmonic to the fundamental frequency amplitudes; hence a more reasonable CMV value for the corresponding block. This pattern leads to a high CMV. The source of this problem is transitioning from one pass to other before the roller is in full operational vibration mode. At the beginning of each pass,

the roller revs up the system until it reaches the operating frequency whereas, at the end of each pass, the roller is slowed down. In both cases, the recordings are impacted by the change in the operating frequency.

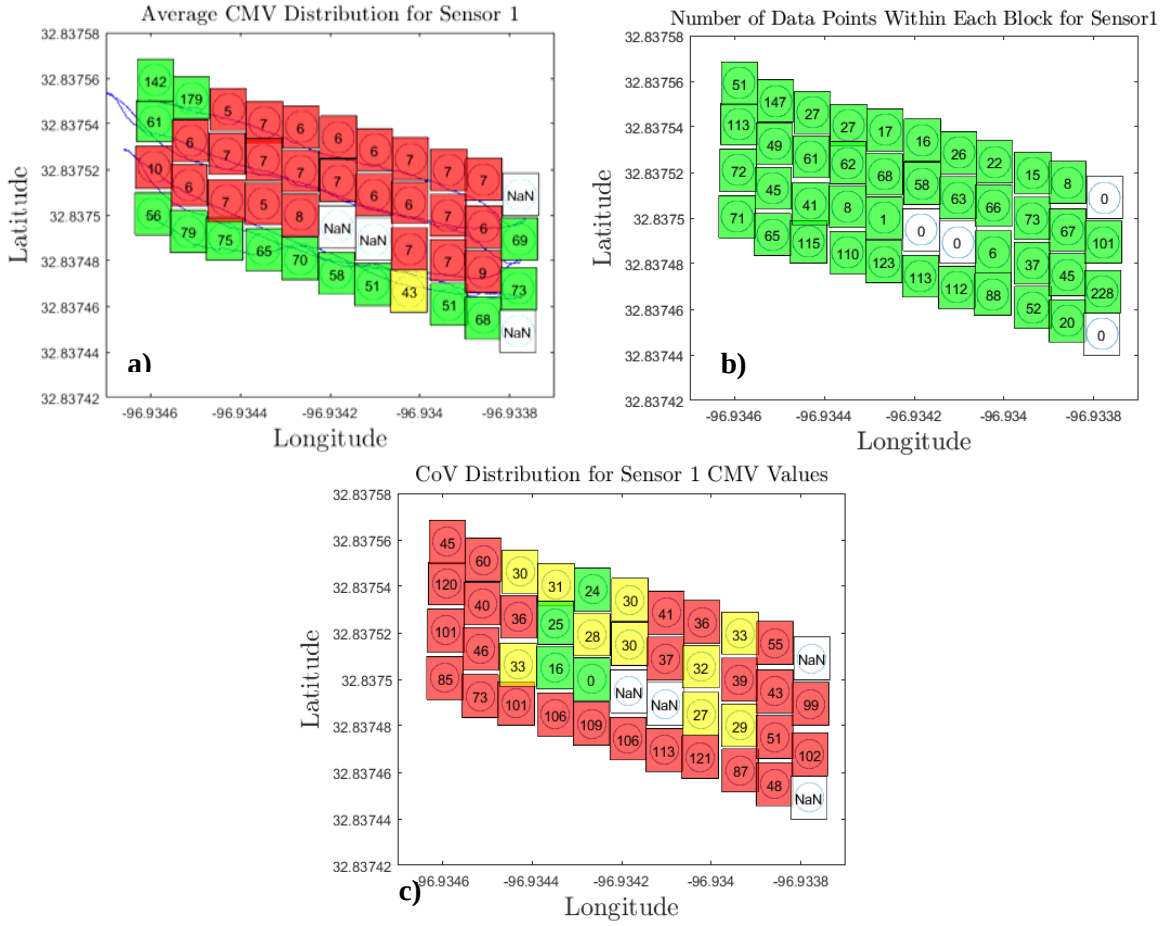

Figure 5.11 – (a) Spatial CMV Distribution Map Obtained from UTEP System. (b) Map of the Number of Data Points Falling within Each Rectangular Block. (c) Coefficient of Variation (COV) Map.

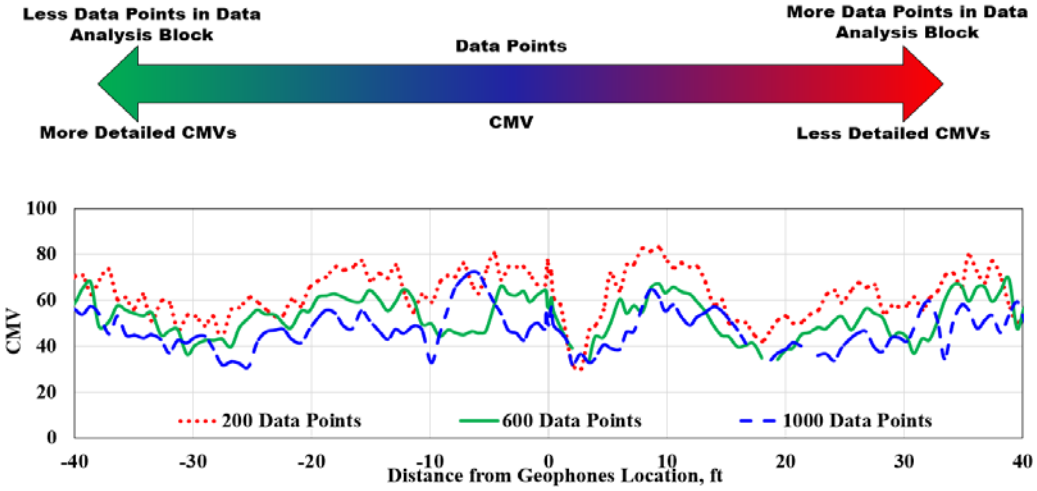

Figure 5.12 – Impact of the Number of Data Points on the Computed CMV Averages.

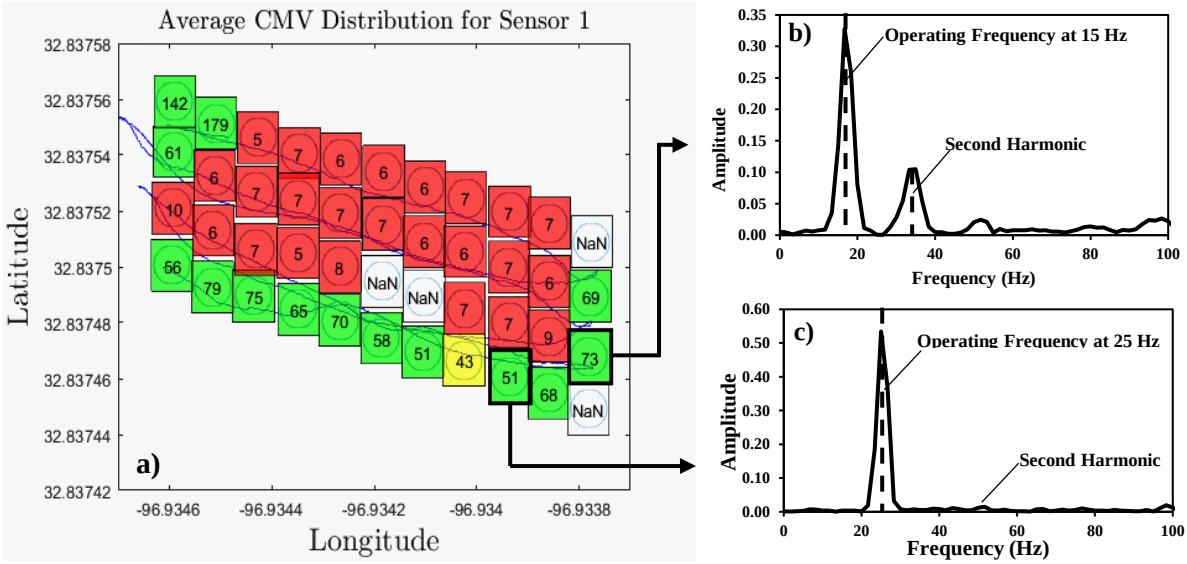

Figure 5.13 – Typical Spatial CMV Distribution Map.

In order to address this complication, it is recommended to either start the data collection after the desired operating frequency is reached or to extend out the test area by a pre-determined length (e.g. 10 ft to 15 ft) at the beginning and the end of each pass.

5.4 In-Situ Spot Tests Performed in Conjunction with IC Roller

The relationships between the measurements and mechanical properties as determined by conventional NDT spot tests and ICMV data were studied using data collected for this and previous projects. All selected test sections were evaluated using one or more of the following devices:

- **Light Weight Deflectometer (LWD)**, is a portable Falling Weight Deflectometer (PFWD) that has been developed as an alternative in-situ testing device to the plate load test as shown in Figure 5.14a. Similar to FWD, the LWD determines the stiffness of pavement system by measuring the material's response under the impact of a load with a known magnitude and dropped from a known height. LWD reports the composite modulus of the layers with the estimated depth of influence of about 6 ft. The LWD tests were performed in this project following the ASTM E2583.
- **Dynamic Cone Penetrometer (DCP)**, test involves driving a cone shaped probe into the soil or aggregate layer using a dynamic load and measuring the advancement of the device for each applied blow or interval of blows as shown in Figure 5.14b. The depth of penetration is a directly impacted by the drop height of the weight, cone size, and cone shape. Also, the resistance to penetration is dependent on the strength of the material. The strength, in turn, is dependent on density, moisture, and material type of the layer evaluated. The standard test method as per ASTM D6951 was followed to perform DCP tests during field evaluations to determine the number of DCP blows.

Field samples of subgrade materials were collected for estimation of index properties and oven dry (as per ASTM D2216) tests. The following moisture/density and stiffness based tests were also performed during at some of the sections:

- **Falling Weight Deflectometer (FWD)**, is a non-destructive test method for achieving in situ characterization of the pavement layer stiffness. The FWD applies dynamic loads to the pavement surface, simulating the magnitude and duration of a single heavy moving wheel load as shown in Figure 5.14c. The deflection bowl resulting from the impulse load is measured using geophones adjusted to a predetermined set of distances from the loading plate. Backcalculation of layer moduli is carried after a complex iterative procedure. TxDOT uses the MODULUS® program to perform the backcalculation of layer moduli.

Figure 5.14 – Nondestructive Tests Carried Out During This Study.

- **Plate Load Test (PLT)** is a field test for determining the ultimate bearing capacity of soil and settlement under a given load. The procedure consists of loading a steel plate placed at the foundation level (as shown in Figure 5.14d and recording the settlements corresponding to each load increment as per ASTM D1195. The test load is gradually increased till the plate starts to sink at a rapid rate.
- **Nuclear Density Gauge (NDG)**, test involves the use of a radioactive source that emits gamma radiation into the soil and a sensor measures the reflected radiation for determining in-place density and moisture of soil following ASTM D6938 procedure as shown in Figure 5.14e.

An extensive implementation of IC in addition to in-situ spot test was conducted by the research staff at the different sites listed in Table 5.1 to investigate the relationships between the IC measurements and measurements determined by conventional modulus-based NDT methods. Detailed information, mapped results and extensive analyses are available for each of the test sites in their respective appendices, also listed in Table 5.1.

Table 5.1 – Field Test Sites

Site	Location	Length	Layer	Section	Appendix
1	I-35W Northbound Frontage Road in Fort Worth, TX	500 ft	LTS	36 in. lime-treated subgrade (LTS) on top of subgrade.	**C**
			FB	12 in. flexible base (FB) on top of the lime-treated subgrade.	
2	FM 1460 in Georgetown, TX	250 ft	LTS	250-ft long section 8 in. of lime-treated subgrade (LTS) on top of subgrade.	**D**
			FB	250-ft long section of 12 in. flexible base (FB) on top of the lime-treated subgrade (LTS)	
3	SH 183 in Irving, TX	250 ft	LTS	250 ft-long section of 12 in. lime-treated subgrade (LTS) on top of subgrade.	**E**
			FB	250 ft-long section of 8 in. flexible base (FB) on top of lime-treated subgrade (LTS).	
4	US 77 North Bound near Victoria, TX in Yoakum District	500 ft	CTB	500-ft section of 12 in. cement treated base (CTB) on top of subgrade.	**F**
5	SH 149 in Carthage, TX	200 ft	CTS	200-ft long section of 6 in. cement treated salvaged base and reclaimed asphalt (RAP) material.	**G**
6	SH 349 near Lamesa, TX	250 ft	Subgrade	250-ft long section of 18 in. recycled base and asphalt on top of subgrade.	**H**
			FB	250-ft long section of 6 in. flexible base (FB) on top of the recycled base and asphalt subgrade.	
7	FM 133 near Cotulla, TX in Laredo District	250 ft	LTS	250-ft long section 6 in. of cement-treated subgrade (CTS) on top of subgrade.	**I**
			CTB	250-ft long section of 6 in. cement-treated base (CTB) on top of the cement-treated subgrade (CTS)	
8	I-45 in Hunstville, TX	250 ft	CTS	250 ft-long section of 12 in. cement-treated subgrade (CTS).	**J**
			CTB	250 ft-long section of 12 in. cement-treated base (CTB) on top of cement-treated subgrade (CTS).	

Table 5.2 includes a list of NDTs performed at different sites. In addition to LWD and DCP, the plate load test (PLT) was included as part of the field testing at the I-35W site in Fort Worth and Falling Weight Deflectometer was performed in Victoria. The analysis of the PLT results are discussed in Appendix F. PLT tests were discarded from other sites due to the duration of the testing procedure compared to other NDT modulus-based field test and due to the uncertainty to select the appropriate location to conduct them. The results of FWD were not evaluated as the test was performed later after the compaction occurred.

Table 5.2 – Summary of Tests Performed at Visited Sites.

Site	Location	Material	Test Performed						
			IC	Modulus-based NDT				Moisture Content	
			ICMV	LWD	DCP	PLT	FWD	In-Situ NDG	Laboratory Oven-Dry
1	I-35W FR NB Fort Worth	LTS	✓	✓	✓	✓		✓	✓
		FB	✓	✓	✓				✓
2	FM 1460 Georgetown	LTS	✓	✓	✓				✓
		FB	✓	✓	✓				✓
3	SH 183 Irving	LTS	✓	✓	✓				✓
		FB	✓	✓					✓
4	US 77 Victoria	CTB	✓	✓			✓		
5	SH 149 Carthage	CTS	✓	✓					
6	SH 349 Lamesa	Subgrade	✓	✓	✓				✓
		FB	✓	✓					
7	FM 133 Cotulla	LTS	✓	✓	✓				✓
		CTB	✓	✓					
8	I-45 Huntsville	CTS	✓	✓	✓				
		CTB	✓	✓					

5.5 Determining Target Field Values

For a robust modulus verification process, the target field values should be set in conjunction with establishing the design moduli, with consideration of the moisture content at the time of compaction and the state of stress imparted by the testing technology to the geomaterial layer. The target value should be the deflection for LWD and/or the rate of penetration for DCP. Most of the deflection-based devices measure the stiffness of the pavement system, and the reported modulus is based on an elastic-half space Boussinesq theory. This is particularly critical for a multi-layered system being tested with deflection.

Nazarian et al. (2014) developed a multi-layered equivalent-linear algorithm that makes use of an iterative process to consider the nonlinear behavior of the pavement materials using the modified MEPDG constitutive model described by Equation 3.1 to determine LWD target deflection.

Two ASTM standards exist for LWDs. Even though the operation of the devices that conform to ASTM E 2835 and ASTM E 2583 is similar, their measured parameters are different. As a result, the LWD target modulus should be adjusted accordingly depending on the LWD device used. For instance, the impact load varies per LWD device. Though devices that adhere to ASTM E 2583 include a load cell that provides the operator the magnitude of the load impact, the peak load F for these devices, as well as for those that conform to ASTM E 2835, can be determined using the following relationship,

$$F = \sqrt{2mghC} \tag{5.2}$$

where h = drop height (in.), m = falling mass (lb·s^2/in.), g = gravitational force (386.2 in/s^2) and C = spring (buffer) constant (lb/in.) provided by the manufacturer. The term mg of Equation 5.2 can be replaced by the weight W (lb) of the falling weight.

Nazarian et al. (2014) demonstrated experimentally the systematic differences in the measured deflections with these two devices. Tirado et al. (2015, 2017) showed that through proper modeling this issue can be addressed in the specifications. Chapter 4 contains a detailed explanation of that process, and hence, is not repeated herein.

5.6 Geospatial Classification for Developing Optimized Color-Coded Maps

The IC data are best described and interpreted as color-coded maps. These maps display the collected geo-referenced ICMV data on a map separated by means of different colors. The selection of a color-coded criteria affects the visualization of the data. The use of more than three colors is common in many geospatial analyses, but in the case of IC data, the use of three colors (i.e. red, yellow and green) is considered practical. The ultimate goal of using the ICMV color-coded maps is to identify the less-stiff areas, highlighted in red. Based on the identified less-stiff areas, supplemental spot testing is suggested to investigate the mechanistic properties of compacted geomaterials as part of the quality control process.

The proper interpretation of the geospatial IC data is dependent on the optimal selection of the values of the class breaks. Different geospatial classification techniques have been proposed by researchers for this purpose. Brewer and Pickle (2002) evaluated the impact of a few classification methods on the interpretation of the georeferenced data and recommended the Quantile method followed by the Natural Breaks and a modified version of the Equal Intervals method to effectively describe the spatial data. Osaragi (2002) evaluated several classification methods using the principles of information theory. He concluded that the distribution of the geospatial data affected the selection of the optimal classification approach. Xiao et al. (2017) studied the effects of geospatial data uncertainty on the classification method. The authors defined a minimum classification uncertainty level and an overall classification robustness factor. They concluded the smaller number of classes yield is, the more robust the classification will be.

Mazari et al. (2017) evaluated different classification methods and their impact on the interpretation of the data using an information theory concept. They attempted to find the optimal class breaks that minimize the information loss ratio using the Akaike's Information Criterion (AIC, Akaike, 2011) using ICMV data collected at a site. They evaluated the following classification methods:

- *Quantile:* classifies data by placing equal number of data points in each class.
- *Natural Breaks*: classifies data based on the maximization of the difference or variance-minimization between the groups of data (Jenks and Caspall, 1971).
- *Geometrical Intervals*: identifies the class breaks based on the intervals that represent a geometric series by optimizing the sum of squares of the number of features in each group.
- *Equal Intervals*: classifies the features in different groups in a way that the width of each class is the same.

The outcome of implementing these methods at a clayey site and on top of a lime-stabilized layer are shown in Figures 5.15 and 5.16, respectively. Table 5.3 shows *AIC* and the ratio of information loss, *L*, as a measure of the appropriateness of each classification method at the clayey site. The Natural Breaks and Quantile were found to have the lowest *AIC* and *L* values meaning these classification methods were more efficient techniques for classifying the georeferenced CMV data.

Table 5.3 – Comparison of Performance of Geospatial Data Classification Methods for CMV Data Collected at a Clayey Site.

Classification Method	*AIC* ($\times 10^6$)	*L* (%)	Percent Marked as Green	Percent Marked as Yellow	Percent Marked as Red
Quantile	2.2535	0.7424	33	33	33
Natural Breaks	2.2533	0.7169	50	20	30
Geometrical Intervals	2.2695	0.9591	60	25	15
Equal Intervals	2.2552	1.0457	32	31	37

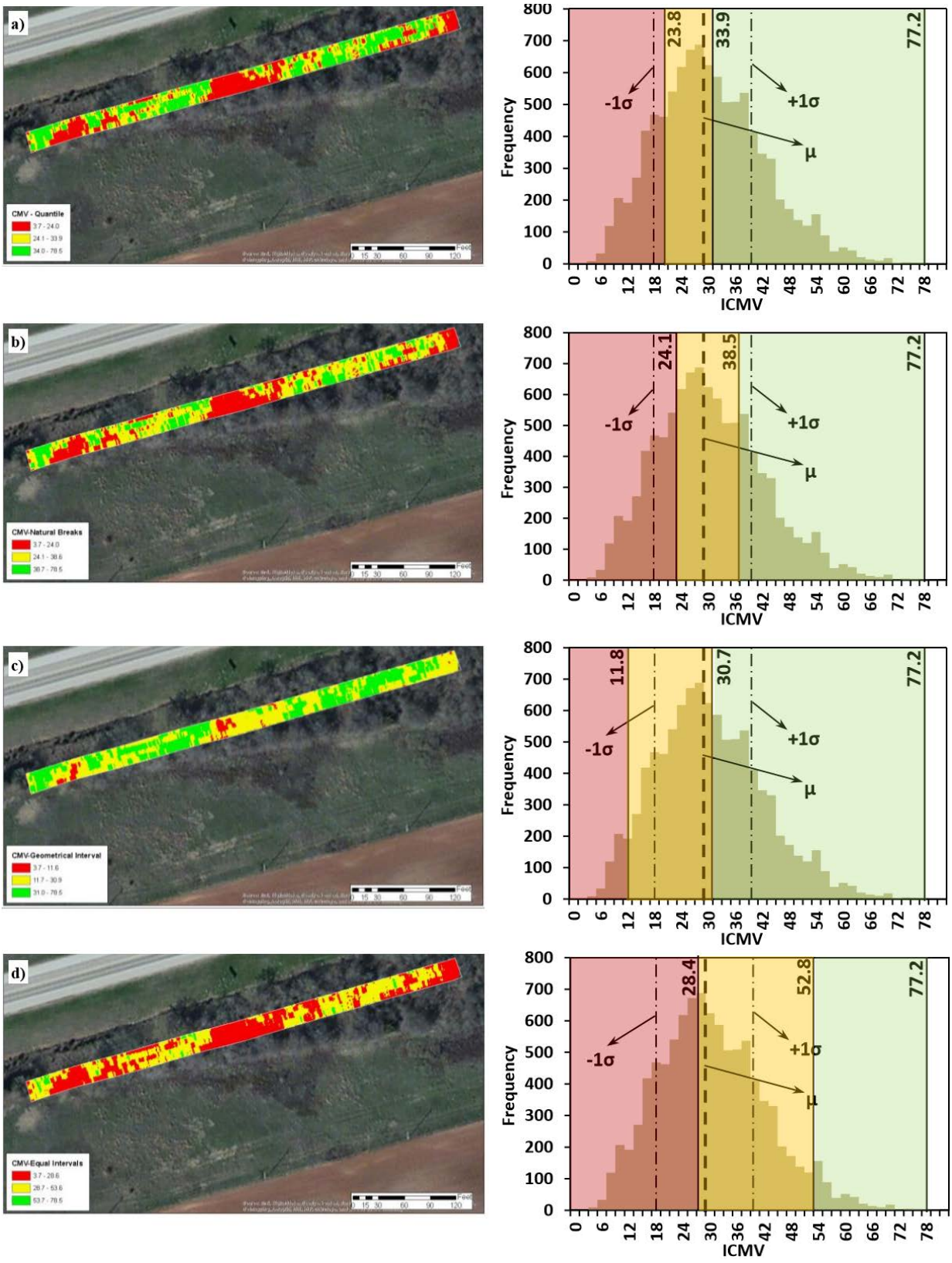

Figure 5.15 – (a) Quantile, (b) Natural Breaks, (c) Geometrical Intervals, and (d) Equal Intervals for Geospatial Analysis of IC Data from a Clayey Site.

The same process was implemented on a lime-stabilized layer. In this case, the Quantile, Natural Breaks, and two methods that are based on fixed breaks using the average of the collected ICMV data as the IC target value (ICTV). The only difference between the last two methods lies on the break for separating ICMVs marked in red color (used to identify less-stiff areas). A 75% and a 50% of ICTV criteria for coloring ICMV areas in red were used for generating color coded-maps. The color-coded maps of the site are shown in Figure 5.16. Table 5.4 shows the AIC criterion for the classifying methods. AIC values were very similar to each other, with AIC for Quantile being the lowest of all.

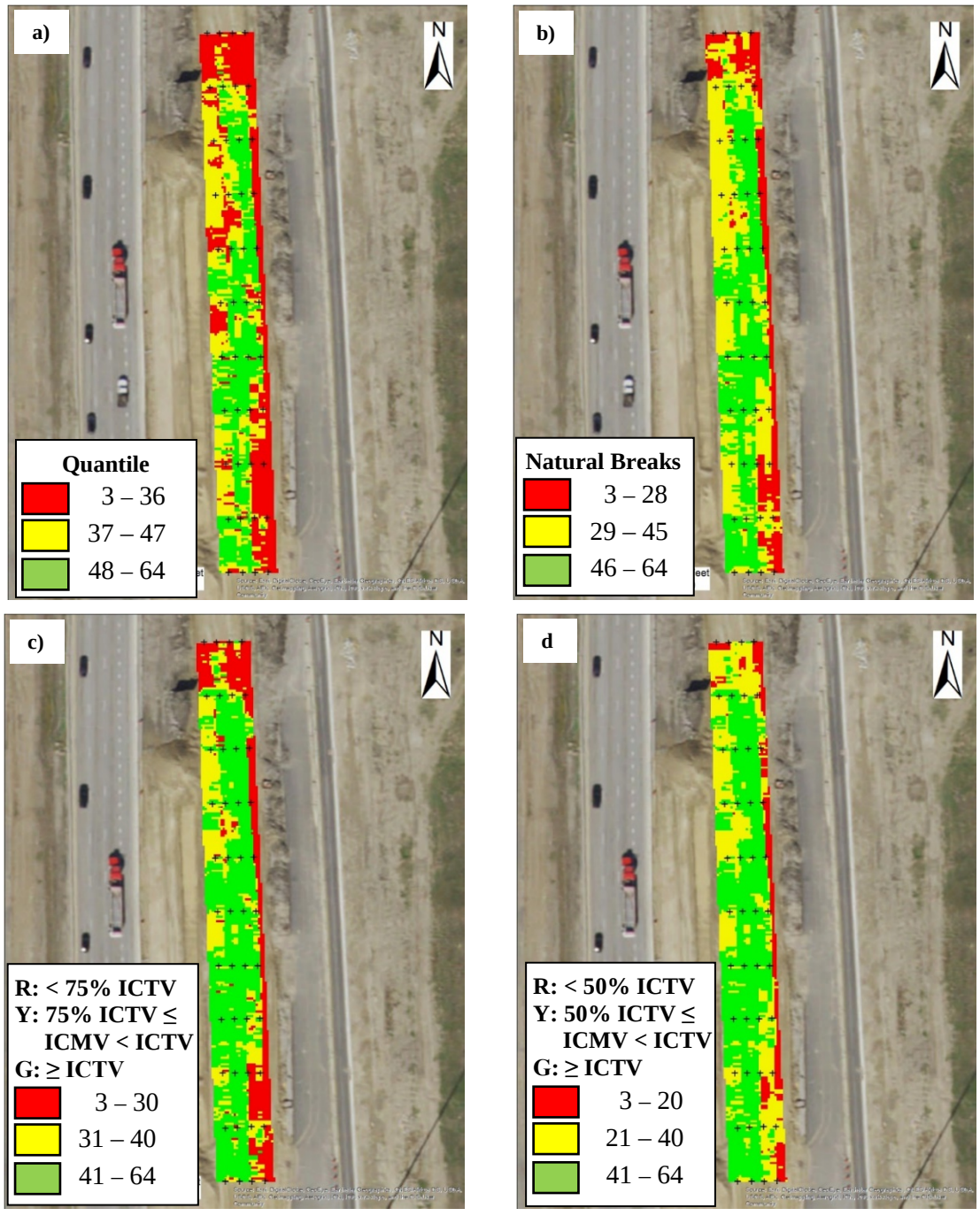

Figure 5.16 – (a) Quantile, (b) Natural Breaks, (c) Red: ICMV < 75% and Green: ICMV > ICTV, and (d) Red: ICMV < 50% and Green: ICMV > ICTV (where ICTV is the Mean of ICMV Data) for Geospatial Analysis of IC Data from a Lime-Stabilized Site.

Table 5.4 – Comparison of Performance of Geospatial Data Classification Methods for CMV Data as Collected by OEM Equipment in Fort Worth Site.

Classification Method	*AIC* ($\times 10^6$)	Percent Marked as Green	Percent Marked as Yellow	Percent Marked as Red
Quantile	1.9348	33	33	33
Natural Breaks	1.9334	19	41	40
Red: ICMV < 75% ICTV Yellow: 75% ICTV ≤ ICMV < ICTV Red: ICMV ≥ ICTV	1.9339	21	24	55
Red: ICMV < 50% ICTV Yellow: 50% ICTV ≤ ICMV < ICTV Red: ICMV ≥ ICTV	1.9335	32	31	37

* ICTV = Average of ICMV collected data

In an effort to reduce the number of spot test measurements based an optimal classification system it is necessary to link the spot test measurements to the collected ICMV data. As indicated before, the vibration data is collected at a discrete point on the roller. The current IC data analysis programs incorporate various interpolation processes in order to extrapolate the ICMV data points over the width of the roller prior to generating the color-coded maps. Some of the extrapolation techniques that are used include the Inverse Distance Weighting (IDW), spline and ordinary kriging. The use of these methods enhance the visualization of the data by smoothing the color-coded contours and by filling gaps in information. Unfortunately, ICMV data is affected by the inclusion of these tools, as ICMV outliers can be cropped resulting in reduced ranges of ICMVs array of values. Kriging, for instance, does not pass through any of the point values and causes interpolated values to be higher or lower than real values. Spline interpolation does not work well when sample points have extreme differences in magnitude and are close together.

Being a heterogeneous material, compacted geomaterials may exhibit high spatial variability in their mechanical properties. Since it is impractical to estimate the exact position of the roller due to its size, it is virtually impossible to estimate ICMV exactly on top of the spot where the LWD test is performed. Instead of point-by-point comparison, it may be prudent to establish a grid equal to the width of the roller and the length equal the minimum length of the compacted section that is practical to rework (e.g., 25 ft or 50 ft). All ICMV measurements falling inside each rectangular area can be averaged to obtain a representative CMV characterizing the stiffness of that grid. This would facilitate the comparison of the geospatial data obtained with IC roller and the spot tests such as LWD. For this purpose, spot test measurements using LWD and DCP were performed at equidistant distances along several sites. An example of such a grid is shown in Figure 5.17.

Usually, a set of 44 spots test were performed, comprising a grid of an array of eleven recordings along the longitudinal direction and four along the transverse direction of the test section. Following the process discussed before, a rectangular buffer area was selected around each spot test location. Color-coded maps were created for the representative CMV values and the spot test measured values, with the purpose of relating the less stiff geospatially referenced data from the two devices. The coefficient of variation of the ICMV values in each grid will represent the variability of the compaction quality. The average value for ICMV and LWD along with their associated ±1 standard deviation bounds can be used for a more rational comparison. This approach was implemented at several sites.

A comparison is provided in Figure 5.18 showing the IC mapping for a 500 ft long and 27 ft wide test section on top of a lime-treated subgrade when an interpolation technique, such as spline, is used and when only the average CMVs of their respective rectangular buffer areas are used. Both data sets show similar trends.

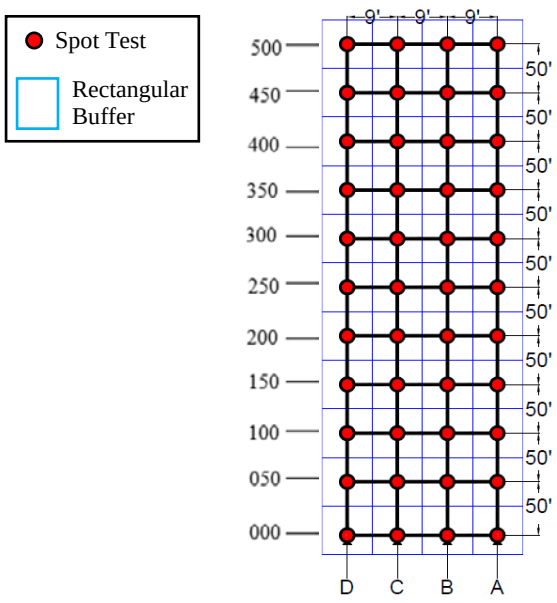

Figure 5.17 – Schematic of Location of Georeferenced LWD and DCP Spot Tests for a 500-ft Long Test Section.

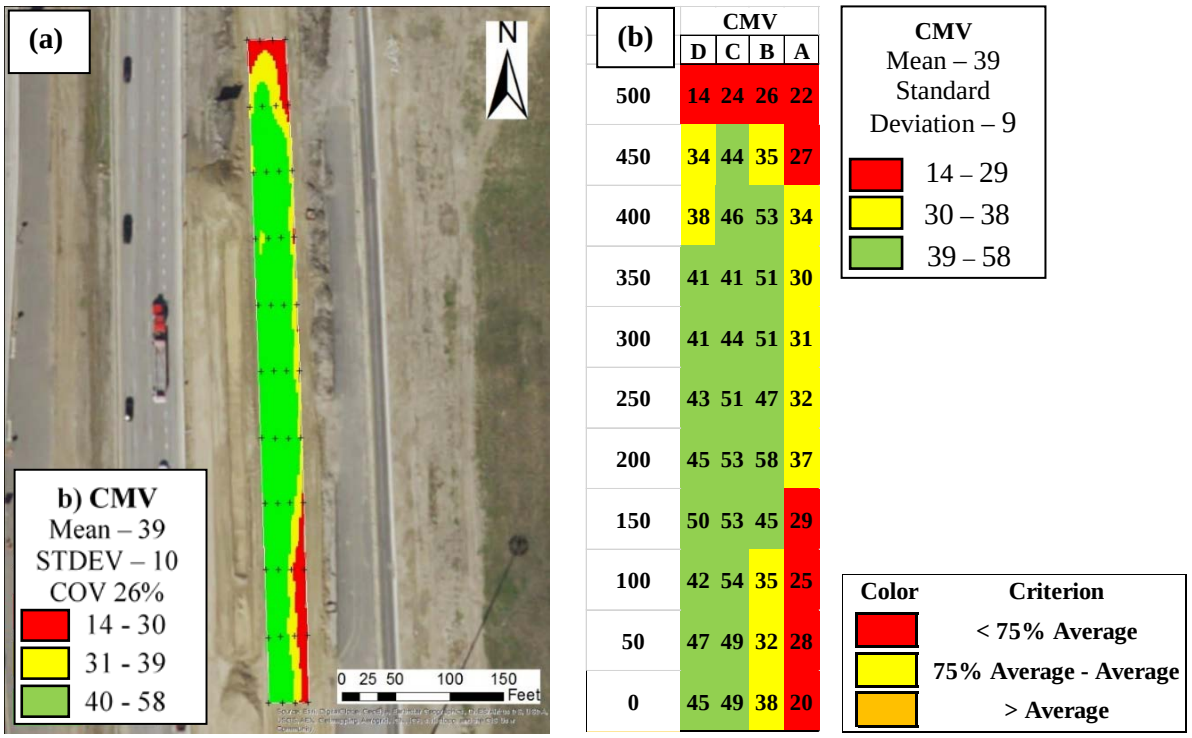

Figure 5.18 – Mapping of CMVs on Lime-Treated Subgrade after (a) Implementation of Interpolation Techniques and (b) Rectangular Buffer Areas without any Interpolation.

Figure 5.19 compares the collected and processed CMV data and LWD modulus for the same lime-stabilized layer. A relationship seems to exist between the measurements, as the red color indicating less-stiff areas lie on the northern and southern parts of the test section.

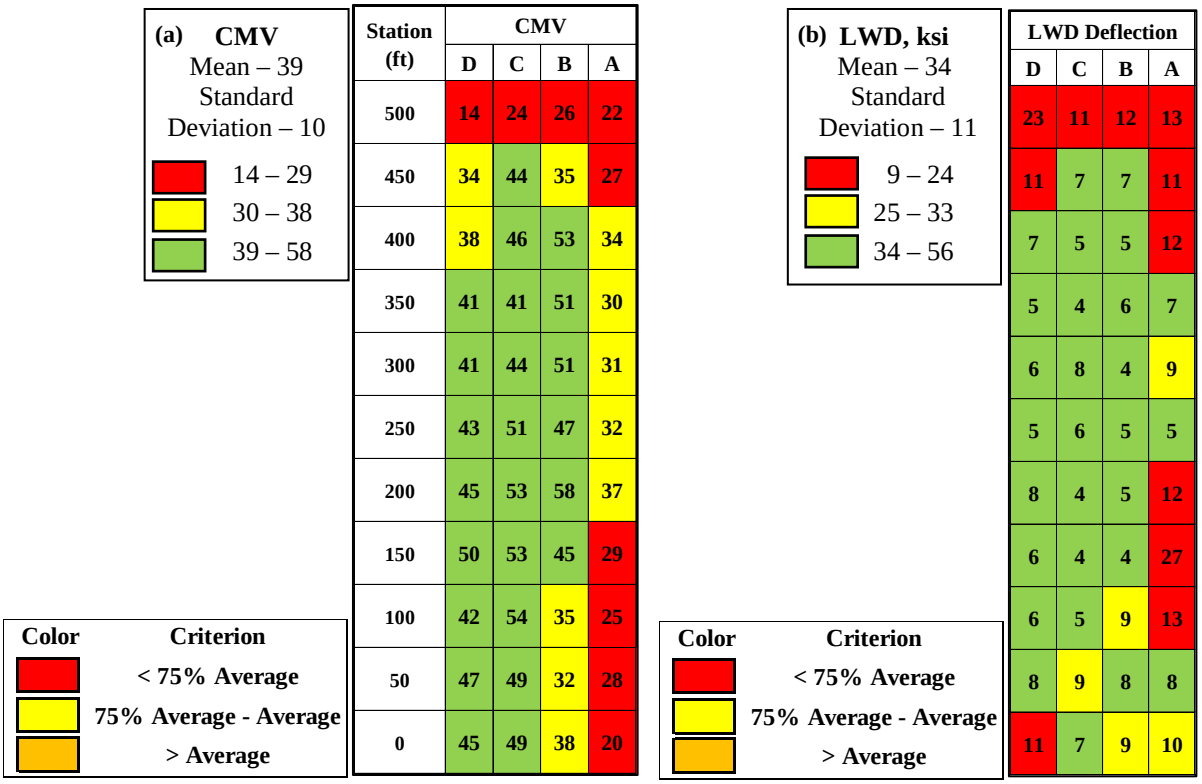

Figure 5.19 – Spatial Representation of (a) CMVs and (b) LWD Deflection-Based Spot Testing on Lime-Treated Subgrade.

5.7 Relationships between Modulus-based Measurements and ICMV

This section summarizes the key findings from the field evaluation of the sites. The objectives of the evaluation were to investigate simple relationships between ICMV and various in-situ modulus-based spot test measurements, identify key factors that affect the relationships, and evaluate different approaches to improve the relationships for identifying less-stiff areas. The proper identification of less-stiff areas by means of IC is critical for performing evaluation of compaction by means of modulus-based measurements.

Compacted geomaterials may exhibit spatial variability in their mechanical properties due to different factors that can be attributed to heterogeneous conditions of underlying layers, moisture content variation and even to limited number of measurements.

To evaluate whether a relationship existed between the modulus-based measurements and ICMVs, the grid with 44 spot test points was used, as illustrated in Figure 5.17. Rectangular buffered areas were superimposed over the spot tests for delimiting the areas with dimensions suitable for rework. All ICMVs falling within the rectangular areas were averaged to obtain a unique ICMV representative of that area. Compaction Meter Value (CMV) was used as the representative unit for roller-based ICMVs. This dimensionless parameter characterizes the phenomenon that different harmonic components of the drum rebounds occur due to soil stiffness, roller dimensions and operating characteristics. CMV is defined as

$$CMV = 300\frac{A_{2\Omega}}{A_{\Omega}}, \tag{5.3}$$

where A_{Ω} is the amplitude of the acceleration at the fundamental frequency, i.e. operating frequency, of the roller, and $A_{2\Omega}$ is the amplitude of the acceleration of the second harmonic frequency (Sandström and Pettersson, 2004).

Color-coded maps for CMV, coefficient of variation of CMVs and spot test measurements are available in the appendices for each of the visited sites, including a discussion of the findings, and are omitted in this section. A summary of the descriptive statistics of the deflection-based devices and the roller CMV collected from the visited sites is offered in Table 5.5.

Table 5.5 – Descriptive Statistics of NDT Devices on Different Sections in Evaluated Sites

Section*		Device	Mean	Standard Deviation	Coefficient of Variation	Sample Size	First Quartile	Third Quartile	Median
1	LTS	CMV	13	3	27	44	11	16	14
		DCP, No. of Blows	42	8	20	44	39	46	43
		LWD Deflection, mils	33	12	37	44	25	43	32
		Moisture Content, %	18	2	11	43	17	19	18
		PLT, ksi	28	11	41	5	24	37	28
	FB	CMV	13	4	30	44	10	16	14
		DCP, No. of Blows	16	4	26	34	13	20	17
		LWD Deflection, mils	30	10	32	34	24	37	31
		Moisture Content, %	15	3	21	32	13	16	14
2	LTS	CMV	2	1	50	44	2	3	2
		DCP, No. of Blows	31	17	54	44	23	29	25
		LWD Deflection, mils	7	2	35	44	5	7	6
		Moisture Content, %	14	1	10	43	13	15	14
	FB	CMV	10	5	52	43	5	13	9
		DCP, No. of Blows	178	108	61	20	45	260	215
		LWD Deflection, mils	28	13	46	44	16	36	30
		Moisture Content, %	10	2	21	37	9	11	9
3	LTS	CMV	3	1	22	35	2	3	3
		DCP, No. of Blows	36	16	45	44	24	43	33
		LWD Deflection, mils	22	9	40	44	18	24	20
		Moisture Content, %	14	2	14	44	13	16	15
	FB	CMV	9	3	29	33	8	11	9
		LWD Deflection, mils	17	9	55	44	11	17	13
		Moisture Content, %	7	1	18	44	7	8	7
4†	CTB	CMV	17	3	21	44	15	20	16
		LWD Deflection, mils	42	13	30	44	33	50	40
		FWD, ksi	55	13	24	11	45	66	61
5	CTS	CMV	24	7	30	36	18	28	25
		LWD Deflection, mils	14	5	33	36	10	16	14
6	Subgrade	CMV	58	9	15	43	51	64	55
		DCP, No. of Blows	45	13	29	28	33	55	48
		LWD Deflection, mils	9	2	26	44	7	10	9
		Moisture Content, %	3	1	0.2	44	3	4	3
	FB	CMV	29	9	30	43	23	33	28
		LWD Deflection, mils	15	4	31	43	12	16	14

Table 5.5, cont. – Descriptive Statistics of NDT Devices on Different Sections in Evaluated Sites

Section*		Device	Mean	Standard Deviation	Coefficient of Variation	Sample Size	First Quartile	Third Quartile	Median
7	LTS	CMV	35	9	25	44	31	38	34
		DCP, No. of Blows	21	5	24	44	19	24	21
		LWD Deflection, mils	15	8	51	44	12	16	14
		Moisture Content, %	15	2	16	44	14	16	15
	CTB	CMV	50	12	24	41	43	56	51
		LWD Deflection, mils	7	2	22	44	7	8	7
8	CTS	CMV	18	5	28	42	15	21	18
		DCP, No. of Blows	21	6	30	23	18	22	21
		LWD Deflection, mils	6	2	36	44	4	8	7
	CTB	CMV	17	5	29	44	15	20	17
		LWD Deflection, mils	7	2	35	44	5	8	7

Notes: * CMV values normalized using a factor of 100 for comparative purposes. LTS – lime treated subgrade, FB – flexible base, CTB – cement treated base.

† FWD testing occurred days after compaction.

5.7.1 Relationship between CMV and LWD Deflection Measurements.

Figure 5.20 shows the relationship between the LWD deflection and the average CMV for each of the 44 rectangular areas from the subgrade materials at the evaluated sites, excluding cement treated sites. A factor of 100 was used, rather than the value of 300, to have uniformity in all sites. Quality control on the ICMV datasets was performed to remove ICMVs that occurred in rectangular buffer areas that exhibited high variability (COV > 50%) and those calculated at fundamental frequencies beyond ±5 Hz of the roller operating frequency, which usually lead to erroneous CMVs. Figure 5.20f, which compiles the data from all five sites, reveals that higher CMVs occur when lower LWD deflections are recorded (i.e. material became stiffer). A logarithmic relationship yielded a relatively good coefficient of determination.

Sites 2 and 3 exhibit very low CMVs (below 5) in accordance to large LWD deflection measurements, usually above 11 mils. This is an indicator that these two sites have subgrades that are considerably less stiff than other sites.

Figure 5.21 shows the relationship between the LWD deflections and the average CMVs for the 44 rectangular areas as measured on top of flexible base layers. Sites with cement treated bases are excluded. A summary of all sites with flexible base layers is provided Figure 5.21e. Though no appreciable correlation is observed in every single site, it is evident measured CMVs are generally higher than those measured in subgrades, while LWD deflection measurements are lower as well, due to the stiffer materials present in flexible base layers.

Sites 2 and 3 exhibit the effect of the base layer when compared to measurements on top of their respective subgrades, shown in Figure 5.20b and 5.20c, respectively. LWD deflection measurements decreased in magnitude, while CMVs increased from values below 5 to values higher than 5, when the flexible base was laid upon subgrade, indicating that testing occurred in a stiffer layer. However, CMVs of these two sites are relatively low when compared to other sites. This is attributed to the influence depth of the roller penetrating into the less-stiff subgrades present in these sites. This suggests that the IC roller proof-mapping of bases is impacted by the subgrade and as such it is prudent to conduct a pre-mapping before mapping the base.

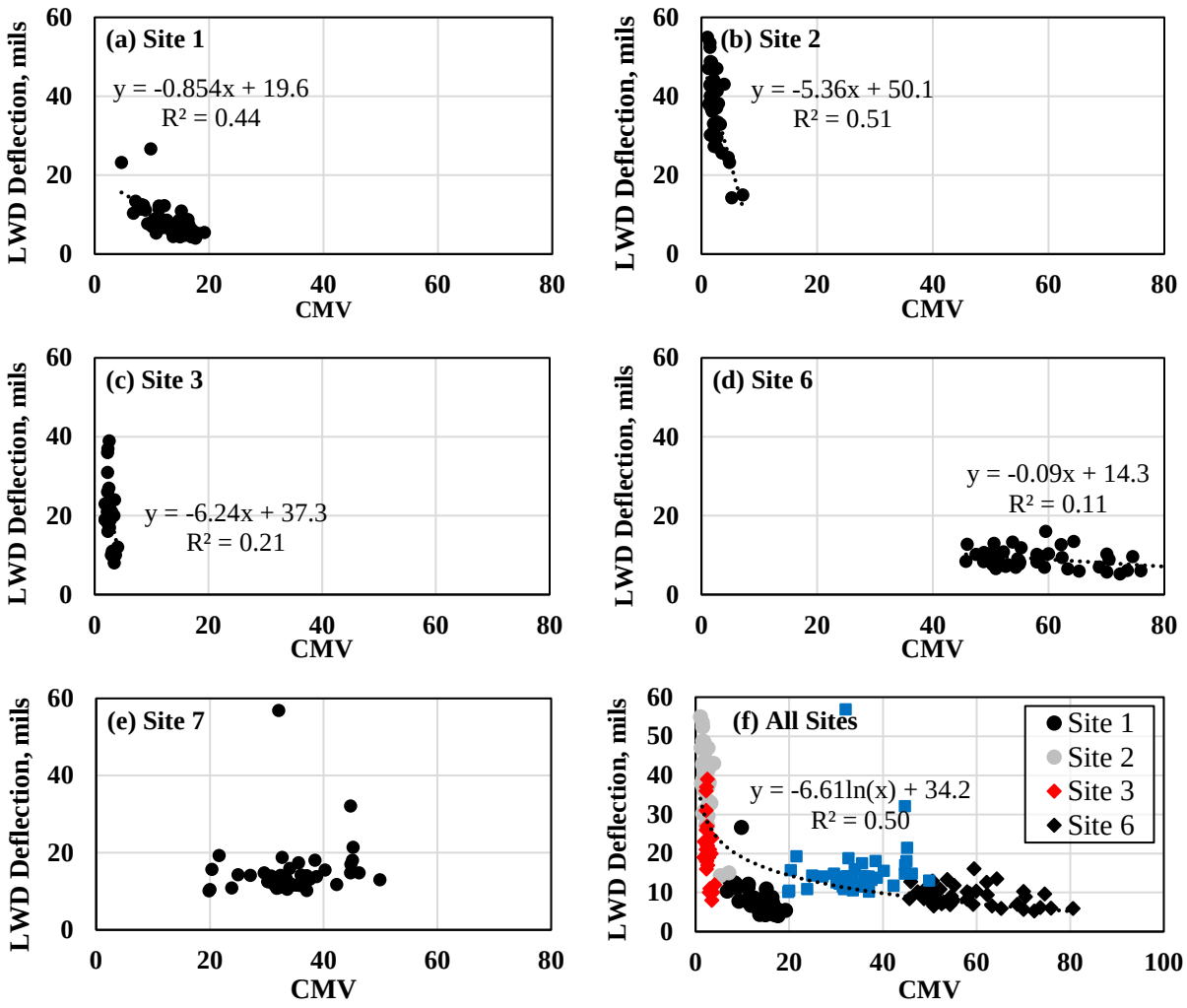

Figure 5.20 – Relationship between CMV and Deflections Measured from LWD Mass Drops in Lime-Treated Subgrade and Recycled Base and Asphalt Material for (a-e) Sites 1, 2, 3, 6, and 7, respectively, and (f) All Sites Compiled.

On the other hand, site 6 shows lower CMVs and higher LWD deflections when measured in the base layer compared to those measured in subgrade (Figure 5.20d). This indicates the base layer to be less stiff than the subgrade, the latter being comprised of recycled base and asphalt material that produced a very stiff subgrade.

Figure 5.22 shows the relationship between CMV and LWD deflection measurements for sites with cement treated subgrade and cement treated base materials, 24 hours after treatment. In site 7, cement treatment of base material induced higher CMV and smaller LWD deflections measurements than its respective subgrade. However, no significant change in the magnitude of both measurements is seen in site 8, indicating similar stiffness in both base and subgrade.

Figure 5.23 summarizes the relationship between CMV and LWD deflection measurements, and their respective LWD modulus, for all sites with subgrade and flexible bases combined, excluding sites with cement treatment. Sites 2 and 3 exhibit CMVs below 5, while most LWD deflection measurements lie above 11 mils. Figure 5.24 shows the relationship between CMV and LWD deflection for all sites. The trends are similar to Figure 5.23a, with LWD deflections for cement treated bases being lower than those obtained in flexible bases.

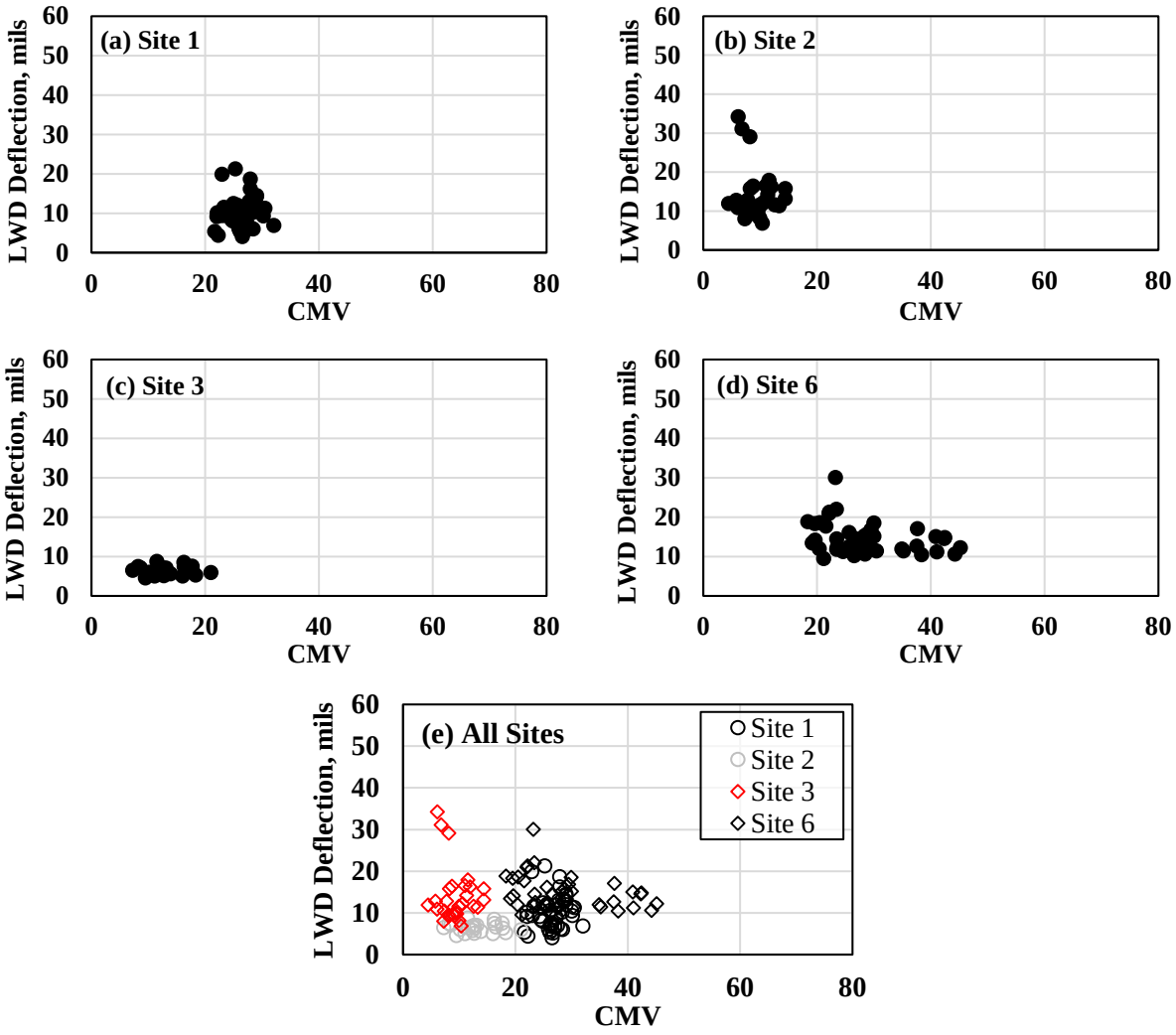

Figure 5.21 – Relationship between CMV and Deflections Measured from LWD Mass Drops in Flexible Base Material for (a-d) Sites 1, 2, 3, and 6, respectively, and (f) All Sites Compiled.

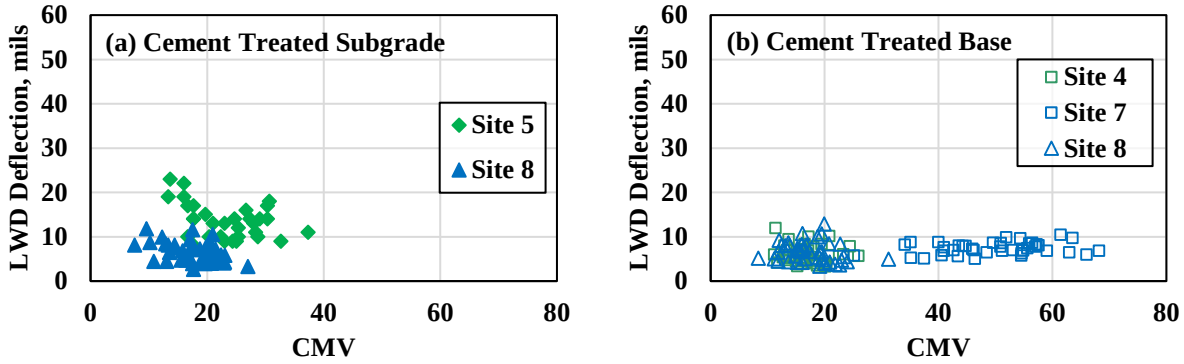

Figure 5.22 – Relationship between CMV and Deflections Measured from LWD Mass Drops in (a) Cement Treated Subgrade Sites and (b) Cement Treated Base Sites.

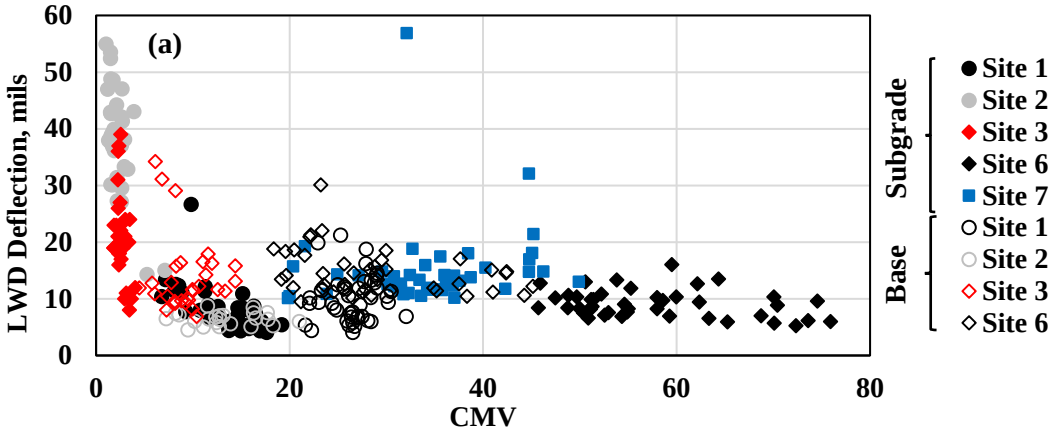

Figure 5.23 – Relationship between CMV and (a) Deflections Measured from LWD Mass Drops for All Subgrade and Flexible Bases.

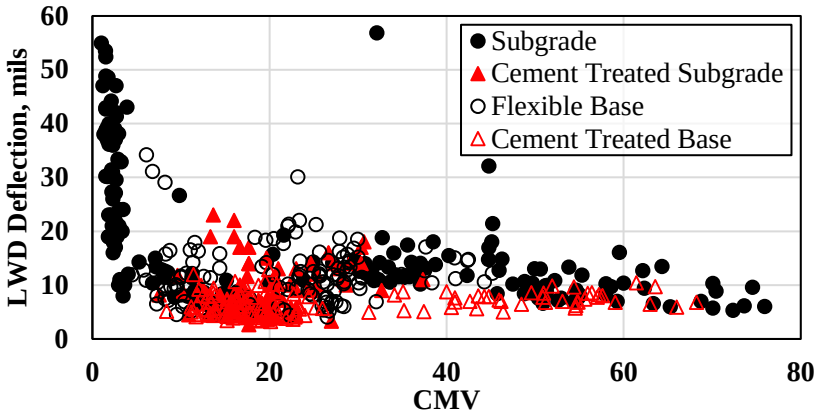

Figure 5.24 – Relationship between CMV and Deflections Measured from LWD Mass Drops for All Sites.

As shown in Figure 5.21, a direct correlation of the measurements at the buffer areas cannot be provided for each site. However, the representation of the average measurements along the stations may yield trends indicating the stiffness of the mapped section. Data points were averaged by station reducing the amount of data from 44 points to 11 points for subgrade at Sites 1, 2, 3, and 6 (Figure 5.25a through 5.25d, respectively). Error bars included in the figures show the standard deviation of the measurements per station. A good trend between the LWD deflection and CMV measurements seems to exist in all sites.

The trends obtained between CMV and the LWD spot test measurements show that CMV is not effective when the material is too soft and LWD is not very effective when the material is very stiff (i.e., for CTB). A careful review of Figure 5.24 shows that for very soft materials (e.g., LWD deflections greater than 20 mils), the intelligent compaction is not very effective. On the other hand, for very stiff materials such as CTB, the LWD deflections are too small to be measured effectively with LWD.

5.7.2 Relationship between CMV and DCP Measurements.

Figure 5.26 shows the relationship observed between the number of DCP blows to penetrate the subgrade to a certain depth (24 in. for sites 1 and 2, 18 in. for Site 3, 16 in. for Sites 6 and 7) and the rectangular buffered areas averaged CMV values for each of the 44 areas in the test sections. Though no direct correlation is seen, similar to the relationships observed with LWD deflections in subgrade, a trend is seen relating both measurements, particularly when all tested sites are compiled together (shown Figure 5.26f),

and where the dynamic cone penetration index (DCPI) was compared to CMV. The DCP drives the cone deeper per blow in those subgrade materials where lower CMVs are measured (Sites 1 and 2). Conversely, a lower DCPI value, i.e. a lower penetration rate, is observed in the stiffer subgrade in site 6, which also yielded higher CMV measurements. Unlike the other sites which were lime-treated subgrades, site 6 has a subgrade prepared with recycled base and asphalt material.

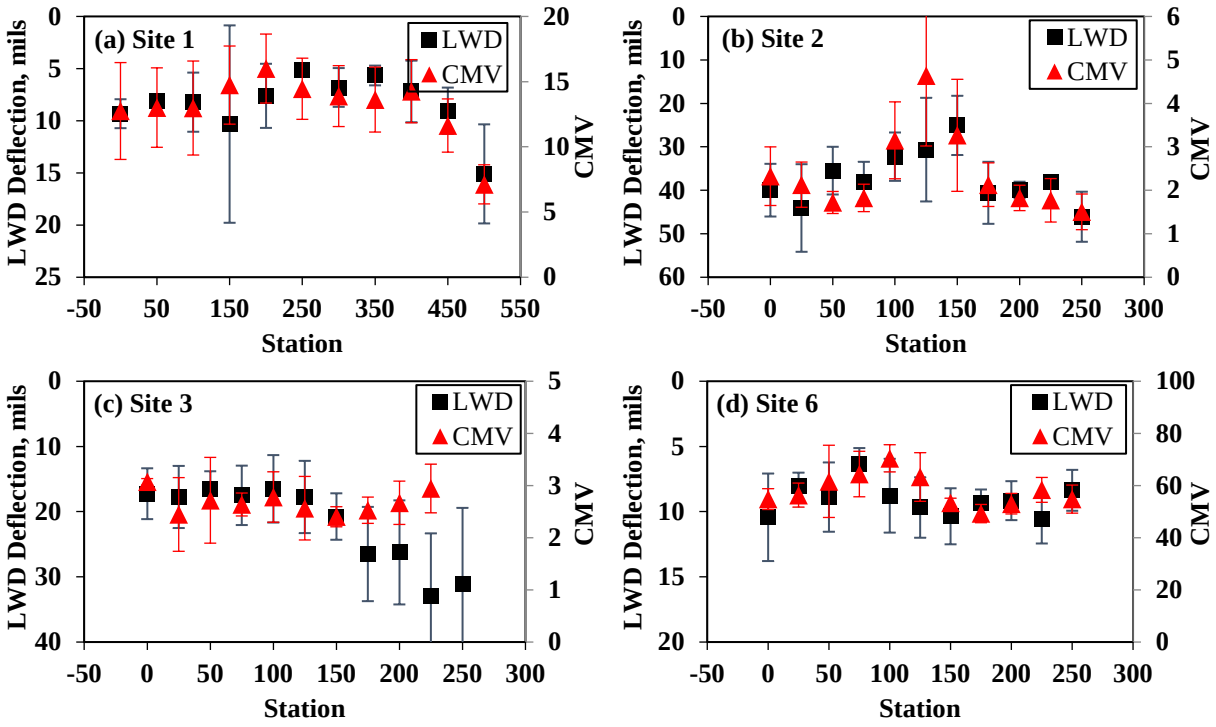

Figure 5.25 – Relationship between CMV and LWD Mass Drop Deflection per Station in Lime Treated Subgrade Material

DCP tests were also performed at cement treated subgrades in Site 7, and the base layers of sites 1 and 2. Their penetration rates for these materials are shown in Figure 5.27 along those obtained for lime-treated subgrades. DCP tests in the 24-hour cement treated subgrade showed similar penetration rates to the lime treated subgrades. However, for flexible base layers, penetration rates were considerably lower than those obtained in subgrade materials due to the base material granularity. Unlike the subgrades, no trend is observed for between the DCPI and CMVs for the flexible base layers, again indicating the importance of pre-mapping.

Finally, Figure 5.28 shows that a good trend develops between the CMV measurements and the number of DCP blows when averaged along stations, indicating that the CMV is somewhat related to the stiffness of the tested geomaterials. It must be pointed out that these trends improve considerably if a quality control on the CMV measurements is provided by eliminating measurements obtained at frequencies deviating from the ±5 Hz from the operating frequency, thus reducing the variability of the measurements.

5.7.3 Relationship between CMV and PLT Measurements.

Because of the long duration of PLT test, few PLT tests can be executed in a reasonable amount of time. The number of PLT tests are not sufficient for generating a color-coded map to compare with the IC roller mapped data. Figure 5.29 shows an example of the spatial distribution of LWD modulus around a PLT site. Given the variability of the soil in the area (both observed visually and with spot tests), the test point may not be a representative of the test section. As such, the location of the PLT tests should be selected with extreme care.

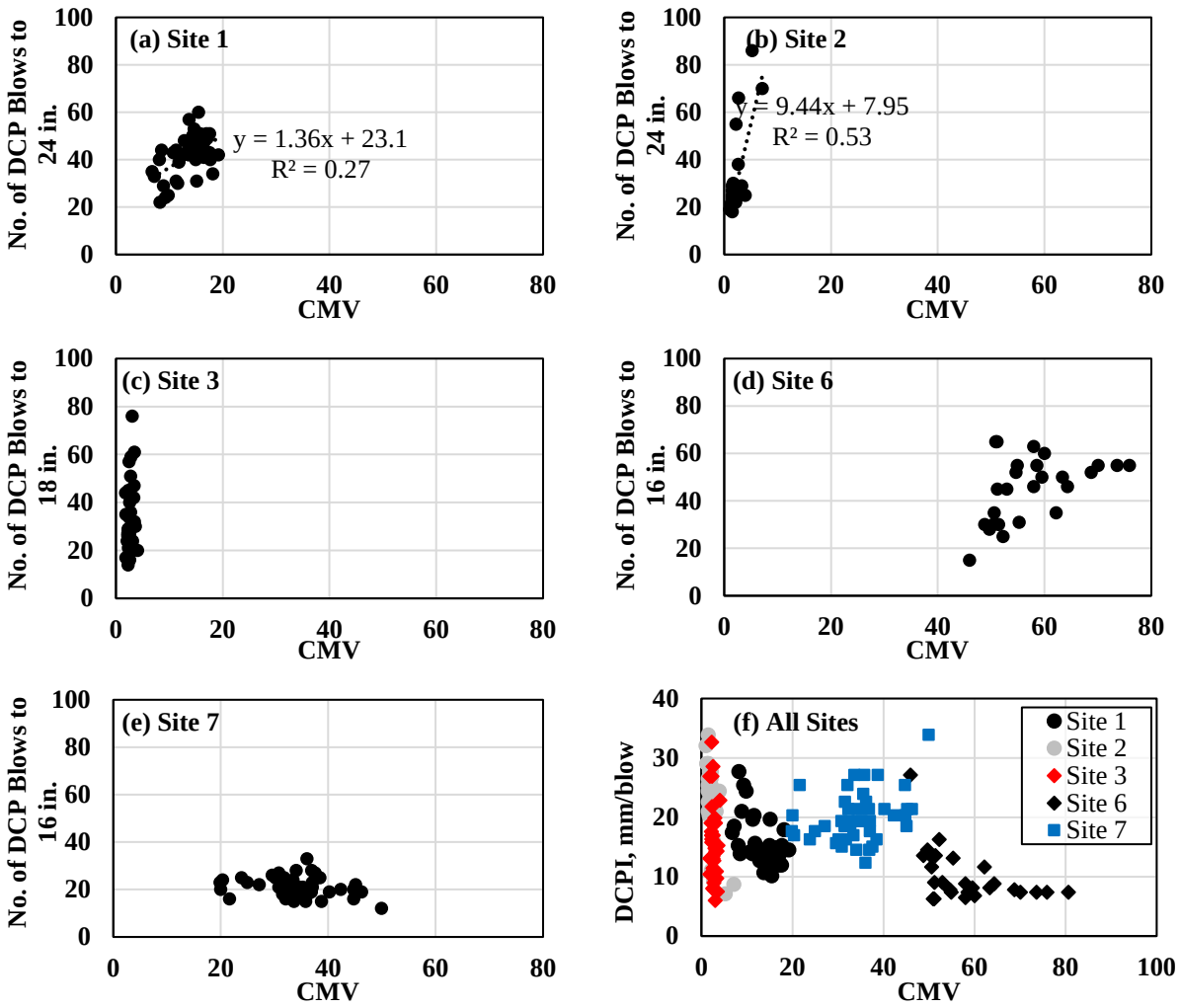

Figure 5.26 – Relationship between CMV and Number of DCP Blows to Penetrate the Indicated Depth in Lime Treated Subgrade Material for (a-e) Sites 1, 2, 3, 6 and 7, respectively, and (d) Relationship between CMV and Dynamic Cone Penetration Index (DCPI) for All Sites.

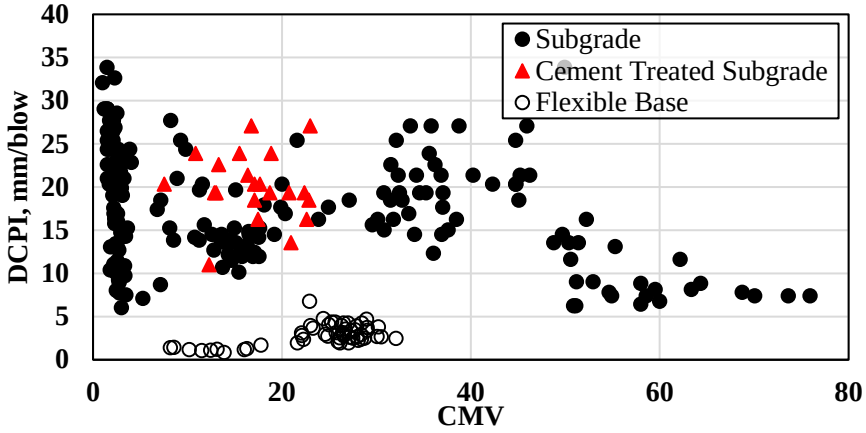

Figure 5.27 – Relationship between CMV and Dynamic Cone Penetration Index (DCPI) in All Subgrade, Cement-Treated Subgrades and Flexible Base Sites.

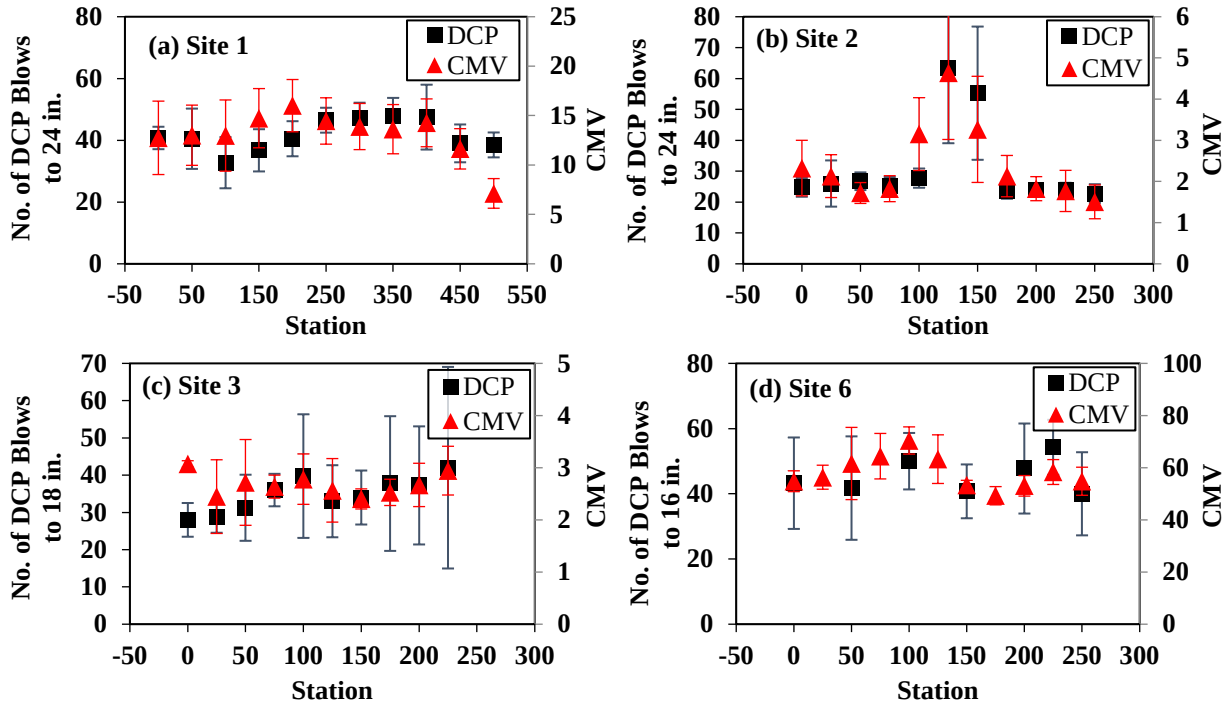

Figure 5.28 – Relationship between CMV and Number of DCP Blows per Station in Lime Treated Subgrade Material for (a) Site 1, (b) Site 2, (c) Site 3 and (d) Site 6.

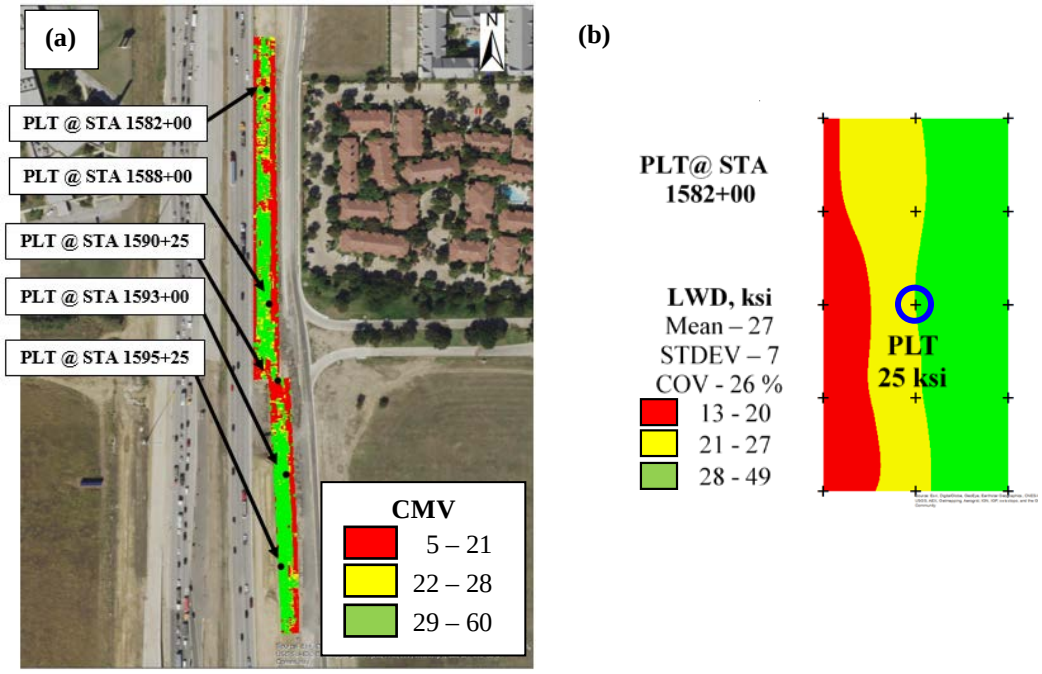

Figure 5.29 – (a) Locations of PLT Spot Tests in Lime-Treated Subgrade Site and (b) Spatial Distribution of LWD Modulus at PLT Location.

5.7.4 Relationship between CMV and Moisture Content Measurements.

No direct correlation seem to exist between moisture content and CMVs, as shown in Figure 5.30. For instance the subgrade of Site 1 is among the stiffer tested subgrade materials, according to Figure 5.23; however, it has higher moisture content than other sites that were similar in stiffness. Mapping of both measurements, available in the appendices for each site where moisture content was measured, have not yielded similar trends.

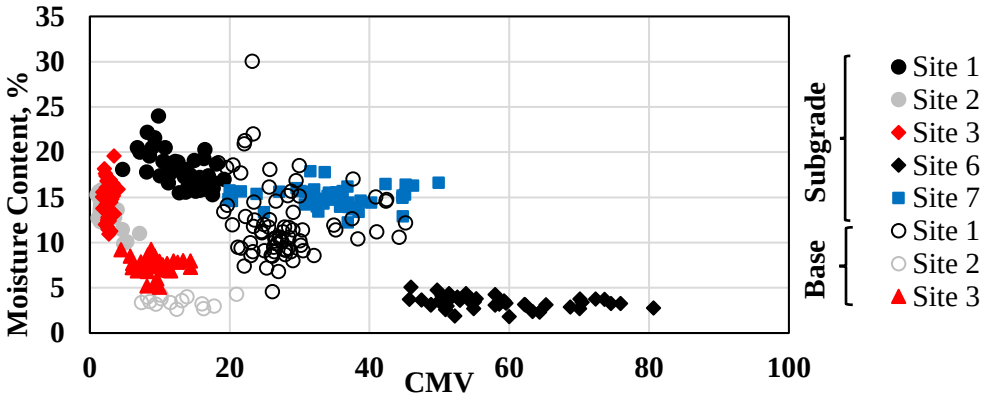

Figure 5.30 – Relationship between CMV and Moisture Content across All Sites.

5.8 Optimization Process for Identifying Low Stiff Areas using IC

In an effort to reduce the number of spot tests, ICMVs are usually represented in color-coded maps. Since ICMVs are collected at a discrete point on the roller, an interpolation technique have to be used in order to extrapolate ICMV data points over the width of the roller. These methods enhance the visualization of the data by smoothing the color-coded contours and by filling the gaps of information. However, the use of these tools can affect the visual representation of the ICMV data, as outliers can be cropped resulting in arrays with reduced ranges of ICMVs, as discussed previously. To overcome these problems, a different approach for developing color-coded maps was followed. This approach consisted of allocating ICMVs into cells of rectangular shapes that are aligned with the roller passes. Color-coded maps are then generated for the representative ICMVs and the spot tests measurements with the purpose of relating the less stiff geospatially referenced data from different devices. Spot tests can then be performed within the cells that yield low average ICMVs.

Figure 5.31 provides the result of the mapping process implemented in a lime treated subgrade test site, showing the mapping of the proof-mapped ICMVs, LWD deflection measurements and DCP blows. Table 5.6 shows the criteria for color-coding the maps. Less-stiff areas are identified as those areas with measurements below 75% the average measurements (being CMV, LWD deflection or number of DCP blows). For the particular case of LWD deflection, since larger deflections occur in less-stiff areas, the criterion was reversed, i.e. less-stiff areas are identified when LWD deflections were greater than 125% of the mean LWD deflections. The IC roller map shows a total of nine cells with CMVs below 75% of the mean CMV (marked in red). Seven of these nine areas identified by the roller were marked as less-stiff on the LWD color-coded map. The rectangular areas enclosed by a blue border indicate the areas identified as less-stiff in the CMV map but not in the LWD deflection map. This indicates that 22% of less-stiff areas spotted in the CMV map were not in agreement with the less-stiff areas found in the LWD map. The percentage of mis-estimated areas increased to 56% when CMVs are compared to the number of DCP blows to penetrate 24 in. into the subgrade.

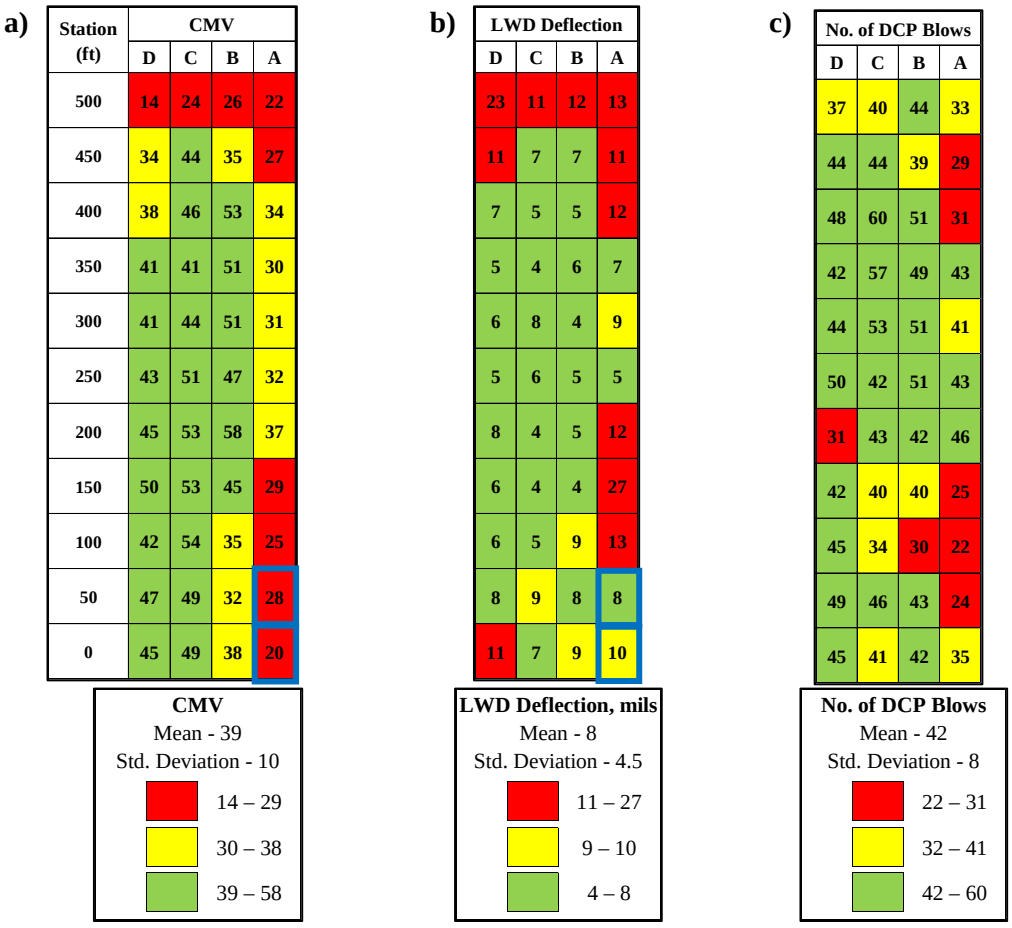

Figure 5.31 – Color-Coded Map Comparison between (a) CMV, (b) LWD Mass Drop Deflection and (c) Number of DCP Blows to Penetrate 24 in. as Obtained in Lime-Treated Subgrade at Site 1.

Table 5.6 – Criterion for Color-Coded Maps.

Color	Criterion
Red	< 0.75 Mean
Yellow	0.75 Mean – Mean
Green	> Mean

The color-coding criteria should also consider the number of data points per cell as well as the level of certainty in the reported values. To reduce the percentage of mis-estimated areas, a systematic search for a different coloring criteria for identifying less-stiff areas was carried out. The color-coded criteria optimization approach consisted of varying the class-break for identifying the less-stiff areas for both the CMV and the spot test measurements. This criterion varied within a range defined from 60% to 90% of the average measured values, for the ICMV data and the NDT spot test values. In the case of the LWD deflection, as the stiffness trend is reversed, a range between 110% and 140% of the average deflection was used for setting the less-stiff class-break.

Table 5.7 shows the percentage of mis-estimated areas in the subgrade of site 1 when color-coded maps are generated with different levels. For that particular site, the IC roller was able to predict all less-stiff areas (shaded cells in Table 5.7), when a class-break criteria were set at 70% of the average CMV (or lower) and at 120% of the average LWD deflection (or lower).

Table 5.7 – Percentage of Misestimated Roller Measurements (Rectangular Buffered Areas CMVs) with Respect to LWD Measurements Based on Different Percentages of Average Measurements for the Identification of Less-Stiff (Red) Areas in Site 1

Percentage of IC Roller Misestimated Areas		Less-Stiff (Red) Area Above % of Average LWD Deflection						
		110	115	120	125	130	135	140
Less-Stiff (Red) Area Below % of Average CMV	90	41	41	41	47	47	53	65
	85	38	38	38	46	46	54	62
	80	27	27	27	36	36	45	55
	75	11	11	11	22	22	33	44
	70	0	0	0	14	14	29	43
	65	0	0	0	17	17	17	33
	60	0	0	0	33	33	33	33

That process was also implemented for the DCP in Table 5.8. The shaded area indicating the best combinations of class-break criteria as concluded from Table 5.7 is superimposed in Table 5.8. Though the comparison of the roller's CMVs to the DCP measurements indicate a larger number of mis-estimated areas by the roller; the optimization process was able to identify the combinations of class-breaks best suited for identifying less-stiff areas for the subgrade in site 1. The criterion for less-stiff area class break for CMV was lowered to 60% of the mean, while for the DCP the class break was set at 80% of the average number of DCP blows for the entire section, as shown in Table 5.9.

Table 5.8 – Percentage of Mis-estimated Roller Measurements (Rectangular Buffered Areas CMVs) with respect to DCP Measurements Based on Different Percentages of Average Measurements for the Identification of Less-Stiff (Red) Areas in Site 1

Percentage of IC Roller Misestimated Areas		Less-Stiff (Red) Area Below % of Average No. of DCP Blows (0-24 in.)						
		90	85	80	75	70	65	60
Less-Stiff (Red) Area Below % of Average CMV	90	47	53	59	65	76	82	88
	85	46	54	62	69	69	77	85
	80	36	45	55	64	64	73	82
	75	22	33	44	56	56	67	78
	70	29	43	57	71	71	86	86
	65	33	50	67	83	83	83	83
	60	0	33	67	100	100	100	100

Table 5.9 – Optimized Class-Break Criterion for Color-Coded Maps.

Color	Criterion for CMV	Criterion for LWD Deflection	Criterion for No. of DCP Blows
Red	< 60% Mean	> 120% Mean	< 80% Mean
Yellow	60% Mean – Mean	Mean – 120% Mean	80% Mean – Mean
Green	> Mean	< Mean	> Mean

Figure 5.10 shows the new areas identified as less-stiff, in red. Lowering the less-stiff criterion for the roller's CMVs reduced the number of areas identified as less-stiff to 3, while increasing the number of areas considered as marginally stiff. This process allowed the identification of the areas with the lowest CMVs that correlated well with those areas that were identified as less-stiff by LWD. However, the percentage of mis-estimated areas with the new criteria did not decrease for the DCP measurements.

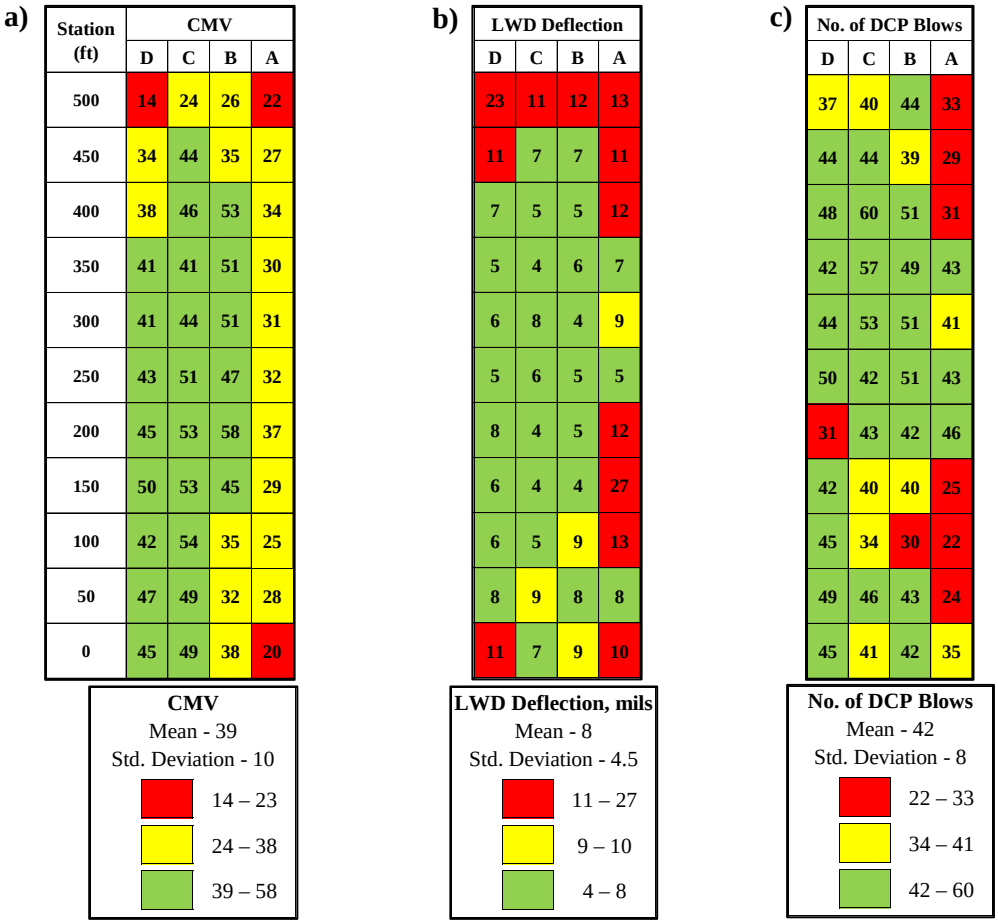

Figure 5.32 – Optimized Color-Coded Map Comparison between (a) CMV, (b) LWD Deflection and (c) Number of DCP Blows to Penetrate 24 in. as Obtained in Lime-Treated Subgrade at Site 1.

The use of an optimized class-break allowed for a better estimation of the less-stiff areas using the IC data. To evaluate this process for all sites, a comprehensive database with ICMVs and spot test measurements was assembled and the color-coded class-break was varied for identifying the less-stiff areas for both the CMV and the spot test measurements across all sites. However, in some sites and layers the optimized class-break still yielded an estimation of less-stiff areas with high uncertainty. This problem occurred mostly with flexible bases. The identification of less-stiff areas was also difficult to assess in sections with IC data measurements that had very low variability, since there is the possibility that no areas will be marked in red. For less-stiff subgrade sites, that generally exhibit more variability (coefficient of variation of CMVs > 35%), the optimization approach yielded an optimum class-break criteria set at 70% of the average CMV (or lower) and at 120% of the average LWD deflection (or lower), as shown in Table 5.10.

The results of this study showed the significance of maintaining uniformity of the compaction. As such, maps were generated with the coefficient of variations of the collected measurements as discussed next.

5.8.1 Effect of Variability of Measurements in Identification of Less-Stiff Areas

The roller measurements collected after proof-mapping of the subgrade at site 3 are shown in Figure 5.33 prior to performing any quality control. The figure shows the variability of the roller data using the coefficient of variation of the CMVs of each cell. High variability is present in the CMV measurements along Line A, and within a distance of 25 ft from the edges of the test section (all roller passes along Stations 0 and 250).

Table 5.10 – Percentage of Misestimated Roller Measurements (Rectangular Buffered Areas CMVs) with Respect to LWD Measurements Based on Different Percentages of Average Measurements for the Identification of Less-Stiff (Red) Areas

Percentage of IC Roller Misestimated Areas		Less-Stiff (Red) Area Above % of Average LWD Deflection						
		110	115	120	125	130	135	140
Less-Stiff (Red) Area Below % of Average CMV	90	32	32	32	39	58	68	68
	85	22	22	22	30	48	61	61
	80	24	24	24	33	48	62	62
	75	28	28	28	33	50	56	56
	70	14	14	14	21	43	50	50
	65	9	9	9	9	36	36	36
	60	0	0	0	0	33	33	33

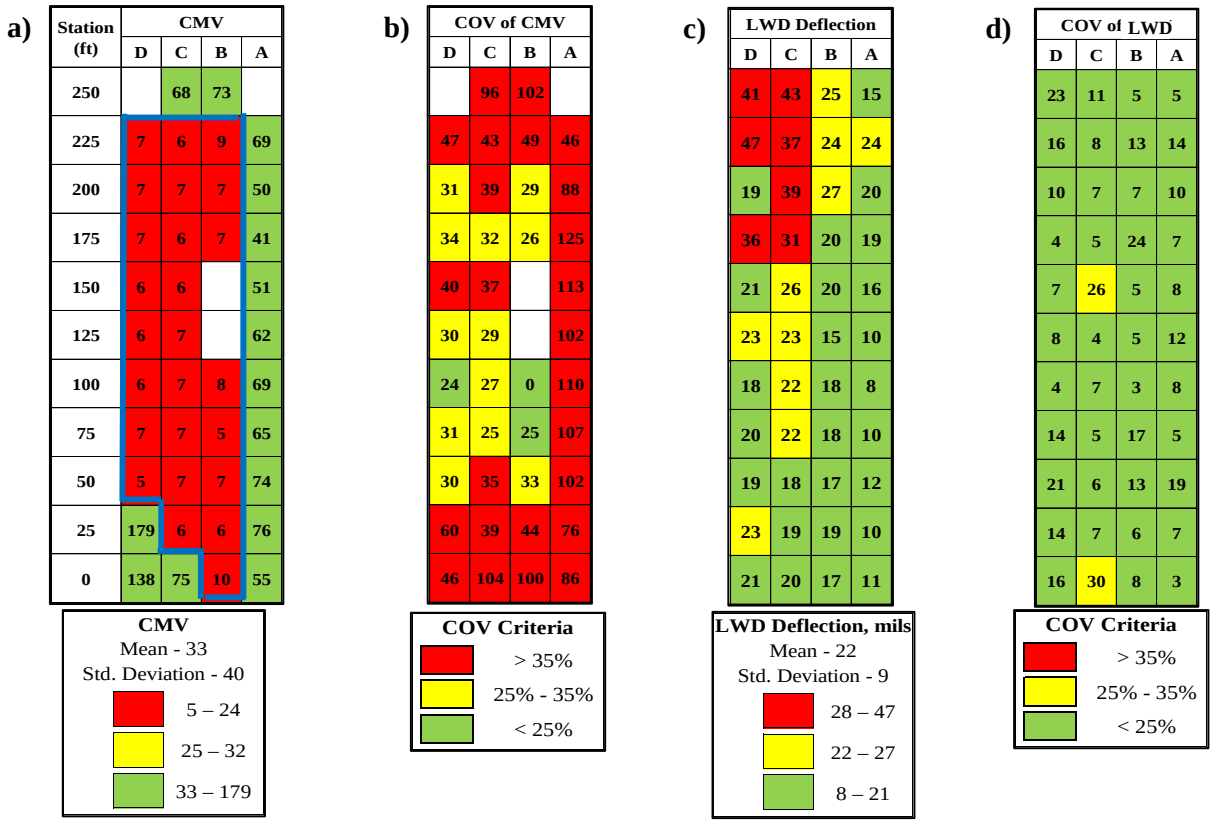

Figure 5.33 – Spatial Variation of CMV in Subgrade at Site 3: (a) Roller Collected CMV Data, (b) Mapping of Coefficient of Variation of CMV Data, (c) Mapping of LWD Deflection and (d) its Coefficient of Variation.

The latter is an indication that the roller had not reached its operating frequency and velocity, usually at about 30 Hz and 3 mph, respectively, before it started mapping. The CMV data contained between 25 and 50 ft away from the limits of the test section were also contaminated with high CMV measurements due to the aforementioned condition of the roller operation, but CMVs decreased considerably as the roller started to reach the adequate operating conditions. This is further supported by the map depicting the LWD deflections along the test section. Areas with low LWD deflection, i.e. stiffer areas, lie along Line A and within the areas estimated to be less-stiff by the CMV mapping, i.e. along Station 0 and 25. The variation

of the LWD measurements was considered to be uniform (COV < 25%) throughout the test section, as shown in Figure 5.33d.

Figure 5.34 shows the spatial variation of CMV in subgrade at Site 3 after the data with the high variability along Line A and within the 25 ft from the limits are removed. Using the color-criterion shown in Table 5.6, a new reconfigured color-coded map depicts the new areas that fall below the average CMV (see Figure 5.34a). Yet, only one buffered area was identified as less-stiff. Figure 5.34b depicts the results of making use of the optimized class-break shown in Table 5.10. None of the color-coded criteria was able to reveal less-stiff cells that matched the less-stiff areas since the section is reasonably uniform. The optimized class-breaks shown in Table 5.3 were also applied to the LWD deflections in Figure 5.12d. Visually the CMVs and LWD deflection color-coded maps are different. The reason for this pattern lies in the color-coded map of the coefficients of variation of CMVs. (see Figure 5.34c). Areas with high variability were defined as those COV areas that exceeded a COV of 35%. Despite the reasonably constant CMV maps, the COVs of a number of cells are large, indicating lack of the uniformity.

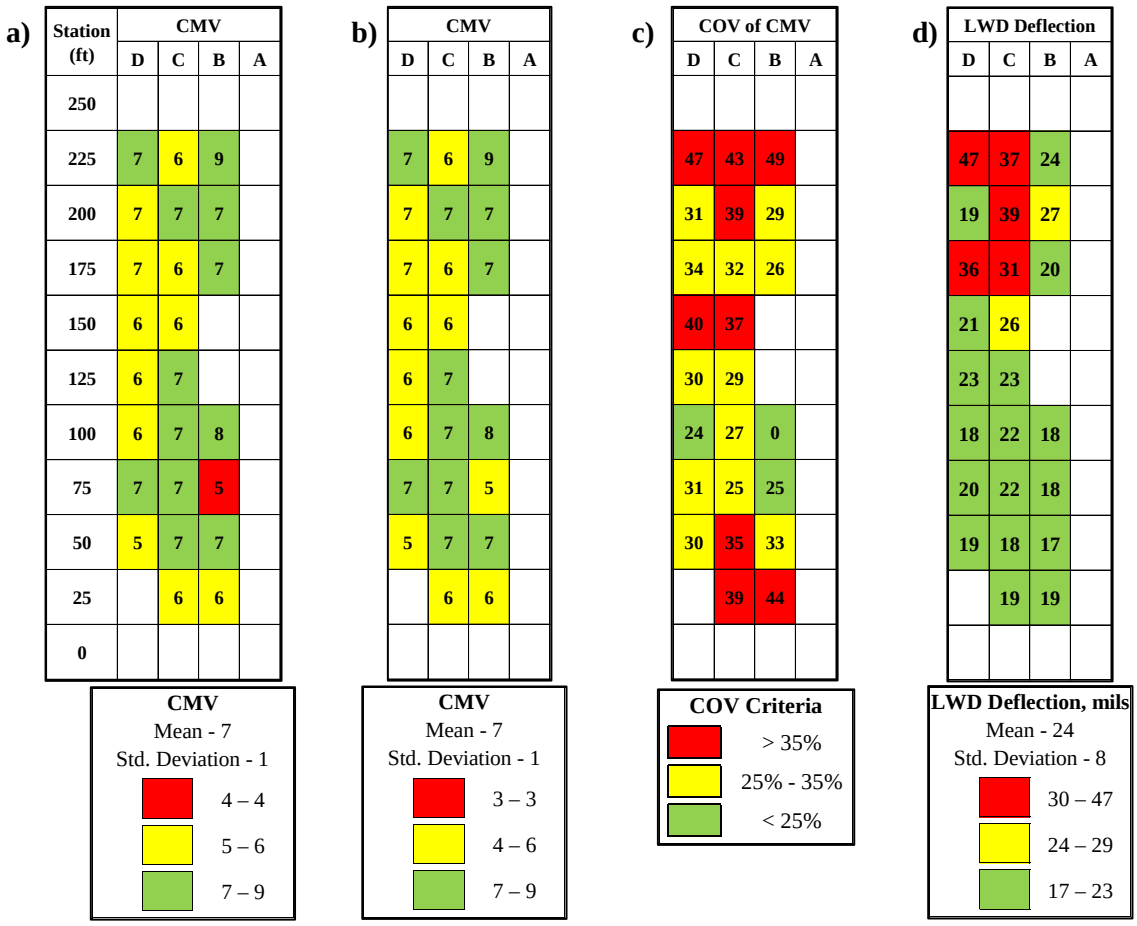

Figure 5.34 – Spatial Variation of CMV in Subgrade at Site 3 after Removal of CMV Data with High Variability: (a) Roller Collected CMV Data, (b) Mapping of CMV Data after Class-Break Optimization, (c) Mapping of Coefficient of Variation of CMV Data, and (d) Mapping of LWD Deflection.

Partially, the high COVs are the result of the poor operation of the roller during the proof-mapping process. This in turn can lead to a poor selection of areas for performing the quality control using modulus-based testing. It would be difficult to select a representative point for LWD in a cell.

This analysis allowed us to implement quality control on the acquired data from the UTEP-developed DAQ system by removing CMV measurements obtained at frequencies beyond ±5 Hz the roller operating frequency. This quality control permitted the generation of maps with almost all cells having a variability of COV < 50% in the last visited sites.

5.8.2 Recommendations for the Improvement of Proof-Mapping Process

The roller operator has to be aware of several factors which may affect the collection of IC data. One of these factors is the importance of maintaining a constant speed. At a constant rate of readings, any significant variation in the roller speed would lead to an uneven distribution of number of data points falling within each block which could dramatically impact the CMV average values for each of the blocks as well as the output map.

Figure 5.35 demonstrates the influence of variation of the roller vibration frequency by comparing the spectrograms from two data points in two different cells. One of these cells is at the beginning of a section and the other one is located 50 ft beyond the start of the section. As shown in Figure 5.35c, the second harmonic (first multiple of the operating frequency) has a relatively high amplitude as compared to the fundamental frequency. Conversely, the spectrogram in Figure 5.35d exhibits a lower ratio of second harmonic to the operating frequency amplitude; hence a more reasonable CMV for the corresponding block. Operating the roller without reaching its desired operating frequency leads to large CMVs, as previously discussed for the mapping obtained for the subgrade of Site 3. A cause of this problem is the transitioning from one pass to another before the roller is in full operational vibration mode. At the beginning of each pass, the roller revs up the system until it reaches the operating frequency whereas, at the end of each pass, the roller is slowed down. In both cases, the roller measurements are impacted by the change in the operating frequency. In order to prevent this issue, it is recommended to either start the data collection after the desired operating frequency is reached or to extend out the test area by a pre-determined length at least 50 ft from the beginning and the end of each roller pass.

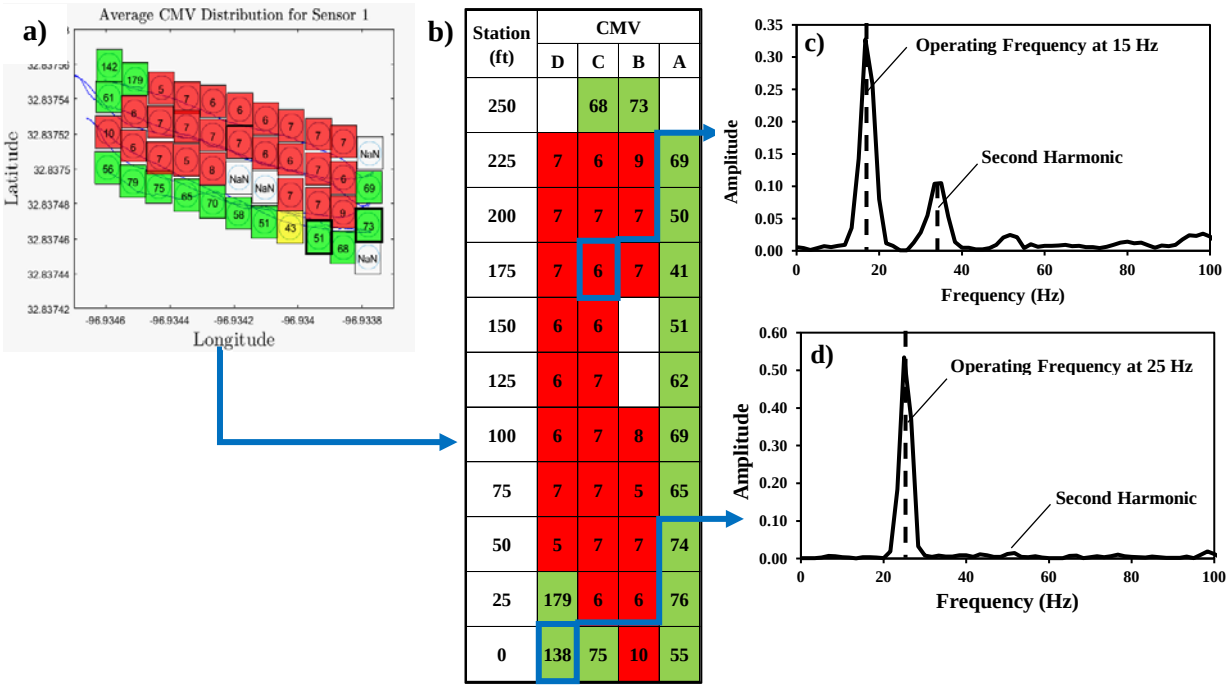

Figure 5.35 – CMV Mapping of Subgrade in Site 3 (a) with Roller Passes Overlapped and (b) per Station Showing High CMVs due to Poor Operation, and Accelerometer-Based Sample Measurement for Calculation of CMV on Section Proof-Mapped with (c) Proper Operating Settings and (d) Inadequate Operating Settings.

Another factor worth mentioning that hinders the correlation of ICMVs and NDT measurements lies on the number of measurements along the path driven by the roller operator. A wobbly direction of the roller pass can affect the number of measurements collected within each averaged rectangular area. For instance, Figure 5.35a shows four rectangular areas where no IC data were collected. This reduces the amount of CMV data for comparison with other modulus-based NDTs. To prevent this from happening, the roller operator must be instructed clearly beforehand the path where IC data needs to be collected.

5.9 Design Verification

The selection of the NDT devices depends on the variability, sensitivity to construction anomalies and the levels of risk to the contractor and TxDOT. Device-related uncertainties can be classified into three categories: accuracy, repeatability (precision) and reproducibility. Mazari et al. (2013) studied the precision and bias of the LWD. The parameters reported by Mazari et al. were repeatability of the equipment, reproducibility or the operator variability, and specimen variability. Table 5.11 summarizes the results of that study for the same LWD device used in this study, i.e. Zorn LWD.

Table 5.11 – Analyses of Variability of the LWD (after Mazari et al., 2013).

Measurement Device	Mean of Modulus Measurements, ksi	Equipment Variation, σ due to Repeatability, ksi*	Operator Variation, σ due to Reproducibility, ksi	Combined Device Variation, Gauge R&R†, ksi	Specimen Variation, SV, ksi	Total Variation, TV, ksi	COV‡ of Total Variation, %
LWD	3.48	0.27 (8%)	0.24 (7%)	0.36 (10%)	1.18 (34%)	1.23	35

Confidence level = 95%, Study variation = ±6σ, σ = standard deviation, no. of specimens = 18, no. of operators = 2, no. of measurement repetitions = 9, *numbers in parenthesis is the variation divided by the mean, †R&R = Repeatability and Reproducibility, ‡COV = Coefficient of Variation.

As summarized in Table 5.12, aside from the repeatability and reproducibility, about 91% of estimated variability was due to the variability in the specimens' moisture content and density.

Table 5.12 – Contribution of each Variability Parameter to Total Variability of the LWD (after Mazari et al., 2013).

Measurement Device	Equipment Variation (Repeatability) Proportion, %	Operator Variation (Reproducibility) Proportion, %	Combined R&R Proportion, %	Specimen Variation Proportion, %
LWD	5	4	9	91

The following equation can be used to estimate the sample size, *n* (Burati et al., 2004):

$$n = \frac{\left(Z_\alpha + Z_\beta\right)^2 \sigma^2}{e^2} \tag{5.4}$$

where α = Type I (contractor's) risk, β = Type II (owner's) risk, Z_α = the $(1-\alpha)^{th}$ percentile of the standard normal distribution, Z_β = the $(1-\beta)^{th}$ percentile of the standard normal distribution, σ = standard deviation, and e = tolerable error. Typically, σ is an approximation of the variability of modulus of compacted geomaterials tested by each device. The overall pattern of sample size based on different α and β, σ and e is presented in Figure 3.2. Parameter e is assumed to be equal to 1.5 times σ_t (i.e. total variation in Table 5.12) and σ is assumed to be equal to σ_{Gauge} (LWD device variation). Based on the values reported in Table 5.12 for σ_t and σ_{Gauge} for each device, the number of samples necessary per lot for a given level of α and β can be estimated. AASHTO (1984) categorizes projects into four groups (critical, major, minor and contractual) with corresponding α and β values shown in Figure 5.36. Based on Figure 5.36, using α = 5.0% and β = 0.5% (critical project), the sample sizes necessary are three for LWD used in the evaluated sites.

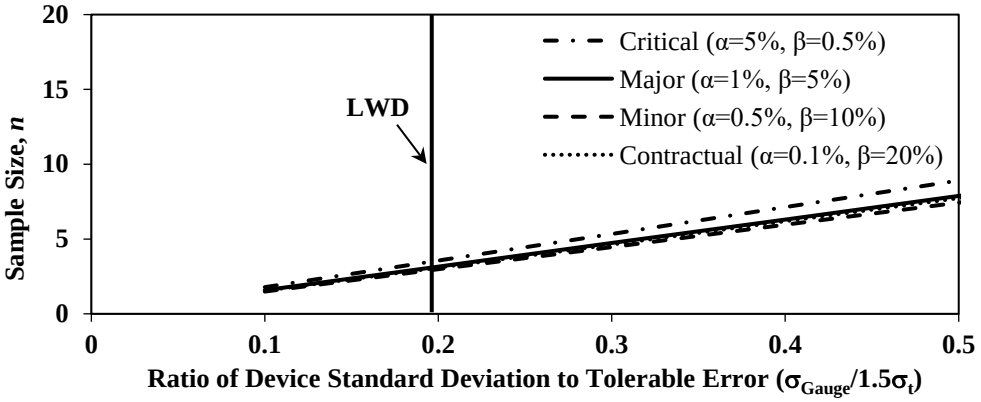

Figure 5.36 – Suggested Sample Size for LWD.

There is some degree of uncertainty (risk) in the measurement for acceptance because only a fraction of the material is sampled and tested. The Contractor's risk is the probability that material produced at the acceptable quality level is rejected or subjected to a pay adjustment. The Owner's risk is the probability that material produced at the rejectable quality level is accepted. Material should be rejected when a considerable number of field QA tests produce deflection measurements beyond an acceptable limit. To implement this, the percentage within specification limit (PWL) methodology in AASHTO R 9-05 based on the quality index can be used. For single sided specification limits, the lower quality index *Q* is computed using

$$Q = \frac{\bar{X} - LSL}{s}, \tag{5.5}$$

where $\bar{X}$ is the sample mean for the lot, *LSL* is the lower specification limit, and *s* is the sample standard deviation for the lot. The PWL is estimated after using the column appropriate to the total *n* number of measurements from the percent within limits estimation tables, available in TxDOT's Aviation General Construction Provisions, Section 110. Appropriate remedial procedures should be adopted for lots with an estimated PWL less than the agency minimum.

5.9.1 Determining Target Field Values and Adjustment of LWD Effective Deflection

For a robust modulus verification process, the target field values should be set in conjunction with establishing the design moduli, with consideration of the moisture content at the time of compaction and the state of stress imparted by the testing technology to the geomaterial layer. The target value should be the deflection for LWD and/or the rate of penetration for DCP. Most of the deflection-based devices measure the stiffness of the pavement system, and the reported modulus is based on an elastic-half space Boussinesq theory. This is particularly critical for a multi-layered system being tested with deflection.

Nazarian et al. (2014) developed a multi-layered equivalent-linear algorithm that makes use of an iterative process to consider the nonlinear behavior of the pavement materials using the modified MEPDG constitutive model described by Equation 3.1 to determine LWD target deflection, described in Chapter 3 of this report.

Research done on the effect of moisture content variation on the responses of unbounded geomaterials has demonstrated that suitable consideration must be given to this factor for pavement design. Even when unbound materials are compacted at values close to their optimum moisture content and maximum dry density, they do not remain under the same conditions over time. The moisture content will change from the compaction moisture content to an equilibrium moisture content. The moisture content will be heavily dependent on the environmental conditions, water table location, and properties of the soil materials at the site. It is important to take into account the variations of in moisture as one of the environmentally driven variables that can affect pavement layers and the subgrade capacity for carrying loads. The following

procedure can be used to adjust the LWD deflections based on moisture content obtained from the oven-dried samples.

To account the changes in moisture content in the subgrade over the design life of a pavement the model proposed by Witczak et al. (2002) using the enhanced integrated climatic model (EICM) can be incorporated to adjust the effective LWD deflection, d_{eff}, as follows:

$$d_{adj\ MEPDG} = d_{eff} \times F_U, \tag{5.6}$$

where F_U is determined from:

$$\log F_U = \left[a + \frac{b-a}{1+e^{\left[\ln\left(\frac{-b}{a}\right)+k_m\times\left(S-S_{opt}\right)\right]}} \right], \tag{5.7}$$

where a = -0.3123 for coarse-grained materials and a = -0.5934 for fine-grained materials (minimum of log F_U), b = 0.3010 for coarse-grained materials and b = 0.3979 for fine-grained materials (maximum of log F_U), k_m = regression parameter (6.8157 and 6.1324 for coarse and fine-grained materials, respectively), and S_{opt} = degree of saturation at optimum moisture content and S = degree of saturation at compaction moisture content, expressed in decimal.

Further development of this model by Cary and Zapata (2010) yielded the following approach where an composite environmental adjustment factor F_{env} is calculated. The measured LWD deflection, d_{eff}, can be converted to adjusted deflection, d_{adj}, from

$$d_{adj} = d_{eff} / F_{env}, \tag{5.8}$$

where F_{env} is calculated from:

$$\log F_{env} = \left[-0.40535 + \frac{1.20693}{1+e^{\left[0.68184+1.33194\times\left(\frac{S-S_{opt}}{100}\right)\right]}} \right]. \tag{5.9}$$

The degree of saturation of the compacted soil samples was determined using the following equation,

$$S = \frac{MC}{\left(\frac{G_s \cdot \gamma_w}{\gamma_d} - 1\right)}, \tag{5.10}$$

where MC is the moisture content at compaction (%), G_s is the specific gravity, γ_w is the unit weight of water and γ_d is the dry unit weight of soil. Moisture content from the soil samples obtained from the spot test locations was obtained from Tex-113-E test procedure. Likewise, the dry density was estimated from the moisture-density (M-D) curve as per Tex-113-E.

5.9.2 Determining Target Field Values

Table 5.13 provides the target LWD deflection values as determined from numerical simulation of the pavement structure using a multi-layered equivalent-linear algorithm and the design provided by TxDOT personnel for the specific sites. A target LWD deflection was calculated at 25% above target deflection, this to be equivalent to an 80% of the target modulus, to serve as a limit for marginally acceptance.

Figure 5.14 compares the averaged effective LWD deflections to the adjusted LWD deflections using both approaches, per station. Moisture content conditions had a significant effect on the adjusted deflections of site 3, marginally on the adjusted deflection of site 2 and none in site 1 where the higher moisture content values were obtained than the other two sites. Nonetheless, site 1 was the only site the testing of the subgrade yielded deflection measurements that at least marginally passed the +25% target deflection. None of the adjusted LWD deflection-based measurements passed the lower passing limit of +25% LWD target

deflection in site 2, while the LWD measurements after station 125 exhibit a significant drop of stiffness for site 3.

Table 5.13 – Descriptive Statistics of NDT Devices on Different Sections in Evaluated Sites

Site	Layer	Thickness, in.	Design Modulus, ksi	Target LWD Deflection, mils	+25% Target LWD Deflection, mils
1	LTS	36	35	7.2	9.0
	FB	12	50	5.2	6.5
2	LTS	8	35	8.9	11.1
	FB	12	50	5.8	7.3
3	LTS	12	75	10.4	13.0
	FB	8	30	5.4	6.8

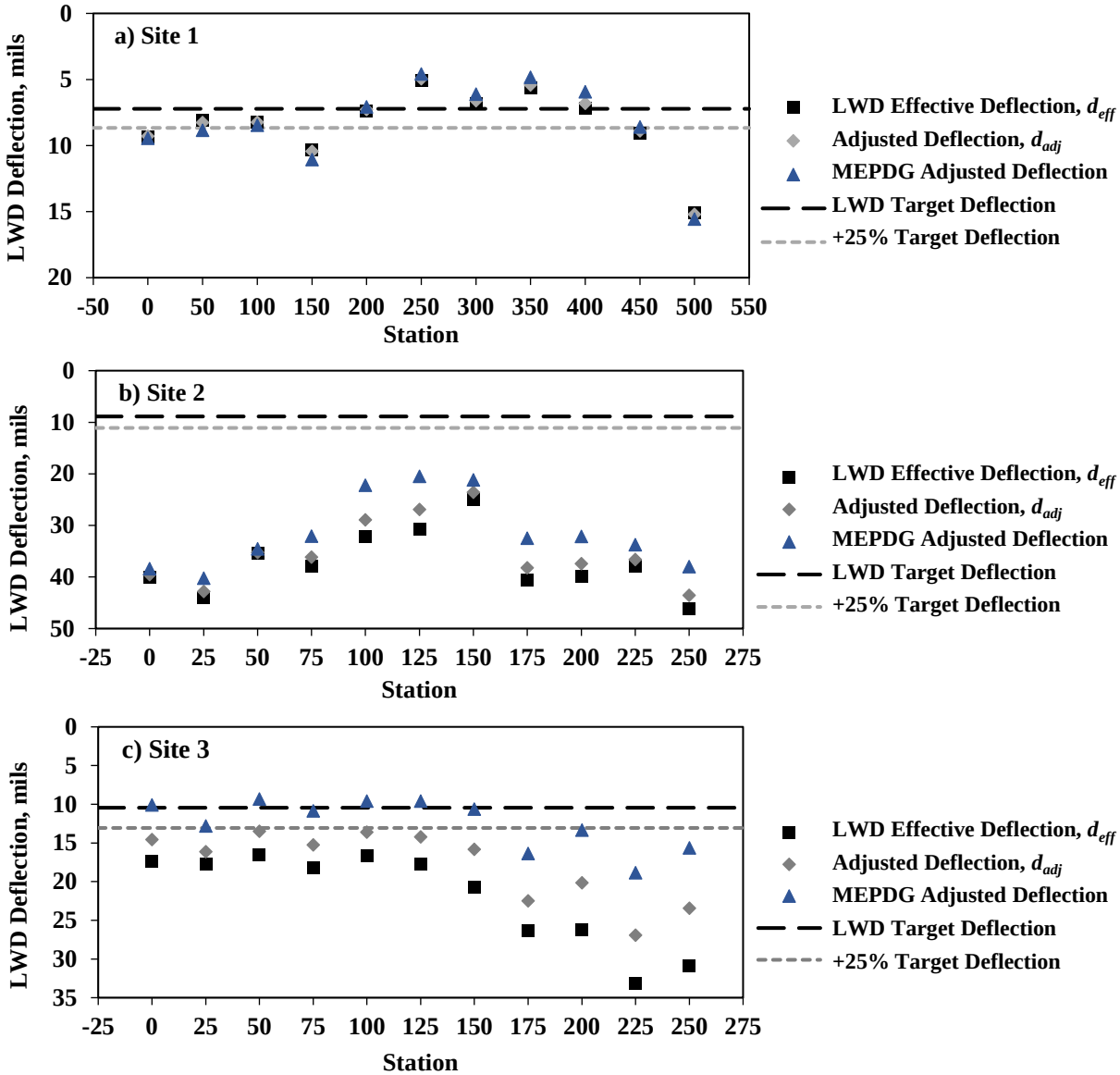

Figure 5.37 – Averaged LWD Deflections per Station in Lime Treated Subgrade Material with Corresponding Target LWD Deflection for (a) Site 1, (b) Site 2 and (c) Site 3.

Table 5.14 summarizes the percentage of LWD deflection-based measurements, after adjustment, in terms of the 44 spot tests (representative of a rectangular buffer area) that was below the target modulus in the subgrade sections of all evaluated sites. Percentages for measurements that marginally passed the +25% target modulus and the total percentage that passed the lower limit of +25% target deflection are also included. Extensive areas of Sites 1 and 3 meet the target deflection limits. However, the LWD deflections measurements of Site 2 indicate that this site did not met the design stiffness, as almost all LWD deflections are much greater than the acceptable limit.

Table 5.14 – Percentage of LWD Deflection-Based Measurements on Subgrade in Evaluated Sites

Site	Percent Passing	Percent Marginal	Percent Passing Lower Limit
1	55	9	64
2	5	0	5
3	39	36	75

To evaluate the impact of the LWD deflection measurements in Site 2, the reduction of service life in the different buffer areas of the test section was determined in terms of rutting. For this purpose, the base modulus was backcalculated by using the developed multi-layered equivalent-linear algorithm by means of an iterative process of adjusting the base modulus until the LWD deflection on top of the base layer was attained. Once the base moduli were backcalculated, the pavement structure as designed for that corresponding site was simulated using IntPave, a finite element analysis program suited for the analysis of flexible pavement subjected under truck traffic, to determine the number of passes of 34 kip tandem axles to reach a rutting failure (defined as 0.5 in.). This process is shown in Figure 5.38. This number was then compared to the number of passes to reach failure for each of the individual cells using their respective backcalculated properties to determine the reduction in service life.

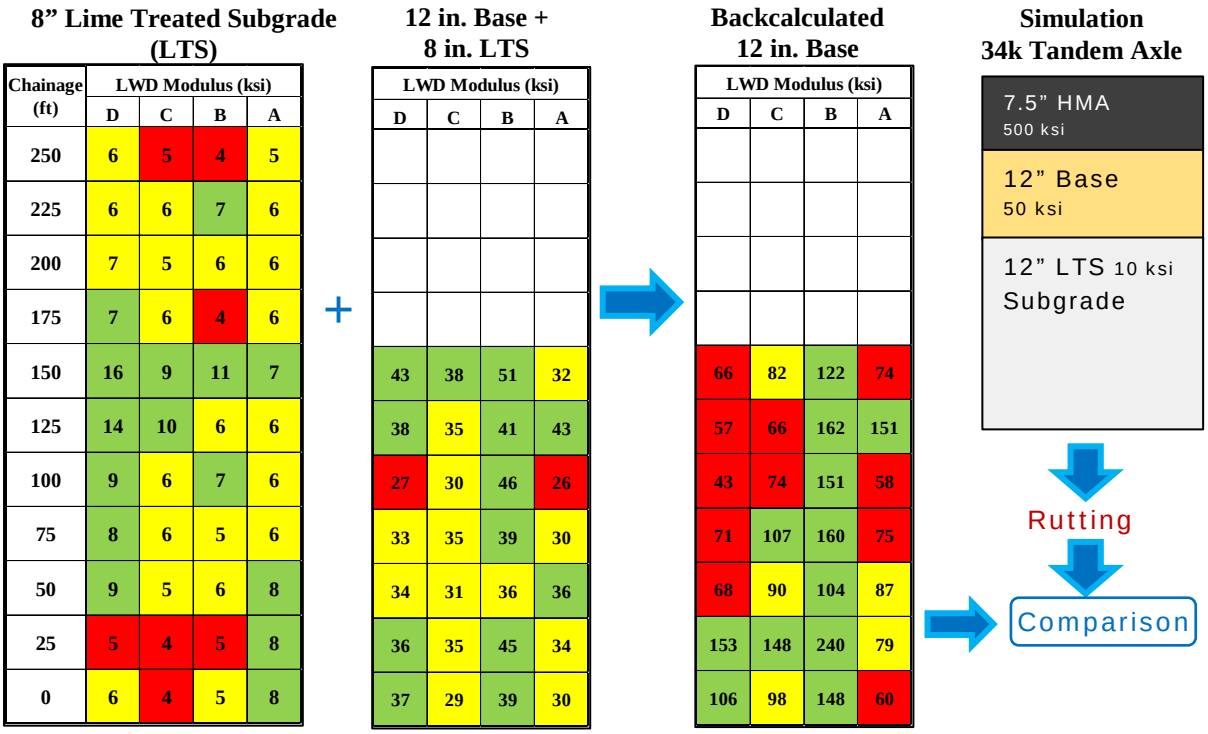

Figure 5.38 – Backcalculation of Base Modulus for the Prediction of Reduction of Service Life.

Figure 5.39 shows the predicted reduction in service life in terms of rutting as obtained for each of the rectangular buffer areas and averaged per station for Site 2. The mapped life reduction shows that service life in some areas will be far from meeting their designed service life. This example underlines the need to identify less-stiff areas by means of a tool that can provide full coverage of the site that relates to stiffness.

a)

Chainage (ft)	Life reduction %			
	D	C	B	A
250				
225				
200				
175				
150	234%	84%	180%	44%
125	168%	87%	57%	75%
100	52%	34%	94%	26%
75	55%	44%	49%	33%
50	65%	29%	48%	62%
25	38%	31%	64%	57%
0	52%	20%	50%	44%

b)

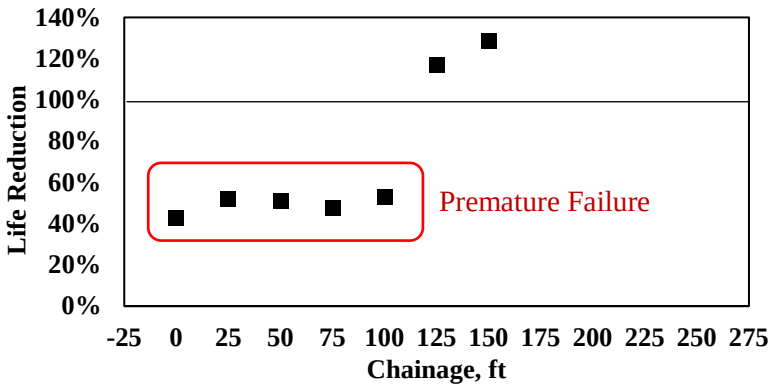

Figure 5.39 – Reduction in Service Life (a) in Rectangular Areas and (b) per Station in Site 2.

Based on the plot of the LWD deflection measurements to their respective CMV measurements shown in Figure 5.40, it can be inferred that those CMV measurements below 5 are indicative of less-stiff measurements, as discussed before. These areas must be reworked to achieve the desired target stiffness. CMV measurements above 30 are indicative of stiffer materials. Since these materials offer less variability, testing can performed at any location along the site. Those areas within a range of $5 \leq CMV < 30$ must be evaluated at the identified less-stiff (red) areas. Using class-break of 60% of the average CMV measurements, and a 120% of the average LWD deflection measurements are recommended to reduce the mis-estimated areas marked as less-stiff.

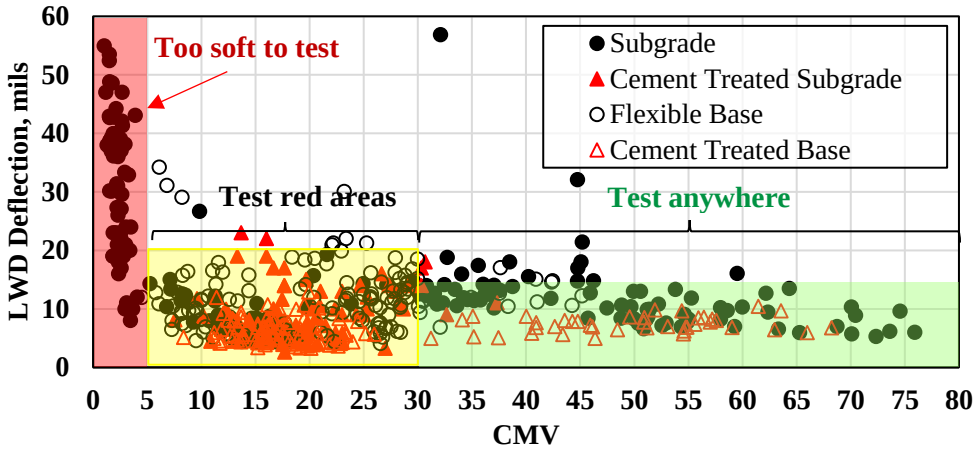

Figure 5.40 – Relationship between CMV and Deflections Measured from LWD Mass Drops for All Sites.

The proposed protocol for acceptance is illustrated by the decision tree provided in Figure 5.41. This protocol is based on the mapped coefficient of variation of the CMV measurements as well as the CMV measurements.

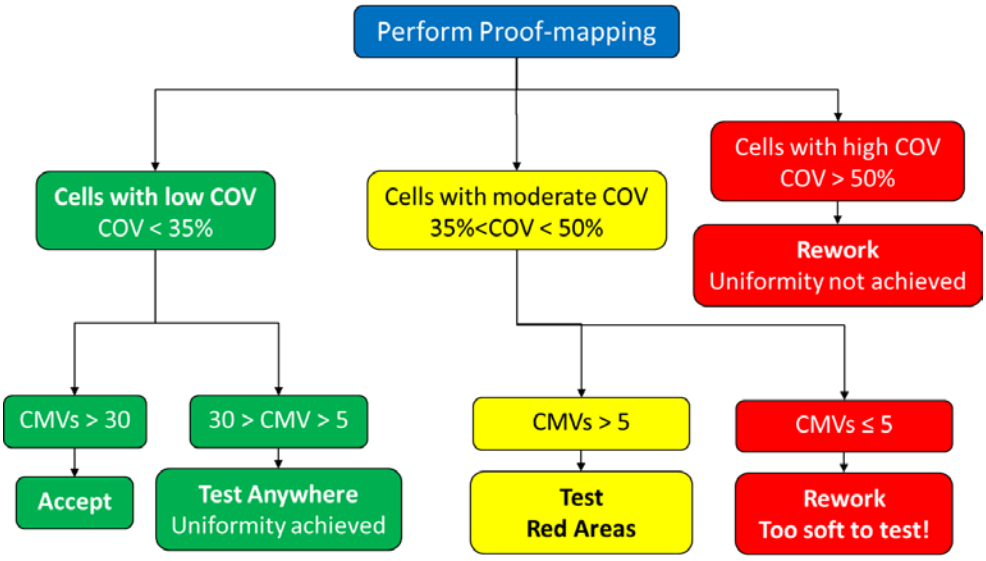

Figure 5.41 – Proposed Protocol for Project Acceptance.

Mapping of ICMVs and COV: After proof-mapping is performed, the mapping of ICMVs and their respective coefficient of variation should be provided using a rectangular grid based on areas practical for rework.

High COV (COV > 50%): Maps with cells with high coefficient of variation indicate that uniformity was not achieved and must be subject to rework.

Low COV (COV < 35%): Maps with cells with coefficient of variation less than 35% can be evaluated in two different ways. Cells with CMVs higher than 30 are indicative of a geomaterial that is stiff and can be accepted. A sample site with this condition is provided in Figure 5.42b. Cells within a range of $5 \leq CMV < 30$ with COV less than 35% indicate that uniformity was achieved but their stiffness must still be evaluated by means of deflection-based measurements. Due to the uniformity of the site, any point would suffice for performing deflection-based testing.

Moderate COV (35% < COV < 50%): Maps with moderate COV should be evaluated based on the CMV measurement. Those cells with CMV > 5 must be evaluated by performing deflection-based testing on the areas marked as less-stiff (in red color). Using class-break of 60% of the average CMV measurements and a 120% of the average LWD deflection measurements are recommended to reduce the mis-estimated areas marked as less-stiff. Cells with CMVs ≤ 5 indicate material is too soft to test and should be reworked.

5.10 Summary

A summary of the results obtained from field tests performed in all sites has been provided. The collected information and its analysis were used for assessing the weaknesses, bottlenecks and shortcomings of the process for implementing modulus-based field tests for project acceptance. The relationship between in-situ modulus-based NDT measurements and roller-based ICMVs was explored. A proposed protocol for project acceptance is proposed after the analysis of these relationships.

6 KEY FINDINGS AND RECOMMENDATIONS

The following key factors affect these relationships:

- A relationship can be seen between the LWD deflections and CMVs when the results are averaged within a buffer area as long as the variability of the CMV measurements within a buffer is small. This was also observed when DCP measurements were compared to the average CMVs.
- To identify areas with high variability, a mapping of the coefficient of variation of the roller measurements can be used for further assessment of the identified less-stiff areas.
- LWD testing was not sensitive enough on very stiff cement treated base that has cured for some time.
- High variability in the roller ICMV measurements occurs before the roller reaches its operating frequency and speed. Quality control to remove ICMV measurements obtained at frequencies other the roller's operating frequency reduces considerably the variability of the measurements.
- Visual correlations between ICMV and modulus-based measurements can be established using rectangular buffer areas and an established color-criteria.
- An optimization approach to improve the color-criteria was proposed to establish better relationships for identifying less-stiff areas.

REFERENCES

AASHTO (1984). "Acceptance Sampling Plans for Highway Construction, AASHTO Materials, Part 43 I Specifications: R-9." American Association of State Highway and Transportation Officials.

Abu-Farsakh, M., Nazzal, M., and Mohammad, L. (2015). "Effect of reinforcement on resilient and permanent deformations of base course material." *Transportation Research Record: Journal of the Transportation Research Board*, No. 2004, Transportation Research Board of the National Academies, Washington, D.C., pp. 120–131.

Abu-Farsakh, M. Y., Nazzal, M. D., Alshibli, K., Seyman, E., (2005), "Application of DCP in pavement construction control," Submitted to *84th Transportation Research Board Annual Meeting*, January 9-13, Washington, DC.

Akaike, H. (2011). "Akaike's Information Criterion." International Encyclopedia of Statistical Science, Springer, Berlin Heidelberg, pp. 25-25.

Akkinepally, R., and Attoh-Okine, N. (2006). "Quality control and quality assurance of hot mix asphalt construction in Delaware." *Report DCT 173*, Univ. of Delaware, Delaware Center for Transportation, Newark, DE.

Alavi, S., LeCates, J. F., and Tavares, M. P. (2008). "Falling weight deflectometer usage." *NCHRP Synthesis 381 Report*, Project 20-5 (Topic 38-15), Transportation Research Board, Washington, D.C.

Alshibli, K. A., Abu-Farsakh, M., and Seyman, E., (2005), "Laboratory evaluation of the Geogauge and light falling weight deflectometer as construction control tools." *Journal of Materials in Civil Engineering*, 17(5), 560–569.

Amber, Y., and Von Quintus, H. L. 2002. "Study of LTPP laboratory resilient modulus test data and response characteristics." *Report No. FHWA- RD-02-051*, Fugro-BRE, Inc. Austin, TX

Amini, F., (2003), "Potential applications of the static and dynamic cone penetrometers in MDOT pavement design and construction," In cooperation with the Mississippi Department of Transportation and the U.S. Department of Transportation Federal Highway Administration, September 2003.

Anderegg, R., Dominik A. von Felten., and Kaufmann, K. (2006). "Compaction monitoring using intelligent soil compactors." *Geo Congress 2006*, Atlanta, pp. 1-6.

Anderegg, R., and Kaufmann, K. (2004). "Intelligent compaction with vibratory rollers feedback control systems in automatic compaction and compaction control." *Transportation Research Record: Journal of the Transportation Research Board*, (1898), 124-134.

Barman, M., Nazari, M., Imran, S. A., Commuri, S., Zaman, M., Beainy, F., and Singh, D. (2014). "Application of intelligent compaction technique in real-time evaluation of compaction level during construction of subgrade." In *Transportation Research Board 93rd Annual Meeting*, Paper No. 14-5183, Washington D.C.

Bennert, T., and Maher, A. (2008), "The use of recycled concrete aggregate in a dense graded aggregate base course." *Final Report FHWA-NJ-2008-002*, Center for Advanced Infrastructure & Transportation (CAIT), Rutgers, The State University, Piscataway, NJ.

Berney, I.V., Ernest, S., and Wahl, R.E. (2011), "Device comparison for determining field soil moisture content," *Report No. ERDC/GSL-TR-08-3*, U.S. Army Corps of Engineers, Washington, D.C.

Brewer, C. A., and Pickle, L. (2002). "Evaluation of Methods for Classifying Epidemiological Data on Choropleth Maps in Series." Annals of the Association of American Geographers, 92, pp. 662-681.

Burati, J. L., Weed, R. M., Hughes, C.S., Hill, H.S. (2003), "Optimal procedures for quality assurance specifications." *Report No. FHWA-RD-02-095*, Federal Highway Administration (FHWA), pp. 57-59.

Cao, Y.-W., Liang, N.-X., Qin, M., and Lu, Z.-F. (2010). "Research on the correlation between vibration acceleration of roller and compaction degree of subgrade soil." *ICCTP 2010: Integrated Transportation Systems-Green, Intelligent, Reliable*, American Society of Civil Engineers, pp. 3738–3746.

Cary, C. E., and Zapata, C. E. (2011). "Resilient modulus for unsaturated unbound materials." *Road Materials Pavement Design*, 12 (3), pp. 615–638.

Celaya, M., Nazarian, S., and Yuan, D., (2010), "Implementation of quality management of base materials with seismic methods: case study in Texas." *Transportation Research Record: Journal of the Transportation Research Board*, (2186), Washington, D.C., 11-20.

Chang, G., Xu, Q., Rutledge, J., Horan, B., Michael, L., White, D. J., and Vennapusa, P. (2012). "Accelerated implementation of intelligent compaction technology for embankment subgrade soils, aggregate base, and asphalt pavement materials." *Report FHWA-IF-12-002*, Federal Highway Administration, U.S. Department of Transportation, Washington, D.C.

Chen, D. H., Wang, J. N., and Bilyeu, J., (2001), "Application of dynamic cone penetrometer in evaluation of base and subgrade layers," *Transportation Research Record: Journal of the Transportation Research Board* 1764, Washington, D.C, pp. 1-10.

D'Appolonia, D.J., R.V. Whitman, and E.D'Appolonia. (1969). "Sand compaction with vibratory rollers." *Journal of Soil Mechanics & Foundations Division*, ASCE, Vol. 95, pp. 263–284.

Dai, S. and Kremer, C., (2006), "Improvement and validation of MnDOT DCP specifications for aggregate base materials and select granular." *Report No. MN/RC-2005-32*, Minnesota Department of Transportation Office of Materials and Road Research, Maplewood, MN.

Duncan, J. M., Williams, G. W., Sehn, A. L., and Seed, R. B. (1991). "Estimation earth pressures due to compaction." *Journal of Geotechnical Engineering*, 117(12), pp. 1833-1847.

Ellis, R., and Bloomquist, D. (2003), "Development of compaction quality control guidelines that account for variability in pavement embankments in Florida." *Report UF 4504-710-12*, University of Florida Department of Civil and Coastal Engineering, Gainesville, FL.

Fathi, A., Tirado, C., Gholamy, A., Lemus, L., Mazari, M., and Nazarian, S. (2018). "Consideration of Depth of Influence in Implementation of Intelligent Compaction in Earthwork Quality Management." *Transportation Research Board 97th Annual Meeting, 2018*, Washington, DC, United States, 18-02100. https://trid.trb.org/view/1495174

Fleming, P. R., Frost, M. W., and Lambert, J. P., (2007), "Review of lightweight deflectometer for routine in situ assessment of pavement material stiffness." *Transportation Research Record: Journal of the Transportation Research Board*, No. 2004, Transportation Research Board of the National Academies, Washington, D.C., pp. 80–87.

Gallivan, V. L., Chang, G. K., and Horan, D. R. (2011). "Intelligent compaction for improving roadway construction." *GeoHunan 2011: Emerging Technologies for Material, Design, Rehabilitation, and Inspection of Roadway Pavements, GSP 218*, ASCE, pp. 117-124.

Gu, F., Sahin, H., Luo, X., Luo, R., and Lytton, R. (2014). "Estimation of resilient modulus of unbound aggregates using performance-related base course properties." *Journal of Materials in Civil Engineering*, 27(6).

Gudishala, R. (2004). "Development of resilient modulus prediction models for base and subgrade pavement layers from in situ devices test results." M.S. Thesis, Louisiana State University, Baton Rouge, LA.

Gupta, S., Ranaivoson, A., Edil, T., Benson, C., Sawangsuriya, A. (2007), "Pavement design using unsaturated soil technology." *Report No. MN/RC-2007-11*, Final Research Report submitted to Minnesota Department of Transportation, University of Minnesota, Minneapolis.

Guzina, B. B., and Osburn, R. H. (2002). "Effective Tool for Enhancing Elastostatic Pavement Diagnosis." *Transportation Research Record: Journal of the Transportation Research Board*, 1806, 30–37.

Heersink, D. K., Furrer, R., and Mooney, M. A. (2013). "Intelligent compaction and quality assurance of roller measurement values utilizing backfitting and multiresolution scale space analysis," arXiv preprint arXiv:1302.4631.

Hossain, M. S., Mulandi, J., Keach, L., Hunt, M., and Romanoschi, S. (2006). "Intelligent compaction control." *Airfield and Highway Pavements*, American Society of Civil Engineers, 304-316.

Hughes, C. S. (2005). "State construction quality assurance programs: a synthesis of highway pracrice." *NCHRP Synthesis 346*, Transportation Research Board., Washington, D.C.

Jenks, G.F., and Caspall, F.C. (1971). “Error on Choroplethic Maps: Definition, Measurement, Reduction.” Annals of the Association of American Geographers. 61(2), 1971, pp. 217-244.

Khalid, F., Vetter, D., Hill, B., and Esposito, R., (2005), “Evaluation of soil compaction measuring devices.” *Final Report GRI-004/0067*, Gas Technology Institute, Des Plaines, IL.

Khoury, N., Brooks, R., Boeni, S. Y., and Yada, D. (2012). “Variation of resilient modulus, strength, and modulus of elasticity of stabilized soils with postcompaction moisture contents.” *Journal of Materials in Civil Engineering*, 25(2), pp. 160–166.

Khoury, N. N., and Zaman, M. M. (2004), “Correlation between Resilient Modulus, Moisture Variation, and Soil Suction for Subgrade Soils,” *Transportation Research Record: Journal of Transportation Research Board*, No. 1874, pp. 99-107.

Kim, Y. R., and Park, H. G. (2002). “Use of falling weight deflectometer multi-load data for pavement strength estimation.” *Report FHWA/NC/2002-006*, NCSU, North Carolina Department of Transportation, Raileigh, NC.

Kim, S. H., Yang, J., and Jeong, J. H. (2014). “Prediction of subgrade resilient modulus using artificial neural network.” *KSCE Journal of Civil Engineering*, 18(5), 1372-1379.

Kung, J. H. S., Lin, H. D., Yang, S.-J., and Huang, W.-H. (2006). “Resilient modulus and plastic strain of unsaturated cohesive subgrade soils.” *Unsaturated Soils*, 1247–1258.

Lekarp, F., Isacsson, U., and Dawson, A. (2000). “State of the art. I: Resilient response of unbound aggregates.” *Journal of Transportation Engineering*, 126(1), pp. 68–75.

Lemus, L., Fathi, A., Gholamy, A., Tirado, C., Mazari, M, and Nazarian, S. (2018). “Geospatial relationship of intelligent compaction measurement values with in-situ testing for quality assessment of geomaterials.” *International Conference on Transportation & Development*, 2018, American Society of Civil Engineers, 2018, ASCE, (p. 293). https://doi.org/10.1061/9780784481554.030

Lin, D., Liau, C., and Lin, J. (2006). “Factors Affecting Portable Falling Weight Deflectometer Measurement.” *Journal of Geotechnical and Geoenvironmental Engineering*, 132(6), 804–808.

Li, D., and Sun, Z. (2015). “The effects of moisture content fluctuation on a dynamic resilient modulus of compacted clay.” *Advances in Civil Engineering and Building Materials IV*, Taylor & Francis Group, London, pp. 29-33.

Maher, A., Bennert T., Gucunski, N., and Papp, W. J., (2000). “Resilient Modulus of New Jersey Subgrade Soils,” *FHWA Report No. 2000-01*, Washington D.C.

Majidzadeh, K., Tashman, L., Redinger, D., Saraf, C., Hedrick, D., and Albrecht, D. (2014). “Application of innovative tools in optimizing risk and cost of subgrade QA/QC.” *Geo-Congress 2014, Geo-characterization and Modeling for Sustainability*, ASCE, pp. 2355-2364.

Malla, R., and Joshi, S. (2007). “Resilient modulus prediction models based on analysis of LTPP data for subgrade soils and experimental verification.” *Journal of Transportation Engineering*, 133(9), 491–500.

Malla, R., and Joshi, S. (2008). "Subgrade resilient modulus prediction models for coarse and fine-grained soils based on long-term pavement performance data." *International Journal of Pavement Engineering*, Vol. 9(6), 431-444.

Mazari, M., Navarro, E., Abdallah, I., and Nazarian, S. (2012). “Role of Resilient Modulus Constitutive Models on Response of Pavements,” 2nd International Conference on Transportation Geotechnics (ICTG), Sapporo, Japan, 6.

Mazari, M., Garcia, G., Garibay, J., Abdallah, I and Nazarian, S. (2013). “Impact of Modulus Based Device Variability on Quality Control Of Compacted Geomaterials Using Measurement System Analysis.” 92nd Annual Meeting, Transportation Research Board, Washington, DC, http://trid.trb.org/view/2013/C/1241890.

Mazari, M., Tirado, C., Nazarian, N., and Aldouri, R. (2017). “Impact of Geospatial Classification Method on Interpretation of Intelligent Compaction Data”, 2017 TRB Annual Meeting, Paper 17-05453, Washington, D.C.

McDonald, J. H. (2014). “Handbook of Biological Statistics.” 3rd ed. Sparky House Publishing, Baltimore, MD. pp. 209–212.

Miller, H., and Mallick, R. (2003), "Field evaluation of a new compaction monitoring device." Prepared for the New England Transportation Consortium, University of Massachusetts Dartmouth, Dartmouth, MA.

Mohammad, L. N., Gaspard, K., Herath, A., and Nazzal, M. (2007). "Comparative evaluation of subgrade resilient modulus from non-destructive, in-situ, and laboratory methods." *Report FHWA/LA.06/417*, Baton Rouge, LA.

Mohammad, L., Huang, B., Puppala, A., and Allen, A. (1999). "Regression model for resilient modulus of subgrade soils. *Transportation Research Record: Journal of the Transportation Research Board*, (1687), 47-54.

Mooney, M., and Adam, D. (2007). "Vibratory roller integrated measurement of earthwork compaction: An overview." *Seventh International Symposium on Field Measurements in Geomechanics (FMGM 2007)*, American Society of Civil Engineers, 1-12.

Mooney, M. A., and Miller, P. K. (2009). "Analysis of Lightweight Deflectometer Test Based on In Situ Stress and Strain Response." *Journal of Geotechnical and Geoenvironmental Engineering*, 135 (2), 199–208.

Mooney, M. A., and Rinehart, R. V. (2007). "Field monitoring of roller vibration during compaction of subgrade soil." *Journal of Geotechnical and Geoenvironmental Engineering*, American Society of Civil Engineers, 133(3), 257-265.

Mooney, M. A., and Rinehart, R. V. (2009). "In situ soil response to vibratory loading and its relationship to roller-measured soil stiffness." *Journal of Geotechnical and Geoenvironmental Engineering*, American Society of Civil Engineers, 135(8), 1022–1031.

Mooney, M. A., Rinehart, R. V., Facas, N. W., Musimbi, O. M., White, D. J., and Vennapusa, P. K. R. (2010). "Intelligent soil compaction systems." *NCHRP Report 676*. National Cooperative Highway Research Program, Transportation Research Board, Washington, DC.

Mooney, M., Rinehart, R. V., and van Susante, P. (2006). "The influence of heterogeneity on vibratory roller compactor response." *Geo Congress 2006*, American Society of Civil Engineers, 1-6.

Navarro, E., Garibay, J., Abdallah, I., and Nazarian, S. (2012). "Development of models to estimate modulus and permanent deformation of Texas bases," *Technical Memorandum: TXDOT 0-6622-4a*. *Subtask 4.1: MR and PD Model Developments for Granular Base Materials*. Center for Transportation Infrastructure Systems, The University of Texas at El Paso, El Paso, TX.

Nazarian, S., Abdallah, I., and Yuan, D. (2004). "Neural networks for rapid reduction interpretation of spectral analysis of surface waves results." *Transportation Research Record: Journal of the Transportation Research Board*, (1868), 150-155.

Nazarian, S., Mazari, M., Abdallah, I., Puppala, A. J., Mohammad, L. N., and Abu-Farsakh, M. Y. (2014). "Modulus-based construction specification for compaction of earthwork and unbound aggregate." *NCHRP Project 10-84*, Transportation Research Board, Washington, DC.

Nazarian, S., Williams, R., and Yuan, D., (2003), "A simple method for determining modulus of base and subgrade materials," *ASTM STP 1437*, ASTM, West Conshohocken, PA, 152–164.

Nazarian, S., Yuan, D., and Arellano, M., (2002), "Quality management of base and subgrade materials with seismic methods," *Transportation Research Record: Journal of the Transportation Research Board*, (1786), Washington, DC., 3–10.

Nazzal, M. D., and Tatari, O. (2013). "Evaluating the use of neural networks and genetic algorithms for prediction of subgrade resilient modulus." *International Journal of Pavement Engineering*, Taylor & Francis Group, 14(4), 364–373.

Oh, J. H., and Fernando, E. G. (2011). *Comparison of Resilient Modulus Values Used in Pavement Design*. Final Report BDL76-1, Texas Transportation Institute, College Station, Texas, 55–58.

Oman, M. (2004). "Advancement of grading and base material testing." Office of Materials, Minnesota Department of Transportation, Maplewood, MN.

Ooi, P. S. K., Archilla, A. R., and Sandefur, K. G. (2004), "Resilient modulus models for compactive cohesive soils," *Transportation Research Record: Journal of the Transportation Research Board*, No. 1874, pp. 115-124.

Ooi, P. S., Sanderfur, K. G., and Archilla, A. R. (2006). *Correlation of Resilient Modulus of Fine-Grained Soils with Common Soil Parameters for Use in Design of Flexible Pavement*. Report No. HWY-L-2000-06. Hawaii Department of Transportation, Honolulu, Hawaii.

Osaragi, T. (2002). Classification Methods for Spatial Data Representation. Centre for Advanced Spatial Analysis (UCL), London, UK, 2002.

Pacheco, L.G., and Nazarian, S. (2011), "Impact of moisture content and density on stiffness-based acceptance of geomaterials," *Transportation Research Record: Journal of Transportation Research Board*, No. 2212, pp. 1-13.

Parker, F., Brown, E., and Vecellio, R. L. (1993). "Development of new criteria for control of hot-mix asphalt construction." *Transportation Research Record: Journal of Transportation Research Board*, (1389), pp.1-8.

Petersen, D. L., and Peterson, R. (2006). "Intelligent compaction and in-situ testing at MnDOT TH53." *MnDOT Report MN/RC-2006-13*, CNA Consulting, Minnesota Department of Transportation, Minneapolis, MN.

Petersen, J. S., Romanoschi, S. A., and Hossain, M. (2007). "Development of stiffness-based specifications for in-situ embankment compaction quality control." Report No. K-TRAN: KSU-04-6. Kansas State University, Manhattan, KS.

Petersen, D. L., Siekmeier, J., Nelson, C. R., and Peterson, R. L. (2006). "Intelligent soil compaction technology results and a roadmap toward widespread use." Transportation Research Record, *Journal of the Transportation Research Board*, 1975, 81-88.

Ping, W. V., Yang, Z., and Gao, Z. (2002). "Field and laboratory determination of granular subgrade moduli." *Journal of Performance of Constructed Facilities*, 16(4), 149-159.

Pluta, S. E. and Hewitt, J. W., (2009), "Non-destructive impedance spectroscopy measurement for soil characteristics." *2009 GeoHunan International Conference (GSP 189): Characterization, Modeling, and Performance of Geomaterials*, pp. 144–149

Puppala, A.J., (2008), "Estimating stiffness of subgrade and unbound materials for pavement design," *NCHRP Synthesis 382*, Transportation Research Board, Washington, DC.

Rahman, F., Hossain, M., Hunt, M. M., and Romanoschi, S. A. (2007). "Intelligent compaction control of highway embankment soil." *86th Annual Meeting of the Transportation Research Board*, Annual Meeting CD-ROM.

Rahman, F., Hossain, M., Romanoschi, S. A., and Brennan, J. (2012). "Kansas experience with stiffness-based quality control/quality assurance specifications for compaction of highway embankments." *Geo Congress 2012*, American Society of Civil Engineers, 1522-1561.

Richter, C. (2006), "Seasonal variations in the moduli of unbound pavement layers." *Report FHWA-HRT-04-079*, Turner-Fairbanks Highway Research Center, McLean, VA.

Rinehart, R. V., Mooney, M. A., Facas, N. F., and Musimbi, O. (2012). "Examination of roller-integrated continuous compaction control on a Colorado testsite." *91st Annual Meeting of the Transportation Research Board*, Annual Meeting CD-ROM.

Sandström A.J., and Pettersson, C.B. (2004). "Intelligent Systems for QA/QC in Soil Compaction", Proc., *83rd Annual Transportation Research Board Meeting*, January 11-14. Washington, D.C.

Santha, B. L. (1994). "Resilient modulus of subgrade soils: comparison of two constitutive equations." *Transportation Research Record*, (1462), 79–90.

Sebesta, S. D., Scullion, T., Taylor, R. J., and Frazier, J. T. (2012) "Alternative methods of flexible base compaction acceptance." *Texas Transportation Institute, Research Report No. 0-6587-1*, The Texas A&M University System, College Station, TX.

Schuettpelz, C. C., Fratta, D., Edil, T. B., (2010), "Mechanistic corrections for determining the resilient modulus of base course materials based on elastic wave measurements." *Journal of Geotechnical and Geo-environmental Engineering*, 136(8), 1086-1094.

Schmalzer, P., Rada, G. R., and Miller, J. S. (2007). "Falling weight deflectometer (FWD) testing and analysis guidelines volume II: supporting documentation (U.S. customary units version)." *Report No. FHWA-FLH-07-001*, Washington, D.C., 2007, p. 16.

Senseney, C. T., Grasmick, J., and Mooney, M. A. (2015). "Sensitivity of Light Weight Deflectometer Deflections to Layer Stiffness via Finite Element Analysis." *Canadian Geotechnical Journal*, 52(7), 961–970.

Senseney, C. T., Krahenbuhl, R. A., and Mooney, M. A. (2013). "Generic Algorithm to Optimize Layer Parameters in Light Weight Deflectometer Backcalculation." Technical Note. *International Journal of Geomechanics*, 13(4).

Siddagangaiah, A. K., Aldouri, R., Nazarian, S., Chang, C. M., and Puppala, A. (2014), "Improvement of base and soil construction quality by using intelligent compaction technology." *Report FHWA/TX-13/0-6740-1*, Center for Transportation Infrastructure Systems, The University of Texas at El Paso, El Paso, TX.

Siekmeier, J. A., Young, D., and Beberg, D. (2000). "Comparison of the dynamic cone penetrometer with other tests during subgrade and granular base characterization in Minnesota." *Nondestructive testing of pavements and backcalculation of moduli: 3rd Volume, ASTM STP 1375.* S. D. Tayabji and E. O. Lukanen, Eds., ASTM International, West Conshohocken, PA.

Tanyu, B. F., Kim, W. H., Edil, T. B., and Benson, C. H. (2003). "Comparison of laboratory resilient modulus with back-calculated elastic moduli from large-scale model experiments and FWD tests on granular materials." *ASTM STP 1437*, 191-208.

Terzaghi, K., and R. B. Peck (1967). "Soil Mechanics in Engineering Practice." 2nd ed. John Wiley & Sons, Inc., New York, pp. 281–283.

Tirado, C., Mazari, M., Carrasco, C., and Nazarian, S. (2015). "Simulating response of different lightweight deflectometer testing using finite element modeling." In *Transportation Research Board 94th Annual Meeting* (No. 15-2228).

Tirado, C., Rios-Gomes, K. Y., Fathi, A., Mazari. M., Nazarian, S. (2017). "Simulation of Light Weight Deflectometer Measurements Considering Nonlinear Behavior of Geomaterials." Transportation Research Record: Journal of the Transportation Research Board, 2641, Washington, DC, 58–55.

Titus-Glover, L., and Fernando, E. B. (1995). "Evaluation of pavement subgrade material properties and test procedures." *Report No. FHWA/TX-96/1335-2*, Texas Transportation Institute, Texas A&M University, College Station, TX.

Toohey N. M., Mooney, M.A., Ryden, N., (2010), "Quality management of stabilized soil construction using lab and field seismic testing." *SAGEEP 2010*, Keystone, Colorado.

Tutumluer, E. (2013). "Practices for unbound aggregate pavement layers." *NCHRP Synthesis 445*, National Cooperative Highway Research Program, Transportation Research Board, Washington, D.C.

Velasquez, R., Hoegh, K., Yut, I., Funk, N., Cochram, G., Marasteanu, M., and Khazanovich, L. (2009). *Implementation of the MEPDG for New and Rehabilitated Pavement Structures for Design of Concrete and Asphalt Pavements in Minnesota*. Research Report MN/RC 2009-06. St. Paul, Minnesota.

Vennapusa, P. K. R. (2008). "Investigation of Roller-Integrated Compaction Monitoring and In-Situ Testing Technologies for Characterization of Pavement Foundation Layers." Doctoral Dissertation. Iowa State University, Ames, Iowa.

Vennapusa, P., and White, D. J. (2009) "Comparison of light weight deflectometer measurements for pavement foundation materials," *Geotechnical Testing Journal*, Volume 32, Issue 3, ASTM.

Vennapusa, P. K. R., White, D.J., and Morris, M. D. (2010). "Geostatistical analysis for spatially referenced roller-integrated compaction measurements." *Journal of Geotechnical and Geoenvironmental Engineering*, American Society of Civil Engineers, 136(6), 813-822.

Von Quintus, H. L., Rao, C., Bhattacharya, B., Titi, H., and English, R. (2010), "Evaluation of Intelligent compaction technology for Densification of Roadway Subgrades and Structural Layers," Submitted to the Wisconsin Highway Research Program (WHRP), Draft Final Report, WHRP Study No. 00092-08-07, Applied Research

Von Quintus, H. L., Rao, C., Minchin, R. E., Nazarian, S., Maser, K.R., and Prowell, B. (2009), "NDT technology for quality assurance of HMA pavement construction." *NCHRP Report 626*, National Cooperative Highway Research Program, Transportation Research Board, Washington, D.C.

Von Quintus, H. L., and Killingsworth, B. (1998), "Analyses relating to pavement material characterizations and their effects on pavement performance," *FHWA-RD-97-085*, Federal Highway Administration, McLean, VA.

Wacharanon, V., Wachiraporn, S., and Sawangsuriya , A. (2008), "Innovative tools for highway construction quality control." Technical Report, TransTech Systems, Inc.

White, D. J., Becker, P., Vennapusa, P. K. R., Dunn, M., and White, C. (2013). "Assessing Soil Stiffness of Stabilized Pavement Foundations." *Transportation Research Record: Journal of the Transportation Research Board*, (2335), pp. 99-109.

White, D. J., Jaselskis, E. J., Schaefer, V. R., and Cackler, E. T. (2005). "Real-time compaction monitoring in cohesive soils from machine response." *Transportation Research Record: Journal of the Transportation Research Board*, 1936, 173-180.

White, D. J., Morris, M., and Thompson, M. J. (2006). "Power-based compaction monitoring using vibratory padfoot roller." *Geo Congress 2006*, American Society of Civil Engineers, 1-6.

White, D. J., and Thompson, M. J. (2008). "Relationships between in situ and roller-integrated compaction measurements for granular soils." *Journal of Geotechnical and Geoenvironmental Engineering*, American Society of Civil Engineers, 134(12), 1763-1770.

White, D. J., Thompson, M. J., Vennapusa, P K. R.., and Siekmeier, J. (2008). "Implementing intelligent compaction specification on Minnesota TH-64 synopsis of measurement values, data management, and geostatistical analysis." *Transportation Research Record: Journal of the Transportation Research Board*, (2045), pp. 1–9.

White, D. J., Vennapusa, P., and Gieselman, H. (2011). "Field assessment and specification review for roller-intergarated compaction monitoring technologies." *Advances in Civil Engineering*, 2011, 1-15.

White, D. J., Vennapusa, P. K., R. and Thompson, M. J. (2007). "Field validation of intelligent compaction monitoring technology for unbound materials." Center for Transportation Research and Education (CTRE), Iowa State University, Ames, IA.

Williams, R. R., Nazarian, S., Yuan, D., (2002), "Methods of data analysis for correlating resilient modulus and seismic modulus test results," *Journal of Materials in Engineering*, American Society of Civil Engineers, New York, NY.

Witczak, M.W., Andrei, D. and Houston, W.N. Resilient Modulus as Function of Soil Moisture – Summary of Predictive Models. Development of the 2002 Guide for the Development of New and Rehabilitated Pavement Structures, NCHRP 1-37 A, Inter Team Technical Report (Seasonal 1), Tempe, AZ.

Wolfe, W., and Butalia, T. (2004). "Continued monitoring of SHRP pavement instrumentation including soil suction and relationship with resilient modulus." *Report No. FHWA/OH-2004/007*, Ohio State University, Columbus, OH.

Xiao, N., Calder, C.A., and Armstrong, M.P. (2007). "Assessing the Effect of Attribute Uncertainty on the Robustness of Choropleth Map Classification." International Journal of Geographical Information Science, 21(2), pp. 121-144.

Xu, Q., and Chang, G. K. (2016). "Adaptive quality control and acceptance of pavement material density for intelligent road construction." *Automation in Construction*, *62*, 78-88.

Xu, Q., Chang, G. K., Gallivan, V. L., and Horan, R. D. (2012). "Influences of intelligent compaction uniformity on pavement performances of hot mix asphalt." *Construction and Building Materials*, Elsevier Ltd, 30, 746–752.

Yau, A., and Von Quintus, H.L. (2002). "Study of LTPP laboratory resilient modulus test data and response characteristics." *Final Report FHWA-RD- 02-051*, U.S. Department of Transportation, FHWA, Washington, D.C.

Yuan, D., and Nazarian, S. (2003). "Variation in moduli of base and subgrade with moisture." *2003 Annual Meeting of the Transportation Research Board, Road/Pavement Design for Seasonal Effects Session*, Transportation Research Board of the National Academies, Washington, D.C., 15.

Zaman, M., and Khoury, N. (2007). “Effect of soil suction and moisture on resilient modulus of subgrade soils in Oklahoma.” *Report No. ORA 125-662*, Norman, OK.

APPENDIX A - SPECIAL SPECIFICATION FOR DEFLECTION-BASED DESIGN VERIFICATION

SPECIAL SPECIFICATION

XXXX

Deflection-Based Design Verification

1. Description.

The primary objective of this document is to develop procedures and specifications that can be used to estimate the uniformity and mechanical properties of compacted geomaterials for design verification employing stiffness or deflection-based devices and Intelligent Compaction (IC) rollers.

2. Terminology.

A. Dynamic Cone Penetrometer (DCP). A quasi-nondestructive device that involves driving a cone shaped probe into the soil or aggregate layer using a dynamic load and measuring the advancement of the device for each applied blow or interval of blows. The depth of penetration is directly impacted by the height of the drop weight, cone size, and cone shape. Also, the resistance to penetration is dependent on the strength of the material. The strength, in turn, is dependent on density, moisture, and material type of the layer evaluated.

B. Intelligent Compaction. A technology to collect georeferenced stiffness-based data during and after compaction of geomaterial layers.

C. Intelligent Compaction Measurement Values (ICMV). A set of IC data used to assess the uniformity of compaction based on IC roller vibration measurements.

D. Intelligent Compaction Retrofit Kit (a.k.a. Aftermarket Kit). A set of stand-alone IC instrumentation that could be mounted on almost any dynamic vibratory roller to collect ICMV data.

E. Light Weight Deflectometer (LWD). A nondestructive deflection-based device to evaluate the stiffness of compacted layers by applying an impulse load through dropping a weight from a specified height on a loading plate on top of a compacted geomaterial layer.

F. Mapping. Collecting IC data at a specific vibration setting and roller speed after completion of compaction process.

G. Pre-mapping. Collecting IC data at a specific vibration setting and roller speed before placement of a new geomaterial layer.

H. Proof-mapping. The process of using an IC roller to map the uniformity and consistency of compaction for the entire section upon completion of compaction.

I. VETA. A Standardized Intelligent Construction Data Management (ICDM) public domain software that stores, maps and analyzes IC and associated geospatial data, available online at http://www.intelligentcompaction.com,

3. Materials.

Incorporate the requirements included in Section 8.3 of the DB earthwork specifications. Furnish uncontaminated materials of uniform quality that meet the requirements of the

plans and specifications in accordance with Item 110, "Excavation;" Item 132, "Embankment;" Item 247, "Flexible Base;" ~~Item 251, "Reworking Base Courses;" Item 260, "Lime Treatment (Road-Mixed);" Item 263, "Lime Treatment (Plant-Mixed);" Item 265, "Fly Ash or Lime-Fly Ash Treatment (Road-Mixed);" Item 275, "Cement Treatment (Road-Mixed);" and Item 276, "Cement Treatment (Plant-Mixed)."~~ Notify the Engineer of the proposed material sources. Notify the Engineer before changing any material source. The Engineer may sample and test project materials at any time throughout the duration of the project to assure specification compliance. Use Tex-100-E for material definitions.

4. Equipment

Furnish machinery, tools, and equipment necessary for proper execution of the work in accordance with the plans and the applicable Specification Items listed in Section 3, "Materials." The specifications of LWD device and IC rollers shall conform to Tex-998-E and Tex-999-E, respectively. The DCP test apparatus shall conform to ASTM D 6951.

5. Design Verification Process.

Follow the flowchart in Figure 1 to perform the design verification process.

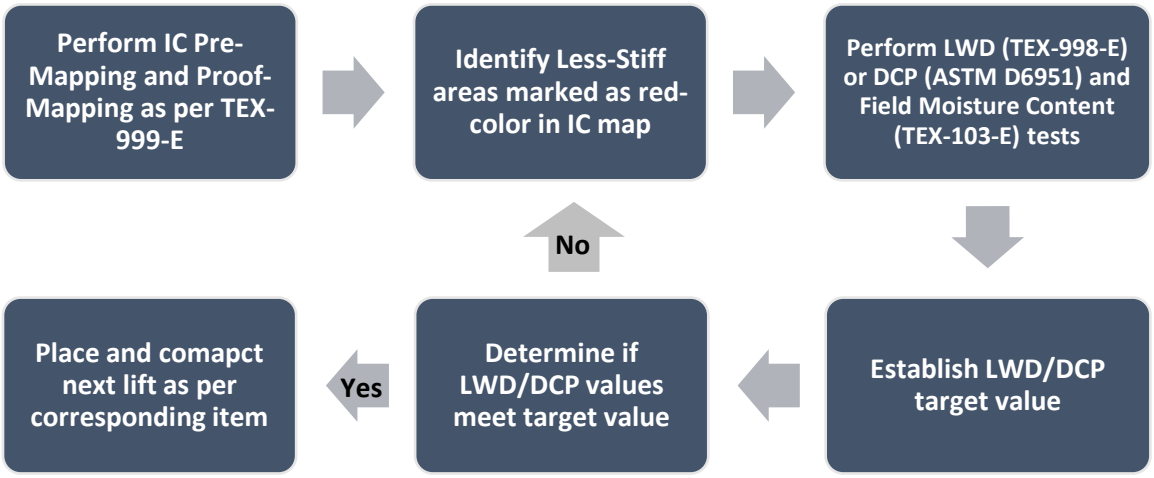

Figure 1 - Design Verification Process for DB Projects

Use the TxDOT test procedures in Table 1 to characterize the compacted geomaterial for design verification.

Table 1 - Materials and Test Procedures

Testing	Material Type
Light Weight Deflectometer (LWD) (ASTM D2835, Tex-998-E)	Subgrade and Base
Intelligent Compaction (IC) Roller (Tex-999-E)	Subgrade and Base
Dynamic Cone Penetration (DCP) (ASTM D6951)	Subgrade
Soil Classification (Tex-142-E)	Subgrade and Base

5.1. Selecting IC System.

Specify the type of IC roller for use prior to the beginning of the compaction process to include the accuracy of the GPS unit. The specifications of the IC system must be approved by the Engineer. The installation of the retrofit kit on conventional rollers needs special configuration and installation processes that should be planned in advance of their use. Furnish the roller model and serial number prior to installation of the retrofit kit to accommodate for any special equipment and installation process.

5.2. Pre-Mapping.

Follow Tex-999-E to pre-map the existing layer prior to placement and compaction of the layer of interest. Use the average ICMV collected from pre-mapping as the target value during the proof-mapping of the new layer/lift. Perform the pre-mapping process at low amplitude and low frequency vibration settings with forward passes of the IC roller over the section at a speed of no more than 3 mph.

5.3. Compaction

Compact the lift in a manner such that the finished layer is adequately and uniformly compacted and conforms to Sections 3 and 4.

5.4. Finishing.

Immediately after completing compaction of the final layer, finish the final section in accordance with the plans and the applicable specification items listed in Section 3, "Materials."

5.5. Curing.

Cure the finished section in accordance with the plans and the applicable specification items listed in Section 3, "Materials."

5.6. Identifying Less Stiff Areas by Proof-Mapping.

Upon completion of the compaction process, map the section using the IC roller with the same vibration settings as in Section 5.2, "Pre-Mapping," to generate a color-coded map. Review the color coded map of the compacted section and identify the relatively less-stiff areas[1].

5.7. Performing Spot Tests.

Perform the LWD/DCP tests within the identified less-stiff areas in Section 5.4, "Finishing." Follow the steps in Tex-998-E to perform the LWD test to obtain deflections. Follow the ASTM D6951 procedure to perform the DCP test to obtain the penetration rate. The density and moisture measurements shall be taken by the Engineer within the red color areas identified by the IC color-coded map. Moisture content may be determined in accordance with Tex-103-E, Part I.

[1] **The research team will work to define less stiff area rigorously.**

5.8. Establishing Target Values.

Establish the target LWD deflection as per Tex-998-E using the provided software package (see Figure 3). Perform the spot tests as soon as possible and before the material loses 2% of its placement moisture content. Determine the in-situ moisture content as per Tex-103-E[2] concurrent with LWD/DCP tests. Adjust the measured value for the moisture content at the time of spot testing. If the adjusted deflection/penetration rate exceeds the established target value, rework the area.

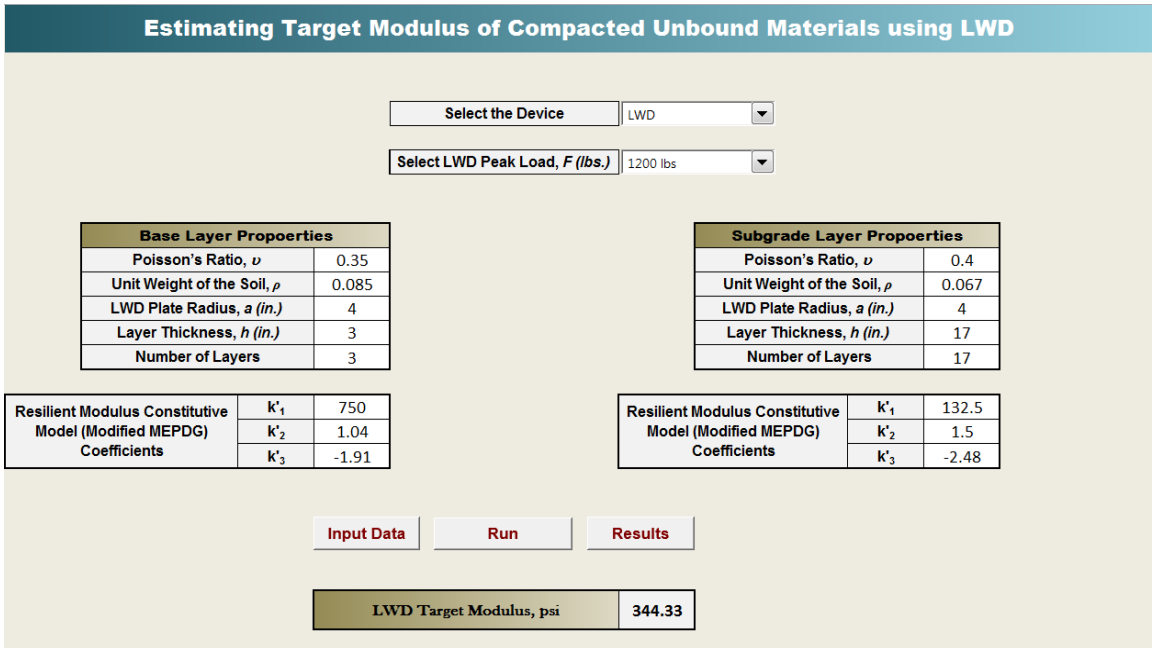

Figure 3 – Establishing LWD Target Field Modulus

6. Measurement and Payment.[3]

The work performed, materials furnished, equipment, labor, tools, and incidentals will not be measured or paid for directly but will be subsidiary to the pertinent Items.

[2] **The research team will work to define the best way to obtain moisture content.**
[3] **The research team will discuss this with TxDOT.**

APPENDIX B - TEST PROCEDURE FOR DETERMINING DEFLECTION OR MODULUS OF GEOMATERIALS USING LIGHT WEIGHT DEFLECTOMETER

Test Procedure for

DETERMINING DEFLECTION OR MODULUS OF GEOMATERIALS USING LIGHT WEIGHT DEFLECTOMETER

TxDOT Designation: Tex-998-E

Effective Date: XXX 201X

1. SCOPE

1.1 This test method describes the procedure for measuring the deflection with a Light Weight Deflectometer (LWD) and for estimating the in-place modulus of compacted geomaterials used in embankments, subgrade and base layers. The method is used for quality control/quality acceptance (QCQA) testing of compacted geomaterials for construction.

1.2 The LWD test relates surface deflection with the modulus and is defined as the maximum axial stress of a material divided by the maximum axial strain during that loading.

1.3 The measurements are made with a device that conforms to ASTM E 2835 or ASTM E 2583.

1.4 The values given in Customary Units are to be regarded as the standard. The values given in parentheses (SI Units if provided) are not standard and may not be exact mathematical conversions. Use each system of units separately. Combining values from the two systems may result in nonconformance with the standard.

2. DEFINITIONS

2.1 *Deflection*—the amount of downward vertical movement due to the application of an external load to the material surface.

2.2 *LWD effective modulus*—a composite surface modulus obtained based on Boussinesq elastic solution obtained from the peak surface deflection response of a layered system of geomaterials to an impact loading.

2.3 *LWD adjusted modulus*—the adjusted composite surface modulus after accounting for difference in the lab and field moduli at the same moisture conditions and density.

3. APPARATUS

3.1 *Loading device,* consists of a falling weight with a guide system, lock pin and spring assembly. The LWD shall conform to either the ASTM E 2835 or ASTM E 2583 (see Figure 1). The fixed drop height shall be in accordance with the manufacturer recommendation. The load is a force pulse, typically 1000 lb to 2000 lb (4.5 kN to 9 kN), generated by a falling mass dropped onto a spring or buffer assembly that transmits the load pulse to a plate resting on the material under test.[1]

3.2 *Handle grip,* is located at the top of the device. It is used to hold the LWD guide rod plumb and to limit the upward movement of the falling weight.

3.3 *Top fix and release mechanism* holds the falling weight at a constant height.

3.4 *Guide rod* allows the falling mass to drop freely.

3.5 *Lock pin* has two positions: locked and unlocked, to release the falling weight for use.

3.6 *Buffer system,* a damping system which provides a controlled transient pulse length to the impact force, typically in the range of 16 to 30 ms, which can be comprised of a spring or a set of steel bearing plates that transmits the load pulse to the plate resting on the material to be tested. The spring element is typically a series of rubber cones/buffers, or a cylindrical pad system.

3.7 *Loading plate,* bearing plate whose diameter typically varies from 8 to 12 in. (200 to 300 mm) in diameter, provides an approximate uniform distribution of the impulse load to the surface.

3.8 *Load cell* measures the applied load of each impact and is only available on devices that conform to ASTM E 2583.

3.9 *Deflection sensor* measures maximum vertical movement with an accelerometer or geophone. Location of deflection sensor may vary depending on manufacturer's design[2].

3.10 *Miscellaneous equipment* consisting of a spade, broom, trowel and cotton gloves for operation of the light weight deflectometer.

[1] Even though the operation of the devices that conform to ASTM E 2835 and ASTM E 2583 is similar, their measured parameters are different. Research team will work with TxDOT for optimal specification.
[2] This needs to be standardized during the project.

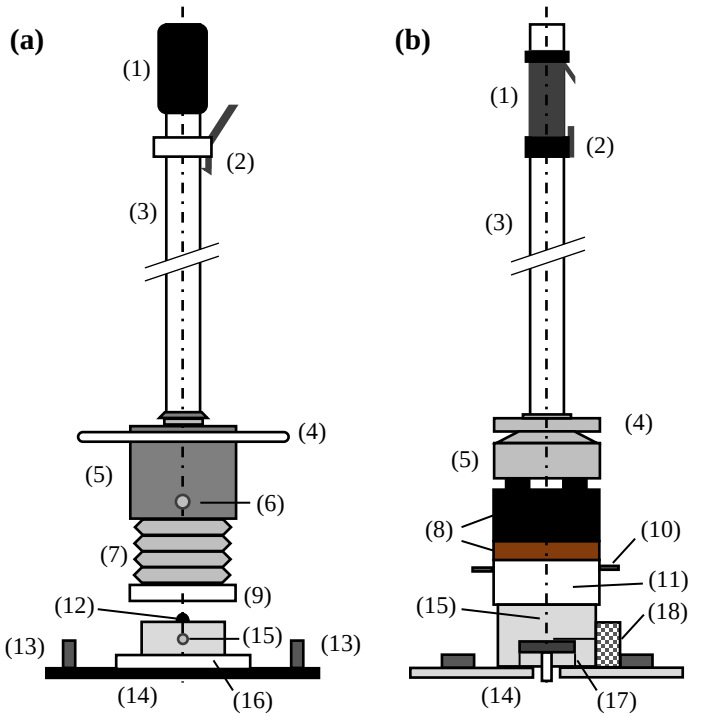

1. Grip
2. Top fix and release mechanism
3. Guide rod
4. Round grip
5. Falling mass
6. Lock pin
7. Set of steel springs
8. Buffers
9. Anti-tipping fixture
10. Geophone seating lever
11. Load cell
12. Load canter ball
13. Carry grip
14. Loading plate
15. Socket for connection to readout unit
16. Adapter plate
17. Geophone (spring loaded)
18. Communication port

Figure 1. Components of light weight deflectometer (LWD) that comply with (a) ASTM E 2835 and (b) ASTM E 2583.

4. PROCEDURE

4.1 Close off the entire testing area from any vehicular or construction equipment for the entire testing period. Clear out any other safety concerns that would impact the testing procedure and safety of the testers prior to testing.

4.2 For surface preparation, the test area shall be leveled so that the entire undersurface of the load plate is in contact with the material being tested. Loose particles on the surface and protruding material shall be removed. If required, any unevenness shall be filled with fine sand. The test shall not be conducted if the temperature is below freezing. The test area shall be at least 1.5 times larger than the loading plate.

4.3 Select the 8 in. (200 mm) or 12 in. (300 mm) diameter load plate. Position the load plate on a properly prepared test site. Set the load plate parallel to the testing surface on a thin (not to exceed ¼ in. thickness) layer of uniform fine sand using the least quantity for uniform loading. Twisting or working the load plate back and forth is permitted to help provide uniform seating of the plate.

4.4 After surface preparation and the load plate is positioned on the surface, center the loading device on the top of the loading plate and connect the data processing and storage system to the deflection sensor using the cable provided. Turn on the readout unit system to be ready for testing.

4.5 Use the following procedure for each drop:

4.5.1 Raise the falling mass to the preset drop height and snap into the release mechanism.

4.5.2 Adjust the guide rod to vertical by either observing the level or visually estimate by others in two perpendicular directions to the rod and itself.

4.5.3 Drop the falling mass by releasing the lock pin.

4.5.4 Catch the falling mass after rebound from striking the plate as recommended by the manufacturer. A test is considered invalid if the operator does not catch the falling weight after the weight rebounds from the load plate or the load plate moves laterally. A new test area is required at least 2 ft away from the original area of testing when the test is invalid.

4.5.5 Raise and snap the load mass into the release mechanism after each rebound.

4.6 Conduct three seating drops by repeating steps 4.5.1 to 4.5.5.

4.7 Following the three seating drops, conduct three drops of the falling mass by repeating steps 4.5.1 to 4.5.5 for analysis and record the deflection and applied load (if applicable) for each drop.

4.8 Record supporting information such as location, material type, and other identification information as needed.

4.9 Measure the in situ moisture content of the material as per Tex-103-E, "Determining Moisture Content in Soil Materials" or other method specified by the Engineer right after the deflection-based measurements are made[3].

4.10 Follow the process described in steps 5.1 to 5.5 to calculate the LWD effective modulus if desired.

5. ADJUSTMENT OF LWD EFFECTIVE DEFLECTION[4]

5.1 The measured LWD deflection, d_{eff}, can be converted to adjusted deflection, d_{adj}, from:

$$d_{adj} = d_{eff} / K_{adj} \quad (2)$$

where K_{adj} is calculated as discussed in Section 6.2.

5.2 To establish the LWD adjustment factor, K_{adj}, obtain K_{adj} from:

$$K_{adj} = K_{lab\text{-}field}\, K_{moist} \quad (3)$$

[3] **Research team will work to improve this step through the operational constraints or more convenient way of measuring moisture content.**

[4] **These adjustments seems crucial based on almost all recent studies. Research team will work to improve this step through the operational constraints or more convenient way of obtaining the parameters.**

where $K_{lab\text{-}field}$ is an adjustment factor that accounts for differences in lab and field moduli at the same moisture content and density, and K_{moist} is an adjustment factor for differences in the compaction and testing moisture contents.

5.3 Estimate $K_{lab\text{-}field}$ from the following relationship:

$$K_{lab\text{-}field} = (F_{env})^{\lambda} \quad (4)$$

where λ = -0.36 and F_{env} is calculated from:

$$\log F_{env} = \left[-0.40535 + \frac{1.20693}{1 + e^{\left[0.68184 + 1.33194 \times \left(\frac{S - S_{opt}}{100}\right)\right]}} \right] \quad (5)$$

where S_{opt} = degree of saturation at optimum moisture content and S = degree of saturation at compaction moisture content.

5.4 Estimate K_{moist} in the following manner:

$$K_{moist} = e^{\eta(\omega_C - \omega_T)} \quad (6)$$

where η = -0.18 for fine grained soils and 1.19 for unbound aggregates, ω_T = moisture content at time of testing (in percent), and ω_C = moisture content at time of compaction (in percent).

6. CALCULATION OF LWD EFFECTIVE MODULUS

6.1 Calculate the average of the three deflection measurements obtained in step 4.7. Report the average deflection in inches (or mm).

6.2 Estimate the peak load, F, as per ASTM E 2835 or ASTM E 2583, based on the LWD model used, following the below equation:

$$F = \sqrt{2mghC} \quad (1)$$

where h = drop height, m = falling mass, g = gravitational force and C = buffer constant provided by the manufacturer.

6.3 Estimate the Poisson's ratio, v, of the geomaterial using recommended values shown in Table 1.

Table 1—Typical Poisson's Ratio Values for Unbound Granular and Subgrade Materials

Material Description	Poisson's Ratio	
	Range	Typical
Clay (Saturated)	0.4 – 0.5	0.45
Clay (Unsaturated)	0.1 – 0.3	0.20
Sandy Clay	0.2 – 0.3	0.25
Silt	0.3 – 0.35	0.32
Dense Sand	0.2 – 0.4	0.30
Coarse-grained Sand	0.15	0.15
Fine-grained Sand	0.25	0.25
Bedrock	0.1 – 0.4	0.25

6.4 Estimate the shape factor, *f*, based on the soil type and plate rigidity. See Table 2 for recommended values.

Table 2—Recommended Shape Factors (*f*) for LWD Effective Modulus Estimation

Soil Type	Plate Type	Shape Factor, *f*
Clay (elastic material)	Rigid	π/2
Cohesionless Sand	Rigid	8/3
Material with intermediate characteristics	Rigid	π/2 to 2
Clay (elastic material)	Flexible	2
Cohesionless Sand	Flexible	8/3

6.5 Calculate the effective modulus of the geomaterials, E_{eff}, from:

$$E_{eff} = \left[\frac{\left(1-\nu^2\right) \times F}{\pi \times a \times d_{eff}} \right] f \qquad (2)$$

where F = LWD peak load, a = radius of load plate, d_{eff} = peak deflection on top of the compacted layer, ν = Poisson's ratio of the geomaterials, and f = plate rigidity factor.

6.6 Follow the process described in steps 5.1 to 5.5 to adjust the LWD effective deflection to account for the differences between laboratory and field conditions as well as the differences in the moisture content of geomaterials at the time of compaction and time of quality management testing.

7. REPORT

7.1 Prepare a one-page report that consists of the following information.

- Date and time of test
- Any unusual observations made during the test
- Layer tested and base layer thickness (if applicable)
- Lift type and thickness (if applicable)

- Nearest station
- Load applied
- Deflection readings for each drop
- Average measured deflection
- Adjusted deflection
- Moisture content of soil at the time of testing
- Estimated effective LWD modulus
- Adjusted effective LWD modulus

APPENDIX C - TEST PROCEDURE FOR DETERMINING INTELLIGENT COMPACTION MEASUREMENT VALUE (ICMV) USING INTELLIGENT COMPACTION (IC) TECHNOLOGY

Test Procedure for

DETERMINING INTELLIGENT COMPACTION MEASUREMENT VALUE (ICMV) USING INTELLIGENT COMPACTION (IC) TECHNOLOGY

TxDOT Designation: Tex-999-E

Effective Date: XXX 201X

1. SCOPE

1.1 This test method describes the procedure for determining the Intelligent Compaction Measurement Value (ICMV) using Intelligent Compaction technology on compacted geomaterials used in embankments, subgrade and base layers. The test method is used for quality control testing of compacted geomaterials during construction.

1.2 The values given in Customary Units are to be regarded as the standard; however, some units are provided in SI. The values given in parentheses are not standard and may not be exact mathematical conversions. Use each system of units separately. Combining values from the two systems may result in nonconformance with the standard.

2. DEFINITIONS

2.1 ***IC***— Intelligent Compaction technology is a system that provides continuous assessment of compaction through roller vibration monitoring and integrates a global positioning system (GPS).

2.2 ***ICMV***—Intelligent Compaction Measurement Value, generic term that refers to a set of IC data for measurements of resistance of deformation of underlying material and to assess uniformity based on the responses of the roller drum vibration measurements in units specific to the roller manufacturer.

2.3 ***Vibration frequency***—rotational speed of roller drum's lifting off and compaction on pavement surface.

2.4 ***Vibration amplitude***— height of roller drum's lift from pavement surface during vibratory compaction.

2.5 ***Roller pass***—the area covered by on width of the roller in a single direction. Roller pass number is the counts of roller machine passes within a given mesh for a construction lift.

2.6 ***Proof-Mapping—***the process of using an IC roller to map the entire section upon completion of compaction for assessing the uniformity and consistency of compaction.

3. EQUIPMENT

3.1 *Intelligent Compaction (IC) roller compactor*, vibratory roller equipped with a data acquisition (DAQ) system that processes compaction data in real time for the roller operator. DAQ can be either factory-installed/Original Equipment Manufacturer (OEM) or a retrofit system. IC roller shall be in accordance with the rollers shown on the Department's Approved Product List, "Intelligent Compaction Rollers" and comply with the following requirements:

3.1.1 IC rollers shall be equipped with accelerometers mounted in or on the side of the drum to measure the interactions between the roller and compacted materials to evaluate the applied compaction effort.

3.1.2 *GPS radio and receiver units* shall be mounted on each IC roller to monitor the drum locations and track the number of passes of the rollers. The recorded GPS data, whether from the IC rollers or hand-held GPS rovers, shall be in the following formats:

- *Date*: The date stamp shall be in either yyyymmdd format.
- *Time*: The time stamp shall be in hh:mm:ss.xx, with a precision of 0.01 seconds required to differentiate sequence of IC data points during post-processing.
- *Latitude and longitude*: shall be in decimal degrees, dd. ddddddddd[8]. Longitudes are negative values when measuring westward from the Prime Meridian.
- *Elevation*: shall be in dddd.ddd in foot.

Essential GPS data elements for each data point are shown in Table 1.

Table 1—GPS Data Elements for Each Data Point

Item No.	Data Field Name	Example of Data
1	Date Stamp (yyyymmdd)	20150205
2	Time Stamp (hh:mm:ss.xx)	16:49:31.18
3	Longitude (decimal degrees)	-101.87905175
4	Latitude (decimal degrees)	35.11711655
5	Elevation (ft.)	737.092

3.1.3 *On-board computer display* to show the location of the roller, number of passes, amplitude and frequency for vibratory rollers, and that provides real-time, color-coded maps of the ICMV. The display unit shall be capable of transferring the data by means of a USB port or by automatic wireless uploading to a cloud computer storage system. On-board computer should have the capability to measure, record, and export compaction parameters in the Comma Delimited Separated Values (*.csv) format data files.

[8] Increase to 8 decimals

4. PROCEDURE

4.1 Close off the entire testing area from any vehicular or construction equipment for the entire testing period. Clear out any other safety concerns that would impact the testing procedure and safety of the testers prior to testing.

4.2 *Calibration of GPS System on IC Roller*. Perform the GPS calibration process prior to any IC data collection. Verify that the handheld survey-grade GPS rover(s) and IC roller are connected with the local/virtual base station.

4.3 Move the IC roller slowly to a designated position to allow the GPS header computation to be stabilized to obtain accurate GPS location. Once the roller stops, record the last reading, which is associated with the center of the drum. Record the coordinates of both sides of the drum (Figure 1) using the handheld survey-grade GPS rover that was previously synchronized with the base station. The coordinates of the drum center shall be interpolated from the coordinates of the two sides of the drum. Compare the coordinates reported by the IC roller with the interpolated coordinates from the GPS rover. Adjust the IC roller coordinates to match the interpolated numbers. The tolerance of the differences is 12 in. (300 mm) in the northing and easting directions.

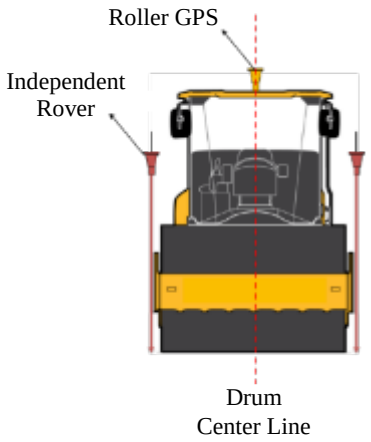

Figure 1. GPS calibration process

4.4 Identify the Layer IDs using Project typical sections. The operator must input (or select) the header information using the on-board display, prior to compacting the given material and enter a file name to store IC data.

IC data file name: operator should name data file using the following convention: data (yyymmdd); material (see Table 2); traffic direction (NB, SB, WB, EB); lane type (ML, FR, RAMP); Stations (to nearest foot, xxxx+xx to xxxx+xx); PM (proof-mapping); Smooth Drum (SD) or Padfoot Roller (PF).

Example: 20160517-SG-NBML-194015TO196045-PM-SD

Required fields in header of each file should contain information about site, material and roller type, see Table 3 for sample header information.

- Design Name, Project ID or Section Title that identifies site. Additional information such as Location Description, Starting Station, Operator, may be added.
- Material Type (Table 2)
- Roller Model, if provided additional roller characteristics (roller type and weight and drum dimensions) may be excluded
- Roller Type, may be excluded if Roller Model provided
- Roller Drum Width (in.), may be excluded if Roller Model provided
- Roller Drum Diameter (in.), may be excluded if Roller Model provided
- Roller Weight (lbs.), may be excluded if Roller Model provided
- GPS Mode
- GPS Tolerance
- Name Index of ICMV Type
- ICMV Type Unit Index (1: CCV, 2: CMV; 3: E_{vib}; 4: HMV; 5: K_b; 6: MDP; 7: Other), when ICMV type name not included

Table 2—Material Type Designation Acronyms

	Material Type	Acronym
1	Untreated Subgrade Soil	SG
2	Lime Treated Subgrade	LTS
3	Cement Treated Subgrade	CTS
4	Untreated Flexible Base	FB
5	Lime Treated Flexible Base	LTB
6	Cement Treated Flexible Base	CTB
7	Asphalt Treated Base	ATB
8	Embankment	EMB
9	Other material not listed above	Specify

Table 3—IC Data Information

Item No.	Data Field Name	Example of Data
1	Design Name	20150205-LTS-NBML-1715+15 to 1745+45-PM
2	Material Type	LTS
3	Roller Model	HAMM3412
4	GPS Mode	RTK Fixed
5	GPS Tolerance (in.)	Medium (2.0 in.)
6	ICMV type	CMV
7	ICMV index	3

4.5 Collect the IC data when the compaction of the entire layer is completed. Start each pass at least 25 ft to 50 ft from test section to allow the IC roller to reach the desired frequency and speed. For this purpose, make each pass continuously, regardless of length, by operating the IC roller according to manufacturer's recommendations to provide reliable and repeatable measurements during proof-mapping, on each lift, using consistent operating settings for the following:

- Low Amplitude and Low Frequency (when in vibration mode)
- Speed = 3 mph (5 km/h)

The output from the roller is designated as the Intelligent Compaction Measurement Value (ICMV) which represents the stiffness of the materials based on the rolling resistance or vibration of the roller drums and the resulting response from the underlying materials.

IC data files must at least include the following information

- Roller Pass Number
- Roller Travel Direction (forward or reverse)
- Roller Travel Speed
- Vibration Setting (on or off)
- Vibration Frequency
- Vibration Amplitude
- Intelligent Compaction Measurement Values (ICMV)

Sample information is available in Table 4.

Table 4—IC Data Elements for Each Data Point

Item No.	Data Field Name	Example of Data
1	Roller pass number	1
2	Direction	Forward, Reverse or index
3	Roller speed (mph)	3
4	Vibration on	Yes, No, On, Off or index
5	Vibration Frequency (Hz)	28.4
6	Vibration Amplitude (mm)	1.95
7	Intelligent Compaction Measurement Value (ICMV)	30.5

4.6 Deliver the electronic IC data files and a hard copy of the color-coded map to the Engineer. The IC data will be color-coded using green, yellow, and red colors as shown in Table 5 and Figure 2.

Table 5—Color-Coded Map Requirements[9]

Color	Criteria[1]
Red	Area less than 60% of Average ICMV Data
Yellow	Area in the range of Average to 60% of Average ICMV Data
Green	Area greater than 60% of Average ICMV Data
1. The criteria listed in this table are for producing color-coded maps using VETA software only. Color sequence is listed from lowest to highest stiffness.	

[9] Research team will work with TxDOT to define the color-coded criteria.

Submit compaction information and data elements using Veta. Operator may combine roller data for multiple rollers operating in echelon into a section file.

4.7 Provide displayed results to the Engineer for review upon request.

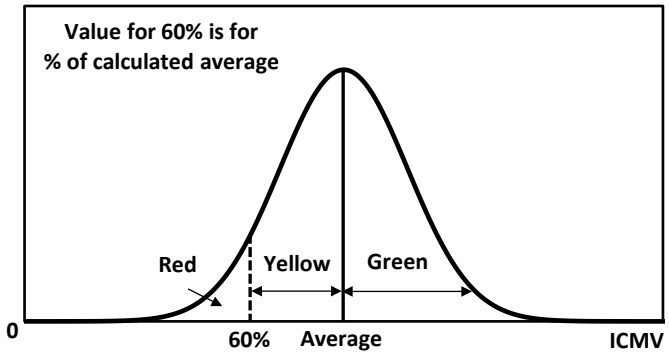

Figure 2. Criteria for color-coded map of ICMV data.[10]

5. REPORT

5.1 *IC Data Quality Control and Report.* Report the collected IC data in the desired format (see Figure 4) upon completion of daily IC operation. The descriptive statistics of the collected ICMVs as well as the vibration amplitude and frequency shall be controlled for any discontinuity or irregular trend in the data. Plots must be scaled to be legible.

[10] Research team will work with TxDOT to define the color-coded criteria.

Inspector Name: Date:

Project Location: Coordinate System:

County: Roller Type:

Material Type: Roller Model:

Layer Type:

Intelligent Compaction Data Report Worksheet

Color-Coded Map of ICMV	Histogram of ICMV

Histogram of Vibration Frequency	Histogram of Vibration Amplitude

Descriptive Statistics of ICMV	Location of Less Stiff Spots

Figure 4. IC data report worksheet.

APPENDIX D - SUMMARY OF RESILIENT MODULUS CONSTITUTIVE MODELS AND MODELS TO PREDICT MODULUS FOR FIELD TEST DEVICES

This appendix provides lists of developed constitutive models and different developed models to predict modulus for different field test devices. Table D.1 summarizes different constitutive models using various definitions of stress state to explain the nonlinear behavior of compacted geomaterials. Table D.2 provides a synthesis of studies that have developed relationships to predict resilient modulus of compacted geomaterials using moisture/suction variables. Table D.3 summarizes the models developed for determining mechanical properties as determined by each of the reviewed modulus-based NDT devices.

Table D.1 – Summary of Constitutive Models Based on Stress States

Reference	Model Form	Stress Parameter
Dunlap (1963)	$MR = k_1 (\sigma_3/P_a)^{k2}$	- Atmospheric pressure (P_a) - $S_{u1.0\%}$ = stress causing 1% strain in conventional unconfined compressive test - Confining stress (σ_3) - Effective confining stress (σ'_3) - Bulk stress (θ) - Deviatoric stress (σ_d) - Octahedral normal stress (σ_{oct}) - Octahedral shear stress (τ_{oct}) - Nonlinear coefficients (k)
Seed et al. (1967)	$MR = k_1 (\theta/P_a)^{k2}$	
Moossazadeh and Witczak (1981)	$MR = k_1 (\sigma_d/P_a)^{k2}$	
Shackel (1973)	$MR = k (\sigma^n_{oct} / \tau^m_{oct})$	
Brown et al. (1975) Brown (1979)	$MR = k_1 (\sigma_d/\sigma'_3)^n$	
Thompson and Robnett (1976)	$MR = k_1 + k_2(\sigma_d)$, when $\sigma_d < \sigma_{di}$ $MR = k_3 + k_4(\sigma_d)$, when $\sigma_d > \sigma_{di}$	
Fredlund et al. (1977)	$MR = 10^{(k-n\sigma d)}$	
Thompson and Elliot (1985)	$MR = k_2 + k_3(k_1 - \sigma_d)$ $MR = k_2 + k_4(\sigma_d - k_1)$	
Drumm et al. (1990)	$MR = (k + n\sigma_d) / \sigma_d$	
Pezo et al. (1991)	$MR = k_1 P_a (\sigma_3/P_a)^{k2}(\sigma_d/P_a)^{k3}$	
Lytton et al. (1993)	$MR = k_1 P_a [(\theta-3k_6)/P_a)]^{k2}(\tau_{oct}/P_a)^{k3}$	
Lee et al. (1997)	$MR = 695.4 (S_{u1.0\%}) – 5.93(S_{u1.0\%})^2$	
Witczak and Uzan (2000)	$MR = k_1 P_a (\theta/P_a)^{k2}(\sigma_d/P_a)^{k3}$	
Ni et al. (2002)	$MR = k_1 P_a (\sigma_3/P_a+1)^{k2}(\sigma_d/P_a+1)^{k3}$	
Wolfe and Butalia (2004)	$MR = k_1 P_a [P_a \sigma_{oct}/\tau^2_{oct}]^{k2}$	
Andrei et al. (2004) NCHRP 1-28A	$MR = k_1 P_a (\theta/P_a)^{k2}(\tau_{oct}/P_a+1)^{k3}$	
Ooi et al. (2004)	$MR = k_1 P_a (\theta/P_a+1)^{k2}(\tau_{oct}/P_a+1)^{k3}$	

Table D.2 – Summary of Models Developed to Predict Modulus Based on Moisture/Suction Variations

Reference	Model Form	Model Parameters
Oloo and Fredlund (1998)	$(Mr)_{us} = k\sigma^{n}_{b}+k_s(u_a - u_w)$, for coarse-grained materials $(Mr)_{us} = k_2 - k_3(k_1 - \sigma_d)+k_s(u_a - u_w)$, when $k_1>\sigma_d$ for fine-grained materials $(Mr)_{us} = k_2 - k_4(\sigma_d - k_1)+k_s(u_a - u_w)$, when $k_1<\sigma_d$ for fine-grained materials	σ_b = *bulk stress* σ_d = deviatoric stress k_i = *regression* parameter M_r = resilient modulus Mr_{us}= unsaturated resilient modulus J_1 = first stress invariant θ_w = volumetric water content θ_s = saturated water content χ = function of degree of saturation u_a = pore air pressure T_s = soil surface tension S_r = degree of saturation T_s = total suction γ_d = dry density θ = volumetric water content β = model parameter χ_w = bishop's parameter $(u_a\text{-}u_w)_b$ = air entry value $(u_a\text{-}u_w) = \Psi_m$ u_a = pore air pressure u_w = pore water presssure p_a = atmospheric pressure σ_{eb} = external bulk stress τ_{oct} = octahedral shear stress $\theta_{net} = \theta\text{-}3u_a$ = net bulk stress $\Delta u_{w\text{-}sat}$ = pore-water pressure under saturated conditions Ψ_m = matric suction Ψ = total soil suction Ψ_{m0} = initial matric suction $\Delta\Psi_m$= relative change in matric suction P = net mean stress P_r = reference pressure q_{cyc} = cyclic shear stress α and β = model parameters $\Theta = \frac{\theta - \theta_r}{\theta_s - \theta_r}$ = normalized water content θ = water content θ_r = water content at residual condition θ_r = water content at saturated condition $k = 1/n$ = fitting parameter m = fitting parameter MC = moisture content
Johnson et al. (1986)	$M_r = 1.35\times10^{6}(101.36 - \Psi)^{-2.36}(J_1)^{-3.25}(\gamma_d)^{-3.06}$	
Fredlund and Xing (1994)	$\theta_w = \left[1-\frac{\ln(1+\frac{\psi}{\psi_r})}{\ln(1+\frac{10^6}{\psi_r})}\right]\frac{\theta_s}{\left[\ln(e+\left(\frac{\psi}{a}\right)^{n}\right]^{m}}$	
Drumm et al. (1997)	$M_r = k_3\,(\sigma_d + \chi\Psi_m)^{k4}$	
Yang et al. (2005)	$M_r = k_3\,(\sigma_d - u_a + \chi\Psi_m)^{k4}$	
Ling et al. (2006)	$S_r = -0.5913\,T_s + 95.2$, when $T_s \geq 24$ kPa $S_r = -0.47847\,\ln(T_s) + 95.2$, when $T_s < 24$ kPa $M_r = 8\,e^{0.0437Ts}$	
Drumm and Meier (2003)	$M_r = 27.06 - 0.526\theta$, if $\gamma_d > 100$ pcf $M_r = 18.18 - 0.404\theta$, if $\gamma_d < 100$ pcf	
Gupta et al. (2007)	$M_r = k_1 P_a\left[\frac{\theta_b - 3k_4}{P_a}\right]^{k2}\left[\frac{\tau_{oct}}{P_a} + k_5\right]^{k3} + \alpha(u_a - u_w)^{\beta}$	
Liang et al. (2008)	$M_r = k_1 P_a\left[\frac{\theta + \chi_w\psi_m}{P_a}\right]^{k2}\left[\frac{\tau_{oct}}{P_a} + 1\right]^{k3}$ $\chi_w = \left[\frac{(u_a - u_w)_b}{u_a - u_w}\right]^{0.55}$	
Seikmeier (2011)	$M_r = k_1 \times p_a \times \left(\frac{\sigma_{eb} + f_s\,\theta_w\,\psi}{p_a}\right)^{k_2} \times \left(\frac{\tau_{oct}}{p_a} + 1\right)^{k_3}$	

Table D.2, cont. – Summary of Models Developed to Predict Modulus Based on Moisture/Suction Variations

Reference	Model Form	Model Parameters
Cary and Zapata (2011)	$M_r = k_1 P_a \left[\frac{\theta_{net} - 3\Delta u_{w-sat}}{P_a}\right]^{k2} \left[\frac{\tau_{oct}}{P_a}\right]^{k3} \left[\frac{\psi_{m0} - \Delta\psi_m}{P_a} + 1\right]$	σ_b = *bulk stress* σ_d = deviatoric stress k_i = *regression* parameter M_r = resilient modulus Mr_{us}= unsaturated resilient modulus J_1 = first stress invariant θ_w = volumetric water content θ_s = saturated water content χ = function of degree of saturation u_a = pore air pressure T_s = soil surface tension S_r = degree of saturation T_s = total suction γ_d = dry density θ = volumetric water content β = model parameter χ_w = bishop's parameter $(u_a\text{-}u_w)_b$ = air entry value $(u_a\text{-}u_w) = \Psi_m$ u_a = pore air pressure u_w = pore water presssure p_a = atmospheric pressure σ_{eb} = external bulk stress τ_{oct} = octahedral shear stress $\theta_{net} = \theta\text{-}3u_a$ = net bulk stress $\Delta u_{w\text{-}sat}$ = pore-water pressure under saturated conditions Ψ_m = matric suction Ψ = total soil suction Ψ_{m0} = initial matric suction $\Delta\Psi_m$= relative change in matric suction P = net mean stress P_r = reference pressure q_{cyc} = cyclic shear stress α and β = model parameters $\Theta = \frac{\theta - \theta_r}{\theta_s - \theta_r}$ = normalized water content θ = water content θ_r = water content at residual condition θ_r = water content at saturated condition $k = 1/n$ = fitting parameter m = fitting parameter MC = moisture content
Ng et al. (2013)	$M_r = M_0 \left[\frac{P}{P_r}\right]^{k1} \left[1 + \frac{q_{cyc}}{P_r}\right]^{k2} \left[1 + \frac{u_a - u_w}{P}\right]^{k3}$	
Nazarian et al. (2014)	$Modulus_{Testing} / Modulus_{Compaction} = EXP[0.18(MC_{Compaction} - MC_{Testing})]$, for subgrade materials $Modulus_{Testing} / Modulus_{Compaction} = EXP[1.19(MC_{Compaction} - MC_{Testing})]$, for GP Base materials $Modulus_{Testing} / Modulus_{Compaction} = EXP[0.66(MC_{Compaction} - MC_{Testing})]$, for GW Base materials	
Han and Vanapali (2014)	$M_r = M_{rsat} + \alpha(u_a - u_w)S^{\beta}$	
Abu-Farsakh et al. (2015)	$M_r = k_1 P_a \left[\frac{\theta + \Theta^{k\psi}}{P_a}\right]^{k2} \left[\frac{\tau_{oct}}{P_a}\right]^{k3}$ $\theta_w = \frac{\theta_s}{\left[\ln(e + \left(\frac{\psi}{a}\right)^n\right]^m}$	
Sawangsuriya et al. (2009)	$M_r / M_{rsat} = -5.61 + 4.54 \log(u_a - u_w)$ $M_r / M_{ropt} = -0.24 + 0.25 \log(u_a - u_w)$	

Table D.3 – Summary of Models to Predict Modulus for Field Test Devices

Reference	Model Form	Model Parameters
Dynamic Cone Penetrometer (DCP)	$E = 17.6 \cdot \text{CBR}^{0.64}$ where $CBR = \left(\frac{292}{DPI^{1.12}} \right)$ when $CBR > 10\%$ $CBR = \left(\frac{1}{0.017019 DPI} \right)^2$ when $CBR < 10\%$ E (in MPa) $= 2224 \cdot \text{CBR}^{0.99}$ (Chai and Roslie, 1998) MR (psi) $= 7013.0 - 2040.8 \ln(DPI)$	CBR = California bearing ratio DPI = DCP penetration index (mm/blow) E = effective DCP elastic deformation modulus MR = resilient modulus
Electro-Mechanical Stiffness Device (Geogauge)	$E_{SSG} = \frac{F}{d} \cdot \frac{1-\nu^2}{1.77R}$ (Humboldt Mfg. Co, 2000; White et al. 2007)	E_{SSG} = GeoGauge modulus (MPa) F = dynamic force (N) d = geophone deflection measurement (mm) R = radius of annular ring (mm) ν = Poisson's ratio
Light Weight Deflectometer (LWD)	$E_{LWD} = \frac{\left(1-\nu^2\right) a \sigma_0}{d_{LWD}} \times f$ (Rahman et al. 2007)	E_{LWD} = surface modulus σ_0 = uniformly distributed applied stress under the plate a = radius of the plate f = shape factor (=2 for flexible plate, =π/2 for rigid plate) ν = Poisson's ratio d_{LWD} = surface deflection under the plate
Portable Seismic Proprty Analyzer (PSPA)	$E_{seismic} = 2\rho\left[\left(1.13 - 0.16\nu\right) V_R\right]^2 \left(1+\nu\right)$ (Celaya and Nazarian. 2006)	$E_{seismic}$ = seismic modulus V_R = velocity of surface waves ρ = mass density ν = Poisson's ratio

APPENDIX E - CURRENT STATE DOT PRACTICES

E.1 Review of Current State DOT Modulus/Deflection Based Specifications

Based on the review of existing documents, relatively little work has been done toward developing comprehensive approaches that tie the design moduli of compacted geomaterials to the moduli measured in the field for acceptance. The existing approaches are summarized in Table E.1. One weakness of most of these methods is relating the design and target moduli.

Table E.1 – Current Specifications for Modulus-Based Quality Management

Reference	Tool Used	Principal Constraints
MnDOT (2005)	DCP	Target modulus is not tied to design
MoDOT (2010)		
MnDOT (2009)	LWD	Target modulus is not tied to design
InDOT (2012)		
European Union (EU)		
United Kingdom (UK)		
Celaya et al. (2010)	PSPA	Should be adapted to all NDT devices

Only MnDOT has developed specifications in the US. MoDOT and TxDOT have developed internal specifications that are still in the draft stages. In the following sections, a few salient points of the MnDOT specification is presented followed brief summary of the other specifications. It should be noted that even though a majority of the highway agencies have not developed modulus based compaction specifications, a number of them have been involved in research studies related to intelligent compaction and modulus based compaction as discussed in Chapter 3. These studies are expected to help in the future development of specifications. Hence, it can be anticipated that specification development and their usage by other states are still feasible in the near future.

E.1.1 Minnesota DOT Specifications

MnDOT has developed specifications that use interpreted moduli from LWD and DCP field studies for compacted geomaterials. MnDOT specifications can be accessed from the following web site: http://www.dot.state.mn.us/materials/gblwd.html . According to Siekmeier (2010), LWD is considered as a practical tool to evaluate the compacted soils in pavement foundations.

As per the LWD-based MnDOT specifications, the plate diameter should be 200 mm and the falling mass should weigh 10 kg. The height of fall is close to 500 mm. To obtain reliable measurements the deflection range should be between 0.3 to 3.0 mm. The deflection is measured from the average of the fourth, fifth and sixth drops in their testing sequence. The first three drops in the testing sequence are seating drops.

The upper 50 to 100 mm of soil should be removed before starting the test to produce a flat testing area, especially on non-granular soils. The moisture content of the embankment materials should be maintained from 65 to 95% of the target moisture content.

Constraints imposed on the LWD testing include the timing when tests should be performed (immediately after compaction). In addition, the LWD tests are not allowed when the water table is less than 600 mm or when the embankment thickness is less than 300 mm (when no site preparation is needed) and 460 mm (when site preparation is needed).

In the MnDOT DCP-based specifications (see http://www.dot.state.mn.us/materials/ gbmodpi.html), the dynamic penetration index (DPI) is used to judge the quality of the compacted geomaterials. In order to

estimate this DPI, five hammer blows are required with the first two treated as seating drop. Penetration depths of the third, fourth, and fifth drop are used to calculate the value of DPI as show in the following equation:

$$\text{Dynamic Penetration Index, } DPI \text{ (mm/blow)} = \frac{penetration_{blow\#5} - penetration_{blow\#2}}{3\ blows} \quad \text{(E.1)}$$

The most recent DCP penetration requirements from MnDOT are shown in Table E.2 and summarized in Equation 5.2.

$$DPI \text{ (mm/blow)} = (4.76\ GN + 1.68\ MC - 14.4), \quad \text{(E.2)}$$

where *MC* is the moisture content at the time of testing and *GN*, Grading Number, is obtained from Equation E.3.

$$GN \text{ (\%passing)} = \frac{25mm+19mm+9.5mm+4.75mm+2.00mm+425\mu m+75\mu m}{100} \quad \text{(E.3)}$$

To obtain GN, a sieve analysis containing the following seven sieves 25 mm, 19 mm, 9.5 mm, 4.75 mm, 2.00 mm, 425 µm and 75 µm should be performed on the geomaterial. The terms in the numerator of Equation 3.3 are the percent passing for each of sieve. A material with an extremely fine gradation will yield a GN close to 7, whereas an extremely coarse material yields a GN close to zero.

Table E.2 – Modified DCP Penetration Requirements

GN	In-Situ Moisture (% by dry weight)	Maximum Allowable Seating (mm)	Maximum Allowable DPI (mm/blow)
3.1-3.5	< 4.0	40	10
	4.1-6.0	40	10
	6.1-8.0	40	13
	8.1-10.0	40	16
3.6-4.0	< 4.0	40	10
	4.1-6.0	40	12
	6.1-8.0	45	16
	8.1-10.0	55	19
4.1-4.5	< 4.0	45	11
	4.1-6.0	55	15
	6.1-8.0	65	18
	8.1-10.0	70	21
4.6-5.0	< 4.0	65	14
	4.1-6.0	75	17
	6.1-8.0	80	20
	8.1-10.0	90	24
5.1-5.5	< 6.0	90	19
	6.1-8.0	100	23
	8.1-10.0	110	26
	10.1-12.0	115	29
5.6-6.0	< 6.0	110	22
	6.1-8.0	120	25
	8.1-10.0	125	28
	10.1-12.0	135	32

For LWD tests, a test strip is proposed. On the basis of a series of research on the use of a range of LWDs (Hoffmann et al. 2003; Davich et al. 2006; Siekmeier et al. 2009, Siekmeier, 2011), MnDOT is pioneering the implementation of the LWD in their quality management. In order to use the LWD as a more effective

tool for construction quality control/assurance, MnDOT suggested defining target LWD modulus for each particular base course material and subgrade soil. Since the LWD device is currently non-standardized nationally, MnDOT selected a specific LWD to serve its purpose such that the buffer and plate stiffness are also constant along with the specified falling mass, peak force, and plate diameter.

For granular material, the grading number (GN) and field moisture content are used by MnDOT to select the LWD target modulus values (see Table E.3). For compacted fine grained soil, the plastic limit and field moisture content are used by MnDOT to determine the target moduli (Table E.4).

Table E.3 – LWD Target Values for Granular Material (Siekmeier et al. 2009)

Grading Number GN	Moisture Content	Target LWD Modulus		Target LWD Deflection Zorn*
		Keros/Dynatest#	Zorn&	
	%	MPa	MPa	mm
3.1 – 3.5	5 -7	120	80	0.38
	7- 9	100	67	0.45
	9 - 11	75	50	0.60
3.6 – 4.0	5 -7	120	80	0.38
	7- 9	80	53	0.56
	9 - 11	63	42	0.71
4.1 – 4.5	5 -7	92	62	0.49
	7- 9	71	47	0.64
	9 - 11	57	38	0.79
4.6 – 5.0	5 -7	80	53	0.56
	7- 9	63	42	0.71
	9 - 11	52	35	0.86
5.1 – 5.5	5 -7	71	47	0.64
	7- 9	57	38	0.79
	9 - 11	48	32	0.94
5.6 – 6.0	5 -7	63	42	0.71
	7- 9	50	33	0.90
	9 - 11	43	29	1.05

#Keros/Dynatest LWD target assume v = 0.35, and R = 0.789;
&Target LWD modulus values assume falling mass = 10 kg, plate diameter = 20 cm, and drop height = 50 cm;
*Zorn LWD target deflection values assume v = 0.5, R = 1, and peak force = 6.28 kN resulting in a peak stress of 0.2 MPa.

E.1.2 Missouri DOT

The Missouri DOT specifications are still in the draft stage. DCP is considered in that specification. The framework for DCP assessment is similar to MnDOT's DCP specification. The method is predominantly used for bases that contain Type 1, 5, 7 aggregates and the procedure is per ASTM D6951. Type 1 aggregate for base is essentially limestone or dolomite and Type 5 aggregate consist of crushed stone or sand and gravel. Type 7 aggregate base layers under both roadway and shoulders shall be compacted to achieve an average dynamic cone penetration index value through the base lift thickness less than or equal to 10mm per blow, as determined by a standard DCP device with a 18 kg hammer. Type 7 bases should be tested with the DCP within 24 hours of placement and final compaction. DCP index values are determined similar to MnDOT's DPI procedure reflected in Equation E.1.

Table E.4 – LWD Target Values for Fine Grained Soil (Siekmeier et al. 2009)

Plastic Limit	Estimated Optimum Moisture	Field Moisture as a Percent of Optimum Moisture[#]	Zorn Deflection Target at Field Moisture	
			Minimum	Maximum
%	%	%	mm	mm
Non-plastic	10-14	70 – 74	0.5	1.1
		75 - 79	0.6	1.2
		80 - 84	0.7	1.3
		85 - 89	0.8	1.4
		90 - 94	1.0	1.6
15 – 19	10 - 14	70 – 74	0.5	1.1
		75 - 79	0.6	1.2
		80 - 84	0.7	1.3
		85 - 89	0.8	1.4
		90 - 94	1.0	1.6
20 – 24	15 - 19	70 – 74	0.8	1.4
		75 - 79	0.9	1.6
		80 - 84	1.0	1.7
		85 - 89	1.2	1.9
		90 - 94	1.4	2.1
25 – 29	20 - 24	70 – 74	1.0	1.7
		75 - 79	1.2	1.9
		80 - 84	1.4	2.1
		85 - 89	1.6	2.3
		90 - 94	1.8	2.6
30 – 34	25 - 29	70 – 74	1.3	2.0
		75 - 79	1.5	2.2
		80 - 84	1.7	2.4
		85 - 89	1.9	2.7
		90 - 94	2.2	3.0

E.1.3 Indiana DOT

Indiana DOT also developed a test method for "Field Determination of Deflection Using Light Weight Deflectometer." This test method may be used for granular soils, coarse aggregates and chemical modified soils. The method generally follows the ASTM E2583 standard for measuring deflections with a lightweight deflectometer. Similar to the other LWD specifications, the field modulus is not correlated to the target modulus. This protocol specifies that if the change in deflection reading of LWD between two consecutive drops is more than 10%, the layer may require additional compaction.

InDOT has also developed a separate specification for field determination of strength using DCP. This test method may be used for fine-grained materials (clay and silty soils) as well as sandy, granular and chemically modified soils. The number of DCP blows for a specific amount of penetration in each type of geomaterials is used as the indicator of soil strength.

E.1.4 UTEP Protocol

Celaya et al. (2010) presented a procedure to close the gap between design and quality management of aggregate layers based on a modulus-based process. Even though seismic devices, such as the Free-free Resonant Column (FFRC) and the Portable Seismic Property Analyzer (PSPA) for laboratory and field experiments, were recommended, the process is applicable to all modulus based devices. To describe the process briefly, the appropriateness of a material is evaluated first. The acceptable design modulus and the target filed modulus are then determined using conventional and seismic laboratory tests. Finally, field

modulus is measured on constructed materials and compared to the established target modulus. The researchers present case studies to demonstrate the benefits of the proposed method.

E.2 Review of Modulus Based Specifications in Europe

E.2.1 European Union.

The European Union (EU), especially Austria, Germany, Sweden and the UK have developed specifications for LWD (PFWD) implementation (CEN ICS 93.020). As a summary, the unbound or geomaterial layer needs to be investigated by performing the following test based on their corresponding specifications: a) compactibility (EN 13286-2), b) grain-size distribution (EN 933-2), c) water content (EN 1097-5), d) water absorption, and d) saturation lines and as built water-content limits (EN 1097-6).

Table E.5 provides the technical requirements and specification for performing the LWD testing. The test process involves using the LWD at a drop height of 72 cm and a load of 7 kN using a loading plate diameter of 163 mm. Six measurements with three drop per measurement are averaged. The dynamic modulus is calculated using the elastic Boussinesq method based on the average deflection. The averages of the deflections measurements need to be less than 0.1 mm.

Table E.5 – Technical Requirements and Specifications for Performing the LWD Test

Informative Requirements of the design of the mechanical loading deflectometer	
• Mass of the falling weight (including handle)	10.5 kg ± 0.5 kg
• Total mass of guide rod (including the spring consisting of spring elements, transportation structure and tilting protection)	Max. 5 ± 0.5 kg
• Dynamic loading	0.35 MPa
• Loading time	18 ± 2ms
Design requirements of the loading disc	
• Diameter of the loading disk	163 ± 2 mm
• Thickness of the loading disk	Min. 20 mm
• Total mass of the loading disc complete masse (including measuring cell for the sensor and handles)	15 ± 1.0 kg
Fixed technical data of acceleration gauge applied, for definition measurement	
• Measurement range of in-built acceleration gauge	0-50 g
In case of applying other strain gauge and the acceleration gauge	
• Measurement time	18 ± 2 ms
• Processed measurement signal	Min. signals/18 ms
• Reading accuracy of deformation	Min. .01mm
• Quartz clock accuracy	Max. ± 1.5 s per day
• Reading accuracy of deformation	Min. 0.01 mm

The following Boussinesq formula is used to determine the modulus *E*:

$$E = \frac{c\,(1-\mu^2)\rho_{dyn} r}{s_{1a}} = \frac{c\mu}{s_{1a}} \quad \text{(E.4)}$$

where:

c = Boussinesq plate multiplier (considering π/2 rigid plate)
s_{1a} = Average vertical travel of the center of the plate
μ = Poisson's ratio (according to MSZ 2509-3 standard)
r = Radius of the loading disc, mm

$\rho_{dyn} = F_{dyn}/A$ = theoretical pressure applied to soil
A = Loading plate area , mm²
$F_{dyn} = \sqrt{2m \cdot g \cdot h \cdot K}$
m = Mass of falling body,
g = Acceleration of gravity m/s²
h = Drop height, m
K = spring constant, N/m

The test location must be prepared for the measurement. The prepared surface must be even, and must have an even texture typifying the material layer. The load plate must seat on the surface without tilting. The diameter of the prepared surface must be approx. 100 mm larger than the diameter of the loading disc and almost horizontal. The uneven surface must be corrected. Loose, dried, cracked or uneven materials must be removed. The reliability of the LWD measurements is questionable when the degree of saturation is greater than 95% (which can be determined from site water-content measurement) due to the incompressibility of water.

For quality control purposes, at least two measurements need to be executed simultaneously within one meter. If they differ from average by more than 20%, a third measurement is incorporated in the averaging. In the cases where the difference in deflections measured at two locations is greater than 3 mm, and the modulus is less than 10 MPa, the section should be re-compacted.

A parameter called the dynamic compactness, T_{rd}, is used to determine the degree of compaction of the compacted geomaterials. This parameter is estimated from:

$$T_{rd} = T_{rE} . T_{rw} \quad \text{(E.5)}$$

where T_{rE} site relative compaction at a given water content, and T_{rw} is the moisture correction coefficient to adjust for differences between the measured moisture content and optimum moisture content.

E.2.2 United Kingdom (UK)

In the UK specifications (Highway Agency, 2009), four foundation classes based on the long-term in-service foundation surface modulus value (a composite value with contributions from all underlying layers) are defined (Table E.6). Which foundation class is used is usually based on the materials that are available, the size of the scheme and relevant costing information. For construction quality control, the target mean and minimum modulus values are specified for the four foundation classes as shown in Table E.6. The moving mean of five consecutive in-situ foundation surface modulus measurements must be equal or exceed the target mean foundation surface modulus. All individual in-situ foundation surface modulus measurements must equal or exceed the target minimum foundation surface modulus. These in-situ foundation surface measurements are based on the standard dynamic plate test device (an FWD). If a LWD is used, a correlation exercise in the demonstration area is needed by using both the proposed LWD and the FWD. Twenty five measurement points are required in this correlation procedure. The U.K. specifications also specify a minimum subgrade CBR of 2.5. Subgrades with a CBR lower than 2.5 must be improved before they can be included in the permanent pavement works.

Table E.6 – Target Pavement Foundation Surface Modulus Values (Highways Agency, 2009)

Long-Term In-Service Modulus (MPa)			Class I	Class II	Class III	Class IV
			≥50	≥100	≥200	≥400
Target Mean Modulus (MPa)	Unbound		40	80	…	…
	Bound	Fast Curing	50	100	300	600
		Slow Curing	40	80	150	300
Target Minimum Modulus (MPa)	Unbound		25	50	…	…
	Bound	Fast Curing	25	50	150	300
		Slow Curing	25	50	75	150

E.3 Review of Existing Intelligent Compaction Specifications

A summary of existing IC specifications is provided in Table E.7. Most of the specifications require the roller measurement values to be higher than 70 to 90% of the target values established from the control section for 90% of the area being considered. The weak areas not meeting the target value requirements are marked for rework or reconstruction. For acceptance of the compaction work, both roller measurement values and density or modulus are checked to meet the specified requirements.

For a particular type of soil, the important factors influencing the measurement values are moisture content, density and compaction energy. The nonlinear relation between the density and moisture content is well represented by a parabolic fit. Similar densities can be obtained at both dry and wet of optimum moisture contents. Even at same density, the modulus or stiffness values may not be comparable and hence the compaction control may not be possible with density measurements alone (Hossain et al., 2006). Also the variation in modulus and stiffness depends upon on the type of soil (cohesive or granular). White et al., (2005) have demonstrated the influence of moisture content on the density and stiffness measurements. The findings have shown that laboratory density and compaction energy required is significantly influenced by the moisture content. Similarly studies (Petersen and Peterson, 2006, Rahman et al., 2007) have also high lightened the importance of moisture content in developing target values.

The German specifications recommends correlating three to five static plate load tests or density results on each control section to the roller measurement values. To establish the target roller measurement values the correlation coefficient must be greater than 0.7. However, there are no moisture content requirements. Most importantly to address the uniformity of compaction, the areas with roller measurement values lower than the target values should be distributed throughout the evaluation area. However, the definition of such distributed area is subjective. Specification prohibits the use of automatic feedback control rollers during calibration and acceptance testing (Mooney et al., 2010).

The Austrian/ISSME specifications are applicable to subgrade, subbase and base, and recycled materials (Mooney et al., 2010). Compaction is allowed with both static and vibratory rollers. However, dynamic measurements are needed for process control and acceptance. The target value is selected based on the minimum Portable FWD modulus, E_{LWD}, or plate load test results EV1 requirements. Moisture content needs attention if the fines exceed 15%. The roller measurements for calibration and correlation development are valid only during for continuous contact or partial loss of contact conditions.

The Sweden specifications for intelligent compaction are primarily for subbase and base layers (Mooney et al., 2010). The target values are established for the minimum requirements of plate load test results EV2. Since the subbase and base layers are primarily granular materials (cohesionless soil), the moisture content requirements are not specified.

Table E.7 – Summary of Existing Intelligent Compaction Specifications

Specification	Control section	QC/QA
Germany (1997)	Existing IC specifications are only for soils and embankments. Three 20 m long test strips should be selected as calibration sections. Develop the correlations between the roller MV and soil density or PLT modulus (E_{v2}). The correlation coefficient shall be of minimum 0.70. Identify the roller MV target value (MV-TV) for the required density or modulus.	90% of all roller MVs shall be higher than MV-TV. To use CCC as a QA tool the soil type and the underlying stratigraphy should be homogeneous. The soil shall be reworked if density or modulus measurements made on the identified weak areas using CCC is not greater or equal to the desired value. Speed of the roller shall be constant.
Swedish (2004)	IC specifications are not recommended for subgrades since the base and subbase layers are considerable thick. Predominantly cohesionless soil compaction is monitored using IC.	PLT at eight randomly locations within 5000 m^2 control area have to be carried out. Mean of compaction values for two inspection points ≥ 89% for sub-base under base and for protective layers over 0.5 m thick; mean should be ≥ 90% for bases. Required mean for two bearing capacity ratios varies depending on layer type.
ISSMGE/ Austria (2007)	At least 100 m long and width equal to the site width and overlap of each roller shall be <10% of the drum width. Compaction shall continue until the mean measurement value of a pass is no more than 5% higher than the mean measurement value of the preceding pass. Roller measurement values shall be correlated to PLT. The correlation coefficient shall be greater than 0.70.	The measured roller values shall be between 95 to 105% of PLT modulus values. Speed shall be constant between 2-6 km/h and frequency be constant within ± 2 Hz.
FHWA (2012)	Test section should be of minimum 75 m long and 8 m wide. A minimum of 10 locations shall be used to measure nondestructive density or stiffness. Target values for the optimal passes shall be determined from the compaction curve between the roller values and number of passes. The pass where the measurement values do not increase by 5% is considered as the optimal pass. Target values (IC-MV) for required density shall be established from linear regression between the density and the roller measurement values. The variation in moisture content allowed is between -3 % and + 2 % of OMC.	The magnitude of the evaluation areas may vary but not less than 25,000 ft^2. Around 90% of the construction area should meet the optimal number of roller passes and 70 % of the target values.
INDOT (2012)	Test section should be of minimum 30 m long and 6 m wide. The minimum thickness of the test section shall be 300 mm. The variation in moisture content allowed is between -3 % and + 2 % of the OMC. The target IC-MV should be established from the number of DCP blows required as determined in the laboratory.	The compaction acceptance should be determined by DCP testing. The frequency of tests is one test for each 1000 cum for each lift. A minimum of 90% of the mapped construction area should have a minimum of 70 % of the target IC-MV.
MnDOT (2012)	At least 100 m x 10 m. Thickness shall be same as layer to be constructed. One control section for each type/source of material at site. Determine the optimum passes based on the stiffness increment. The total thickness of the granular layer shall be equal to planned granular layer thickness being constructed. Moisture content shall be varied from 65 to 100% of optimum.	On all sections 90% of the IC stiffness measurements should be at least 90% of the target value prior to placing the next lift. If localized areas have IC stiffness of less than 80% of the target value, the areas shall be re-compacted. If a significant portion of the section is more than 30% in excess of the selected target value, the Engineer shall re-evaluate the target value (IC-TV).

In addition to the general procedure for establishing the target values using intelligent compaction rollers, Minnesota specifications requires mapping subsurface before placing the layer. This will help to identify the weak areas to be corrected prior to compaction process. Also Minnesota specifications recommend to construct the control section with moisture near 65% and 95% of the optimum and to establish the correction factors for LWD testing.

In summary, heterogeneity of the underlying layer, measurement depth and variation in moisture content were found to be the challenges to implement the IC technology (White et al., 2005, Mooney et al., 2006, Petersen and Peterson, 2006, Mooney and Rinehart, 2007). The stress dependent characteristic of the granular materials is a potential source of problem to compare stiffness and modulus results from different test and roller measurement values (Rinehart et al., 2012). Incorporation of moisture content, density and modulus measurements from the spot tests will improve to correlation between the roller measurement values and spot test results.

APPENDIX F - TEST SITE ALONG I-35W IN FORT WORTH, TX

F.1 Introduction

Field evaluation was performed on a north-bound frontage road section along IH-35W in Fort Worth, Texas, where reconstruction of the road was taking place. Figure 4.1 shows an aerial view alongside a map with the location of the test section

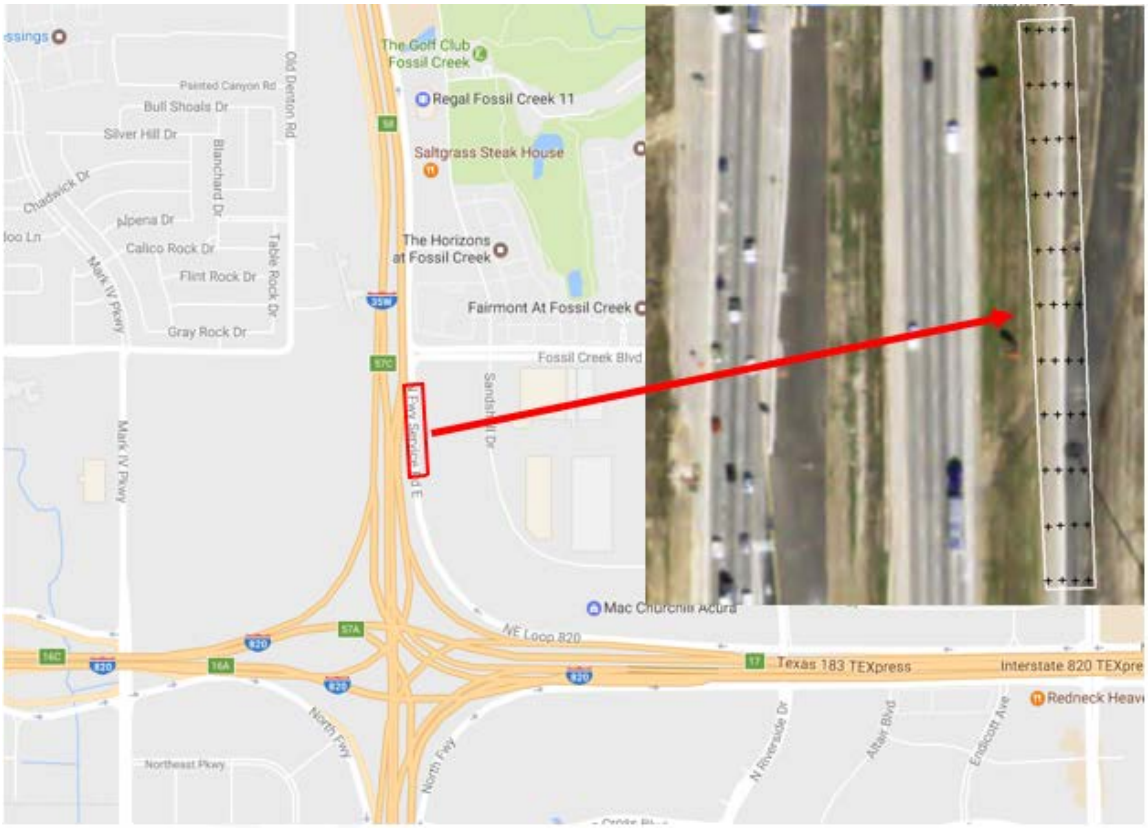

Figure F.1 – Location of Test Site on I-35W in Fort Worth, TX.

Two layers were evaluated for this study as shown in Figure F.2. The first layer consisted of a lime-treated subgrade (LTS) with a design thickness of 36 in. Field assessment of the LTS by the UTEP team took place on April 14, 2016. The second layer evaluated in this section was a Flexible Base with design thickness of 12 in. Field evaluation for the Flexible Base was carried out on May 13, 2016. A figure representative of the pavement structure is shown in Figure F.2.

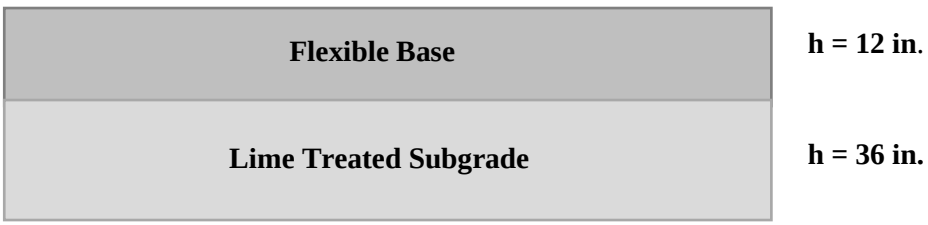

Figure F.2 – Pavement Structure of Test Section.

F.2 Field Testing Program

Modulus-based nondestructive spot testing was carried out along a 500 ft-long and 27 ft wide section. For this purpose, a grid of spot tests was arranged on the test section along 4 rows, each row consisting of 11 spot tests, yielding a total of 44 measurements. Rows of spot test measurements follows the paths of the IC roller line passes. The grid was designed to have a spacing of 50 ft between measurements longitudinally, and a spacing of 9-ft between each transverse point as shown in Figure F.3a. The following tests were performed on the test section:

- **Light Weight Deflectometer (LWD).** LWD testing was performed on all 44 points on the grid. At each location, two consecutive LWD drops were performed and their surface displacement measurements were averaged. In those cases where the consecutive measurements exceeded 10% of change in deflection, a third LWD measurement was recorded. In addition to the spot testing on the grid, LWD testing was also performed at 15 spots surrounding each location where the Plate Load Tests were performed. The grid formed by these 15 spots is shown in Figure F.3b.

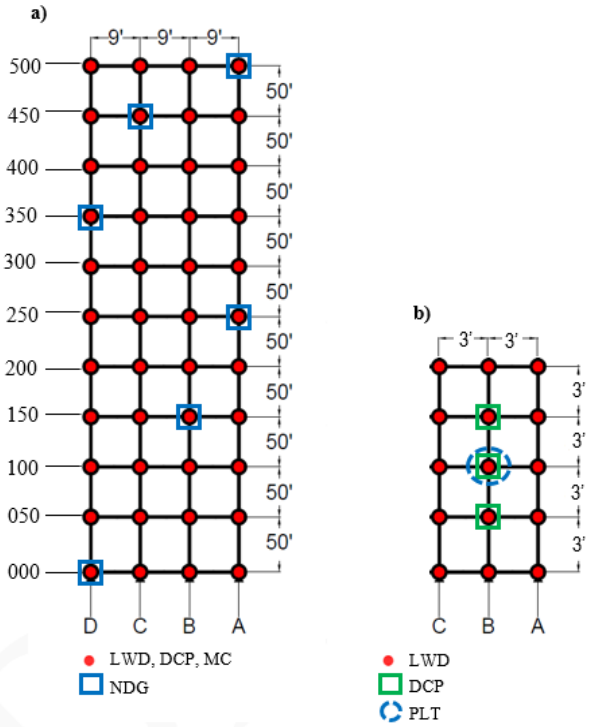

Figure F.3 – (a) Schematic of the Typical Test Section and Location of Spot Tests and (b) Diagram of the Testing Area around the PLT Locations.

- **Dynamic Cone Penetrometer (DCP).** The lime-treated subgrade layer was tested with the DCP in all 44 points of the grid. Similar to LWD, DCP was also performed on three locations adjacent to the spots where the Plate Load Tests were conducted, as shown in Figure F.3b.
- **Nuclear Density Gauge (NDG).** NDG readings were obtained from 6 different spots selected by the contractor. The location of these spots are shown in Figure F.3a.
- **Plate Load Test (PLT).** PLT was performed at five different spots on top of the subgrade layer. These points were chosen by TxDOT personnel based on the mapping of CMVs, provided by the contractor. The Plate Load Tests locations are shown in Figure F.4.
- **Moisture Content (MC).** Samples of the lime-treated subgrade from 44 gridded points shown in Figure F.3a were collected to measure their moisture contents.

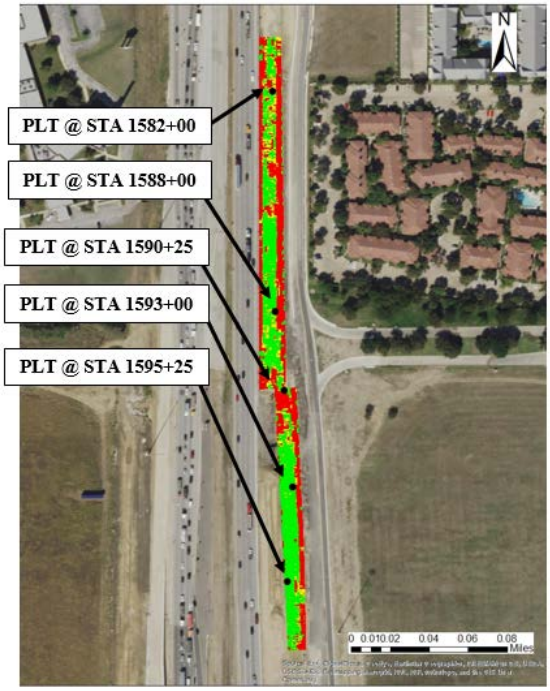

Figure F.4 – Aerial View of the PLT Locations.

F.3 Lime-Treated Subgrade

The lime-treated subgrade layer was mapped using a smooth CAT roller equipped with a Trimble® IC retrofit kit. The first phase of the construction work was involved with stabilizing the subgrade soil using hydrated lime. The spatial distribution of the CMVs collected during the mapping of the LTS layer is shown in Figure F.5a. Kriging was used to create the extrapolated colored figure with CMV values. Figure F.5b shows the spatial distribution of averaged buffered CMVs when the entire section was divided into 44 rectangular areas measuring 9 ft × 50 ft. The location of the less stiff areas on both maps are comparable. The histogram of the mapped CMVs is summarized in Figure F.6. The maximum CMV is around 75 for the spatial distribution of the raw data and 58 for the averaged data. The coefficient of variation (COV) of the raw collected CMVs is 49% for the LTS layer as shown in Figure F.6.

Once the compaction and mapping of the lime-treated subgrade was completed, field testing was performed with the LWD, NDG, PLT and DCP on the compacted layer at 44 points shown in Figure F.3a. The collected spot test data were imported into ArcGIS software to generate color-coded geospatial distribution maps. The spline spatial interpolation algorithm was employed for the process of spatial interpolation. The classification method for the color criterion was based on the mean as obtained for all the different spot test measurements as shown in Table F.1.

Figure F.7a illustrates the spatial distribution of the LWD modulus on top of the compacted LTS layer. The LWD moduli varied from 9 ksi to 57 ksi with an average of 33 ksi and a COV of 36%. The northern and southeastern areas of the test section showed lower LWD moduli which is in agreement with the CMV data in Figures F.5a and F.5b.

Figure F.7b summarizes the DCP results on the compacted LTS layer. The estimated DCP number of blows required to penetrate to a depth of 24 in. ranged from 22 blows to 60 blows with an average of 42 blows and a COV of 19%. The DCP is a layer specific device since it reflects the properties of the layer of interest as compared to LWD that reports a composite modulus of the underlying layers. Similar to LWD, the southeastern parts required fewer DCP blows than the mid-section, where the LTS is stiffer. This is in agreement with the LWD geospatial distribution shown in Figure F.6 and bears resemblance to the CMV geospatial distribution shown in Figure F.5b.

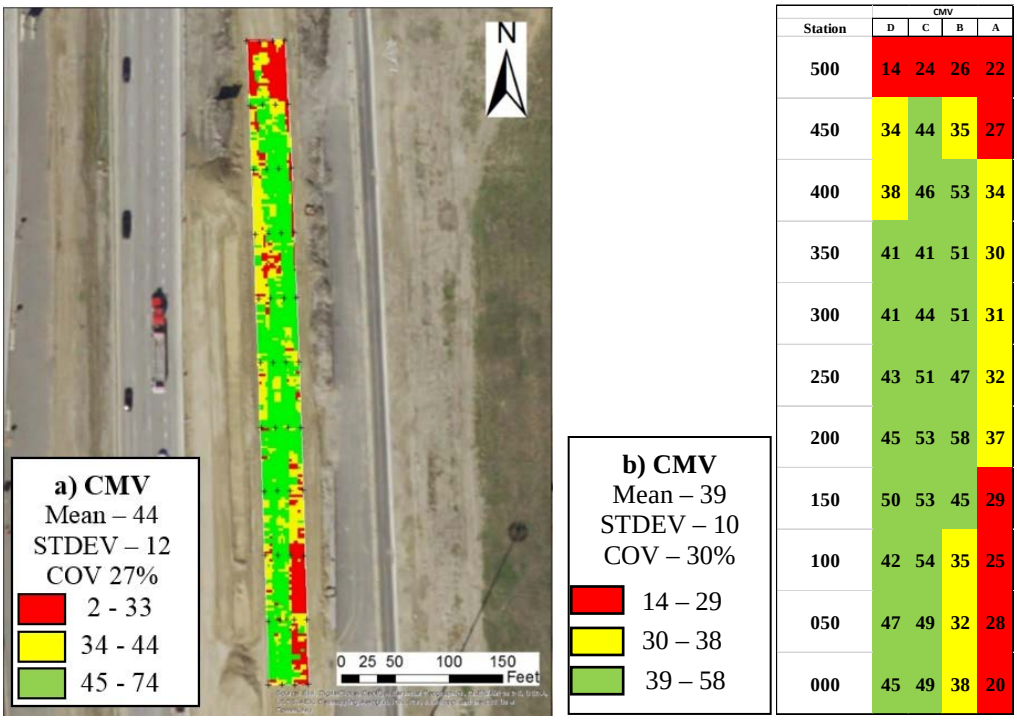

Station	CMV D	CMV C	CMV B	CMV A
500	14	24	26	22
450	34	44	35	27
400	38	46	53	34
350	41	41	51	30
300	41	44	51	31
250	43	51	47	32
200	45	53	58	37
150	50	53	45	29
100	42	54	35	25
050	47	49	32	28
000	45	49	38	20

Figure F.5 – Spatial Distribution of (a) Raw and (b) Rectangular Buffered CMV Data Collected by IC Roller during Proof-Rolling of LTS Layer.

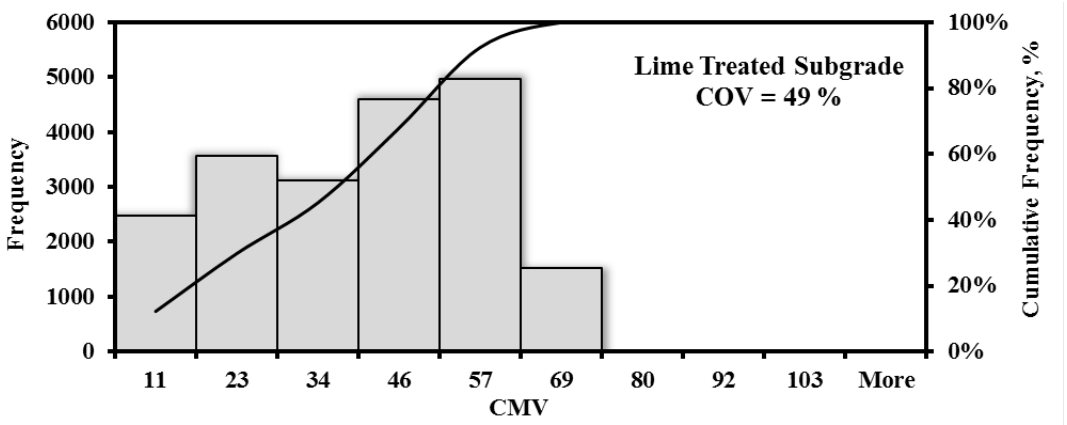

Figure F.6 – Distribution of CMV Data Collected by IC Roller during Proof-Rolling of LTS Layer.

Table F.1 – Criterion for Color-Coded Maps

Color	Criterion
Red	< 0.75 Mean
Yellow	0.75 Mean - Mean
Green	> Mean

Figure F.8 illustrates the spatial distribution of the moisture content found at the surface of the LTS layer. The moisture content varied from 15% to 24% with an average of 19% and a COV of 38%. Throughout the test section the areas with lower moisture content are in agreement with the stiffer areas found in the CMV data.

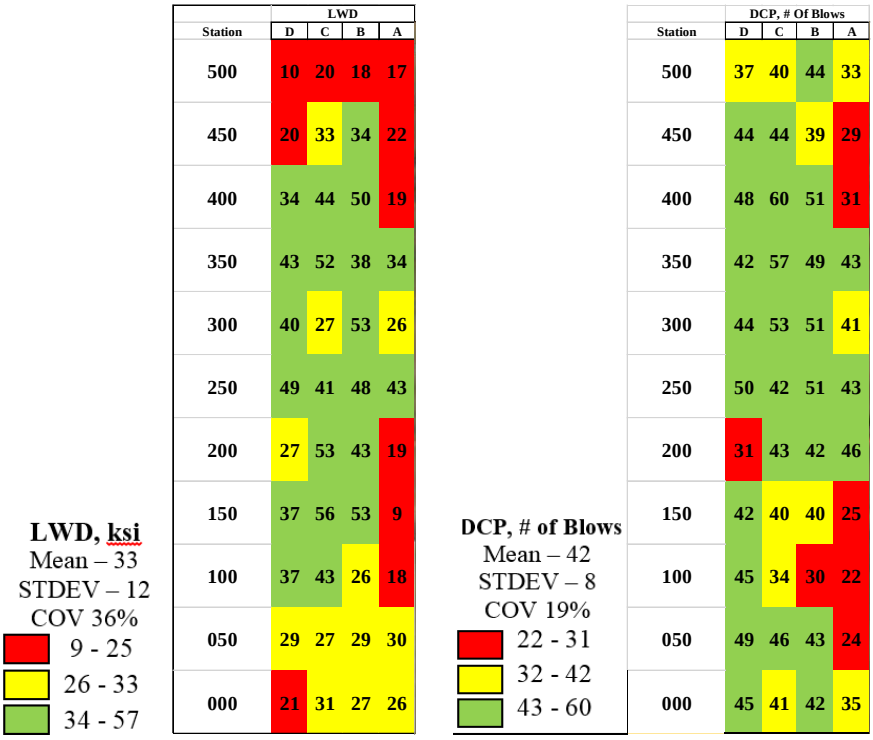

Figure F.7 – Spatial Distribution of (a) LWD Modulus and (b) DCP Blows on LTS Layer.

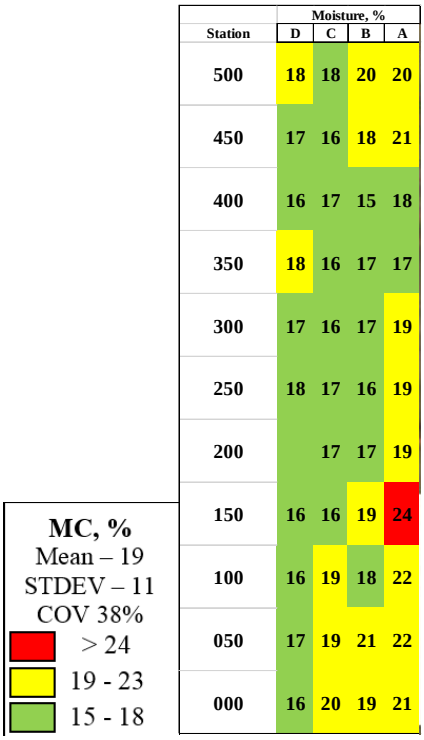

Figure F.8 – Spatial Distribution of Moisture Content of LTS Layer.

A comparison between the LWD modulus and the CMV data at different stations is illustrated in Figure F.9a. An LWD target modulus of 32 ksi, which was determined using a multi-layer linear elastic analysis, is included in Figure F.9a. Both data sets show similar trends. The center part of the test section showed higher LWD modulus and CMVs than the northern and southern ends of the test section. In addition,

average LWD moduli in the center part of the section were greater than the LWD target modulus, while the values reported at the ends of the test section were lower. A similar comparison using the number of DCP blows to penetrate 24 in. in depth and CMV data is shown in Figure F.9b. Though not as manifest as with LWD, some similarity in the trend may be seen between the number of DCP blows and CMV.

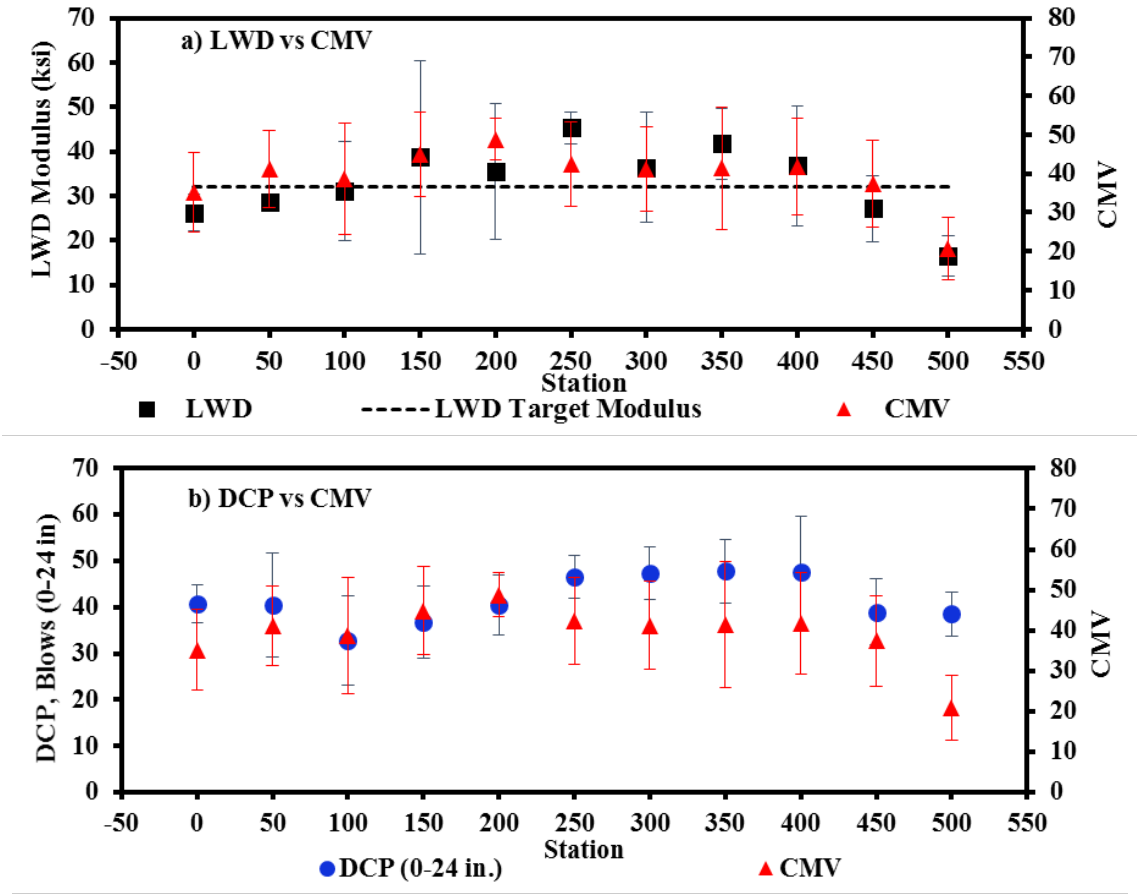

Figure F.9 – Relationship between averaged (a) LWD Modulus and (b) Number of DCP blows vs. CMV.

Plate load tests (PLT) were performed at five different locations shown in Figure F.4. LWD measurements were taken at fifteen points in a 12 ft×6 ft gridded area around the PLT test spot, as shown in Figure F.3b. These measurements were mapped using the same criterion shown in Table F.1. The geospatial variations of the LWD moduli around the PLT locations are shown in Figure F.10. The PLT moduli varied from 10 ksi to 43 ksi with an average of 28 ksi. Descriptive statistics of LWD moduli for each rectangular buffer around the PLT location are included next to the mapped LWD moduli.

Considerable variation around the spot tests can be observed. The maximum COV of LWD moduli was 40% at station 1590+25 as shown in Figure F.10c. Setup of equipment and test duration of the PLT took about 2 hours per spot test, while for the LWD took no more than 5 minutes. In general, the results in terms of moduli obtained by both NDT devices were similar in magnitude.

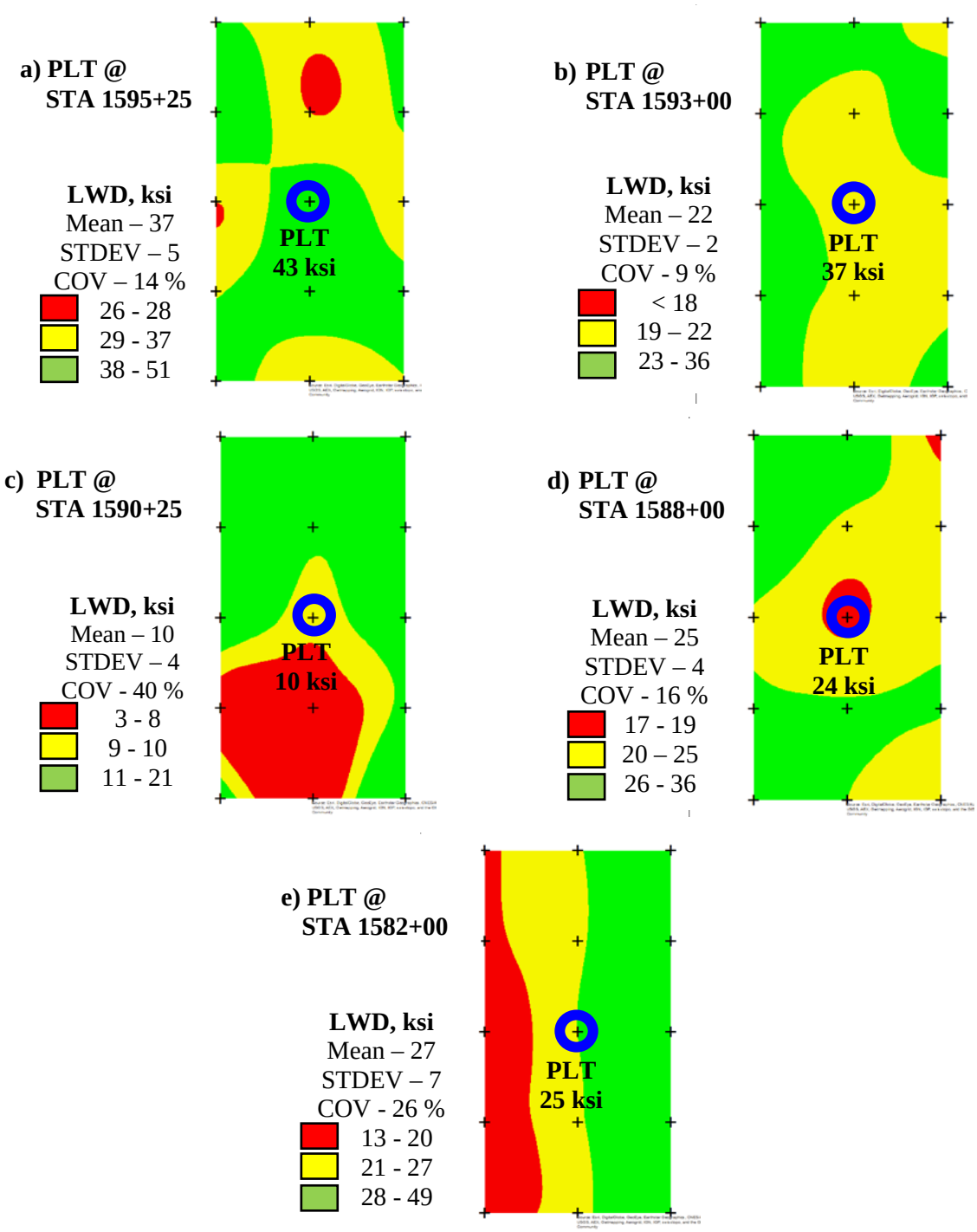

Figure F.10 – Spatial Distribution of LWD at Different PLT locations.

F.4 Geospatial Classification for Developing Optimized Color-Coded Maps

Figure F.11 compares the collected and processed CMV data and LWD modulus for a 500 ft long and 27 ft wide lime-stabilized layer. Using the criterion selected for previous field studies (shown in Table F.1), some rectangular areas marked in red on the CMV map are not shown as less-stiff areas on the LWD surface modulus map. For example, in Figure F.11a, the IC roller predicted nine rectangular areas as less-stiff. Seven of these areas were predicted to be less-stiff on the LWD map as well. As such, 22% of less-stiff areas spotted in the CMV map were not in agreement with the less-stiff areas found in the LWD map.

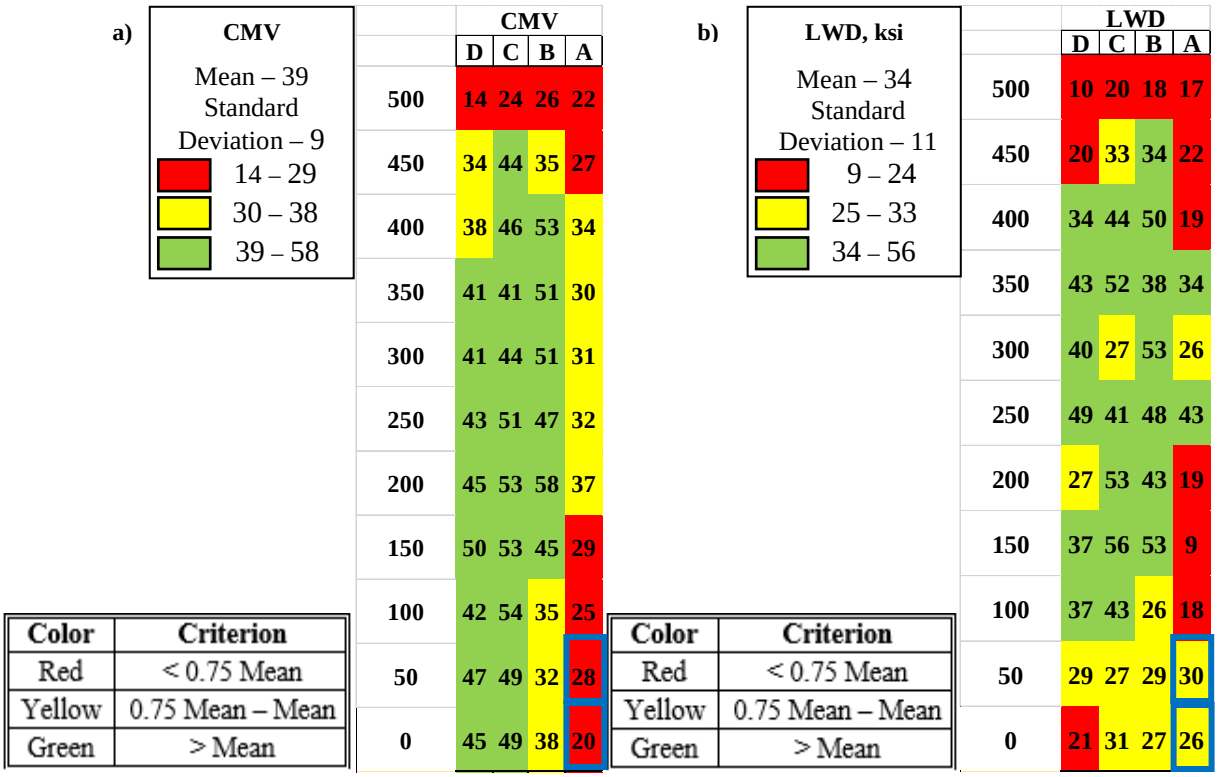

Figure F.11 – Color-Coded Map Comparison between a) CMV and b) LWD Surface Modulus.

In an effort to reduce this percentage, a different color criterion is necessary to improve the IC roller prediction process for identifying the less-stiff areas. The approach consisted of varying the criterion for identifying the less-stiff areas for both the CMV and LWD surface modulus mappings. This criterion varied between a range of 60% to 90% of the average measured values, for the ICMV data and LWD surface moduli. Table F.2 shows the percentage of mismatched areas of the IC roller predicted less-stiff areas. The IC roller was able to predict less-stiff areas, with confidence that all areas were also identified by the LWD as less-stiff, when a criterion mark for less-stiff is set at 70% of the average CMV (or lower), and when a criterion mark for less-stiff is set at 80% of the average LWD surface modulus (or higher). The color maps from this process is shown in Figure F.12. This approach is currently under evaluation at other sites and with the other class breaks discussed above.

Table F.2 – Percentage of Disagreement in Rectangular Buffered Areas between CMV and LWD Modulus Based on Different Color-Criteria for the Less-Stiff (Red) Areas.

		Less-Stiff (Red) Area Below % of Average E_{LWD}						
Less-Stiff (Red) Area Below % of Average CMV		**90**	**85**	**80**	**75**	**70**	**65**	**60**
	90	24	29	29	47	47	53	65
	85	23	31	31	46	46	54	62
	80	18	18	18	36	36	45	55
	75	11	11	11	22	22	33	44
	70	0	0	0	14	14	29	43
	65	0	0	0	17	17	17	33
	60	0	0	0	33	33	33	33

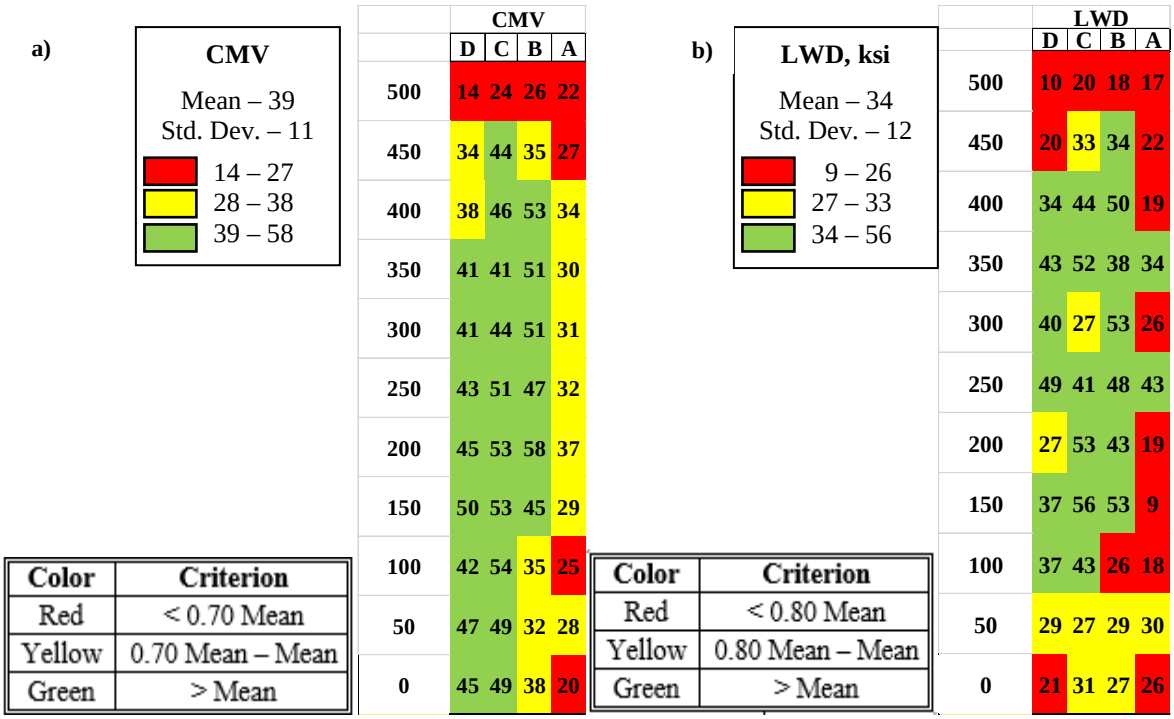

Figure F.12 – Optimized Color-Coded Map Comparison between (a) CMV Using Less-Stiff (Red) Areas when CMV < 75% of Average of CMVs, and (b) LWD Using Less-Stiff (Red) Areas when E_{LWD} < 80% of Average E_{LWD} Values.

F.5 Flexible Base

Figure F.13a illustrates the spatial distribution of the CMV data during the mapping of the compacted base layer. Figure F.13b shows the spatial distribution of averaged buffered CMVs when the entire section was divided into 44 rectangular buffer areas measuring 9 ft × 50 ft. The histogram of the CMV distribution depicted in Figure 4.14 exhibits a considerable change in the trend of the collected CMV data. The average CMV seems to be higher than the previous layer and the COV is reduced to 17%.

The LWD moduli measured at the 44 points vary from 12 ksi to 52 ksi, with an average of 26 ksi and COV of 35% (see Figure F.15a). The areas of the test section showing higher LWD moduli are in accordance with the CMV data shown in Figure F.13a.

Figure F.15b summarizes the DCP results on the compacted FB layer. The estimated number of DCP blows required to penetrate to a depth of 12 in. ranged from 45 blows to 155 blows with an average of 100 blows and a COV of 26%.

Figure F.16 illustrates the spatial distribution of the moisture content of the base layer. The moisture content varied from 5% to 18% with an average of 10% and a COV of 20%. The moisture content was fairly constant except for a few points showing a higher level of moisture. No well-defined visual resemblance was seen between moisture content and CMV.

A comparison between the LWD moduli and the CMV data at different stations is illustrated in Figure F.17a. The LWD moduli and CMV results showed some resemblance, though definitely not as strong as trends seen on the LTS, shown in Figure F.17a. Besides, most LWD moduli were below the target LWD modulus of 32 ksi. A similar comparison using the number of DCP blows and CMV data is shown in Figure F.17b. The trend observed for the number of blows per station was similar to LWD modulus.

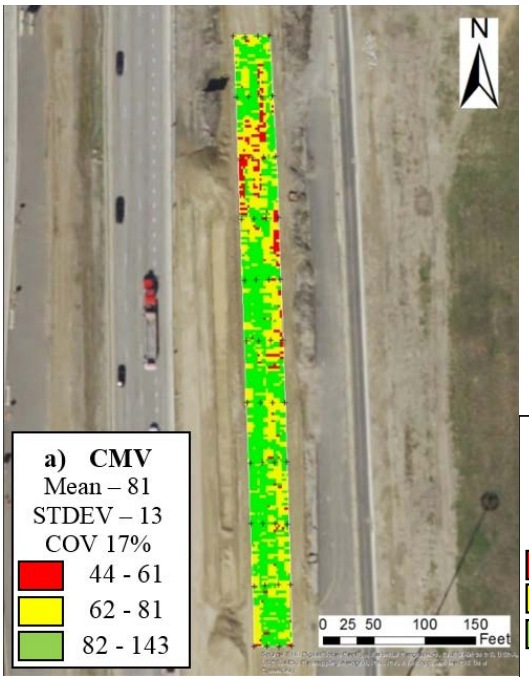

Station	CMV			
	D	C	B	A
250	77	81	81	78
225	85	84	73	82
200	66	65	74	80
175	70	79	80	69
150	85	96	80	67
125	84	87	75	66
100	83	92	83	80
75	87	91	78	79
50	87	90	80	75
25	77	85	82	78
0	69	86	84	76

Figure F.13 – Spatial Distribution of (a) Raw and (b) Rectangular Buffered CMV Data Collected by IC Roller during Proof-Rolling of Flexible Base Layer.

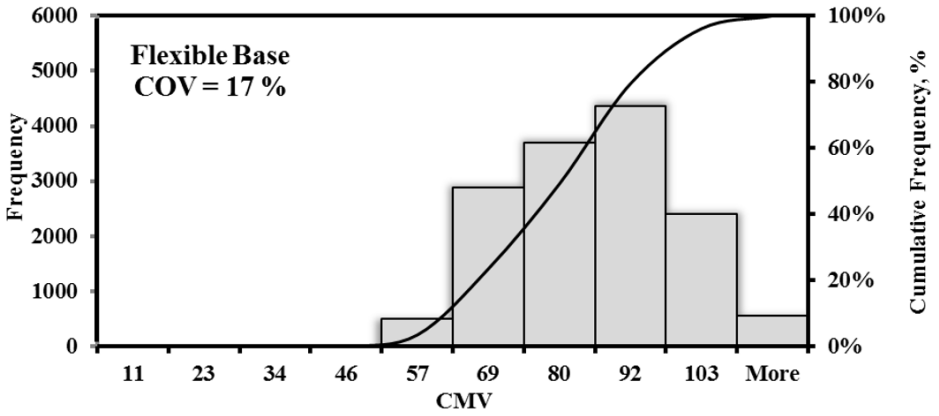

Figure F.14 – Distribution of CMV Data Collected by IC Roller during Proof-Rolling of Flexible Base Layer.

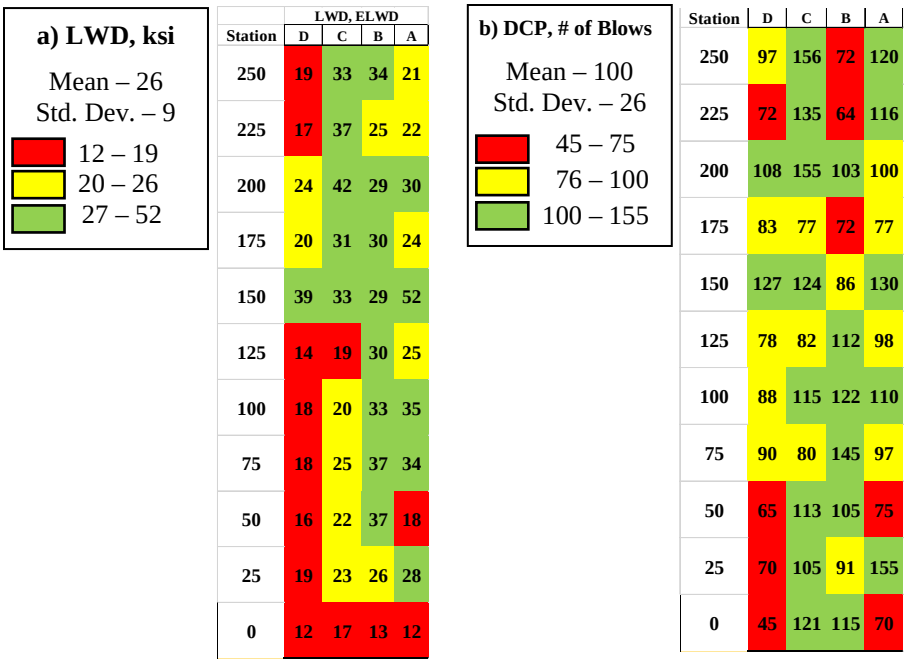

Figure F.15 – Spatial Distribution of (a) LWD Modulus and (b) Number of DCP Blows to Penetrate 12 in. of Flexible Base Layer.

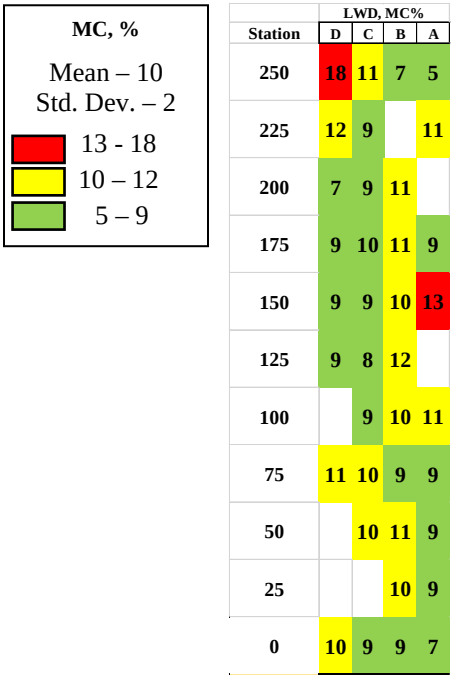

Figure F.16 – Spatial Distribution of Moisture Content of Flexible Base Layer.

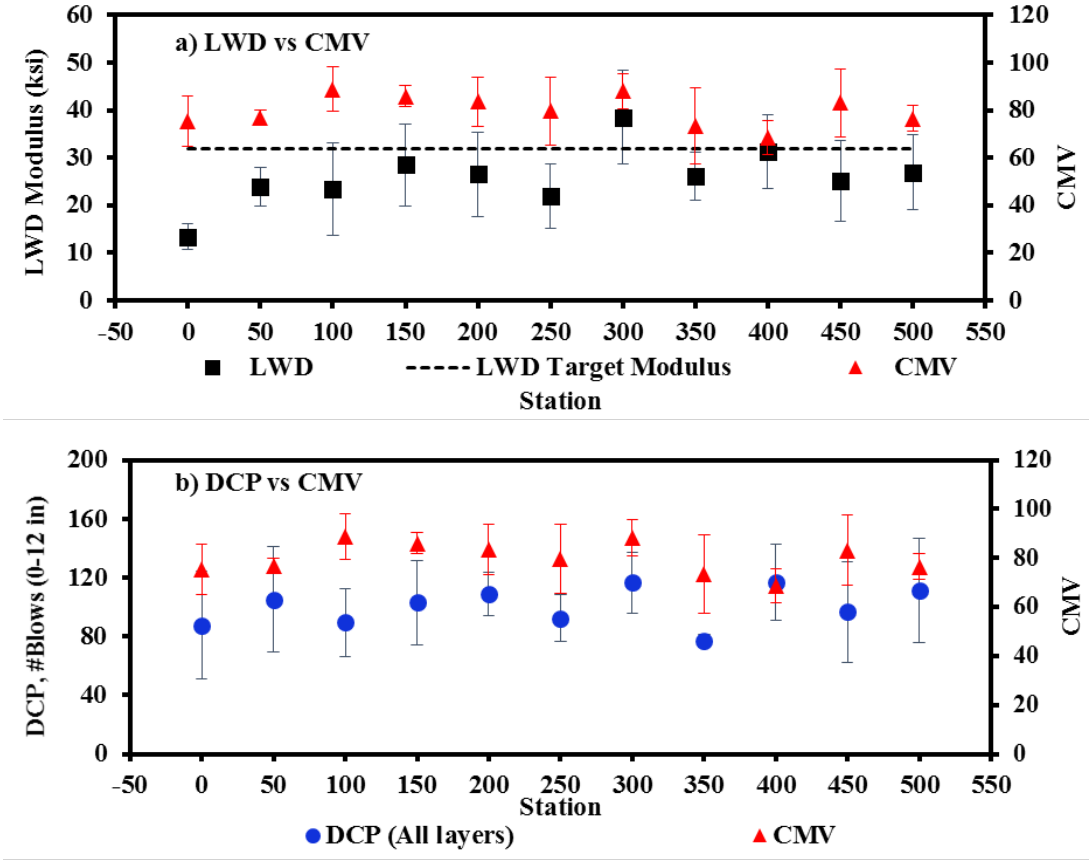

Figure F.17 – Relationship between Averaged (a) LWD Modulus and (b) Number of DCP Blows to Penetrate 12 in vs. CMV.

APPENDIX G - TEST SITE ALONG FM 1460 IN GEORGETOWN, TX

G.1 Introduction

Field evaluation was performed on a 250-ft section as part of an expansion of farm-to-market road FM 1460 in Georgetown, Texas. Figure G.1 shows an aerial view of the of the test section alongside a map with the location of the test section within the Georgetown area.

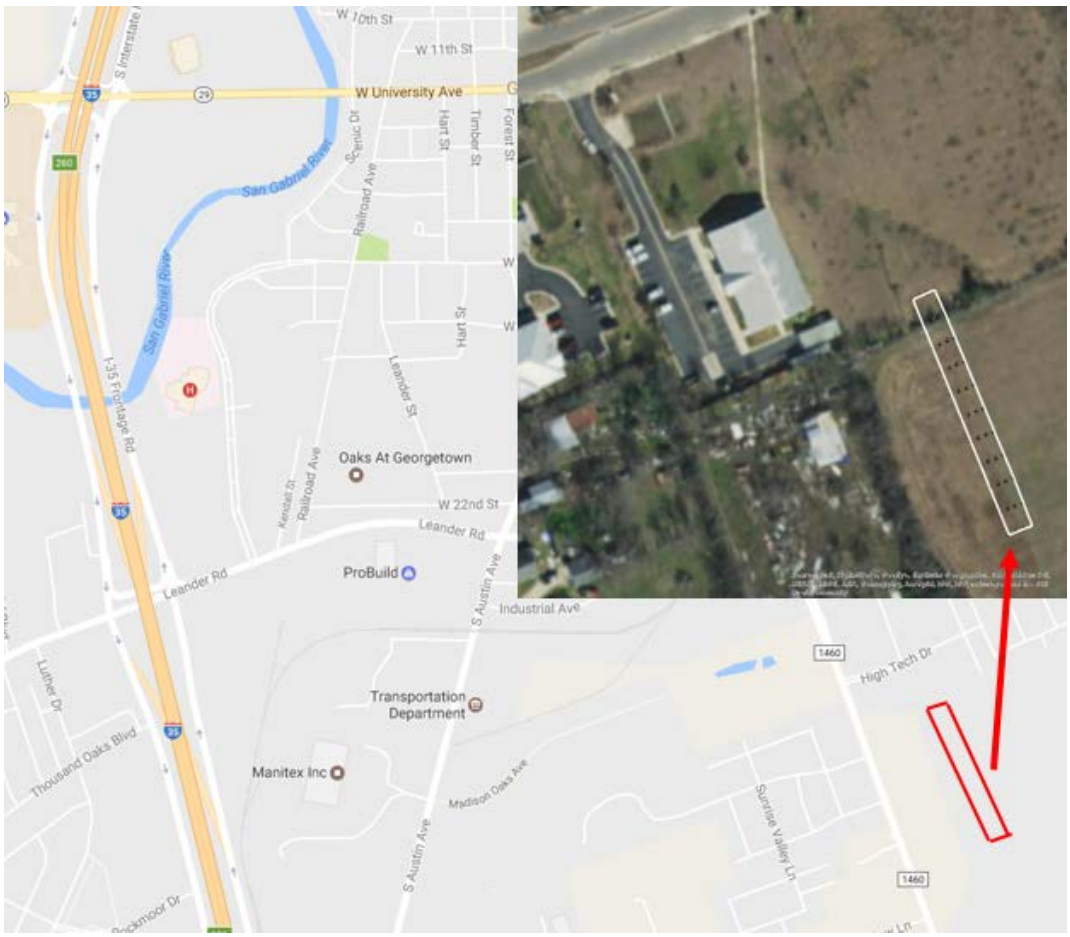

Figure G.1 – Location of Field Evaluation Site on FM140 in Georgetown, TX.

The pavement section consisted of a 12-in. thick flexible (unbound) aggregate base layer over an 8 in. lime-treated subgrade (LTS), on top of subgrade as shown in Figure G.2. Mapping and field evaluation of the LTS took place on June 20, 2016. The evaluation of the base was carried out on July 15, 2016.

G.2 Field Testing Program

Spot testing was carried out along a 250 ft long and 24 ft wide section. A grid consisting of 44 points divided in 4 columns of 11 points each was selected for the location of the spot tests. The grid was designed with a spacing of 25 ft between each of the 11 points, and a spacing of 8 ft between each column as shown in Figure G.3a. The evaluation of the base layer was carried out only along a 150 ft length as shown in Figure G.3b, because the rest of the section was not compacted. LWD and DCP tests were carried out at each point as discussed above. In addition, moisture content samples were collected at all test locations. The lime treated subgrade layer was mapped using a smooth CAT roller equipped with the developed UTEP DAQ system. The first phase of the construction consisted of stabilizing the subgrade soil using hydrated lime.

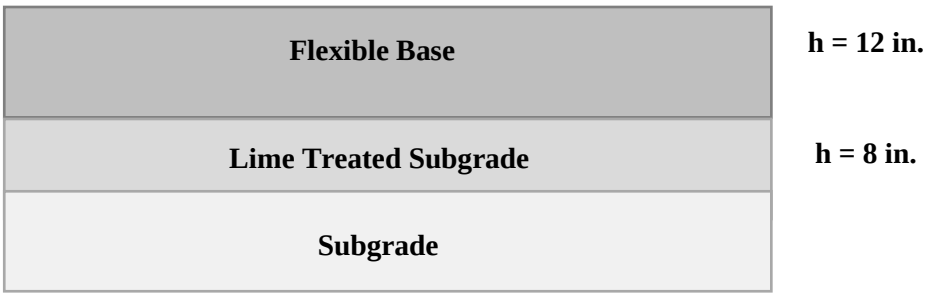

Figure G.2 – Pavement Structure of Test Section

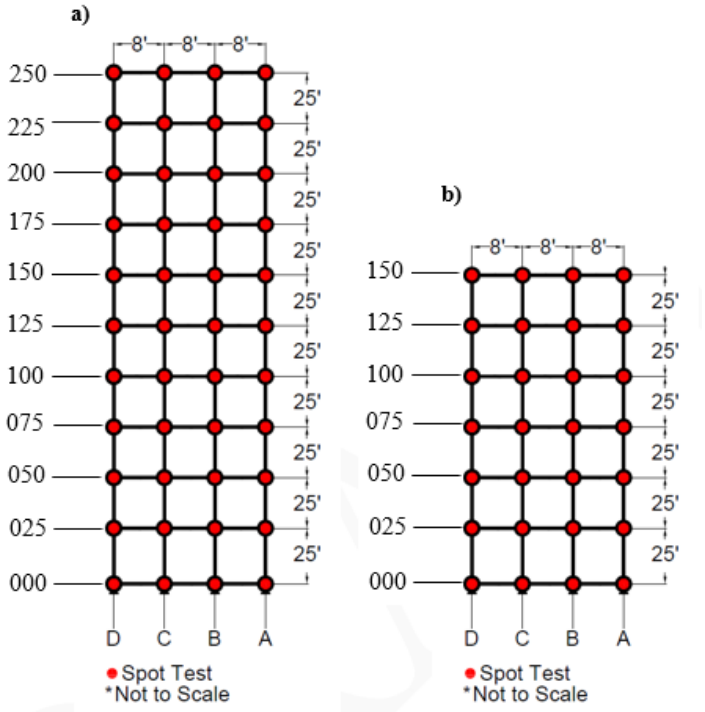

Figure G.3 – Schematic of the Typical Test Section and Location of Spot Tests for (a) Lime-Treated Subgrade and (b) Flexible Base Layer.

The spatial distribution of the CMVs collected during the mapping of the LTS layer is shown in Figure G.4a. Figure G.4b shows the spatial distribution of averaged buffered CMVs when the entire section was divided into 44 rectangular buffer areas measuring 8 ft × 25 ft. The location of the less stiff areas on both maps are comparable.

The histogram of the mapped CMVs is summarized in Figure G.4. The maximum CMV was about 41 for the spatial distribution of the raw data and 36 for the averaged data. COV of CMVs was 46%, as shown in Figure G.5.

Once the compaction and proof-mapping of the lime-treated subgrade was completed, field testing was performed with the LWD and DCP on the compacted layer at 44 points along the test section. The collected spot test data were imported into ArcGIS software to generate color-coded geospatial distribution maps. The spline spatial interpolation algorithm was employed for the process of spatial interpolation. The classification method for the color criterion was based on the mean as obtained for all the different spot test measurements as shown in Table 5.6.

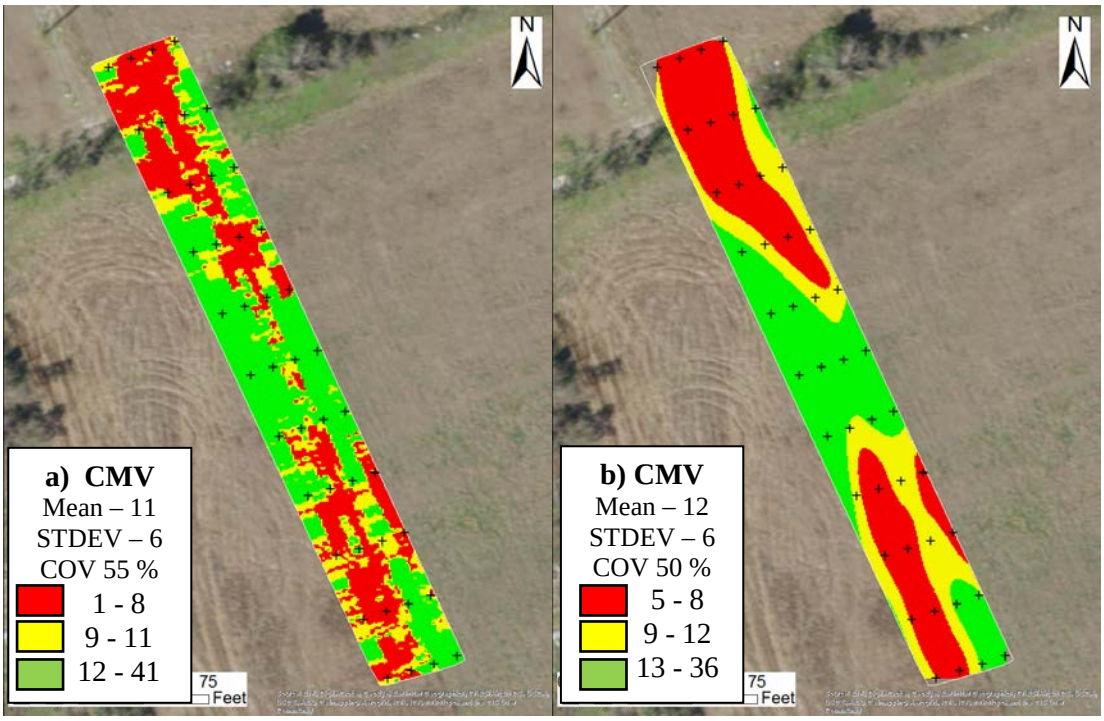

Figure G.4 – Spatial Distribution of (a) Raw and (b) Rectangular Buffered CMV Data Collected by IC Roller during Proof-Rolling of LTS Layer.

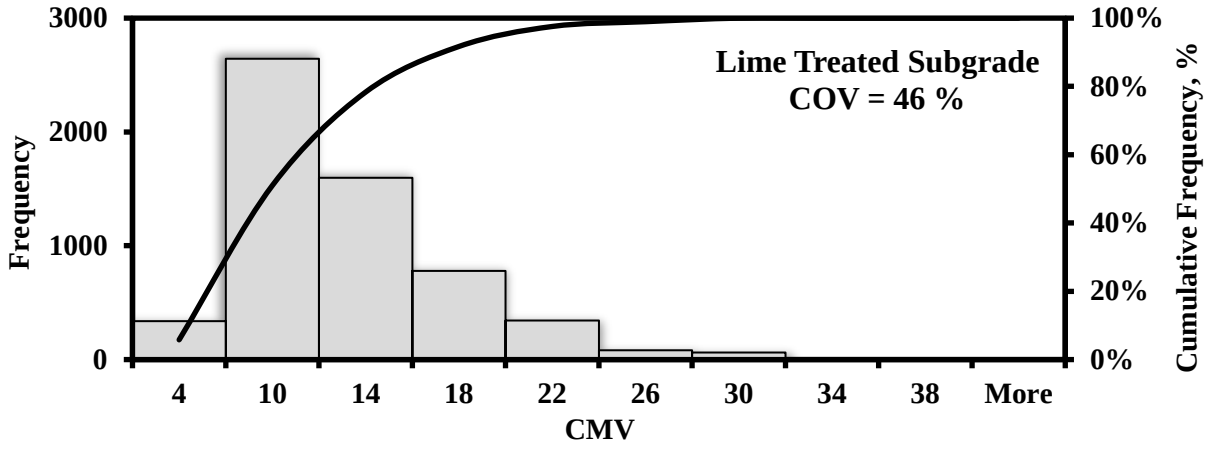

Figure G.5 – Distribution of CMV Data Collected by IC Roller during Proof-Rolling of LTS Layer.

Figure G.6 illustrates the spatial distribution of the LWD modulus on top of the compacted LTS layer. The LWD moduli varied from 4 ksi to 16 ksi with an average of 7 ksi and a COV of 29%. The northern and southern parts of the test section showed lower LWD moduli which is in agreement with the CMV data shown in Figures G.4a and G.4b.

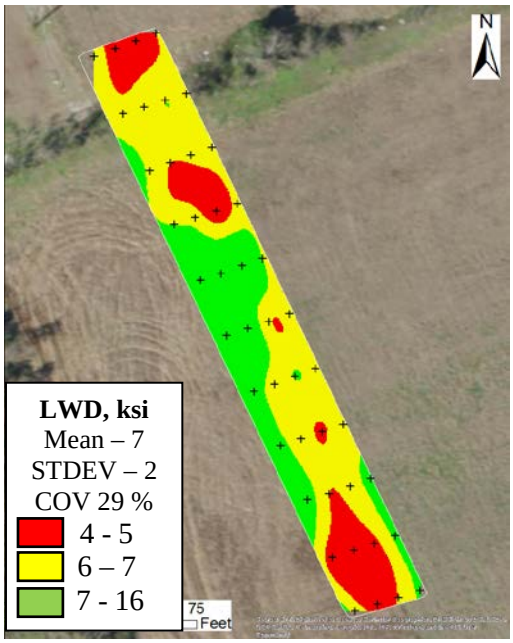

Figure G.6 – Spatial Distribution of LWD Modulus on LTS Layer.

Figure G.7 summarizes the DCP results on the compacted LTS layer. The numbers of DCP blows required to penetrate to a depth of 24 in. ranged from 18 blows to 92 blows with an average of 31 blows and a COV of 55%. Similar to LWD, the northern and southern parts required fewer DCP blows than the mid-section, where the LTS is stiffer. This is in agreement with the LWD geospatial distribution, and bears resemblance to the CMV geospatial distribution.

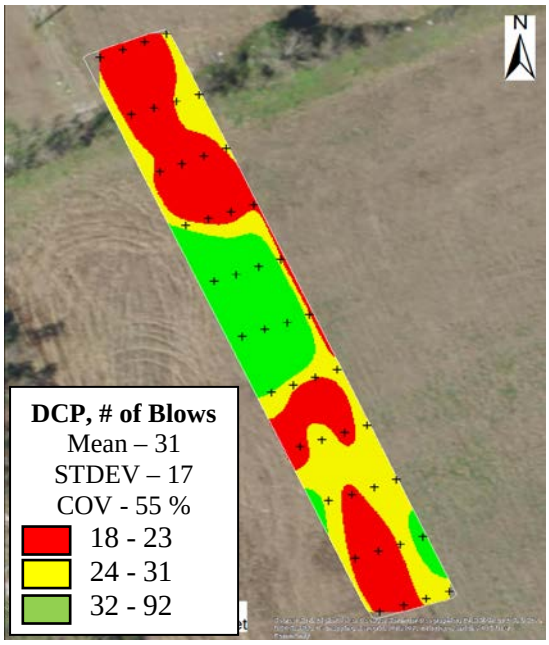

Figure G.7 – Spatial Distribution of Number of DCP Blows on LTS Layer.

Figure G.8 illustrates the spatial distribution of the moisture content of the LTS layer. The moisture content varied from 10% to 16% with an average of 14% and a COV of 7%. No well-defined visual relationship is seen between moisture content and CMV nor with the other modulus-based measurements.

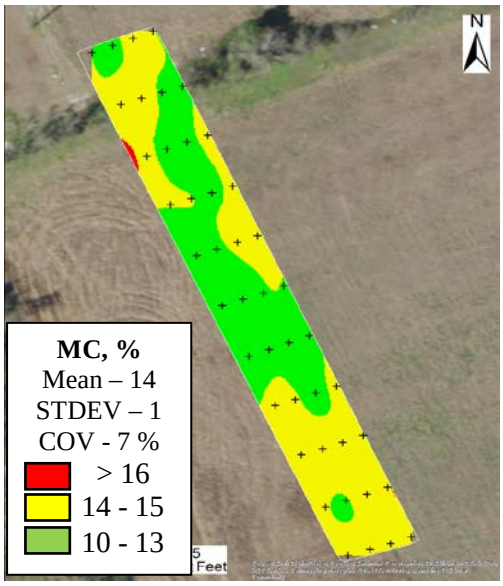

Figure G.8 – Spatial Distribution of Moisture Content of LTS Layer.

A comparison between the LWD moduli and CMV data at different stations is illustrated in Figure G.9a. Likewise, the comparison using the number of DCP blows and CMV data is shown in Figure G.9b. A similar trend is evident between CMV and the modulus-based measurements.

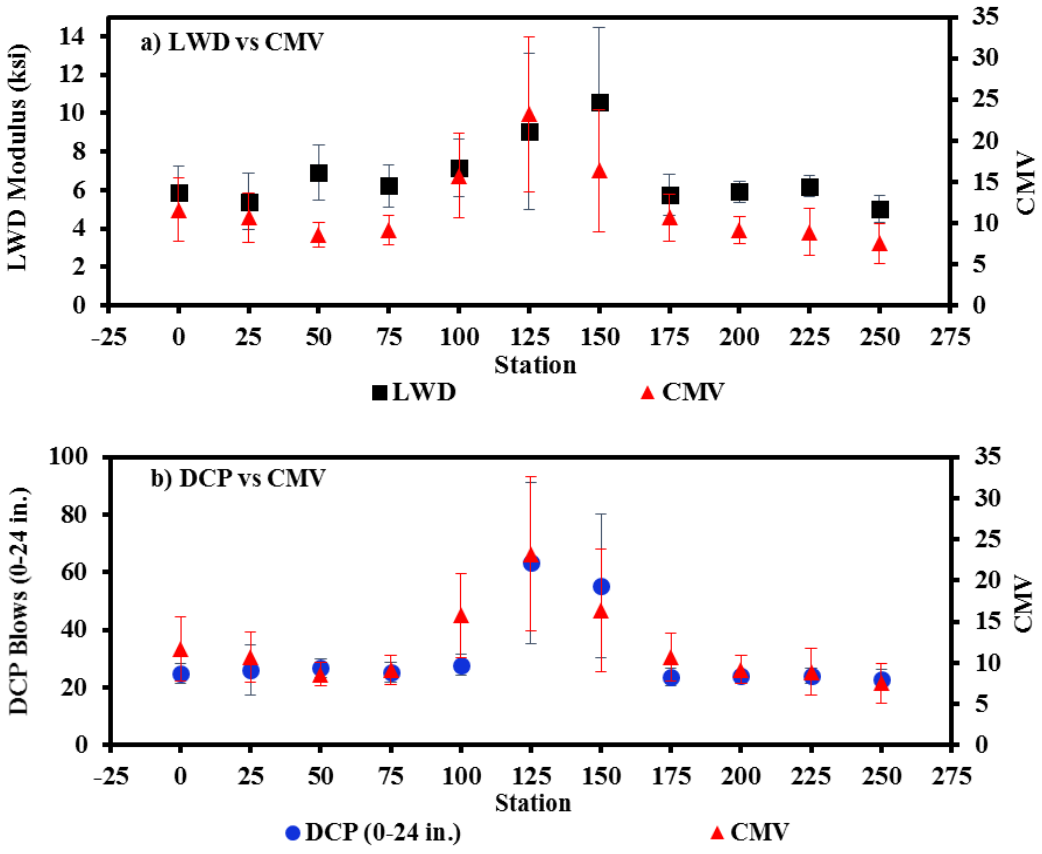

Figure G.9 – Relationship between Averaged (a) LWD Modulus and (b) Number of DCP Blows vs. Average CMV per Station.

G.3 Flexible Base

Figure G.10a illustrates the spatial distribution of CMV data during the mapping of the base layer. Figure G.10b shows the spatial distribution of averaged buffered CMVs when the entire section was divided into 28 rectangular buffer areas measuring 8 ft × 25 ft.

The histogram of the CMV distribution depicted in Figure G.11 exhibits that the average CMV increased to 61, a magnitude greater than that obtained for the LTS, with a COV of 44%.

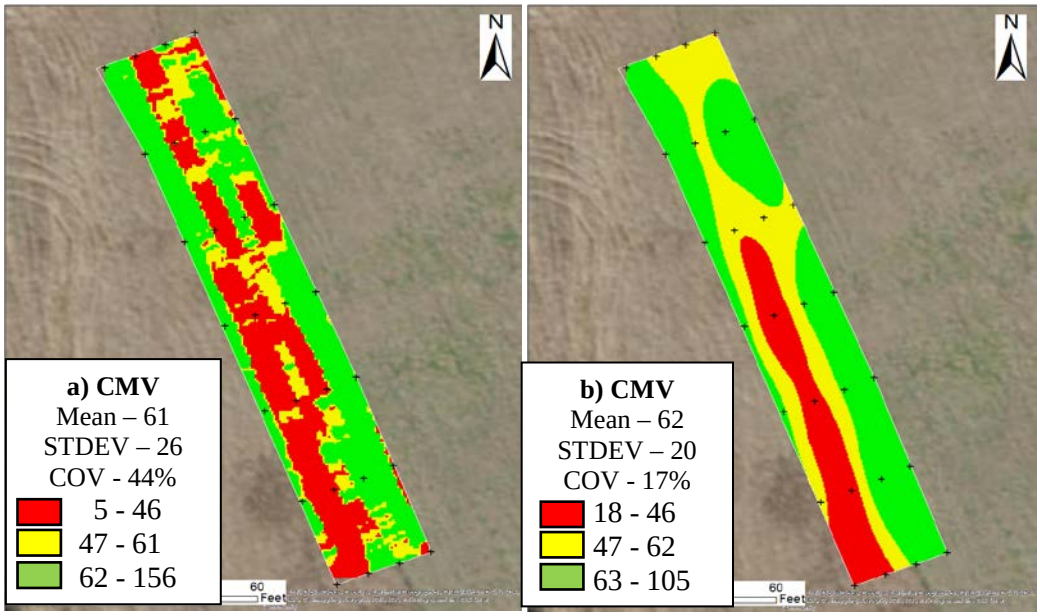

Figure G.10 – Spatial Distribution of (a) Raw and (b) Square Buffered CMV Data Collected by IC Roller during Proof-Rolling of Flexible Base Layer.

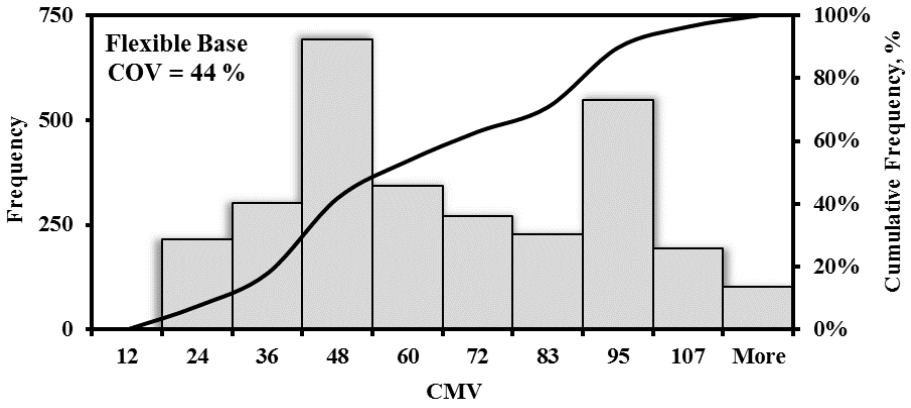

Figure G.11 – Distribution of CMV Data Collected by IC Roller during Proof-Rolling of Flexible Base Layer.

The LWD tests were conducted on the spot locations shown in Figure G.3b within the test section. Figure G.12 illustrates the spatial distribution of the LWD moduli on top of the compacted base. The LWD moduli varied from 26 ksi to 51 ksi, with an average of 35 ksi and COV of 17%. The areas of the test section showing higher LWD moduli are somewhat in accordance with the CMV data shown in Figures G.10a and G.10b; however, less stiff areas as determined by the LWD were not in accordance with the CMV.

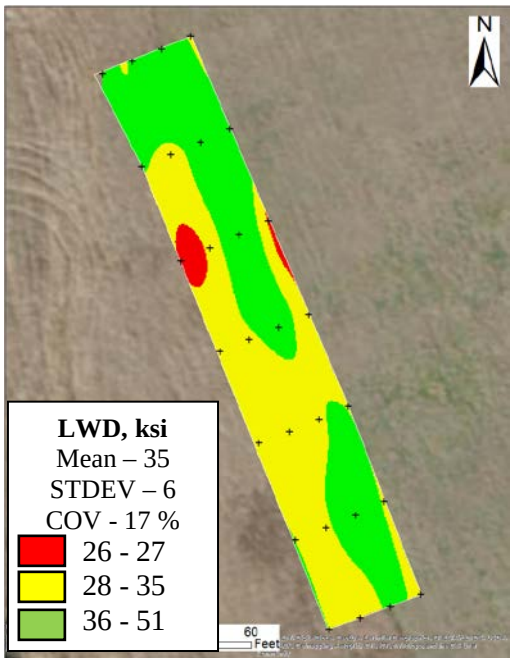

Figure G.12 – Spatial Distribution of LWD Modulus of Flexible Base Layer.

Figure G.13 summarizes the DCP results on the compacted base. The estimated number of DCP blows required to penetrate to a depth of 12 in. ranged from 180 blows to 360 blows with an average of 252 blows and a COV of 17%. Both LWD and DCP indicated that the layer was mostly uniform and stiff, but color maps were not comparable.

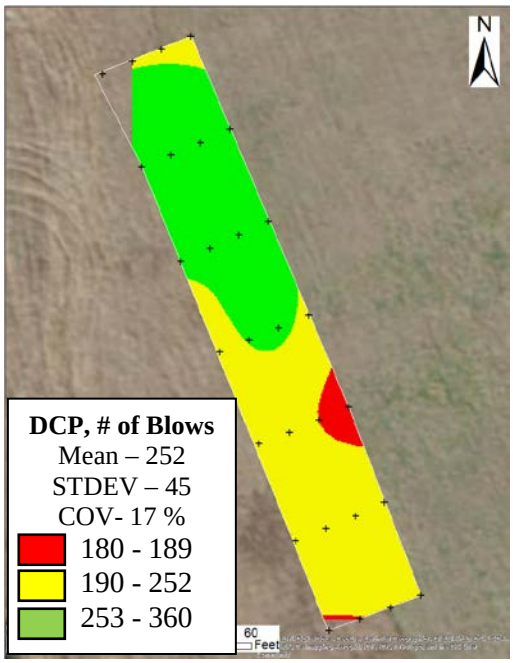

Figure G.13 – Spatial Distribution of Number of DCP Blows of FB Layer.

Figure G.14 illustrates the spatial distribution of the moisture content of the Flexible Base layer. The percentage of moisture content varied from 2% to 5% with an average of 4% and a COV of 14%. Mapping of moisture content did not bear resemblance to the mapping of any of the other measurements, possibly due to low variation of results and the chosen criterion.

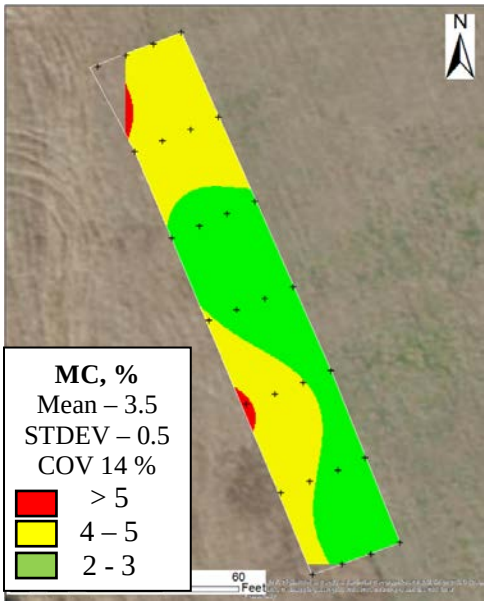

Figure G.14 – Spatial Distribution of Moisture Content of Flexible Base Layer.

A comparison between LWD moduli and CMV data at different stations is illustrated in Figure G.15a. Unlike the mapping, LWD moduli and the CMV results show a similarity in the trends when evaluated with respect to stations. Likewise, the number of DCP blows and CMV data per station, shown in Figure G.15b, indicates good relationship may be seen between the trends of both measurements.

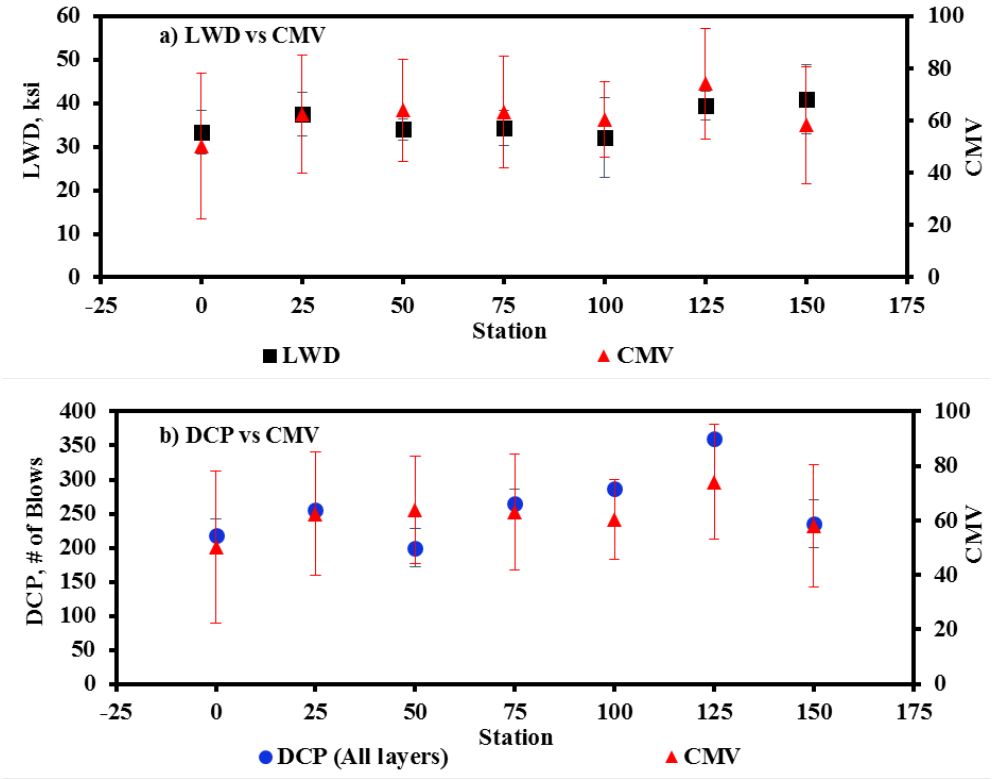

Figure G.15 – Relationship between Averaged (a) LWD Modulus and (b) Number of DCP Blows vs CMV in Flexible Base.

APPENDIX H - TEST SITE ALONG SH 183 IN IRVING, TX

H.1 Introduction

A test section along the west-bound SH 183 in Irving, TX was used for this field evaluation. Figure H.1 shows an aerial view of the test section.

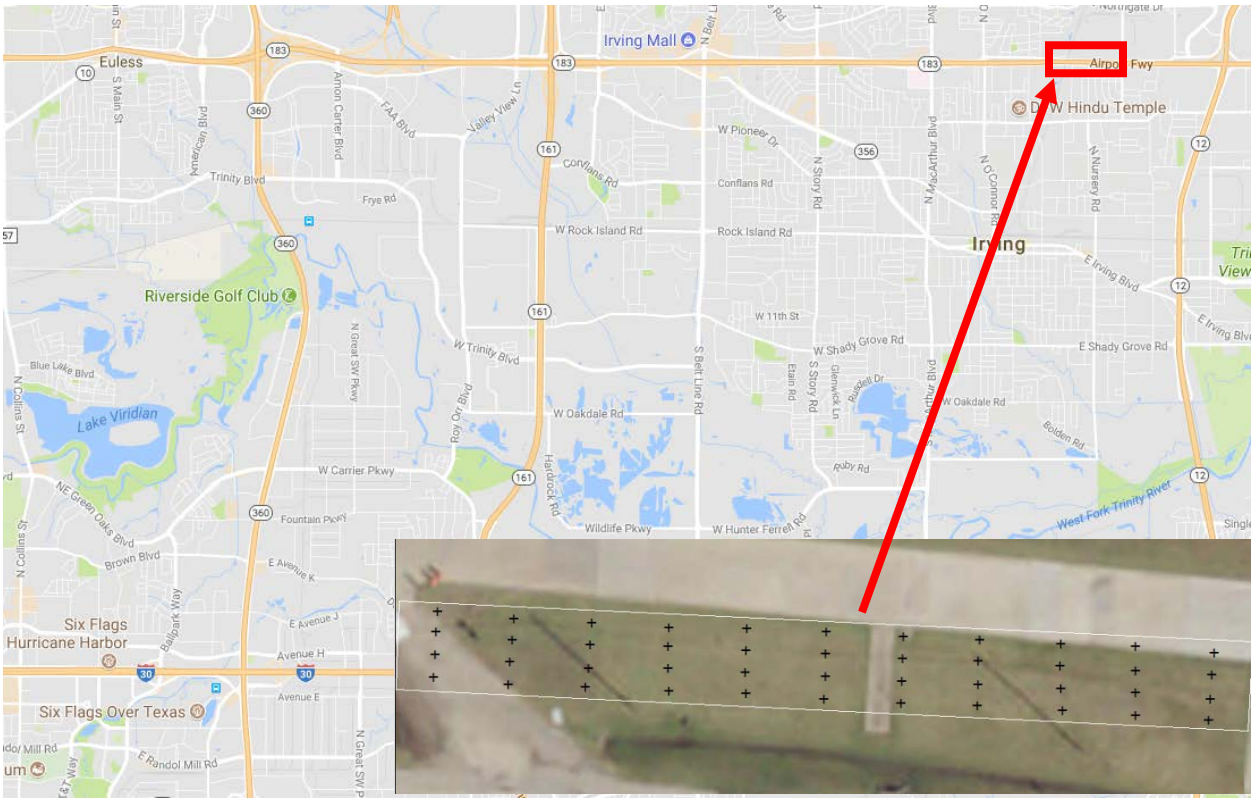

Figure H.1 – Location of Field Evaluation Site on SH 183 in Irving, TX.

The field evaluation was conducted on two different pavement layers. The first layer consisted of an 8 in. lime-treated subgrade (LTS) on top of subgrade. Field evaluation of the LTS took place on April 25, 2017. The second layer evaluated at this section was a 12 in. flexible base layer as shown in Figure H.2. IC roller compaction and NDT testing of the base were carried out on May 9, 2017.

Flexible Base	**h = 12 in.**
Lime Treated Subgrade	**h = 8 in.**
Subgrade	

Figure H.2 – Pavement Structure of Test Section

H.2 Field Testing Program

Nondestructive testing (NDT) and proof-rolling was performed on a 250 ft.-long and 21 ft.-wide section. To locate the spots to carry out the different tests, a grid consisting of 44 points divided in 4 columns of 11 points each was arranged on the site. The grid was designed with a spacing of 25 ft between each of the 11

points, and a spacing of 7 ft between each column, as shown in Figure H.3. LWD and DCP tests were carried out at each point as discussed above. In addition, moisture content samples were collected at all test locations.

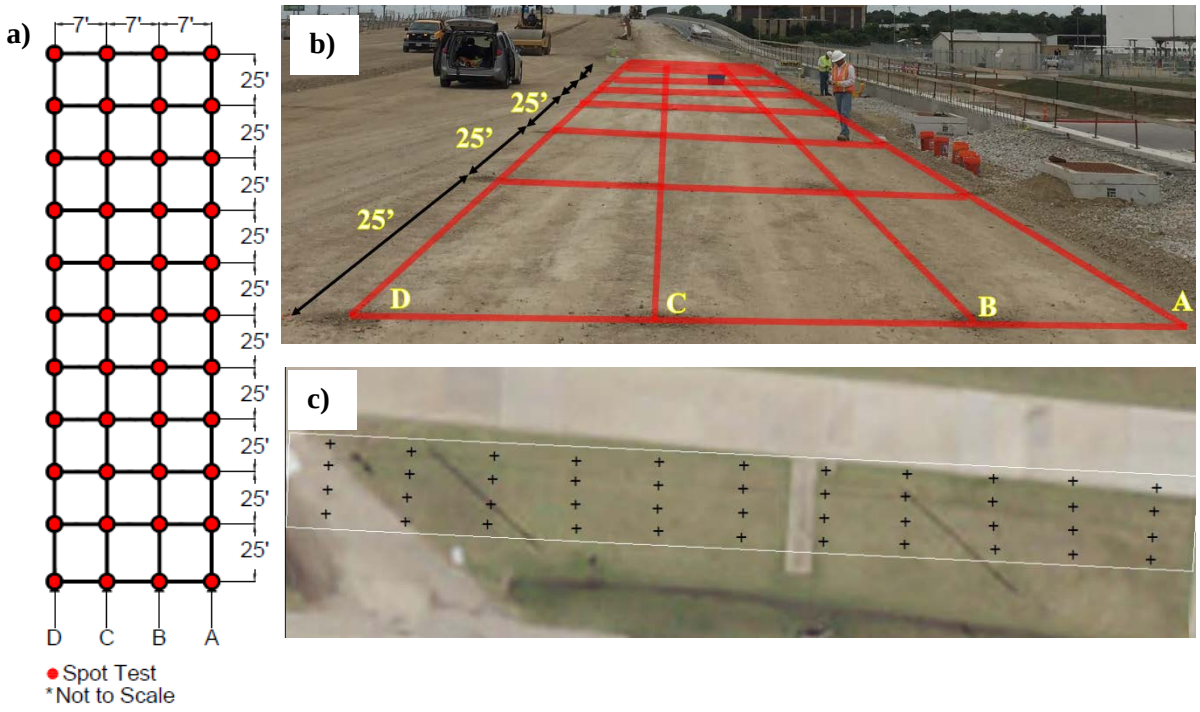

Figure H.3 – (a) Schematic of the Test Section, (b) Site View with Grid Overimposed over Test Section and (c) Satellite View Showing Spot Test Points.

UTEP's data acquisition system was employed for the proof-mapping during this field evaluation. A map of the IC data obtained by the acquisition system during the proof-mapping of the subgrade is shown on Figure H.4.

Figure H.4 – IC Data Points Collected During Proof-Mapping of Subgrade Layer

H.3 Lime-Treated Subgrade

The lime-treated subgrade layer was proof-mapped using a padfoot CAT CS78B roller equipped with an IC retrofit kit. The histogram of the mapped CMVs is summarized in Figure H.5. The average CMV value was 11 with a COV of 86%.

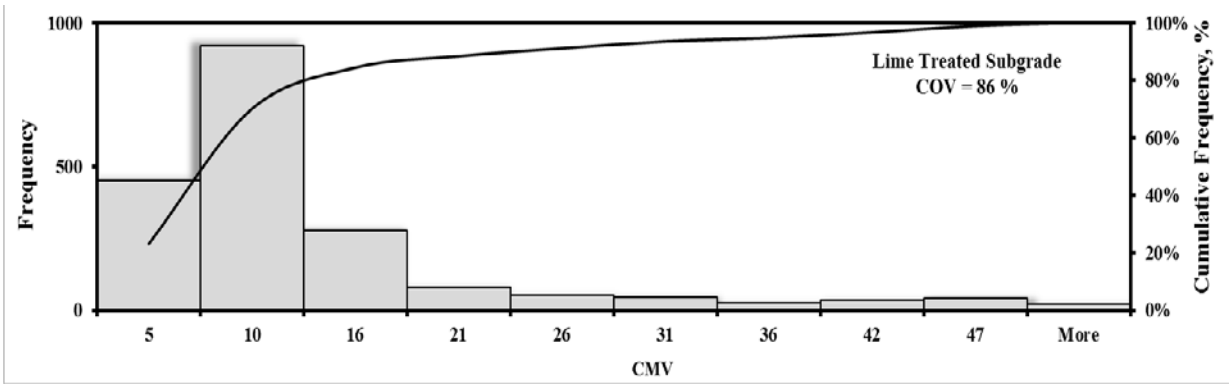

Figure H.5 – Distribution of CMV Data Collected by IC Roller on top of LTS Layer.

Based on the 25 by 7 ft spacing between the locations of the LWD spots, rectangular buffered areas were created around each LWD spot location as shown in Figure 6.5. IC data points found within these blocks was averaged to obtain a unique ICMV to represent that block. In a few cases there were no IC data points found within the limits of the created blocks, as in the case of cells A250, D250, B125, and B150, shown in Figure H.6. Color-coded maps, shown in Figure H.6, were created using the criterion shown in Table 5.6 to compare the values obtained in each block for the IC data and the LWD deflections.

Figure H.6 – Data Collected by IC Roller on top of LTS Divided in Rectangular Buffered Areas.

The spatial distribution of the averaged CMVs is shown in Figure H.7a. The values found in the averaged CMV blocks ranged from a minimum of 5 to a maximum of 179, with a mean of 33. Figure H.7b illustrates the spatial distribution of the deflections created during the LWD testing on top of the LTS layer. The LWD deflections varied from 8 mils to 47 mils with an average of 22 mils. The LWD deflection map reveals a region that is less-stiff at the upper left section of the site, i.e. between Stations 175 to 250, Lines C-D. This area was not revealed on the CMV map.

The coefficient of variation of CMVs within the buffered revealed that the blocks along Line A and along Stations 0 and 250 had highly variable CMVs, as shown in Figure H.8.

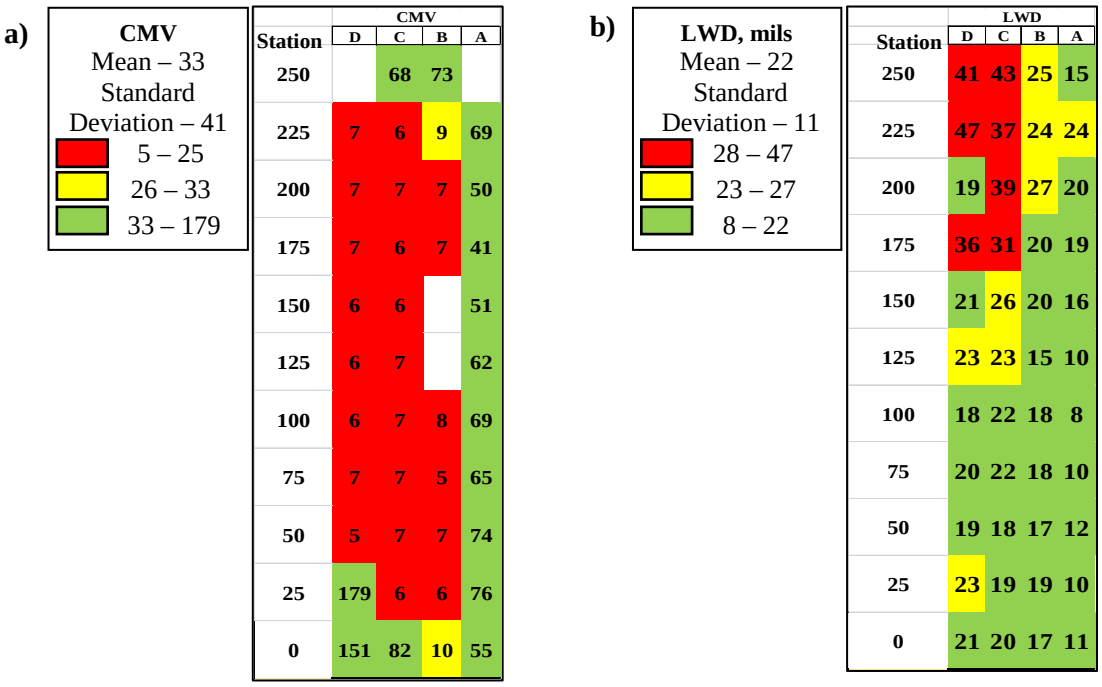

Figure H.7 – Spatial Variation Comparison between (a) CMV and (b) LWD Deflection.

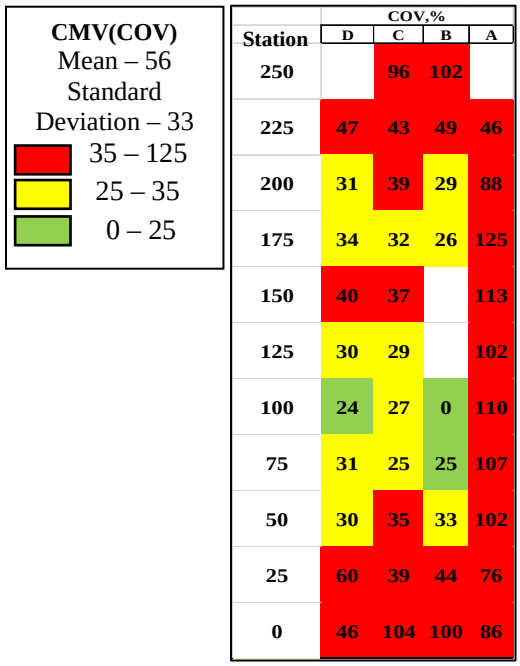

Figure H.8 – Spatial Variation of Coefficient of Variation of CMV within each Buffered Area.

Figure H.9 summarizes the DCP results on the compacted LTS layer. The numbers of DCP blows required to penetrate to a depth of 18 in. ranged from 14 blows to 83 blows with an average of 36 blows and a COV of 45%. Similar to LWD, the upper-left part of the distributed map required fewer DCP blows than the rest of the test section and, thus, is identified as a less-stiff area.

Comparison between the LWD and DCP moduli and the CMV data at different stations are illustrated in Figure H.10. Due to the highly variable nature of the data, it is hard to visualize a correlation among different tests.

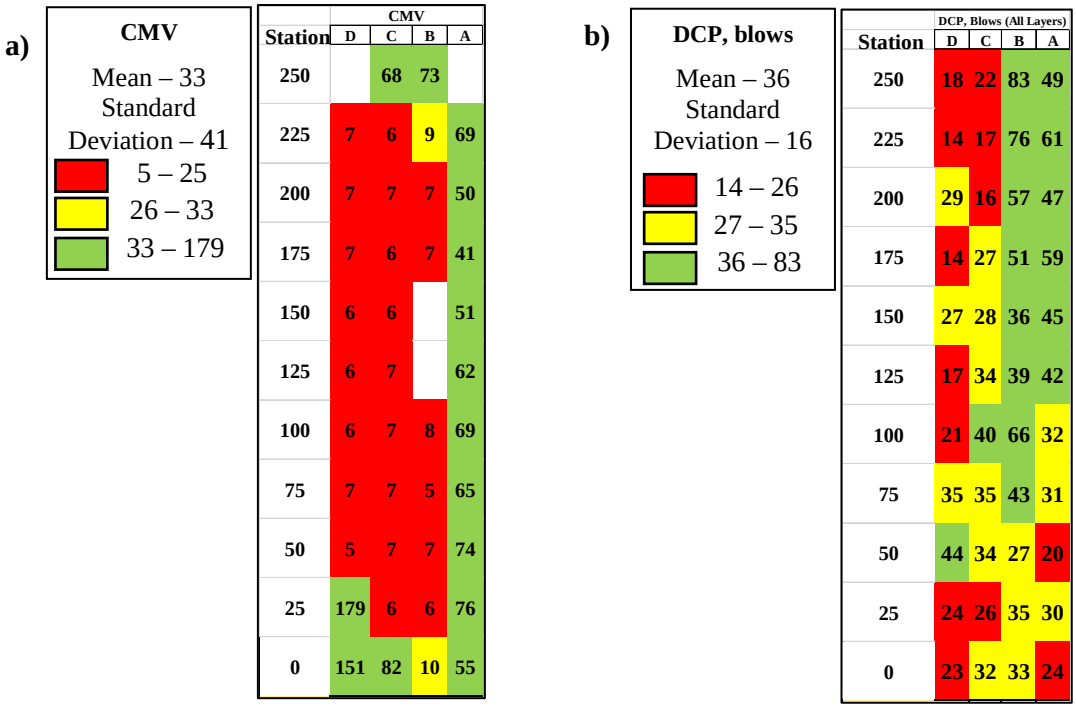

Figure H.9 – Spatial Variation Comparison between (a) CMV and (b) Number of DCP Blows to Penetrate 18 in. on LTS Layer.

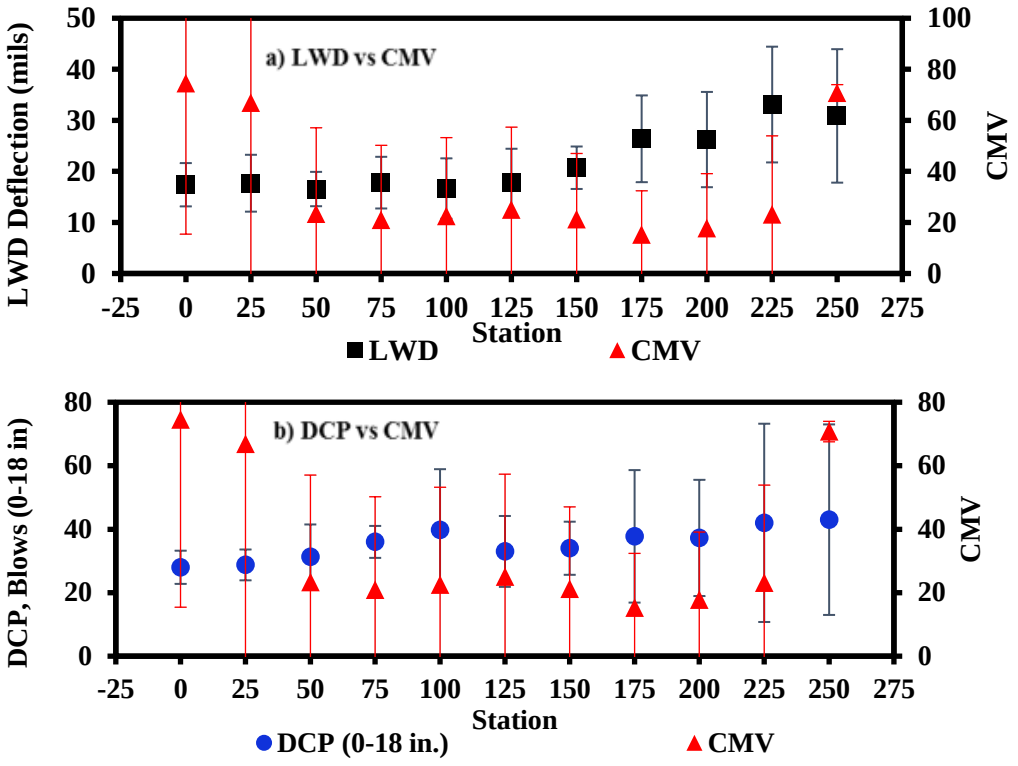

Figure H.10 – Relationship between Averaged (a) LWD Surface Deflection and (b) Number of DCP Blows to Penetrate 18 in. vs. Average CMV per Station.

Figure H.11 illustrates the spatial distribution of the moisture content of the LTS layer. The moisture content varied from 9% to 20% with an average of 14%. Since moisture content was mostly uniform throughout the test section, very minor areas were marked as red (high moisture content). No well-defined visual relationship is seen between moisture content and CMV nor with the other modulus-based measurements.

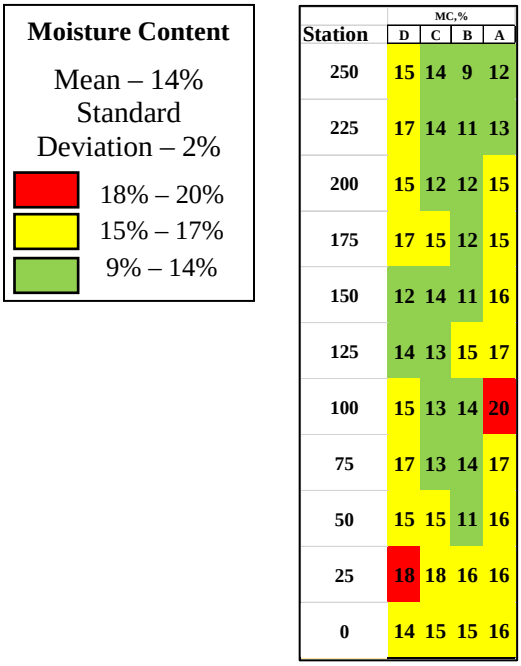

Station	MC,% D	C	B	A
250	15	14	9	12
225	17	14	11	13
200	15	12	12	15
175	17	15	12	15
150	12	14	11	16
125	14	13	15	17
100	15	13	14	20
75	17	13	14	17
50	15	15	11	16
25	18	18	16	16
0	14	15	15	16

Figure H.11 – Spatial Distribution of Moisture Content of LTS Layer.

H.4 Flexible Base

The next phase of the construction consisted of placing and compacting the 8 in. Flexible Base (FB) layer. The tested area for the flexible base was the same area evaluated for the LTS. The histogram of the mapped CMVs is shown in Figure H.12. The average CMV was 25 with a COV of 45%.

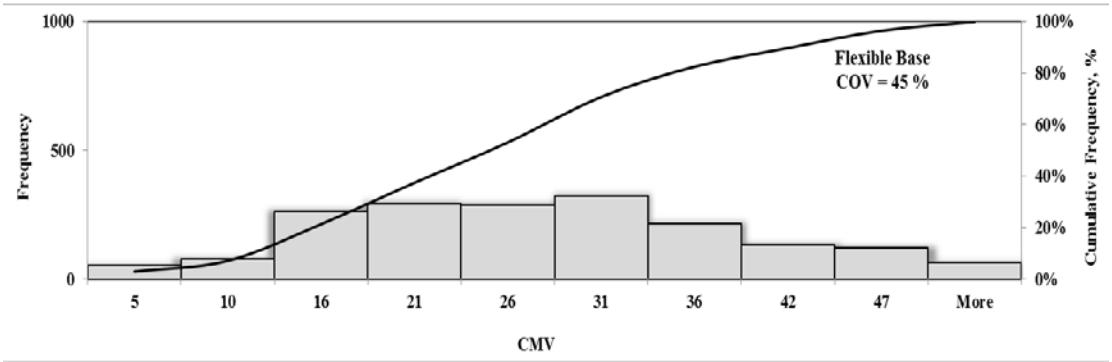

Figure H.12 – Distribution of CMV Data Collected by IC Roller during Proof-Rolling of Flexible Base Layer.

Figure H.13 shows the IC data points collected during the compaction of the layer and the rectangular buffered areas created around the spot tests locations. No data are collected along Line D.

Figure H.13 – Data Collected by IC Roller on top of Base Divided in Rectangular Buffered Areas

The spatial distribution of averaged CMVs is shown in Figure H.14a. The values found in the averaged CMV blocks ranged from a minimum of 20 to a maximum of 93. Figure H.14b illustrates the spatial distribution of the LWD modulus on top of the base layer. The LWD deflections varied from 7 mils to 44 mils with an average of 17 mils. A clear correlation was not found between the two maps. This could be the result of the difference in size of the maps due to the absence of CMV data in some blocks. The LWD map was recreated in Figure H.15 disregarding the information from the left row to reproduce a color-coded map that resembles more the CMV map. Figure H.16 shows a map with the coefficient of variation found within each rectangular buffered areas. The lack of a direct correlation between the LWD and CMV may be attributed to the high percentage of variation found in the CMV map.

a)

CMV

Mean – 38
Standard Deviation–20

20 – 28
29 – 37
38 – 93

	CMV			
Station	D	C	B	A
250		43	67	30
225		46	41	29
200		41	36	36
175		25	36	24
150		25	35	20
125		20	67	27
100		21	88	23
75		28	33	21
50		27	28	53
25		27	28	20
0		43	93	88

b)

LWD, mils

Mean – 17
Standard Deviation – 9

22 – 44
18 – 21
7 – 17

	LWD			
Station	D	C	B	A
250	18	13	12	13
225	22	16	12	12
200	44	11	18	11
175	39	15	10	9
150	28	10	9	11
125	35	13	10	13
100	37	14	12	8
75	31	14	10	13
50	29	16	8	12
25	16	7	10	16
0	34	11	14	17

Figure H.14 – Spatial Variation Comparison between (a) CMV and (b) LWD.

a)

CMV

Mean – 38
Standard
Deviation–20

20 – 28
29 – 37
38 – 93

Station	CMV D	C	B	A
250		43	67	30
225		46	41	29
200		41	36	36
175		25	36	24
150		25	35	20
125		20	67	27
100		21	88	23
75		28	33	21
50		27	28	53
25		27	28	20
0		43	93	88

b)

LWD, mils

Mean – 12
Standard
Deviation – 3

16 – 18
12 – 15
7 – 11

Station	LWD D	C	B	A
250		13	12	13
225		16	12	12
200		11	18	11
175		15	10	9
150		10	9	11
125		13	10	13
100		14	12	8
75		14	10	13
50		16	8	12
25		7	10	16
0		11	14	17

Figure H.15 – Spatial Variation Comparison between (a) CMV and (b) Recreated LWD.

CMV(COV,%)

Mean – 51
Standard
Deviation – 29

36 – 144
25 – 35
18 – 25

Station	COV, % D	C	B	A
250		18	95	86
225		18	27	53
200		98	19	29
175		62	32	46
150		48	29	39
125		58	94	19
100		70	94	29
75		56	32	36
50		42	30	50
25		31	22	45
0		144	66	79

Figure H.16 – Spatial Variation of Coefficient of Variation of CMVs within each Buffered Area.

A comparison between the LWD modulus and the CMV data at different stations is illustrated in Figure H.17. A visual correlation cannot be easily observed in this figure given the uncertainty due to high COVs.

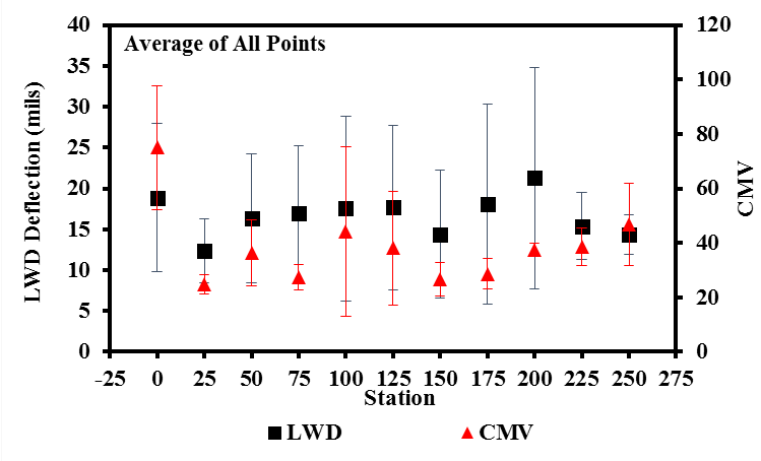

Figure H.17 – Relationship between Averaged LWD Surface Deflection and vs. Average CMV per Station.

Figure H.18 illustrates the spatial distribution of the moisture content of the base layer. The percentage of moisture content varied from 2% to 5% with an average of 4% and a COV of 14%.

CMV

Mean – 14
Standard Deviation – 1
18 – 20
15 – 17
9 – 14

Station	MC,%			
	D	C	B	A
250	5	8	6	7
225	4	7	7	8
200	5	8	7	8
175	5	8	8	9
150	5	8	5	7
125	8	9	6	7
100	6	7	5	8
75	7	7	6	9
50	7	8	8	9
25	7	8	8	9
0	8	7	7	8

Figure H.18 – Spatial Distribution of Moisture Content of FB Layer.

APPENDIX I - TEST SITE ALONG US 77 NEAR VICTORIA, TX

I.1 Introduction

A section of north-bound frontage road of US 77 in Victoria, Texas was used for field evaluation. Figure I.1 shows an aerial view of the of the test section alongside a map with the location of the test section within the Victoria area. A layer consisting of 12 in. cement-treated base (CTB) covered with a tack coat was evaluated. The UTEP research team's field testing took place on February 1, 2017, 24 hours after cement treatment.

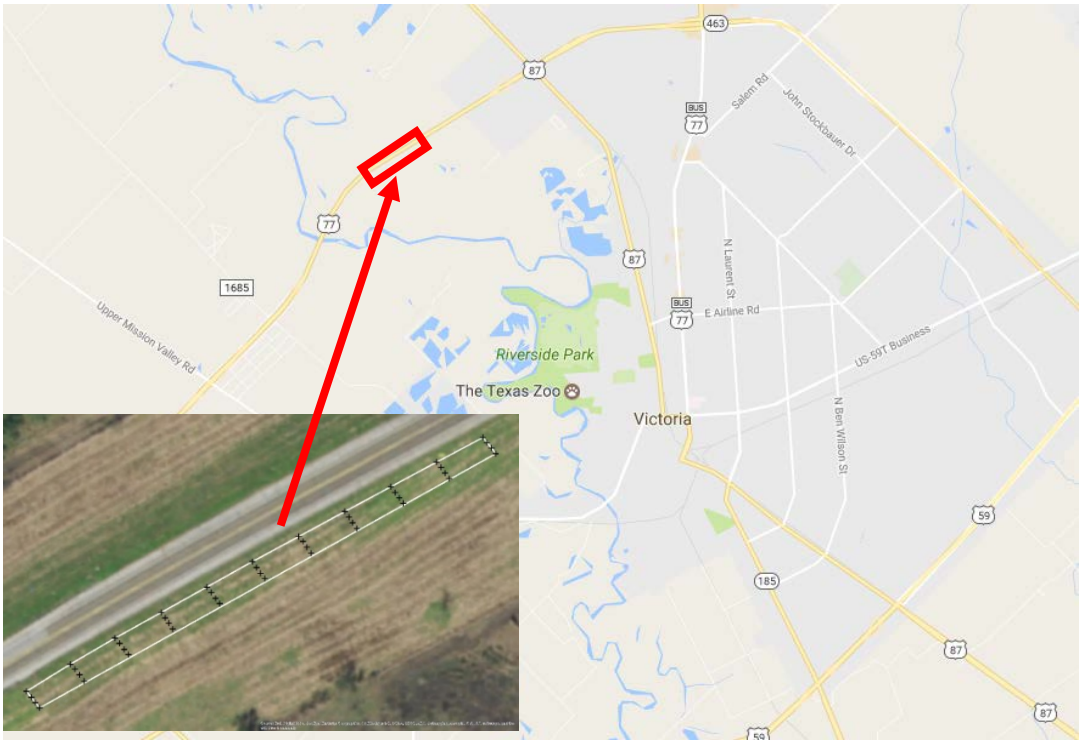

Figure I.1 – Location of Field Evaluation Site on US 77 in Victoria, TX.

I.2 Field Testing Program

A 500-ft long by 21-ft wide section was considered in this study. The location of the spot tests was selected over a grid consisting of 44 points divided in four columns of 11 points. The grid was designed with a spacing of 50 ft longitudinally, and a spacing of 7 ft laterally as shown in Figure I.2. LWD testing was performed on all 44 points on the grid. FWD testing was performed every 25 ft in between lines C and D. The cement treated base was mapped using a padfoot HAMM roller, shown in Figure I.3, equipped with the UTEP DAQ system.

The histogram of the mapped CMVs is summarized in Figure I.4. The average CMV value was 86 with a COV of 35%. Though not shown after data reduction and quality control for generating maps, acquired CMVs had variability that can be attributed to the use of padfoot drum used for testing. Based on the spacing between the locations of the LWD spots, blocks were created around each LWD spot location. IC data points found within these blocks were averaged to obtain one IC measurement to represent that block. Using the IC data results and the LWD moduli color-coded maps were created using the color-coded criteria described in Table 5.6.

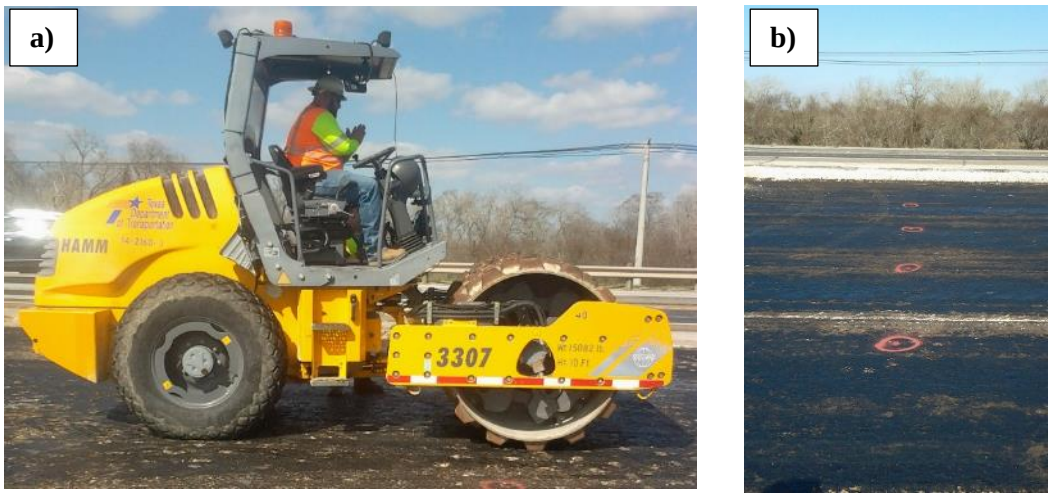

Figure I.2 – (a) Instrumented Pad-foot Roller on Test Site and (b) Spot Tests

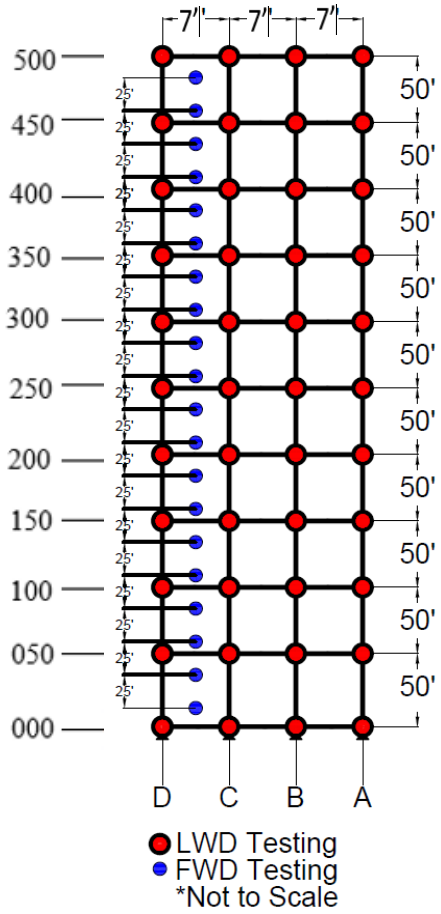

Figure I.3 – Schematic of Test Section.

The spatial distribution of rectangular buffer averaged CMVs and LWD deflections is available in Figure I.5a and I.5c, respectively. The distribution of COVs of the roller CMVs within each of the blocks is shown in Figure I.5b. The values found in the averaged CMV blocks ranged from a minimum of 56 to a maximum of 130. The LWD deflections 3.2 to 11.9 mils, with an average of 6.0 mils.

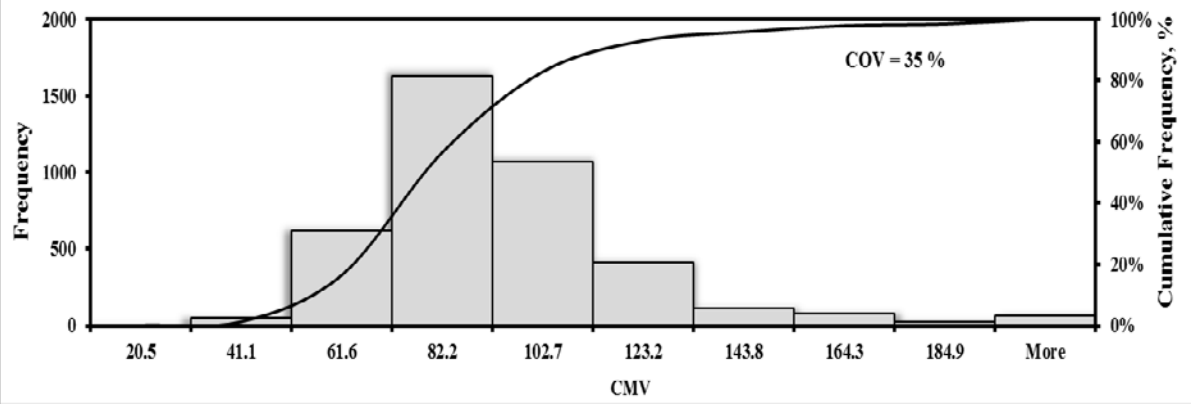

Figure I.4 – Distribution of CMV Collected by IC Roller during Proof-Rolling of CTB Layer.

Station (ft)	D	C	B	A
500	121	130	97	104
450	101	117	81	68
400	99	92	83	57
350	85	76	80	93
300	89	79	86	101
250	90	79	79	102
200	80	65	56	69
150	80	63	65	69
100	91	80	67	59
50	83	86	67	78
0	122	99	75	104

a) CMV

Average – 85
Standard Deviation – 17
56 – 63
64 – 84
85 – 130

D	C	B	A
35	42	45	58
10	12	33	16
18	14	21	17
15	12	13	13
16	17	11	17
16	16	10	16
10	13	9	9
10	12	8	13
8	11	11	17
8	13	41	17
42	35	57	46

b) COV of CMVs, %

Average – 20
> 35%
25%- 35%
≤ 25%

D	C	B	A
10.2	8.3	5.7	5.2
9.4	7.2	6.0	3.2
11.9	6.0	4.0	3.6
3.5	5.3	3.4	6.1
4.0	10.0	3.9	4.9
3.8	6.9	6.6	7.7
5.6	5.9	5.4	5.1
5.2	8.0	5.4	4.7
4.1	6.9	4.4	4.6
6.1	4.7	6.9	8.3
5.8	4.5	6.0	7.8

c) LWD, ksi

Average – 6.0
Standard Deviation – 2.0
7.5 – 11.9
6.1 – 7.4
3.2 – 6.0

Figure I.5 – Spatial Variation Comparison between (a) CMV, (b) Coefficient of Variation of CMVs and (c) LWD.

The mapping of coefficient of variation of CMVs shows that IC mapping was generally uniform, with exception at the beginning and the end parts of the test section. This is attributed to stop and go operation

of the roller toward the beginning and end of the section. However, no visual comparison can be provided by both CMV and LWD maps in Figure I.5.

Similarly, no direct relationship can be seen between the LWD deflection and CMVs as obtained from averaging the measurements at each buffer areas, as shown in Figure I.6. A comparison between the CMV data and the LWD modulus at different stations is illustrated in Figure I.7. Some similarity in the trend may be observed throughout the test section with the exception of the beginning and the end parts of the section, probably due to the same reason explained before.

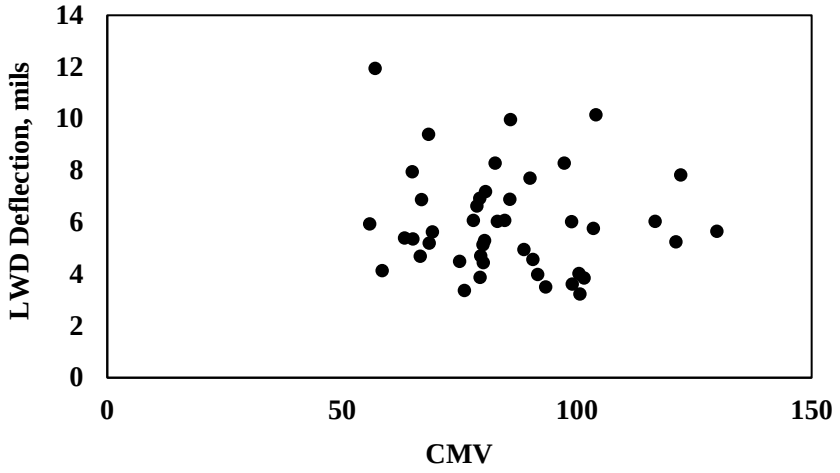

Figure I.6 – Relationship between LWD Deflections and CMVs.

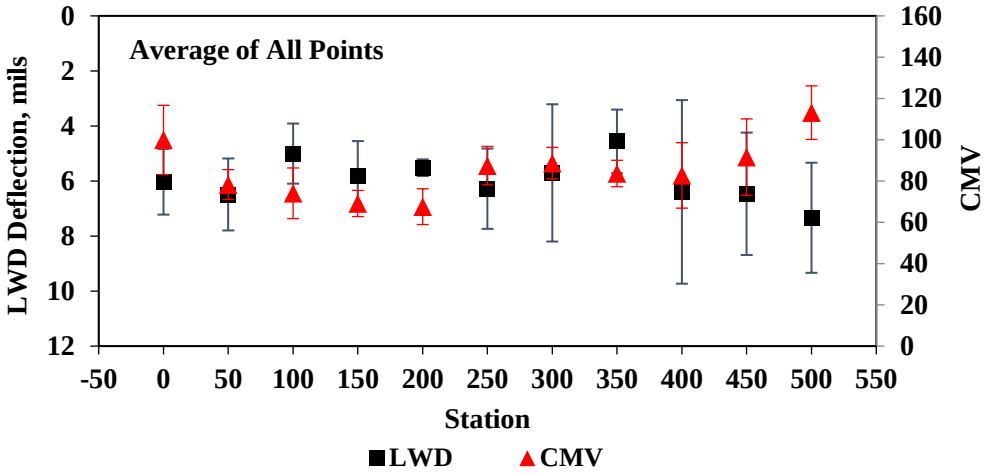

Figure I.7 – Relationship between Averaged LWD Modulus vs CMV.

Figure I.8 shows the spatial distribution of the FWD deflections directly under the load, as well as the LWD deflections and CMV measurements, matching the FWD evaluated cells for better comparison. Since FWD occurred between lines C and D, measurements for LWD and CMVs were averaged to represent a combined single C-D measurement. Color criteria for FWD follows the class breaks used for LWD, described in Table 5.6. No visual relationship is seen among the three measuring devices. FWD deflections do not reflect a clear correlation with the CMV and LWD deflection measurements, as shown in Figure I.9. This can be attributed to testing with FWD occurred a few days later than proof-mapping and testing with LWD.

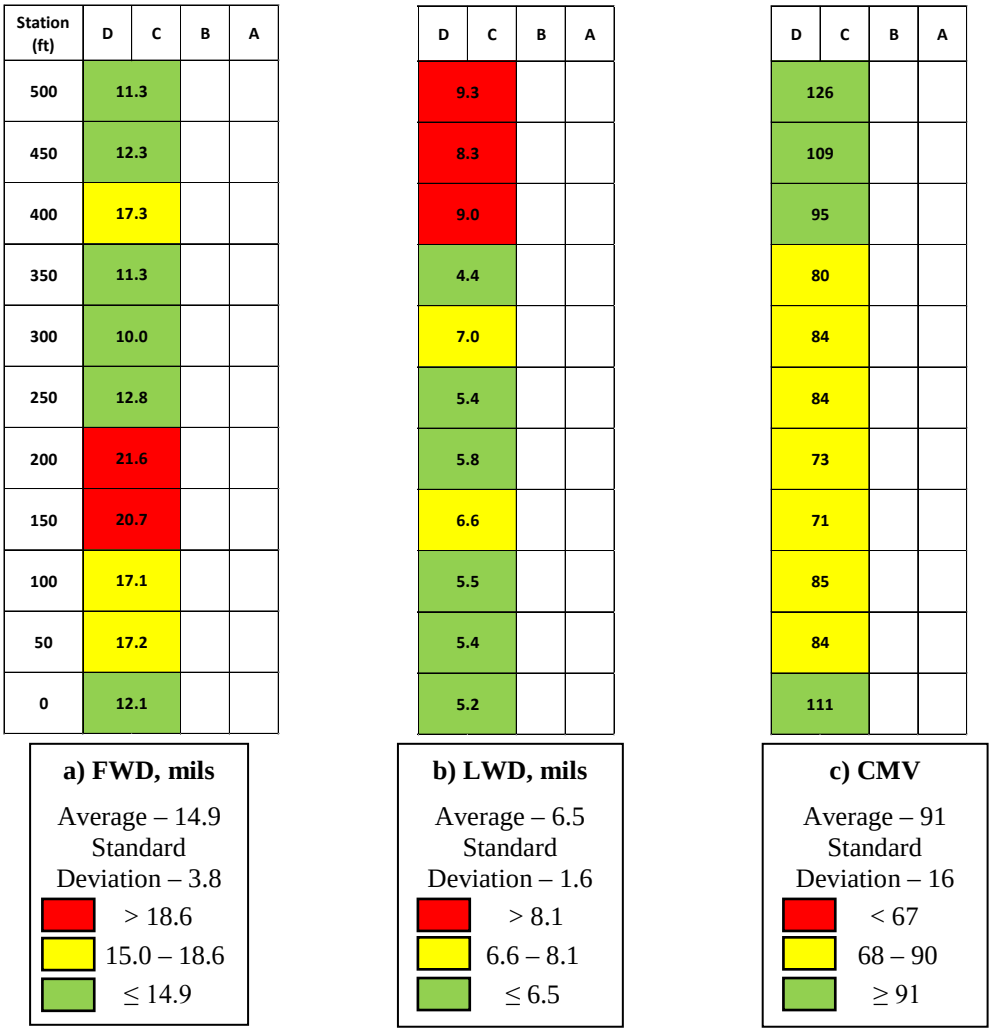

Figure I.8 – Spatial Variation of (a) FWD Deflection under the Load, (b) LWD Deflection and (c) CMV Measurements at the Same Spot Locations of FWD Measurements.

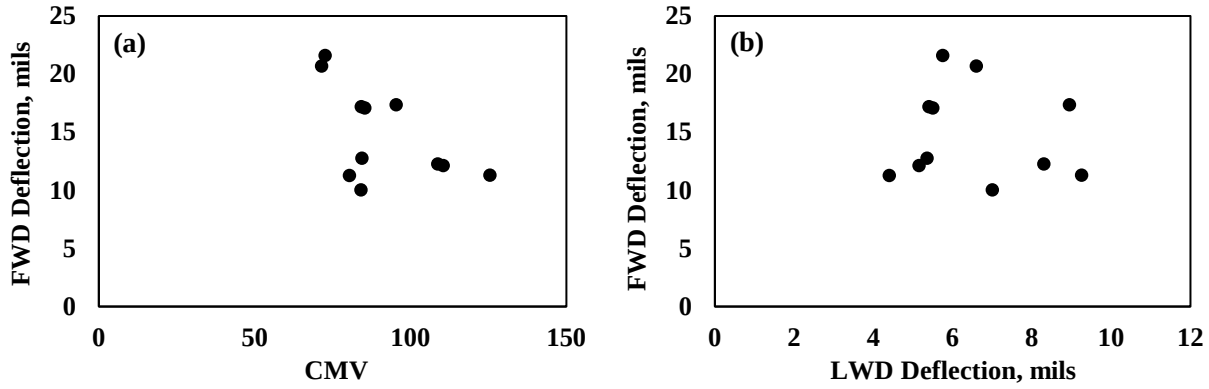

Figure I.9 – Relationship between FWD Deflection Measurements Directly under Load to (a) CMV and (b) LWD Deflection.

No better prediction to minimize the mis-predicted areas by the CMV map was obtained after the implementation of the optimization algorithm, as shown in Figure I.1, where the best combination is already being used by Table 5.6, i.e. red color defined for CMV < 75% of average CMV and LWD deflections > 125% of average LWD deflections. Mapping of the optimized class break is already shown in Figure I.5. For this site, 75% of the red areas were mis-predicted. Similar to other sites that are uniform and a comprised of stiff materials (flexible bases and cement-treated bases), no improvement is attained by lowering the class break for identifying less stiff (red) areas.

Table I.1 – Percentage of Misestimated Roller Measurements (Rectangular Buffered Areas CMVs) with Respect to LWD Measurements Based on Different Percentages of Average Measurements for the Identification of Less-Stiff (Red) Areas in Site 4

Percentage of IC Roller Misestimated Areas		Less-Stiff (Red) Area Above % of Average LWD Deflection						
		110	**115**	**120**	**125**	**130**	**135**	**140**
Less-Stiff (Red) Area Below % of Average CMV	**90**	85	85	92	92	92	100	100
	85	82	82	91	91	91	100	100
	80	78	78	89	89	89	100	100
	75	75	75	75	75	75	100	100
	70	100	100	100	100	100	100	100
	65	-	-	-	-	-	-	-
	60	-	-	-	-	-	-	-

APPENDIX J - FIELD EVALUATION OF CEMENT TREATED SALVAGED BASE AND RAP AT SH 149 IN CARTHAGE, TX

J.1 Introduction

Field evaluation was performed on a 200-ft long section of a reconstruction of State Highway 149 on September 14 and 15, 2017, near State Highway 315 interchange, in Carthage, Texas, as shown in Figure J.1. The pavement structure consists of a 6-in. cement treated salvaged base and reclaimed asphalt (RAP) on top of embankment, as shown in Figure J.2. This layer served as subgrade to be placed beneath concrete pavement (CPCD). Mapping was performed an hour after compaction and cement treatment and 24 hours after compaction and cement treatment. Deflection-based testing was conducted using the Light-Weight Deflectometer (LWD) on the test section 24 hours after compaction and cement treatment. Testing with LWD an hour after compaction was not feasible due to continuous presence of machinery in the test site. For this reason, results are shown for the IC Measurements on the test section 24 hours after compaction.

Figure J.1 – (a) Location and (b) Close-up of Field Evaluation Site on SH 149 in Carthage, TX.

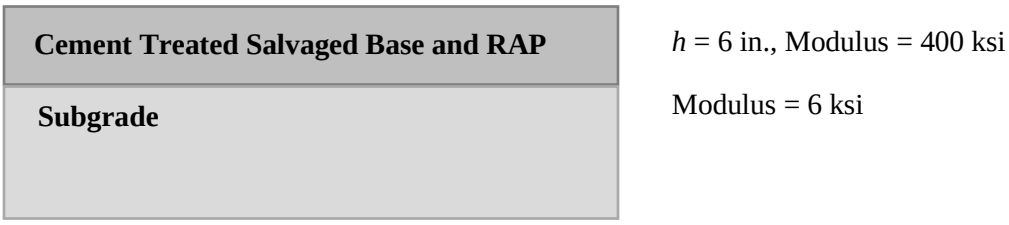

Figure J.2 – Pavement Structure and Design Parameters for SH 149 in Carthage, TX.

J.2 Field Testing Program

Proof-mapping and nondestructive modulus-based testing was performed on a 200 ft.-long and 28 ft.-wide section. The locations of spots for testing were selected to conform a grid consisting of 36 points divided in 4 rows. Each row along a roller line pass consisted of 9 points. The grid was designed to have spot test every 25 ft along a roller line pass, and a line spacing of 7 ft, as shown in Figure J.3.

Light Weight Deflectometer (LWD) testing was performed on all 36 points on the grid 24 hours after cement-stabilization. At each location, two consecutive LWD drops were performed and their surface displacement measurements were averaged. In those cases where the consecutive measurements exceeded 10% of change in deflection, a third LWD measurement was recorded.

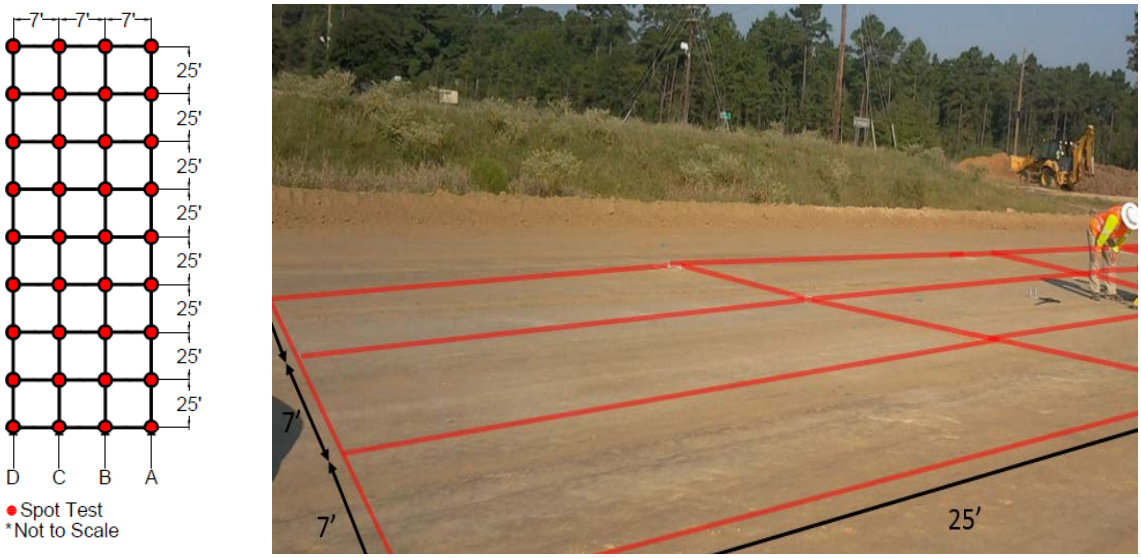

Figure J.3 – (a) Schematic of the Test Section, (b) Site View with Grid Superimposed over Test Section.

To evaluate the compaction uniformity through identification of soft spots and ensuring the complete coverage of the compacted section, proof rolling was implemented at the site using a smooth roller. UTEP's data acquisition system was employed for the proof-mapping during this field evaluation. The system consists of one or two more accelerometers mounted inside the drums to capture the vibration of the drum, a data acquisition system, a GPS antenna/receiver, a power supply and a laptop computer to monitor the data collection process.

J.3 Cement-Treated Salvaged Base and RAP

The cement-treated base layer was mapped using a smooth roller equipped with a data acquisition system. The layer was mapped one hour after the cement treatment and the day after the stabilization occurred. Figure J.4a shows the four roller passes along the test section with the superimposed rectangular buffer areas. The number of IC measurements within each rectangular buffer is shown in Figure J.4b.

The average CMV value for the map one hour after cement treatment was 50 with a coefficient of variation of 65%. The average CMV value increased to 72 with a coefficient of variation of 45% 24 hours after. A coefficient of 100 was used for the calculation of CMV.

Based on the 25 by 7 ft spacing between the locations of the LWD spots, rectangular buffered areas were created around each LWD spot location as shown in Figure J.5. ICMV data points found within these blocks were averaged to obtain a unique ICMV to represent that block. Color-coded maps, shown in Figure A.6, were created using the criterion shown in Table J.1 to compare the values obtained in each block for the IC data and the LWD deflections. Both color-coded maps in Figure J.6 agree on displaying line C to be less-stiff areas.

Table J.1 – Criterion for Color-Coded Maps

Color	*Criterion for ICMV*	*Criterion for LWD Deflection*	*Criterion of Coefficient of Variation*
Red	< 75% Mean	> 120% Mean	≤ 25%
Yellow	75% Mean – Mean	Mean – 120% Mean	25% – 35%
Green	≥ Mean	< Mean	> 35%

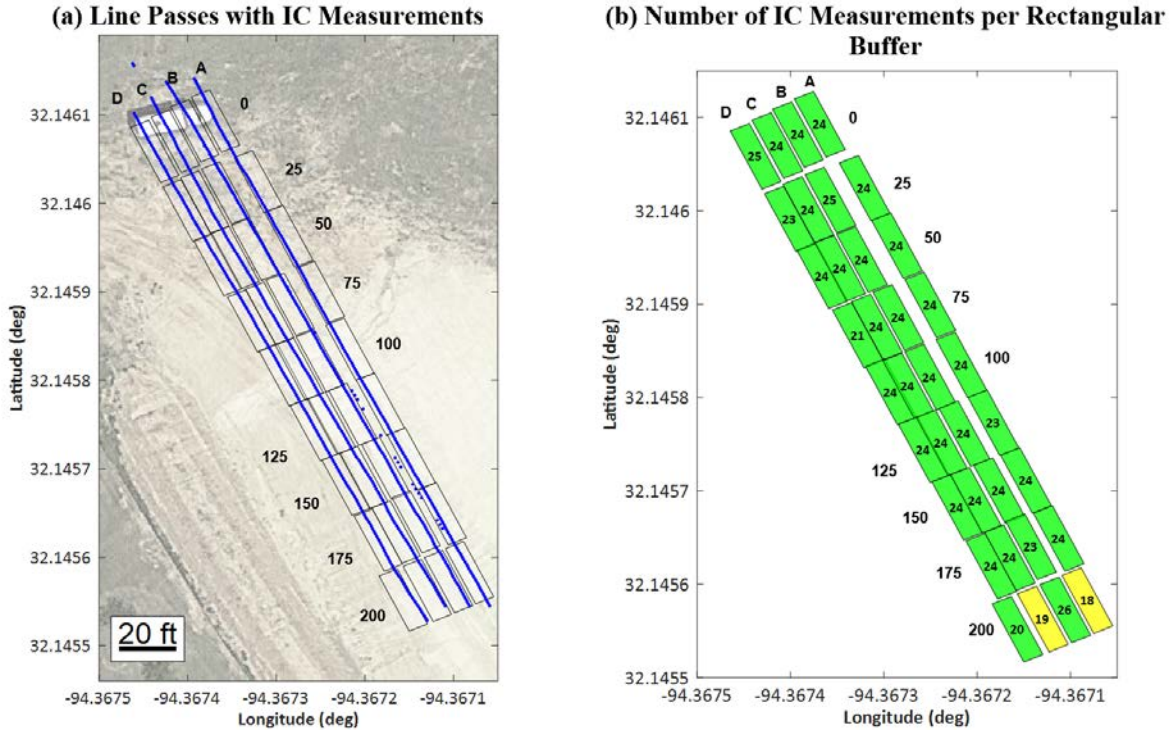

Figure J.4 – (a) Data Collected by IC Roller in Rectangular Buffered Areas and (b) Number of IC Measurement Values within Each Buffer Area.

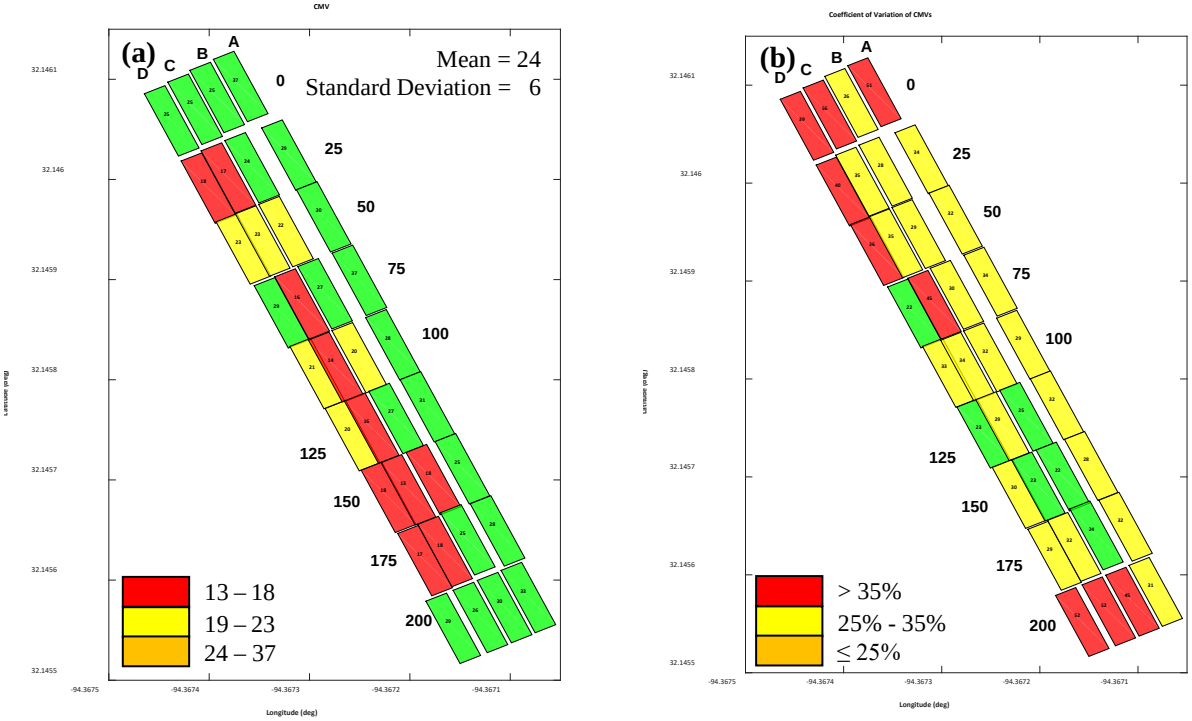

Figure J.5 – Spatial Variation Comparison between (a) IC Roller CMVs and (b) their Corresponding Coefficient of Variation of CMVs 24 Hours after Cement Treatment.

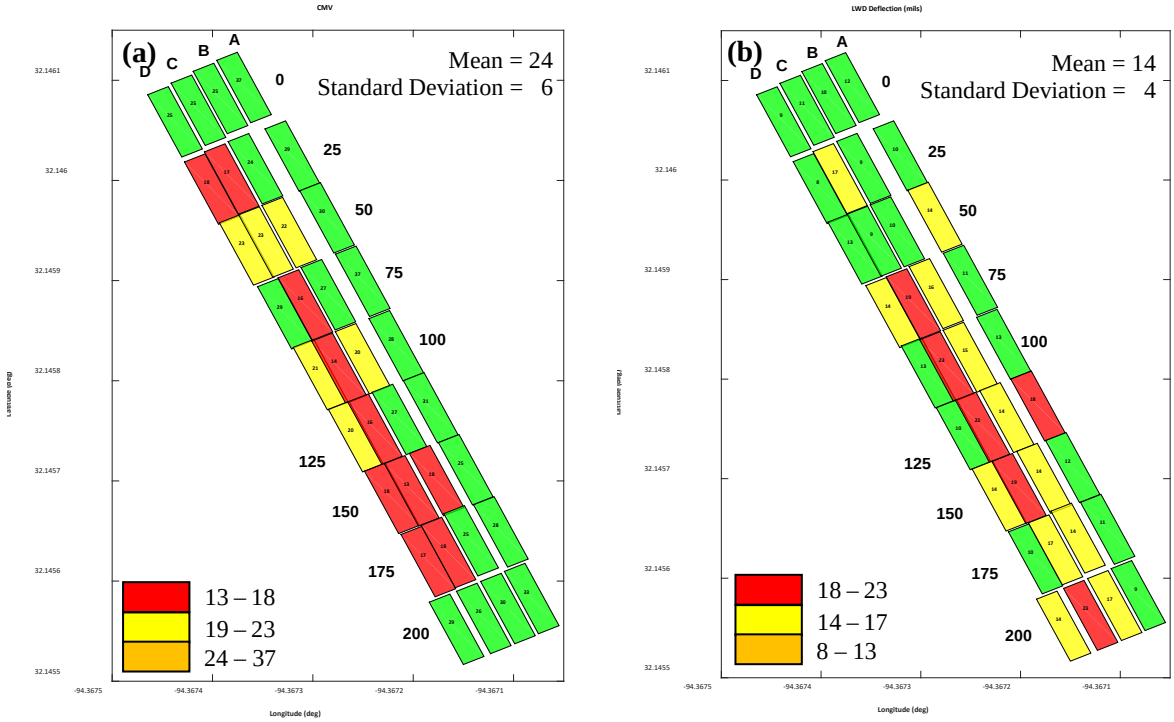

Figure J.6 – Spatial Variation Comparison between (a) IC Roller CMV and (b) LWD Deflections 24 Hours after Cement Treatment.

APPENDIX K - FIELD EVALUATION OF TEST SITE ALONG SH 349 NEAR LAMESA, TX

K.1 Introduction

Field evaluation was performed on a 250-ft long section of a lane widening of State Highway 349, next to FM 2052 intersection, on April 3 and 17, 2018, near Lamesa, Texas, as shown in Figure K.1. The pavement structure consists of a 6 in. flexible base on top of an 18-in. recycled asphalt and base material subgrade on top of embankment, as shown in Figure K.2. Proof-mapping and deflection-based testing was conducted using the Dynamic Cone Penetrometer (DCP) and the Light-Weight Deflectometer (LWD) on the subgrade and using the LWD on the base layer.

Figure K.1 – (a) Location and (b) Close-up of Test Site along SH 349 near Lamesa, TX.

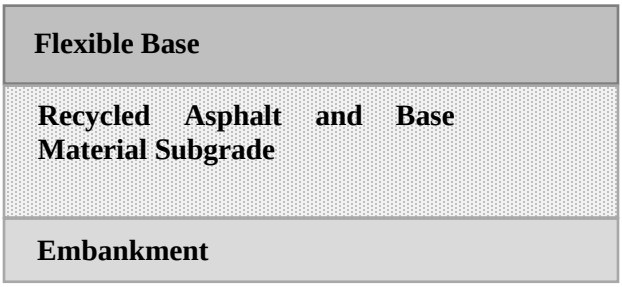

Figure K.2 – Pavement Structure and Design Parameters for SH 349 near Lamesa, TX.

K.2 Field Testing Program

Proof-mapping and nondestructive modulus-based testing was performed on a 250 ft.-long and 24 ft.-wide section. The locations of spots for testing were selected to conform a grid consisting of 44 points divided in 4 rows. Each row along a roller line pass consisted of 11 points. The grid was designed to have spot test every 25 ft along a roller line pass, and a line spacing of 6 ft, as shown in Figure K.3.

LWD testing was performed on all 44 points for both subgrade and flexible base. At each location, two consecutive LWD drops were performed and their surface displacement measurements were averaged. In those cases where the consecutive measurements exceeded 10% of change in deflection, a third LWD measurement was recorded. Due to the stiff recycled material used for subgrade, DCP testing was conducted every 50 ft.

Proof rolling was implemented at the site using a smooth roller using UTEP's data acquisition system to evaluate compaction uniformity. Figure K.3 shows the test section, the instrumentation of the roller compactor with UTEP developed data acquisition system and LWD spot testing conducted at the site.

Figure K.3 – (a) Test Section, (b) Instrumentation of Roller Compactor with Data Acquisition System and Recommendations Provided to Roller Operator and (c) Deflection-Based Spot Testing using the LWD.

K.3 Subgrade

The subgrade was mapped using 4 roller passes, as shown in Figure K.4a. The number of IC measurements within each rectangular buffer, shown in Figure K.4b, indicate the roller passed through all rectangular buffer areas with the exception of a single cell, where the roller nearly missed the buffer area by a few inches. Figure K.5 shows the measured CMVs per buffer area, with their respective coefficient of variation. With exception of two cells, where high variability in the measurements existed, the test section proved to be highly uniform, as no cells were marked as less stiff (in red) by the mapping of CMVs.

Figure K.6 compares the CMV mapping to LWD deflection, the number of DCP blows to penetrate 16 in. and the moisture content of samples retrieved at the site. Though generally uniform, the test section indicates that somewhat less-stiff areas lie along line A, which is consistent with the mapping of the LWD and DCP measurements. The LWD low measured deflections and the numerous blows to penetrate the subgrade indicate a very stiff material consistent to the largely granular material present in the layer.

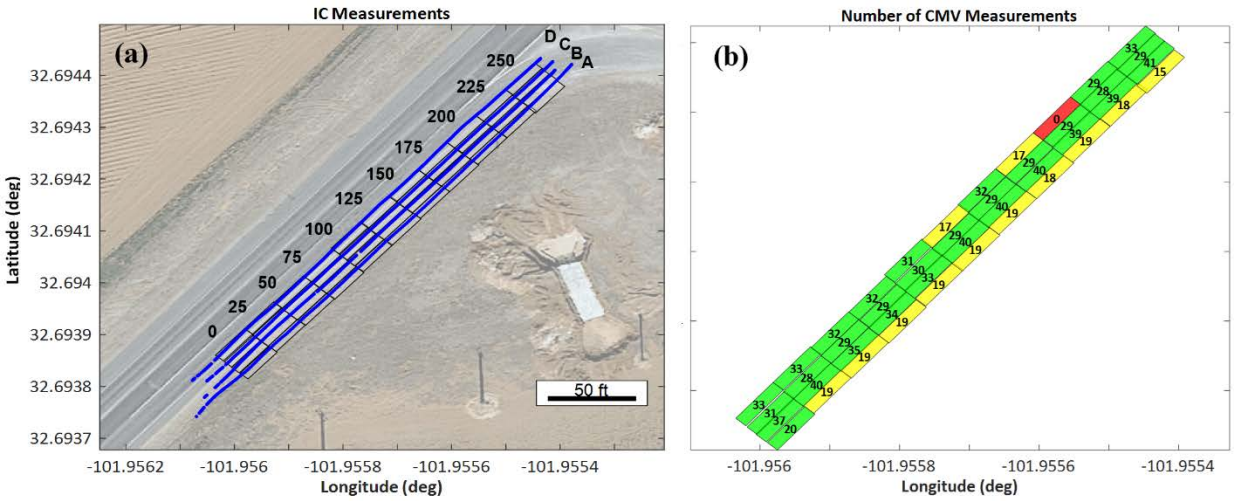

Figure K.4 – (a) Data Collected by IC Roller in Rectangular Buffered Areas and (b) Number of IC Measurement Values within Each Buffer Area.

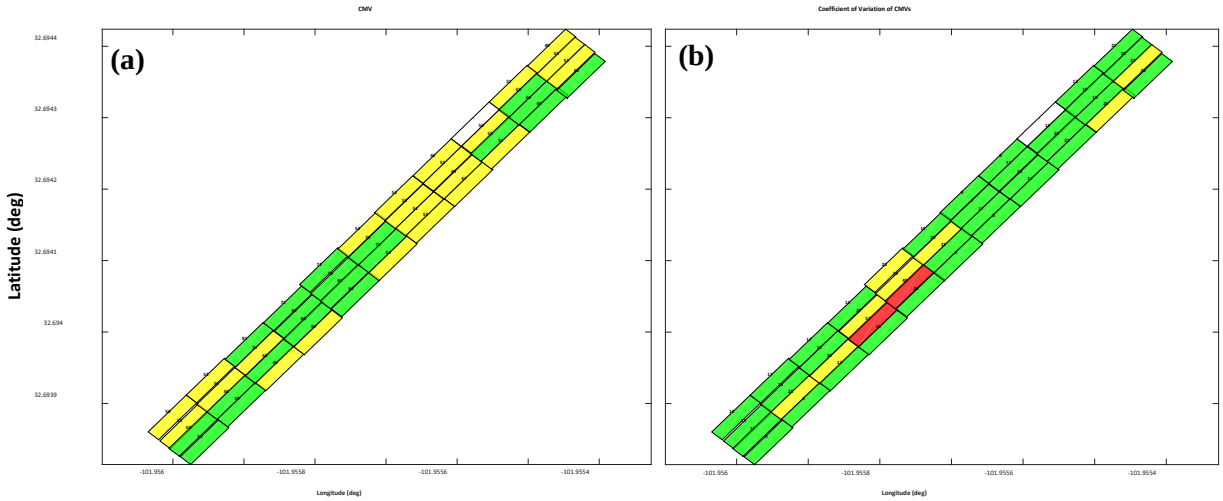

Figure K.5 – Spatial Variation Comparison between (a) IC Roller CMVs and (b) their Corresponding Coefficient of Variation.

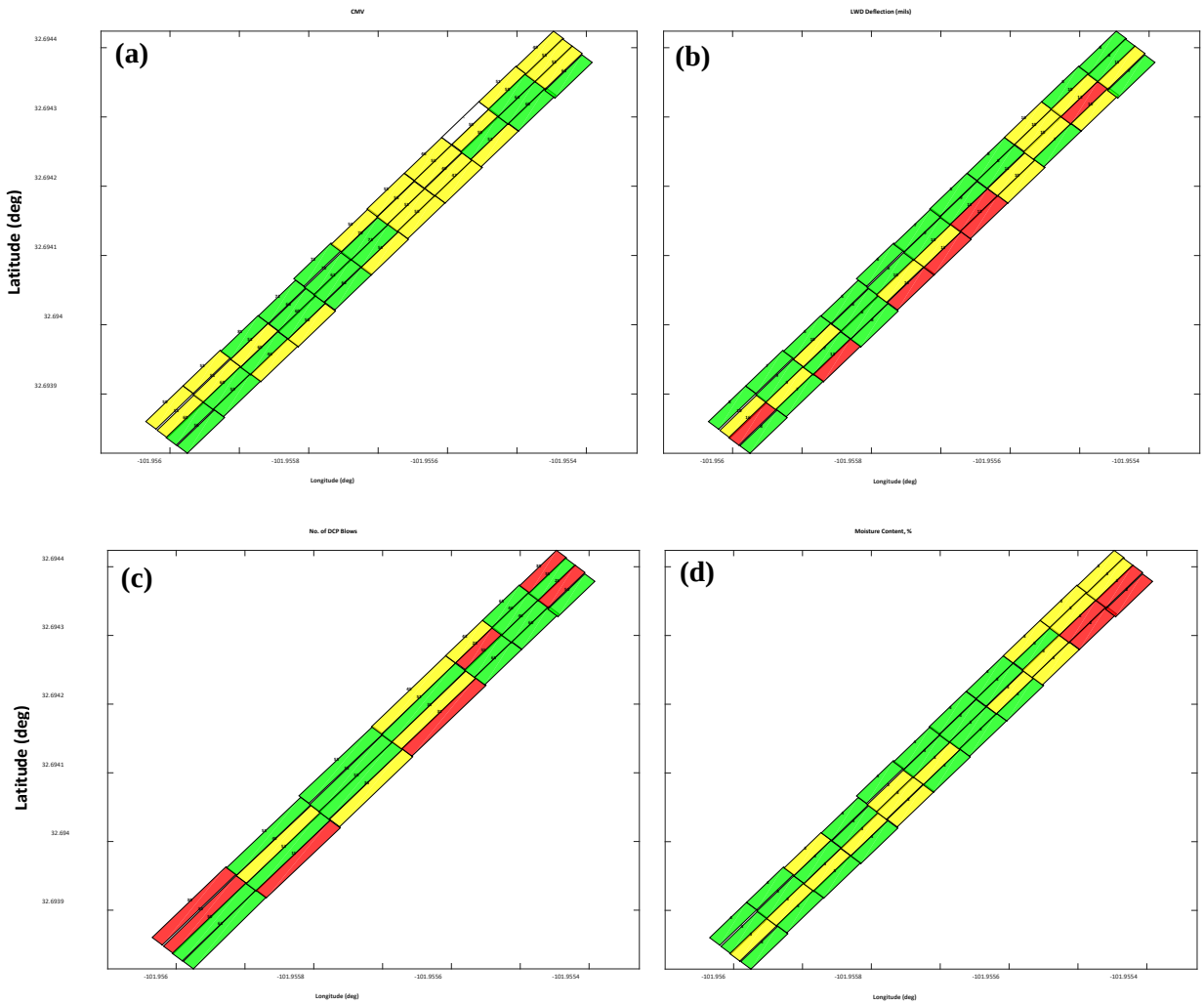

Figure K.6 – Spatial Variation Comparison between (a) IC Roller CMVs, (b) Deflection Imparted by the LWD, (c) Number of DCP Blows to Penetrate 16 in., and (d) Moisture Content.

K.4 Flexible Base

Similar to subgrade, the flexible base was mapped using 4 roller passes, as shown in Figure K.7a. The number of IC measurements is shown in Figure K.7b. Figure K.8 shows the measured CMVs per buffer area measured on top of the base, with their respective coefficient of variation. The mapping of coefficient of variation of CMVs indicates measurements values were uniform within buffer areas; however, the mapping of CMVs expose less stiff areas (in red) mostly along line A. This is somewhat consistent to the mapping of the LWD deflection measurements, shown in Figure K.9. Larger LWD deflection measurements were documented in the base layer when compared to the subgrade (shown in Figure K.6b). Likewise, CMVs for the subgrade (Figure K.6a) are higher in magnitude than those measured for the base layer. A coefficient of 100 has been used for calculation of CMV for both layers. This can be attributed the stiffer conditions of the material used for subgrade.

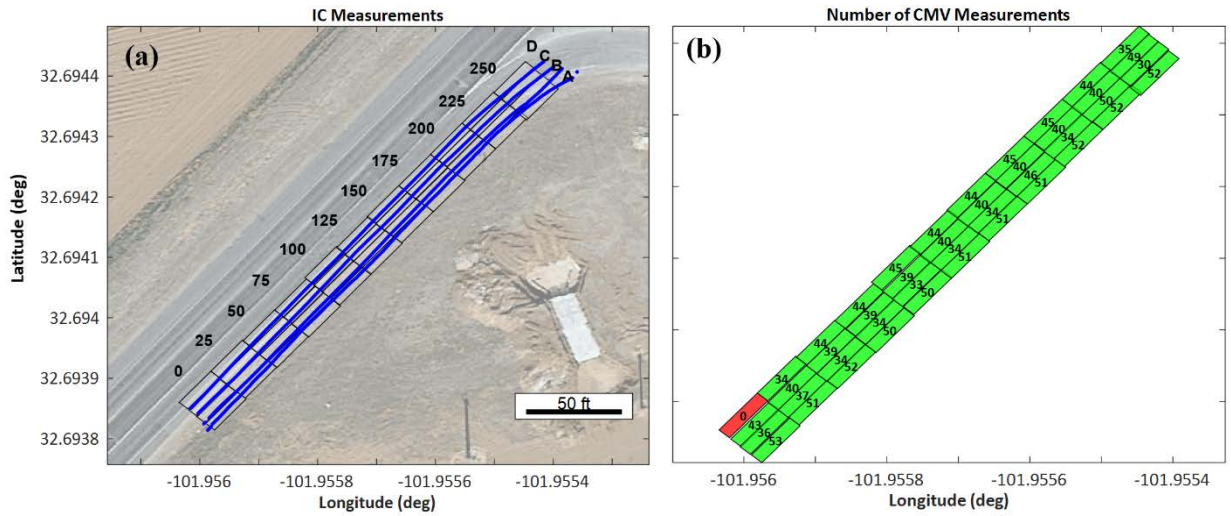

Figure K.7 – (a) Data Collected by IC Roller in Rectangular Buffered Areas and (b) Number of IC Measurement Values within Each Buffer Area.

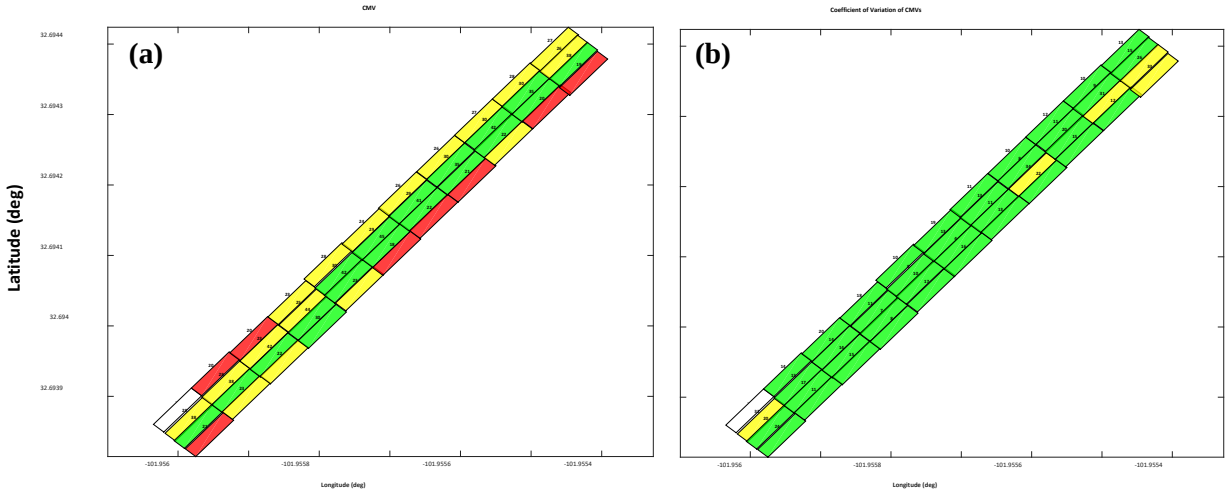

Figure K.8 – Spatial Variation Comparison between (a) IC Roller CMVs and (b) their Corresponding Coefficient of Variation.

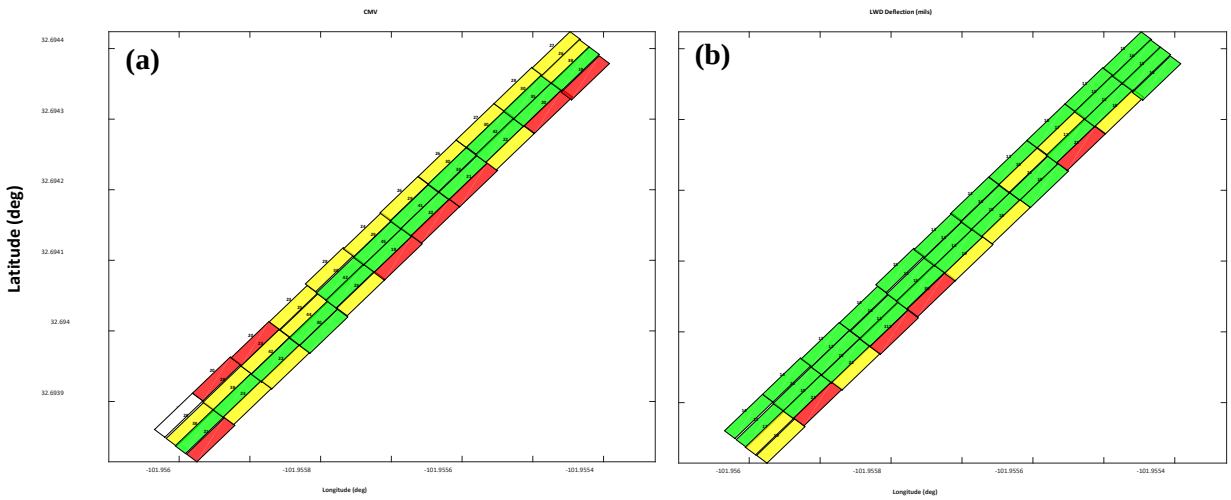

Figure K.9 – Spatial Variation Comparison between (a) IC Roller CMVs and (b) Deflection Imparted by the LWD.

APPENDIX L - FIELD EVALUATION OF TEST SITE ALONG FM 133 NEAR COTULLA, TX

L.1 Introduction

Field evaluation was performed on a 250-ft long section of a reconstruction of Farm-to-Market 133 on April 18 and May 8, 2018, in Dimmit County, near Cotulla, Texas, as shown in Figure L.1. The pavement structure consists of an 8 in. cement treated base with 3% cement, on top of a 6-in. lime treated subgrade, as shown in Figure L.2. Proof-mapping and deflection-based testing was conducted using the Dynamic Cone Penetrometer (DCP) and the Light-Weight Deflectometer (LWD) on the subgrade and using the LWD on the base layer. Figure L.3 shows the test site while arrangements were in preparation to proof-map the base layer.

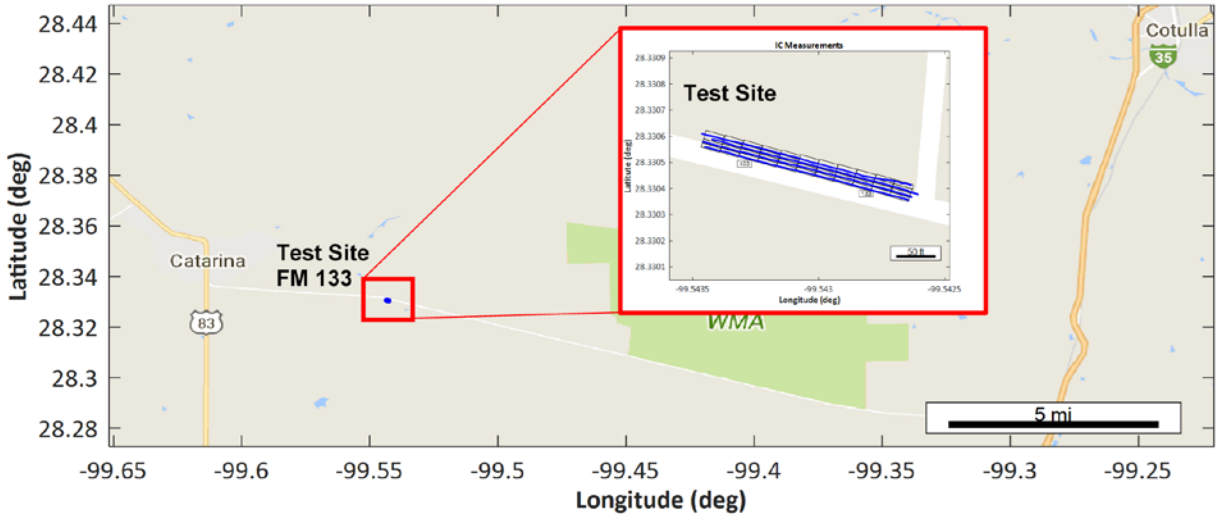

Figure L.1 – (a) Location and Close-up of Test Site along FM 133 in Dimmit County.

Cement Treated Base	*h* = 8 in., Modulus = 400 ksi
Lime Treated Subgrade	*h* = 6 in., Modulus = 10 ksi
Embankment	

Figure L.2 – Pavement Structure and Design Parameters for FM 133 in Dimmit County.

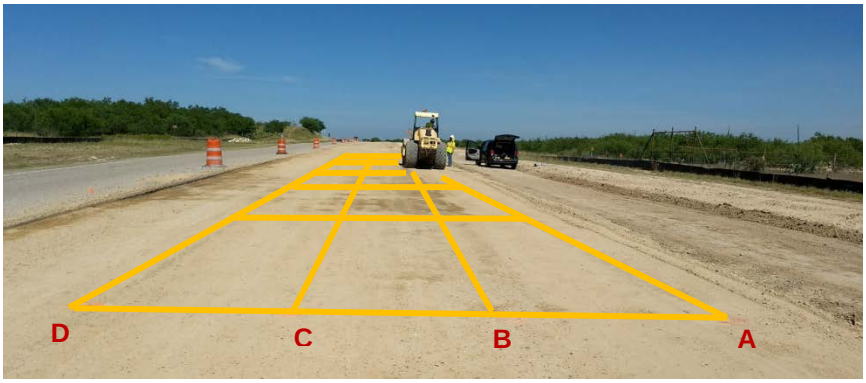

Figure L.3 – Proof-Mapping of Base on Test Site on FM 133 in Dimmit County.

L.2 Subgrade

The subgrade was mapped using 4 roller passes, as shown in Figure L.4a. The number of IC measurements within each rectangular buffer, shown in Figure L.4b. Figure L.5 shows the mapped CMVs per buffer area obtained after proof-mapping the subgrade and the corresponding coefficient of variation of the measured CMVs per buffer area. The latter figure show that ICMVs were generally uniform within the buffer areas.

Figure L.6 shows the mapping of moisture content of samples retrieved at the site, while Figure L.7 shows the mapping of LWD deflection measurements and the number of DCP blows to penetrate 16 in. Line A is shown to be less stiff by the IC proof-mapping; however, mapping of LWD deflection and DCP blows show other areas of the test section as less-stiff .

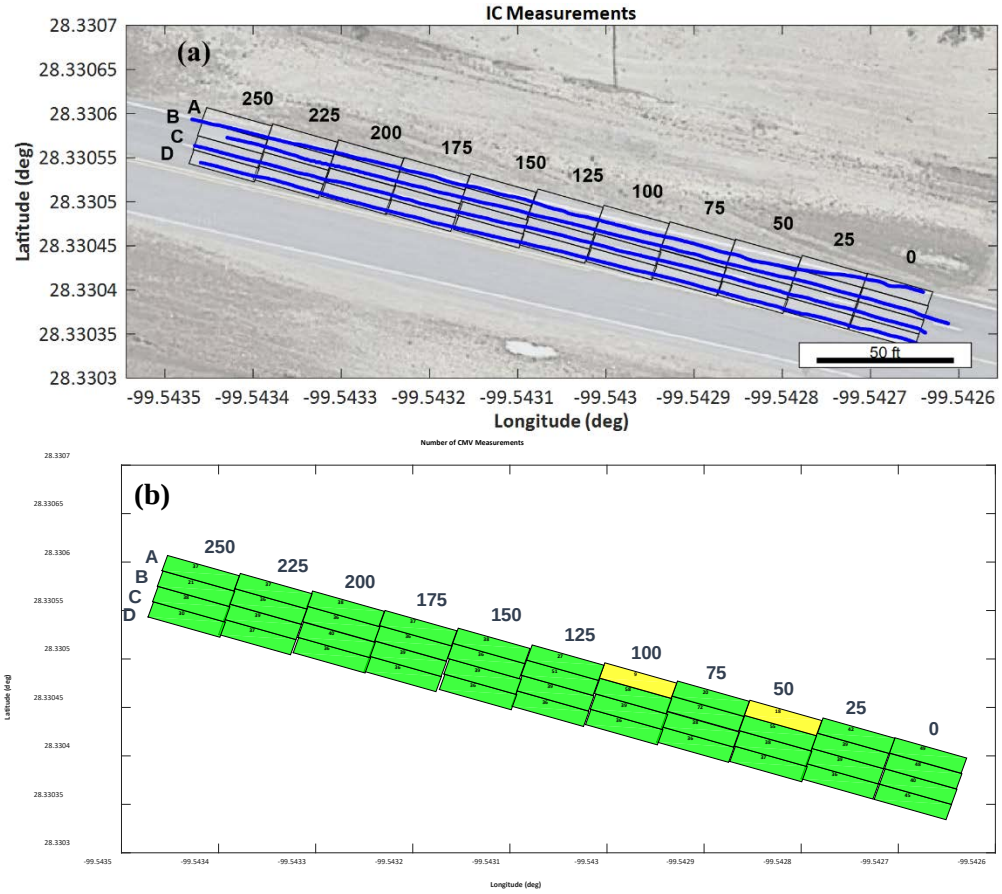

Figure L.4 – (a) Data Collected on Subgrade by IC Roller in Rectangular Buffered Areas and (b) Number of IC Measurement Values within Each Buffer Area.

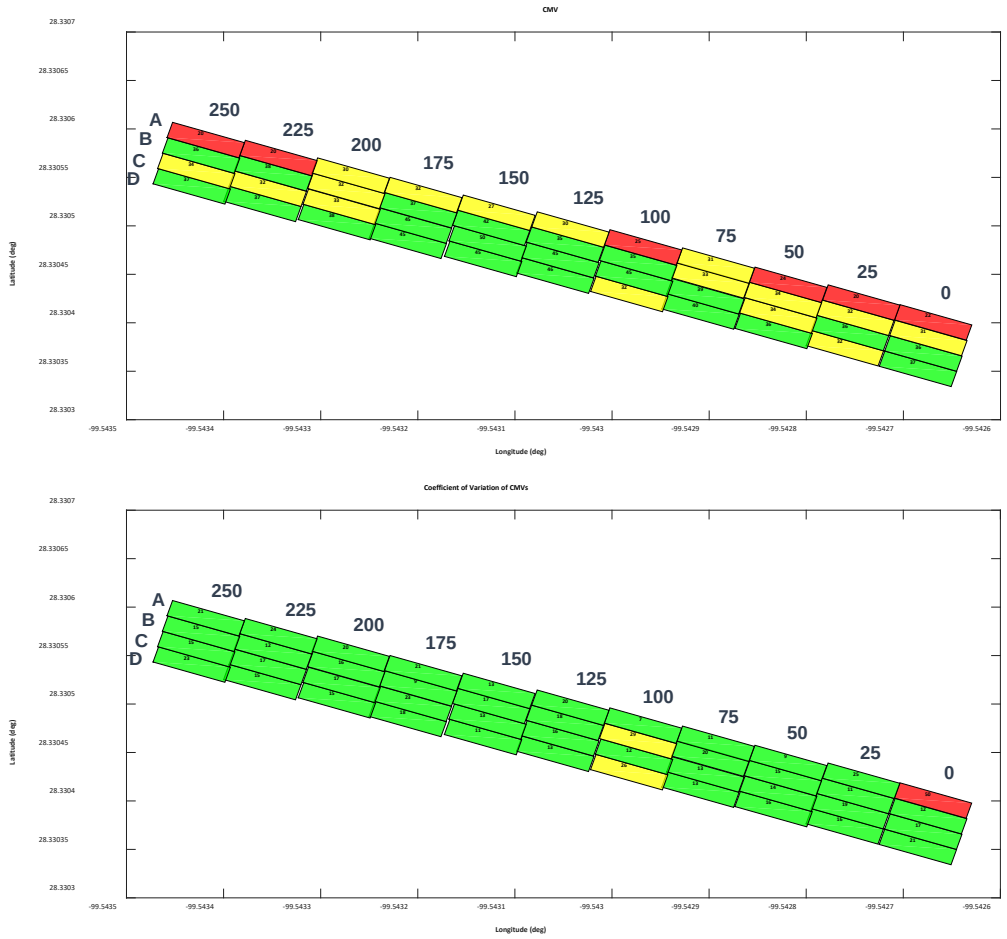

Figure L.5 – Spatial Variation of (a) IC Roller CMVs and (b) their Corresponding Coefficient of Variation.

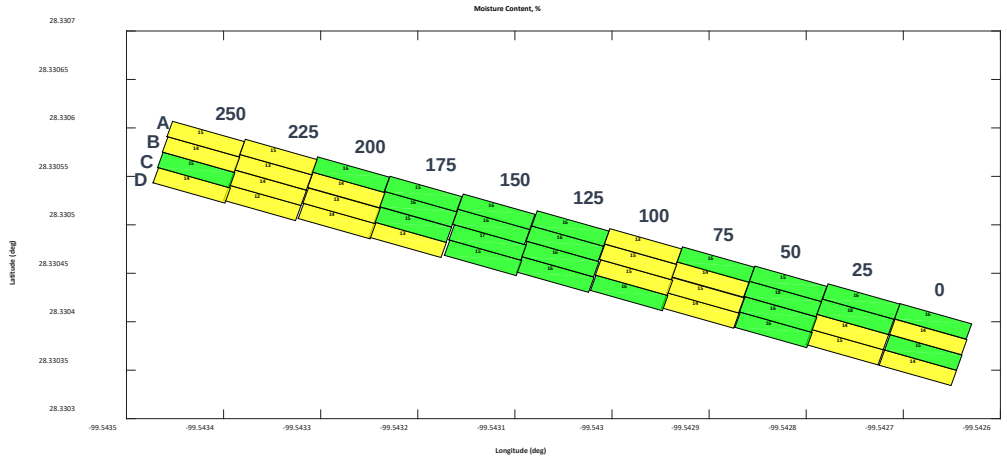

Figure L.6 – Spatial Variation of Moisture Content.

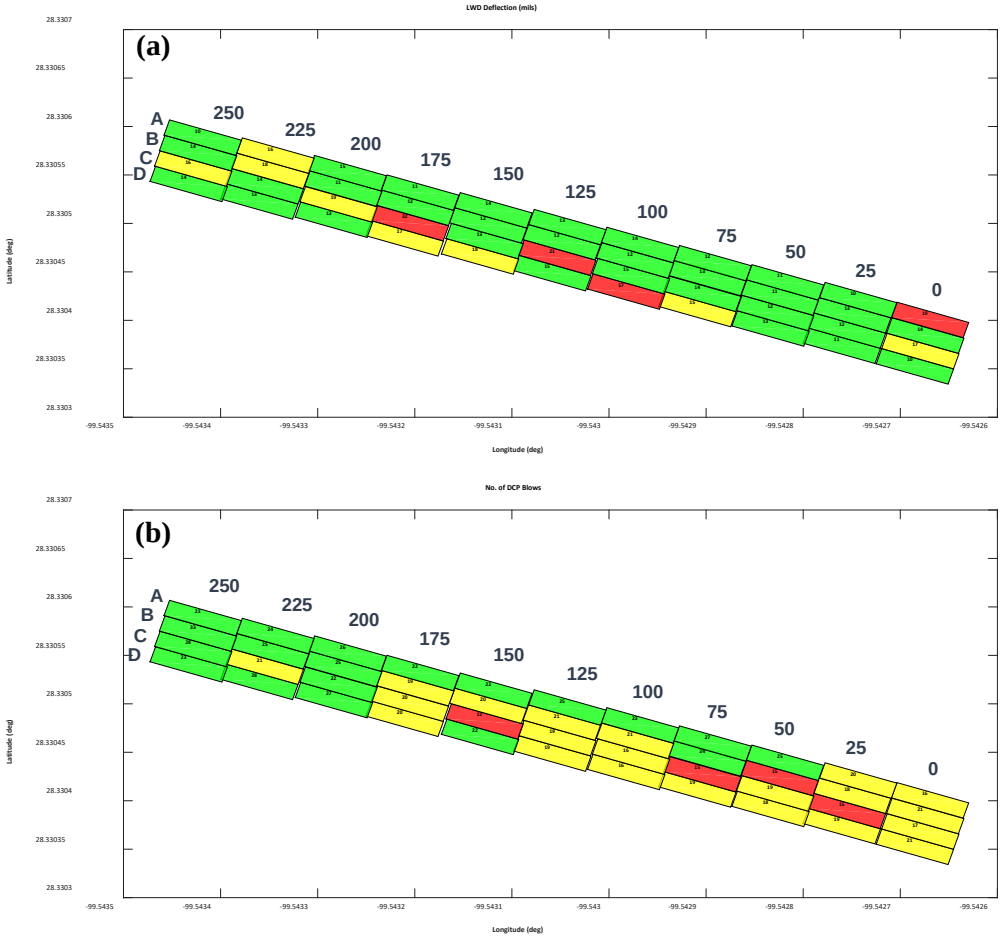

Figure L.7 – Spatial Variation of (a) LWD Deflection and (b) Number of DCP Blows to Penetrate 16 in.

L.3 Base

Figure L.8 shows the mapping of the test section and the number of IC measurements within each rectangular buffer. Figure L.9 shows the mapped CMVs per buffer area obtained after proof-mapping the base and their corresponding coefficient of variation. The latter figure show that ICMVs were generally uniform within the buffer areas. Figure L.10 shows the mapping of LWD deflection measurements. Mapping of LWD deflection shows test section was uniform.

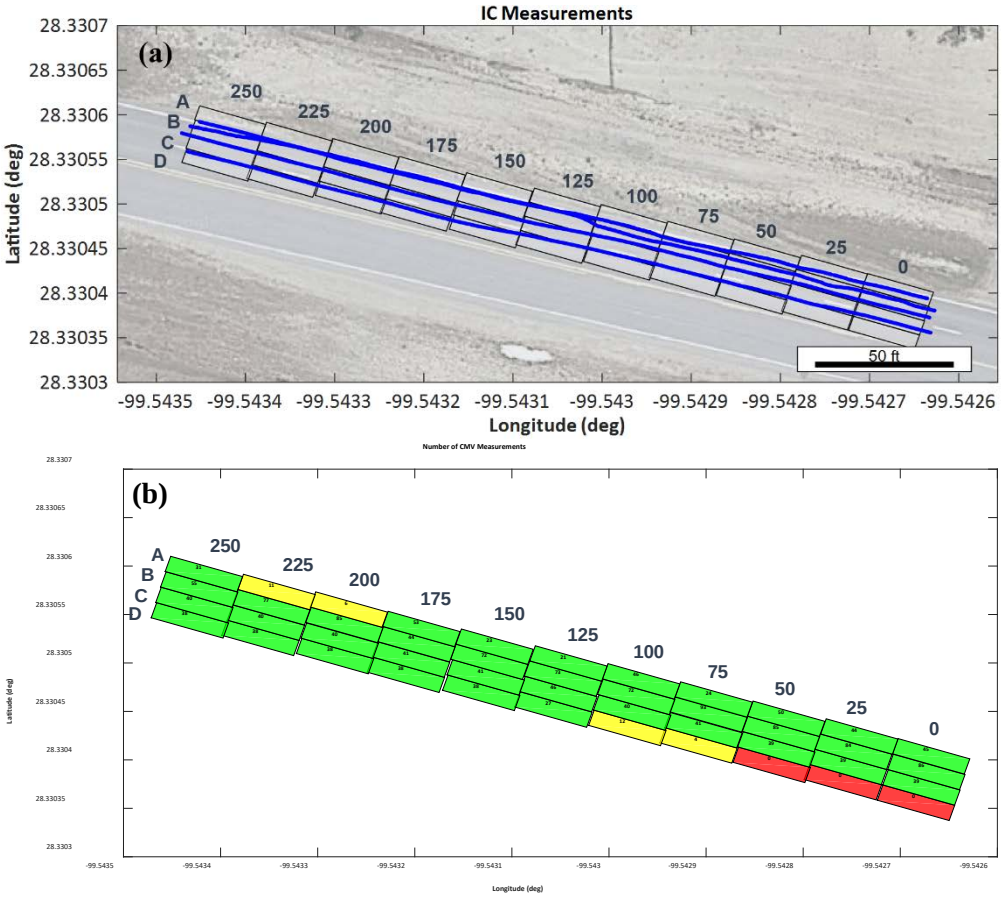

Figure L.8 – (a) Data Collected on Top of Base by IC Roller in Rectangular Buffered Areas and (b) Number of IC Measurement Values within Each Buffer Area.

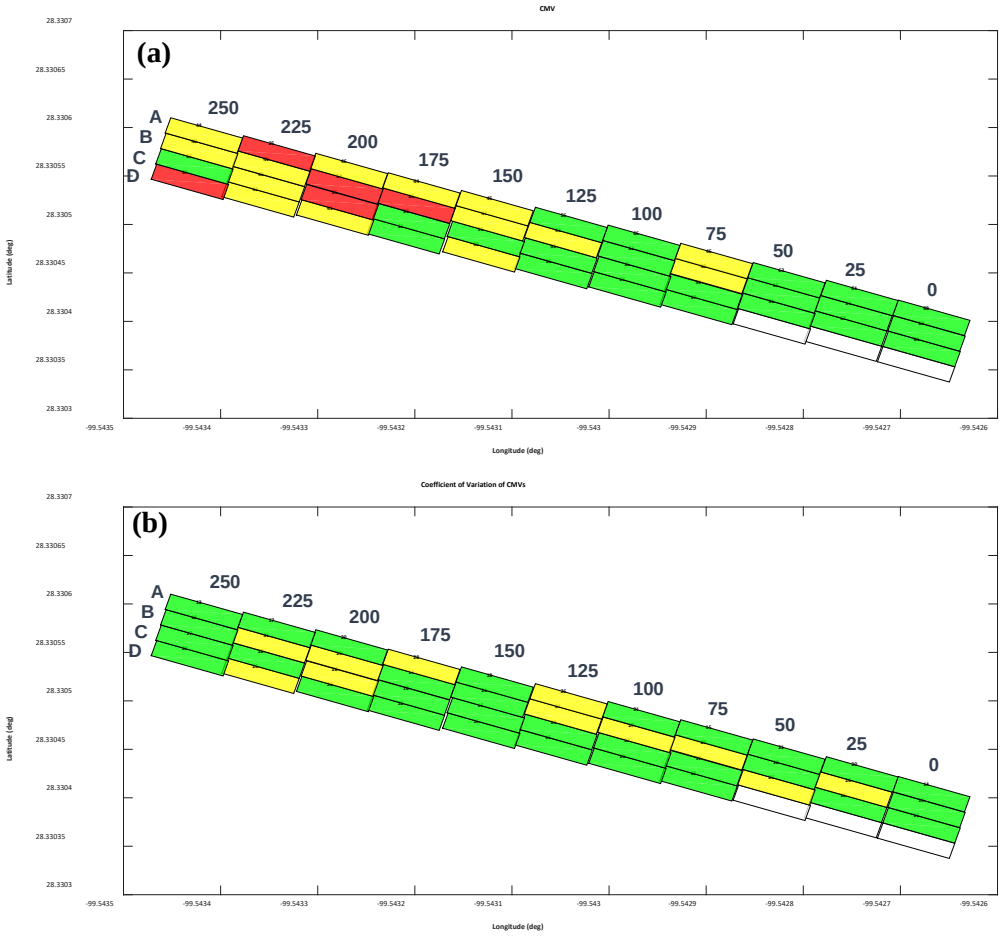

Figure L.9 – Spatial Variation of (a) IC Roller CMVs and (b) their Corresponding Coefficient of Variation in Base Layer.

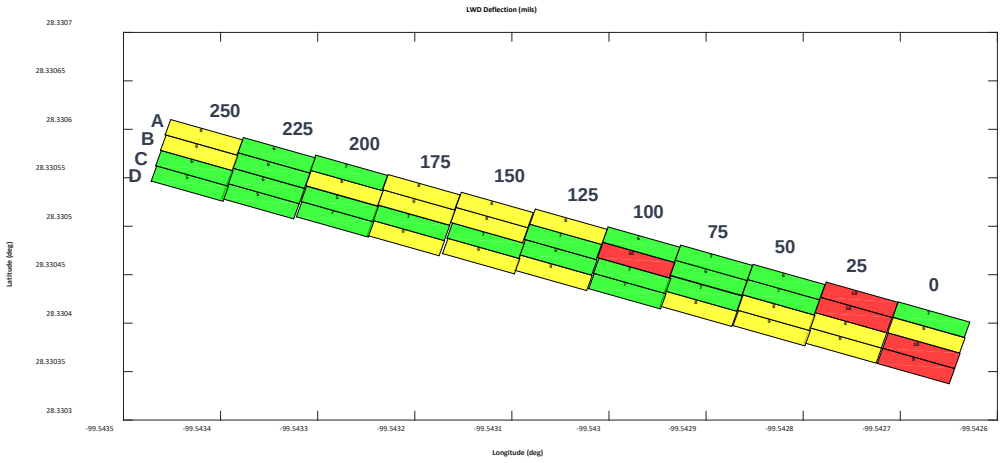

Figure L.10 – Spatial Variation of LWD Deflections in Base Layer.

APPENDIX M - FIELD EVALUATION OF TEST SITE ON I-45 NEAR HUNTSVILLE, TX

M.1 Introduction

Field evaluation was performed on a 250-ft long section of a construction of a south-bound overpass on Interstate Highway I-45 over FM 1374 and SH 150 on May 5, 2018, south of Huntsville, Texas, as shown in Figure M.1. Due to construction operations, testing of the base layer on the same test section was not permitted by the contractor, and the base layer of another section nearby to the subgrade test site along I-45 was tested instead on June 6, 2018. The pavement structure consists of a 6 in. cement treated base (4%) on top of a 12 in. cement treated subgrade with 4% cement, as shown in Figure M.2. Proof-mapping and deflection-based testing on the subgrade was conducted using the Dynamic Cone Penetrometer (DCP) and the Light-Weight Deflectometer (LWD). LWD testing was performed on the base layer.

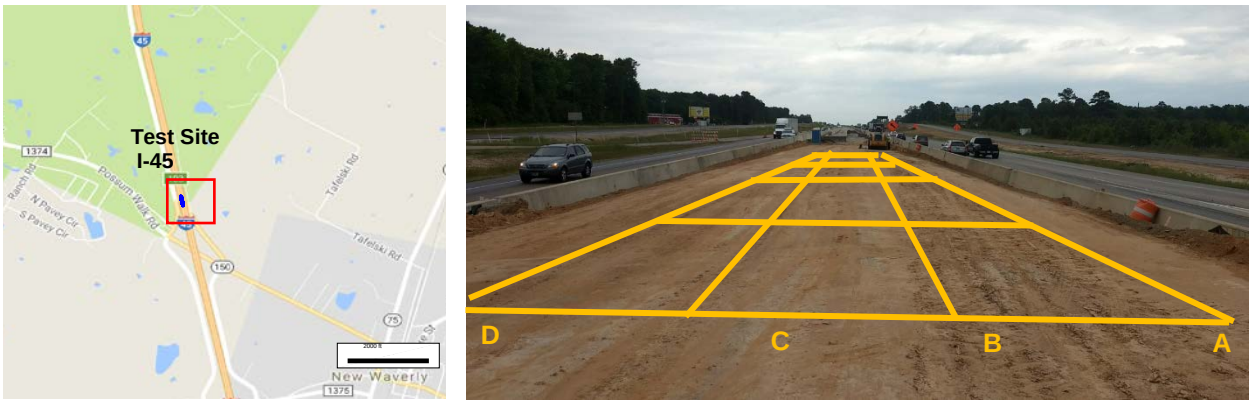

Figure M.1 – Location and View of Test Site on I-45, south of Huntsville, TX.

Cement Treated Base	*h* = 6 in., Modulus = 400 ksi
Cement Treated Subgrade	*h* = 12 in., Modulus = 30 ksi
Embankment	

Figure M.2 – Pavement Structure and Design Parameters for I-45.

M.2 Subgrade

Figure M.3 shows the line passes, the mapping of the number of CMV collected data points within each buffer area, the mapping of CMVs and their respective coefficient of variation within the buffer area. The test site was bounded by the ramp of the overpass on the southern end and by a section with CPCD reinforcement already overlaid on the northern end of the test site. For this reason, proof-mapping was conducted in an area slightly shorter than the limits of the test site, resulting in fewer ICMV data points collected at the extremes of the test site, as shown in Figure M.3b. The mapping of CMVs shows line C as less stiff. The mapping of the LWD deflections and DCP drops also show line C to be less stiff than the other areas, as seen in Figure M.4.

M.3 Base

Figure M.5 shows the line passes, the mapping of the number of CMV collected data points within each buffer area, the mapping of CMVs, their respective coefficient of variation within the buffer area, and the LWD deflection measurements.

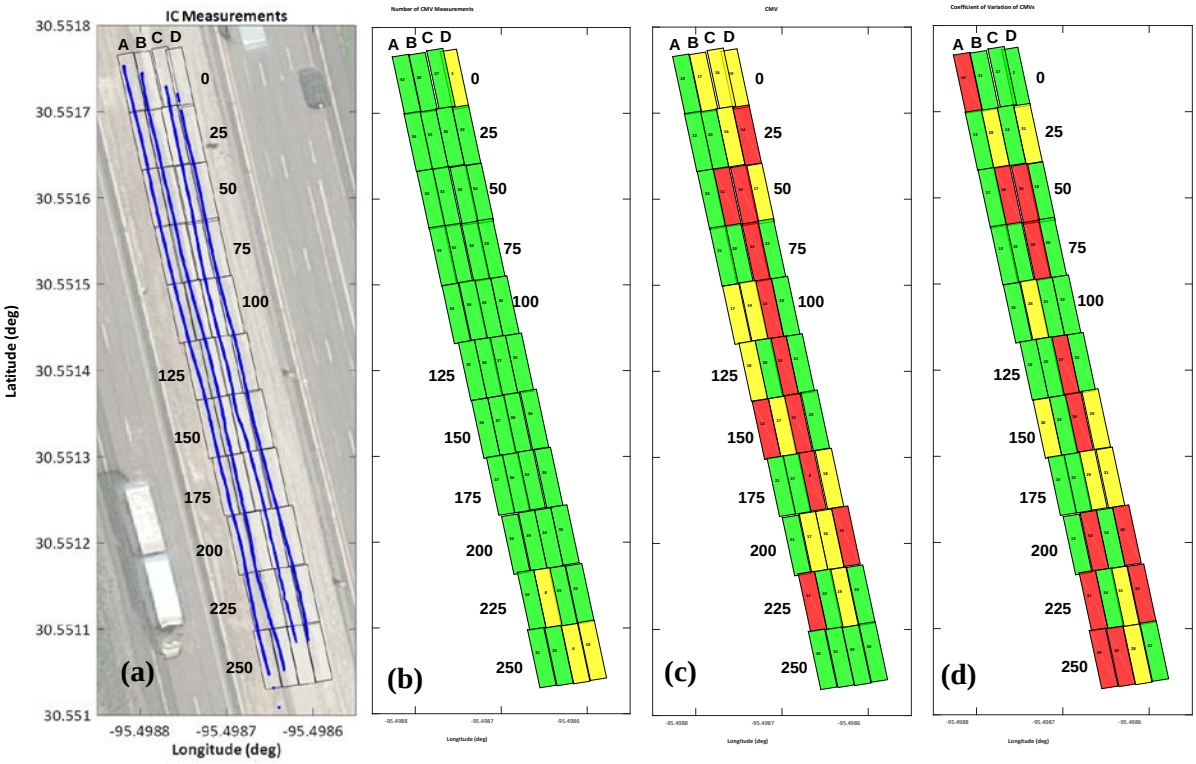

Figure M.3 – (a) Roller Line Passes, (b) Number of ICMV Data Points, (c) CMV Mapping, and (d) Mapping of Coefficient of Variation of CMVs.

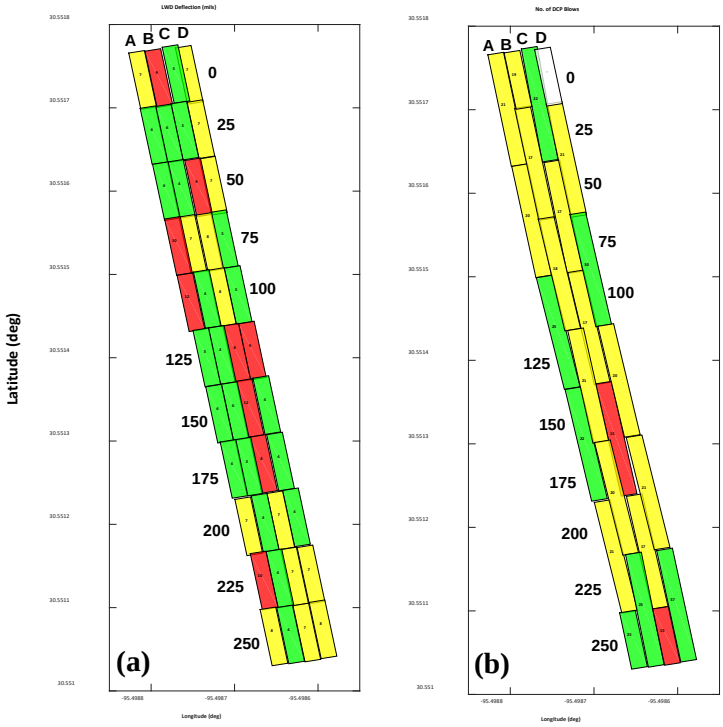

Figure M.4 – Mapping of (a) LWD Deflections and (b) DCP blows to Penetrate 16 in.

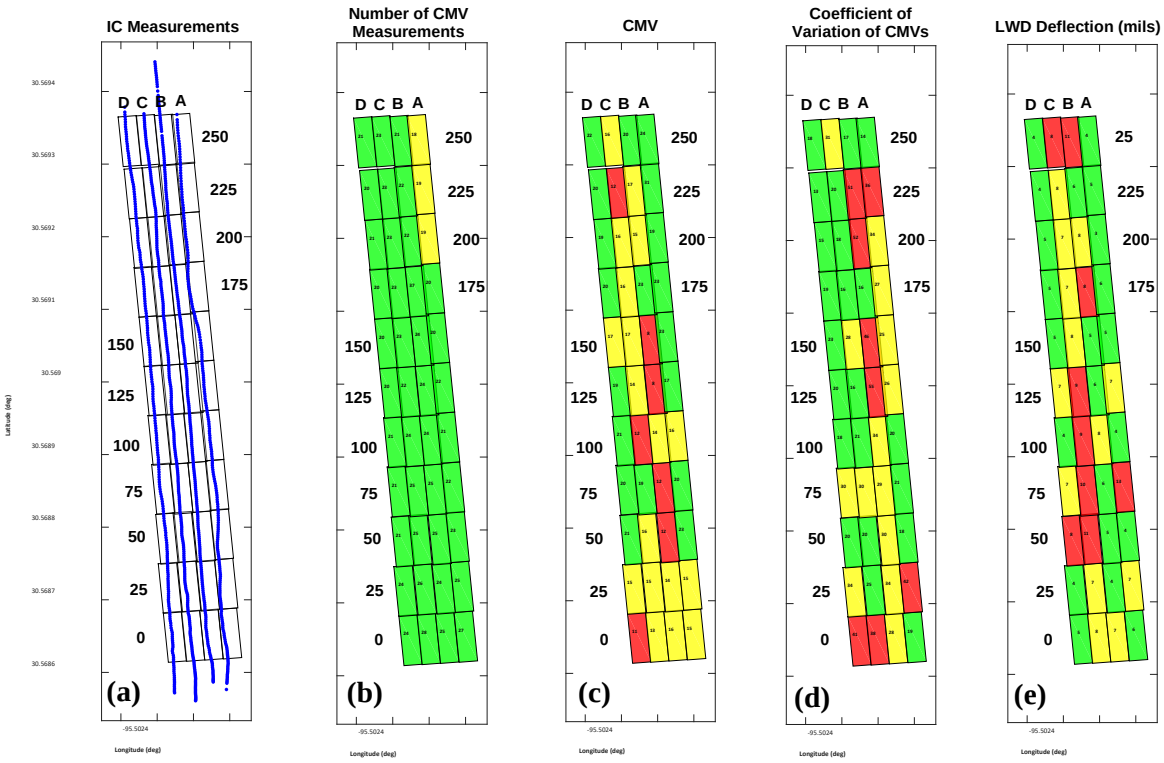

Figure M.5 – (a) Roller Line Passes, (b) Number of ICMV Data Points, (c) CMV Mapping, (d) Mapping of Coefficient of Variation of CMVs, and (e) LWD Deflections.